

Report Title

Laser Drilling – Drilling with the Power of Light

Type of Report:	Final Report
Reporting Period Start Date:	September 2000
Reporting Period End Date:	February 2007
Principal Author(s):	Iraj A. Salehi Brian C. Gahan, P.E. Samih Batarseh, PhD
Date Report was issued:	May 2007
DOE Award Number:	DE-FC26-00NT40917
Submitting Organization:	Gas Technology Institute
Address:	1700 South Mount Prospect Road Des Plaines, Illinois 60018

Disclaimer

This report was prepared as an account of work sponsored by an agency of the United States Government. Neither the United States Government nor any agency thereof, nor any of their employees, makes any warranty, express or implied, or assumes any legal liability or responsibility for the accuracy, completeness, or usefulness of any information, apparatus, product, or process disclosed, or represents that its use would not infringe privately owned rights. Reference herein to any specific commercial product, process, or service by trade name, trademark, manufacturer, or otherwise does not necessarily constitute or imply its endorsement, recommendation, or favoring by the United States Government or any agency thereof. The views and opinions of authors expressed herein do not necessarily state or reflect those of the United States Government or any agency thereof.

Abstract

Gas Technology Institute (GTI) has been the leading investigator in the field of high power laser applications research for well construction and completion applications. Since 1997, GTI (then as Gas Research Institute- GRI) has investigated several military and industrial laser systems and their ability to cut and drill into reservoir type rocks. In this report, GTI continues its investigation with a 5.34 kW ytterbium-doped multi-clad high power fiber laser (HPFL). When compared to its competitors; the HPFL represents a technology that is more cost effective to operate, capable of remote operations, and requires considerably less maintenance and repair.

Work performed under this contract included design and implementation of laboratory experiments to investigate the effects of high power laser energy on a variety of rock types. All previous laser/rock interaction tests were performed on samples in the lab at atmospheric pressure. To determine the effect of downhole pressure conditions, a sophisticated tri-axial cell was designed and tested. For the first time, Berea sandstone, limestone and clad core samples were lased under various combinations of confining, axial and pore pressures. Composite core samples consisted of steel cemented to rock in an effort to represent material penetrated in a cased hole. The results of this experiment will assist in the development of a downhole laser perforation or side tracking prototype tool.

To determine how this promising laser would perform under high pressure in-situ conditions, GTI performed a number of experiments with results directly comparable to previous data. Experiments were designed to investigate the effect of laser input parameters on representative reservoir rock types of sandstone and limestone. The focus of the experiments was on laser/rock interaction under confining pressure as would be the case for all drilling and completion operations. As such, the results would be applicable to drilling, perforation, and side tracking applications.

In the past, several combinations of laser and rock variables were investigated at standard conditions and reported in the literature. More recent experiments determined the technical feasibility of laser perforation on multiple samples of rock, cement and steel. The fiber laser was capable of penetrating these materials under a variety of conditions, to an appropriate depth, and with reasonable energy requirements. It was determined that fiber lasers are capable of cutting rock without causing damage to flow properties. Furthermore, the laser perforation resulted in permeability improvements on the exposed rock surface.

This report has been prepared in two parts and each part may be treated as a stand-alone document. Part 1 (High Energy Laser Drilling) includes the general description of the concept and focuses on results from experiments under the ambient lab conditions. Part 2 (High Energy Laser Perforation and Completion Techniques) discusses the design and development of a customized laser pressure cell; experimental design and procedures, and the resulting data on pressure-charged samples exposed to the laser beam. An analysis provides the resulting effect of downhole pressure conditions on the laser/rock interaction process.

Part 1. High Energy Laser Drilling

Table of Contents

Disclaimer	ii
Abstract	iv
1 Executive Summary	1
1.1 GRI Project, 1997-2000	1
1.2 DOE Project, 2000-2007	1
1.2.1 Conclusions and Recommendations	1
2 Introduction	2
2.1 Drilling Today In the USA	2
2.2 1997-2000 GRI Laser Drilling Research Project	3
2.3 DOE Investigation	4
2.3.1 Phase I – Determination of Energy Requirements	4
2.3.2 Phase II – Multiple Beam Bursts	5
Experimental Approach	7
2.4 Proposed Tasks	7
2.4.1 Determining “Absolute” Specific Energy	7
2.4.2 Determining the Value of Pulsed Lasers	10
2.4.3 Saturated and Submerged Tests	12
2.5 Lasers Used in Drilling Research	13
2.5.1 Laser Parameters	13
2.5.2 Characteristics Of The Lasers Used In This Study	13
2.6 Experimental Approach Summary	15
3 Experimental Procedures and Results	16
3.1 Introduction	16
3.2 Purge Optimization and Calculating Specific Energy	16
3.2.1 Purge Optimization	16
3.2.2 Methods of Calculating Specific Energy	17
3.2.3 Result and Analysis:	19
3.3 Orientation Effect Test:	25
3.4 Determination of Boundary Effect	27
3.5 Effect of Beam Density on Specific Energy	29
3.6 Effect of laser power on Specific Energy (focused beam)	36
3.6.1 Spallation Test:	39
3.6.2 Thermal Effects on Berea Sample	41
3.6.3 Thermal Effects on Limestone Sample	47
Effect of laser power on Specific Energy (Collimated beam)	77
Effect of laser power on Specific Energy (Collimated beam)	110
3.7 Laser Drilling Systems	116
3.7.1 Nd:YAG System	116
3.7.2 Nuvonyx Diode System	116
3.8 Saturated and Submerged Tests	116
3.8.1 Saturated	116
3.8.2 Submerged	117
4 Results and Discussion	118

4.1 Data Analysis	118
4.2 Important Rock Parameters	118
4.3 Spallation and Melting Zones Identified	119
4.4 Spallation Tests with Dry Samples	120
4.4.1 Lithology Samples	121
4.4.2 Specific Energy as Power Increases: Non-melt vs. Melt	122
4.4.3 Effects of Pulse Width and Repetition Rate	122
4.4.4 Temperature Factors	124
4.4.5 Spallation Tests with Saturated Samples	124
4.4.6 Submerged Sample Test	125
4.4.7 Diode Laser Tests with Dry Samples	125
5 Conclusions	127
6 Recommendations	129
6.1 Phase 2 Research Plan	129
6.1.1 Additional Fundamental Research	129
6.1.2 Modeling and Theoretical Studies	130
6.1.3 Engineering Studies	130
7 References	133
8 Appendix: A-F	134
A: GTI Laser Applications Bibliography	135
B: Tables of Results	139
C: Glossary	194
D: Nomenclature	199
E: Petrophysical and Petrographic Studies	202
F: IPG Optical Fluids Report	218

1 Executive Summary

1.1 GRI Project, 1997-2000

Three sandstones, three shales, three limestones, two granites, a salt, and a concrete sample were subjected to energy from three lasers, including the MIRACL of the U.S Army and the COIL and CO₂ lasers belonging to the U. S. Air Force. From the lasing and analysis of more than 240 samples, the following three main conclusions were drawn:

1. Present day lasers have more than enough power to spall, melt and vaporize rock.
2. Qualitatively, there is as much specific energy (SE) variability within as between lithologies.
3. Less power is needed to spall, melt or vaporize rock than calculated from basic principles in the 1960's by orders of magnitude.

1.2 DOE Project, 2000-2007

A work plan for Phase 1 was proposed to DOE to expand upon the GRI-funded work with additional wavelengths of laser power in environments other than air. It was felt necessary to demonstrate that laser parameters could be more carefully defined and to test the idea that pulsed lasers could cut more efficiently, as they do in metal work.

Three objectives were defined:

1. Quantify GRI results,
2. Test effects of varying pulse parameters, and
3. Test laser/rock interaction under water.

A work plan for a follow-on Phase 2 included the following tasks:

1. Continue laser tests under water until the laser/rock interaction is understood similar to dry and saturated rock.
2. Perform additional underwater SE tests in a simulated downhole environment with the development of a vessel that allows a laser beam injection into a pressurized environment with the sample under at least uniaxial stress.
3. Perform modeling and engineering design studies to develop and refine possible downhole assembly configurations.

1.2.1 Conclusions and Recommendations

While some fundamental measurements are still necessary, the minimum energy requirements are much better understood and ideas for system designs are now possible. It is projected that a subsequent study will be necessary to refine the system designs and perform tests targeted at particular system components.

2 Introduction

2.1 Drilling Today In the USA

Rock destruction and removal is a significant issue in the process of oil and gas development. Over the years, billions of cubic feet of rock have been removed, with tremendous capital investment. In 1999, approximately 20,000 wells (oil, gas and dry) were drilled onshore in the United States, averaging about 6,000 feet deep, at a cost of nearly \$15 billion¹. This is equivalent to approximately 23,000 miles, or nearly three times the diameter of the earth (7,926 miles).

According to a GRI study conducted in 1990, 48% of the drilling time of a typical well is spent on making hole, 27% of the time spent changing bits or putting steel tubular casing in place, and 25% of the time spent measuring well and formation characteristics². Major reductions in drilling costs can be obtained by drilling faster and reducing requirements for drill string removal, bit replacement and setting casing.

The 2001 report of the National Energy Policy Development Group, headed by Vice President Dick Cheney titled “Reliable, Affordable, and Environmentally Sound Energy for America’s Future” has a primary recommendation for action “to increase domestic production.” Under this recommendation is a call for the Departments of Energy and Interior to promote enhanced oil and gas recovery from existing wells through new technology. The present project was a response this call.

Characteristics of the laser drilling system make it friendlier to the environment than current state-of-the-art drilling systems and it has the potential to tap known U.S. resources which are currently uneconomical to develop. Drilling is faster so the system is on location for a shorter period of time, thus minimizing interruptions to the natural ecosystems and reducing drilling objections from local residents. It is envisioned that the laser system would have a smaller environmental footprint and the use of hazardous chemicals would be greatly reduced.

Some of the concerns in drilling operations include: rock destruction and removal; drilling time and cost; rig size and transportation; hole shape and deviation; fishing for stuck pipe; and tripping and drilling in hard formations including granite. In well completion operations, perforating with a shaped charge

¹ DeGolyer and MacNaughton, 2000

² Andersen, et al., 1990.

gun causes reduced production by damaging the formation around the perforated tunnel. Depending on the rock type, drilling rates can be significantly increased using lasers when compared to conventional drilling rates. For example, drilling in hard rocks, such as granite, is extremely difficult or impossible. This research has shown that lasers penetrate the hard rocks at about the same rate as for the soft rocks.

Reducing the drilling costs and eliminating problems would have a significant positive impact on the oil and gas industry. New technologies and tools operate using basic rock destruction mechanisms like thermal spalling, fusion and vaporization, mechanical stresses and chemical reactions³. All of these destruction mechanisms can be achieved using lasers. For example, at low laser power, spalling (chipping) can be obtained. Increase in the laser power, with a fixed beam diameter, results in phase changes and reactions in the rock, like dehydration of clays, releasing of gases and inducing thermal stresses. At a certain power, the rock will melt (fuse) and at higher power it will vaporize.

Laser technology applied to drilling and completion operations has the potential to reduce drilling time, eliminate the necessity to remove and dispose of drilling cuttings and improve well performance through improved perforation operations.

2.2 1997-2000 GRI Laser Drilling Research Project

Because reducing drilling costs in an environmentally sensitive manner is critical, in 1997 the Gas Research Institute (now Gas Technology Institute) initiated a two-year research program directed towards revolutionizing drilling. The specific objective of the research was to determine the feasibility of using high power lasers (1 kW and higher) for drilling and completing oil and natural gas wells. A 1994 congressional mandate to transfer cold war military defense technologies to American industry opened the door to begin an investigation of applying “Star War” laser technology to drill and complete oil and natural gas wells.

Two types of military lasers were included in this investigation: the Chemical Oxygen Iodine Laser (COIL) and the Mid-Infrared Advanced Chemical Laser (MIRACL). The COIL was developed at the U.S. Air Force Research Laboratory, Kirtland Air Force Base in Albuquerque, New Mexico. The size of the COIL has been reduced and optimized as part of the Airborne Laser (ABL) research project. Because of its tactical capabilities, it will be placed onboard a Boeing 747 aircraft and used to track and destroy missiles. The MIRACL is located at the U.S. Army’s High Energy Laser Systems Test Facility in White Sands, New Mexico. The MIRACL was tested first because it is the most powerful laser in the Western Hemisphere. It has an output power that can exceed 1200 kW. The initial tests

³ Maurer, 1968, 1980

determined that less power could be used for rock destruction so the remaining tests were conducted using the Air Force's 6.8 kW COIL.

High power lasers were being developed in the former Soviet Union independent of the developments in the U.S. A comprehensive literature review of Russian laser technology and experiment research using a CO and CO₂ was conducted by the P.N. Lebedev Radiophysics Institute in Moscow, Russia. Some preliminary testing using a CO₂ laser was also done at the U.S. Air Force Laser Hardening Material Experimental Laboratory in Dayton, Ohio.

2.3 DOE Investigation

The GRI project to demonstrate the feasibility of using high power lasers for oil and gas applications was very successful. Building on this, the U.S. Department of Energy (DOE) cofunded the next phase to more fully investigate the basic scientific principles that can bring this laser drilling and completions concept within reach of an industry-supported prototype development. Consortium partners in this research with DOE are Gas Technology Institute, Halliburton Energy Services, and the research facility within the Venezuelan National Oil Company, Petroleos de Venezuela – INTEVEP, S.A.(INTEVEP).

The experimental research was conducted at Argonne National Laboratory in Chicago, IL and in the Petroleum Engineering Department at the Colorado School of Mines, Golden, CO under the direction of the Gas Technology Institute. A very preliminary study of the Nuvonyx diode laser was performed at NA Tech, a small metallurgical company in Golden, Colorado.

2.3.1 Phase I – Determination of Energy Requirements

As part of this investigation, GTI identified the minimum specific energy (SE, kJ/cc) required to remove rock from test samples of sandstone, shale and limestone using a 1.6 kW pulsed neodymium yttrium aluminum garnet (Nd:YAG) laser beam. Each sample was subjected to a single exposure of the beam, and the resulting SE calculations were made.

Several changes were incorporated into the experiment design from the previous study. Laser beam bursts onto the rock sample were performed with a 400 scf/m coaxial nitrogen purge to prevent rock particles and exsolved gases from reentering and absorbing energy from the beam, and to prevent damage to the optics. Also, larger spot sizes and shallower holes were created to avoid deeper, energy absorbing holes with depths greater than beam diameter. Both design improvements maximized energy use for hole creation, improved the repeatability of the experiments, and more closely determined the intrinsic SE requirements of each rock type.

The results supported the change in experiment design, with much lower SE values and clear SE differences emerging between lithologies. Shales, in general, required the least energy to remove a unit volume of rock by an order of magnitude. This is fortunate as 70% of the rock drilled in the pursuit of oil and gas is shale. Shale results do not seem to depend on mineralogy as much as the grain size.

The sandstone samples exhibited higher SE values than the shale samples although the range of values is wider. It appears that the SE values determined may correlate to the amount of clays in the rock with more clay content resulting in lower SE values.

2.3.2 Phase II – Multiple Beam Bursts

In July 2002, a series of follow-on experiments were performed lasing multiple holes into rock samples to determine effects on specific energy.

The research team visualized a laser-based drilling system that made use of multiple beams of near-infrared energy placed adjacent to one another, collectively creating a hole. The size of the hole would then depend on the number, arrangement, and burst frequency of beams employed.

The concept is similar to that of a mechanical drill bit in that individual teeth, buttons, or cutters, chip small pieces of rock as the bit turns under the weight of the drill string. Since the rock experiences compressive failure under the concentrated load of each pressure point, the dimensions of the hole are a function of the number, arrangement, and rate at which the points impact the rock under a given load. In both cases, a requisite amount of controlled energy is repeatedly delivered from the system to a point on the rock, causing the rock to fail on a predetermined path.

Key considerations in designing the multiple hole test series included geometric pattern applications, beam overlap and spacing, focal distance changes while lasing, beam intercept angles, purging systems and thermal relaxation time between successive shots.

The results from the multiple burst experiments confirmed that rocks could be removed in a controlled fashion under spallation mechanisms, and that a large hole can be created without the need for moving parts in the bottomhole assembly such as a rastering or rotating system. The application of a significant amount of laser energy to a small rock sample without causing the onset of melting is very important. Avoidance of melt is essential to efficient rock spalling.

The concept of the transport downhole of laser energy by means of fiber optics or other waveguide materials is supported by the low power requirements at each of the many spots to create a large hole in the subsurface. The power requirements are within the tested capabilities of current fiber optics to significant depths, while technology in the research phase, such as hollow core fibers, may provide additional beam transport options in the future.

Results from experiments to date continued to suggest the application of photonic energy may prove to offer a non-explosive alternative for perforating oil and gas wells. By applying this technique downhole through casing and cement, perforations and other directionally controlled completion and stimulation methods could be employed without creating damage to the reservoir. Clearly, with the use of photonic energy, no perforating materials or explosive products are left to contaminate the wellbore and the perforation tunnel; therefore cleaning the perforated tunnel and the wellbore around the perforation area are not required. In fact, the use of lasers in downhole completions techniques, including perforation, has the potential to stimulate the perforation tunnel while it is constructed.

Experimental Approach

2.4 Proposed Tasks

The 1997-2000 GRI Laser Drilling Project consisted of fundamental research testing the feasibility of using the modern generation of lasers for hard rock drilling. The work attempted to measure the specific energy (SE, defined as the amount of energy required to remove a unit volume of rock) needed to cut and melt different lithologies, but found that secondary mechanisms prevented a “true” or “absolute” SE from being measured. The GRI work focused on continuous wave lasers, with little experiment time available for testing pulse efficiencies. The research team was very aware of industry’s need to use pressure controlling weighted (and therefore opaque) drilling fluids, but detailed testing of this environment was not part of the research plan. Time was allotted for one test using the COIL, which showed that even through several inches of opaque drilling mud, a hole could be produced in a block of sandstone.

The research program reported in this document had the purpose of building on and adding to the GRI work in determining the feasibility of using high-power lasers in drilling and completing oil and natural gas wells by quantifying what was only qualitative measurements. The Phase 1 work required a better experiment design that minimized energy losses, while providing greater confidence in the SE calculations. Three tasks were identified:

- Task 1.1 Energy Assessment Series -- GTI shall conduct laser cutting energy assessment series to determine the SE values of five (5) lithologies, of which includes a sandstone and a shale.
- Task 1.2 Conduct Studies of Variable Pulse Laser Effects -- Using a CO₂ laser, GTI shall perform series of tests on identical sandstone samples to determine the pulse, width and repetition rate that spalls the rock matrix most efficiently, then repeat the test using an Nd:YAG laser to determine wavelength effect. The test will be repeated with identical shale samples.
- Task 1.3 Conduct Lasing through Liquids -- GTI shall design and conduct analytical studies to evaluate the optimum placement for the initial laser beam/liquid interface.

2.4.1 Determining “Absolute” Specific Energy

The absolute SE of a given rock sample is an intrinsic physical property of the rock, much like porosity and permeability, and should not change regardless of the rock removal techniques employed. There can be any number of measured values of SE, however, based upon the parameters of any given rock removal technique, these values can approach the absolute SE as the rock removal techniques become more efficient with respect to the responding primary and

secondary mechanisms of the rock itself. Since SE is determined as the beam's power density (irradiance) for a given time duration per volume of rock removed, an accurate means must be available to measure these factors. For purposes of pre- and post-laser rock property measurements, it is important to avoid edge effects, such as micro fractures, that affect the physical properties of the rock, but don't contribute to determining the SE, therefore, no laser spot edges were performed closer than 2 cm from edge or each other.

2.4.1.1 Material Removal

The goal of the experiments was to remove a measurable amount of material with each use of the laser. There was quite a bit of discussion about what the minimum of removed material should be relative to the total mass of the sample. This was complicated by the need for a robust balance to handle the total weight of the sample, and could reduce the number of significant digits for a given sample weight. If the weight of material removed in a single hole was a few milligrams, would it be insignificant relative to the total mass of the rock or be within the error of the balance? The balance available was capable of weighing a maximum of a 160 gram sample with 4 digits to the right of the decimal point, which was sufficient for the experiments. If a particular test removed any material at all, it was in the 10's to 100's of milligrams.

2.4.1.2 Secondary Mechanisms

Several details of the test plan were intended to reduce, if not eliminate, the secondary mechanisms recognized in the GRI study. The hole depth was kept less than its diameter to reduce the amount of spalled material that was melted and vaporized before escaping from the beam; and to reduce the amount of time that exsolved gases were in the beam before being dispersed by the purge gas. A coaxial purge vent was used to provide more efficient material removal.

Critics of the use of lasers in rock drilling point out the deleterious effect of plasmas, formed by the ionizing effect of the laser beam on gas molecules, on the absorption of the beam before reaching the sample. Calculations done by Humberto Figueroa, a member of the team from INTEVEP, indicated that the energy being used in these tests was well below that required for plasma formation.

2.4.1.3 Specific Energy Calculations

In order to break rock by mechanically or thermally induced stresses, sufficient power must be applied to the rock such that the induced stresses exceed the rock's strength. Similarly, when fusing rock, sufficient heat must be generated to produce local temperatures that exceed the melting temperature of the rock. Once these threshold values of power and energy are exceeded, the amount of energy required to break or remove a unit volume of rock remains nearly constant. This energy parameter, which is a measure of the efficiency of the rock destruction

technique, is defined as SE. The term SE is associated with various definitions and is commonly used by the drilling industry in discussions of the efficiency of mechanical drilling, particularly in measuring effectiveness of new bit designs. SE is defined in this experimental work as the amount of energy required to remove a unit volume of rock and is relationally represented as follows:

$$SE \text{ (J/ cc)} = \text{Energy input} / \text{volume removed} \quad (1)$$

2.4.1.3.1 Parameters Affecting SE Measurements.

There are three basic phenomena evident in the process of radiant energy transfer to solids: reflection, scattering and absorption of radiation. The flow of energy of an incident electromagnetic wave (E_{inc}) is divided into these parts:

$$E_{inc} = E_{refl} + E_{sc} + E_{abs} \quad (2)$$

Where E_{refl} , E_{sc} , and E_{abs} are reflected, scattered and absorbed fractions of the energy flow of the incident wave, respectively.

If a surface is a planar one, like a mirror, then much of the energy is reflected. Rough surfaces mainly scatter the incident radiation. The reflectivity is determined by the composition of the solid, while the scattering of radiation is determined by wavelength, λ . It is the absorbed energy that gives rise to the rock heating and destruction. Reflection and scattering represent energy losses that occur apart from the absorbed energy. Minimizing fractions of reflected and scattered energy losses will, consequently, maximize the energy available for transfer to a rock for destruction.

There are factors that affect the amount of absorbed energy transferred to the rock samples, known as secondary effects, and include the creation of melted materials, beam absorbing exsolved gases in the lased hole and induced fractures in the surrounding rock. When applying high power lasers on rocks, the laser can spall, melt, or vaporize the rock as the energy transferred to the rock raises its temperature locally. Mineral melt begins to occur when the rate of heat dissipation by the rock is exceeded by the rate of energy absorbed by the rock. As time increases, energy accumulates in the form of heat, raising the local temperature of the minerals to their melting points, forming a glassy melt.

The amount of melt is a function of the mineralogy of the rock and the intergranular space of the rock matrix. The closer the grains are to one another, the more heat will be transferred, resulting in more melt in the rocks. However, for tightly packed grains, the heat conductivity could reach higher values dissipating the heat at a faster rate, reducing the amount of melted material. Also, some minerals decompose and produce gas. As a result, the melt and gases

require part of the laser energy for their creation, so a smaller percentage of the total laser energy is transmitted to rock.

Fractures that form in the samples also have an impact on SE. It may be that fractures extending out from the laser created hole are beneficial to the removal process. However, it is our conclusion that the fractures seen in the tests are an artifact of the sample size and do not represent what will occur in the subsurface under in situ conditions.

For the purposes of this study, fractures represent losses of energy, which result in higher SE values. Fractures are classified as macro- and micro- fractures. The behavior of fractures is different from one rock type to another. This difference depends on intrinsic factors such as mineralogy, thermal properties of the rocks, volume of void space, dimension of the sample and the amount of stress applied. Mineralogy also affects fracture formation. Clays contain water and by subjecting the clays to higher temperatures, water will escape in the form of vapor. This increases the volume and pressure in the pore and can cause fractures. Sandstones and shales have high thermal conductivities and contain clays. Limestones, on the other hand, have low thermal conductivity and have low amounts of clay and quartz. Therefore, fractures are expected in sandstones and shales, but not in limestones.

Rocks having a high thermal conductivity transfer heat more efficiently and the temperature is more uniform within the rock. Therefore, for this type of rock, cooling occurs gradually along the core sample. For example, fractures in sandstones developed regularly, not randomly. High temperatures resulting from the energy of the laser beam causes quartz grains to expand. At 600°C quartz grains expand by 1.75% of the original size. In the case of full grain contact (low void space), grains have less space to expand and fractures develop⁴.

The dimensions of the sample can affect the behavior of the fractures. It has been observed from the previous tests⁵ that the 2.54-cm diameter cores are highly fractured around the hole, while the 3.09-cm diameter cores are less fractured. Finally, stress applied to the core minimizes the macro fractures, while the micro fractures will still remain.

2.4.2 Determining the Value of Pulsed Lasers

2.4.2.1 What Is A Pulsed Laser?

The discharge of a pulsed laser is characterized by a train of pulses of similar characteristics generated at a fixed time interval as shown in Equation 3.

⁴ W.H. Somerton, 1992.

⁵ R.M. Graves and D.G. O'Brien, 1998

$$P_{av} = P_p \times W_p \times R \quad (3)$$

In this equation, P_p refers to the maximum power in a single pulse, W_p is the width of each pulse in units of time, and P_{av} is the output power averaged over time (Figure 2). An important parameter in pulsed discharges is the pulse repetition rate R , or number of pulses per unit time, defined as the inverse of time, T : $R = 1/T$. Also, the average power and the energy E in each pulse are related to the other laser parameters through the relationship shown in equation 4.

$$E = P_p \times W_p \quad (4)$$

This type of discharge allows for a better control of the laser effects on the rocks than the continuous discharge, since each parameter affects the rock differently. For example, long pulses (W_p on the order of milliseconds) and high repetition rates favor melting, whereas short pulses (small W_p) and low repetition rate favor creation of microfractures. This type of beam manipulation is not possible in the case of the continuous wave CO_2 laser discharge.

For experiments where the laser beam diameter (spot size) is varied, it is best to define the laser intensity, I (also called power density), as the peak power divided by the beam spot size represented by Equation 5.

$$I (W/cm^2) = P_p (W)/\text{spot size (cm}^2) \quad (5)$$

This wide range of parameter values allows for the determination of their effects on SE within that range. Lasers utilize three methods of rock destruction; spallation, melting, and vaporizing; and can be controlled to the extent of the application of these parameters. In this phase of the research, the experiments were carried out using lower powers and less exposure time than in the COIL experiments of the previous GRI laser study⁶.

2.4.2.2 Using a Pulsed Laser on Rock Samples

The purpose of the laser rock interaction experiments is to determine laser and rock threshold parameters required to remove the maximum rock volume from the samples with a minimum amount of energy. This was performed first with dry rock samples, followed by saturated and submerged samples. All of the experiments were conducted at atmospheric pressure.

⁶ R.M. Graves and D.G. O'Brien, 1998

A change in experiment design following the GRI study was to keep the hole depth less than the hole diameter. Previous results determined that the material liberated from the rock remained in the hole as the hole got deeper and was melted and vaporized, absorbing energy from the beam that should have been used for breaking new rock. Also, the deep holes trapped the gases exsolving from the rock, absorbing even more of the beam energy. Except for the limestones, all of the samples had some amount of melt attached to the rock. A power/time range where the rock was spalled and not melted was postulated, but not observed. The large expanse of clean rock evident from the very high power MIRACL laser was attributed to vaporization rather than spalling.

The power density of the laser beams and total power exposed to the rock was known for the continuous wave (CW) work, so some initial estimates were made for the pulse parameters to be used in this study. These estimates were determined from preliminary linear tests described in the next chapter, where a spalling zone was observed on the sandstones for the first time. From this information, several test matrices were created with various combinations of pulse width, repetition rate and duration, in an attempt to determine the specifications for each lithology. It was determined that the calculated average power ($E \cdot L \cdot R$) would be kept at the maximum for the 1.6 kW Nd:YAG laser. Real average power, as measured for each set of parameters, was always somewhat less than calculated because of the limitations of the laser system.

2.4.3 Saturated and Submerged Tests

2.4.3.1 Saturated

The team was interested in determining the behavior of water in the pores of the sandstones. Two possible outcomes were theorized: the water would convert into steam, aiding in the breakage of the rock, or the presence of water would alter the heat conductivity of the system, and allow heat to leave the immediate area quickly enough that reduce or avoid fractures. There could also be some combination of the two. A series of tests were devised to expand the dry rock matrices to investigate the behavior of the wet samples.

2.4.3.2 Submerged

The drilling industry has made it clear during our discussions with them that to claim success, this research program will have to demonstrate that laser drilling can take place in the presence of water and other fluids in the borehole. The full analysis is beyond the scope of this feasibility study; however, an initial test could provide valuable qualitative information. In addition to the saturated sample tests described above, a series of experiments were undertaken to explore the possibility of injecting the laser beam into water and have it impinge on and cut into a rock sample. A full set of test matrices were not envisioned or accomplished, but enough work was done to show the possibilities and give the team a direction forward.

2.5 Lasers Used in Drilling Research

2.5.1 Laser Parameters

LASER is an acronym for Light Amplification by Stimulated Emission of Radiation. Albert Einstein predicted the possibility of stimulated emission (generation of photons or discrete bundles of energy via transitions between atomic or molecular energy levels) in 1917. Laser use in many applications such as medical, metallurgical, and military, is becoming well understood. The principle of the laser is transforming different kinds of energy (chemical, electrical, etc.) into intense electromagnetic beams of monochromatic and coherent waves. The wavelength of a laser beam (λ) depends on laser's active medium, and ranges from 0.1 micrometers (μm) to $103\mu\text{m}$, spanning the ultraviolet, visible, infrared and sub-millimeter ranges of the photonic spectrum⁷.

Laser drilling is a developing technology that has been applied to industrial uses such as creating small holes in metal and other materials. This research examines the possibility of expanding the use of lasers to remove rock for oil and gas exploration and production applications, including conventional and horizontal drilling, cutting windows in steel casing and cement, and other completion techniques.

In rock drilling, the type of laser used plays a crucial role in the efficiency and quality of the cut. Laser properties, including discharge type (continuous or pulsed), wavelength, peak power, average power, intensity, repetition rate, and pulse width define the type of laser rock interaction obtained, and thus, affect the amount of energy transfer to the rock. The results of the previous experimental work show that lasers penetrate well through rocks, as they have a low reflectivity of electromagnetic waves, resulting in a good coupling with the laser radiation. Also, the low thermal conductivity of rocks allows for a rapid heating of the rock sample in the vicinity of the beam.

2.5.2 Characteristics Of The Lasers Used In This Study

Although initial GRI laser drilling investigations utilized megawatt-class military lasers, it was soon apparent that although oversized lasers could effectively remove a rock mass, it did so quite inefficiently due to material phase change and other phenomenon unrelated to cutting and removing rock.

Less powerful industrial lasers were then utilized providing improved SE values when exposed to the same or similar rock types. Under lab conditions, the

⁷W.T. Silfvast, 1996

researchers were successful in proving that the current generation of industrial lasers was capable of removing rock with energy levels comparable to those of existing mechanical rock drilling methods. However, for a laser system to be applied under field conditions, a number of conditions would have to be met, including requisite power delivery to target, reliability, portability, and greater efficiency. Although the overall size or footprint per kilowatt output was improving, industrial class lasers were not necessarily designed to withstand field conditions and would be difficult to economically operate given their low wall plug efficiencies.

GTI advanced its laser/rock cutting research with the acquisition of an IPG Photonics 5 kW ytterbium-doped multi-clad fiber laser in 2003. Currently, it is the most powerful of its kind available for research in the United States, although more powerful ones have been manufactured for industrial use in other countries.

For oil and gas industry applications, the fiber laser presented itself as the most likely near-term candidate for successful laser applications in remote locations, capable of delivering a beam to a rock target some 1 to 2 km beneath the Earth's surface. Given the improvement in the fiber laser's wall plug efficiency (16%) over a comparable diode pumped Nd:YAG (6%), an ytterbium fiber laser requires about 62.5% less electrical energy to produce the same output power beam.

For many of the same reasons fiber lasers represent a breakthrough for field applications in oil and gas, it is also being considered for other applications that include cutting or breaking rock and/or similar materials in remote locations, including those in the energy, mining, defense, space, demolition and construction industries.

2.5.2.1 Characteristics of the Fiber Laser

Recently, high power fiber lasers have become commercially available and have positioned themselves as a serious alternative to other solid-state and carbon dioxide lasers for industrial material-processing. Over the past two years, fiber lasers have increased in power from several watts to kilowatts, and are fully capable of delivering sufficient rock cutting power via fiber optics.

Of interest to the GTI research team were the nearly 10x higher wall plug efficiency; and greater mobility through a smaller overall size and solid state design. In addition, the beam quality was improved, and projected diode failure was in excess of 50,000 continuous hours, projecting low or no maintenance operations (Table 1). Together, these improvements have rapidly advanced fiber lasers as a leading candidate for on-site applications, including hard rock mining, tunneling, pavement cutting and rock drilling.

	CO ₂	LP Nd:YAG	DP Nd:YAG	HPFL
E/O Efficiency, %	5-10	2-3	4-6	16-20
Electric Power, kW (no chiller)	~ 50	~ 130	~ 80	20-25
Footprint, m ² (no chiller)	6	5	3	0.5
Water, m ³ /hr	6-8	20-25	~ 15	<2
Maintenance, Khrs	1-2	0.5	2-3	10-15
Pump Replace, Khrs	n/a	0.5-1	2.5	>50

Source: IPG Photonics Corporation

Table 1. Comparison of laser characteristics for CO₂; lamp-pumped and diode-pumped Nd:YAG; and high power fiber lasers at 4 kW output power.

2.6 Experimental Approach Summary

The team, through many discussions, made a series of test goals and developed test designs to accomplish them. Laser parameters of peak energy, pulse width and repetition rate were used such that the onset of breaking and of melting would be determined as separate events. The secondary mechanisms affecting the results of the GRI study would be avoided to obtain the best estimate of the “absolute” specific energy possible for each lithology tested: sandstone, shale and limestone.

Even though the single most drilled lithology is shale, and anything we develop in this project will have to work as well on shale as on sandstone, the majority of the tests were performed on the Berea gray sandstone, because of the consistency of the rock parameters. Interestingly, as will be discussed in the Results section, the techniques work better on shale than on sandstone, by an order of magnitude.

The lasers used for most of this study were the CO₂ and Nd:YAG at Argonne National Laboratory. A small study was done using the Nuvonyx diode laser at Native American Technologies in Golden, Colorado.

3 Experimental Procedures and Results

3.1 Introduction

The research team all met three times during this phase of the study, in April, May and August. A first set of tests were designed to work with dry sandstone, shale and limestone samples, trying to get as close as possible to the “absolute” specific energy for each lithology. A second set was to extend this work and move on to testing sandstones saturated with water and sandstones submerged in water.

The lasers at the facility in Argonne National Lab were used for these tests. There was much preliminary work necessary to determine safety requirements while working with natural materials and to train the non-ANL members of the team to work safely during the tests.

3.2 Purge Optimization and Calculating Specific Energy

3.2.1 Purge Optimization

Two purging systems were evaluated: an air amplifier and gas nozzle. The principle of the air amplifier is to provide a flow of purge gas on the target, while directing the laser beam through the open center of the amplifier on to the target. (Fig. 1) The air amplifier can operate in both vacuum and purging mode, and each was evaluated to determine any difference on specific energy while lasing. Different gas purging nozzles were also evaluated based on size, shape, angle and purging pressure.

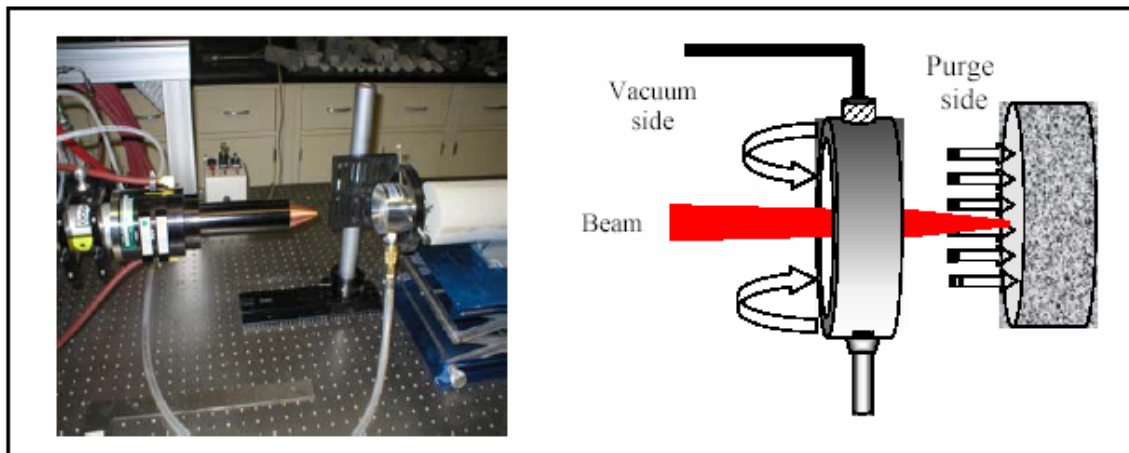


Figure 1. Schematic of purge system and experimental set up for purge optimization

An example of the purging calibration is presented in Figure 2. The calibration was done by adjusting the distance between the purging system and the target, as well as by adjusting the angle of the purging nozzles. The beam was exposed to the target for 4 seconds to get deepest penetration with minimal mineral melt.

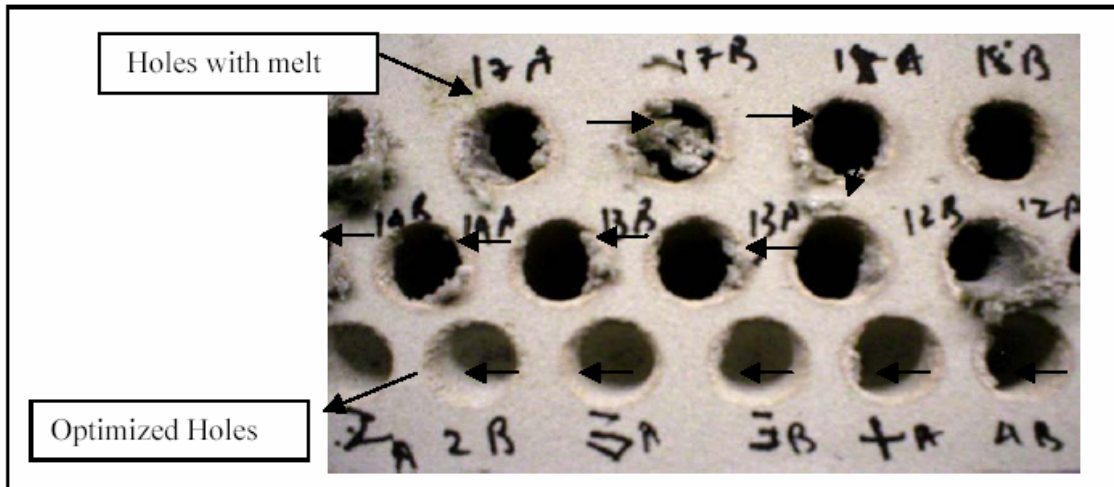


Figure 2. Figure showing holes created by changing purge type and parameters

The selection of the best gas nozzle was based on experimental observation and specific energy calculations. The selected gas nozzle was made from 6.35 mm stainless steel tubing with 519 Kilopascal line pressure (in-house air pressure) and co-axial purging.

It was observed that in the case of limestone, air amplifier and nozzles have the same effect on specific energy, however the nozzles provide for a better purging mechanism on sandstone. Sandstone consists of a high percentage of silica, which melts due to high heat exposure from laser beam and forms a ceramic-like sheath material. The co-axial high velocity-purging nozzle is better at removing this melt than the air amplifier.

3.2.2 Methods of Calculating Specific Energy

Specific energy is defined as amount of energy required to remove unit volume of material.

$$\begin{aligned} \text{Specific energy} &= (\text{energy Input})/(\text{volume removed}) \\ &= (\text{Laser power} * \text{Lasing time}) / (\text{volume removed}) \end{aligned}$$

Volume removed can be calculated by,

- 1) Weighing sample before and after lasing and multiplying weight removed with bulk density of sample

- 2) Measuring diameter and depth of penetration for created hole and applying correct equation for beam shape geometry (Cylindrical structure for collimated beam and conical structure for focused beam)

As mentioned above, creating deep hole in sandstone is more vulnerable to good purge than limestone. Hence, sandstone was used to observe the discrepancy in values of specific energy using above stated methods to calculate volume removed.

Ten core samples of sandstone (2" diameter x 2" depth) were weighed before lasing. Each sample was lased for 8 seconds at 5.34 kW power (CW beam) in presence of optimized purge system (gas nozzle). The spot size was fixed at 8.9 cm (0.35").

Samples were then weighed after lasing. Bulk density of each sample was calculated by measuring their dimensions and weight. Volume removed was then estimated by multiplying bulk density and weight removed by lasing. We called it specific energy based on weight measurement.

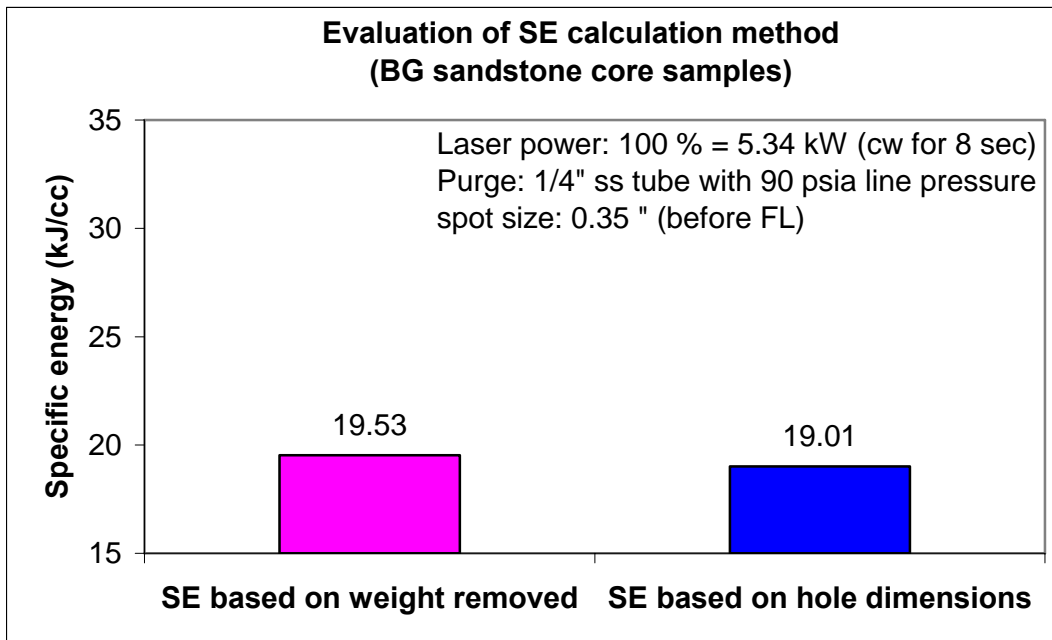


Figure 3. Comparison of specific energy calculated by weight removal and hole dimension

Hole created in each sample was then measured for hole diameter and depth to calculate volume removed. Average results obtained from both methods are show in figure 3. Co-centric purge system with enough airflow and careful

measurement of hole geometry can generate results with same accuracy as weight based calculation method.

3.2.3 Result and Analysis:

The purging is important for cuttings removals and clear the path for the beam to deliver to the rock. Dust, debris and cuttings will absorb the beam and therefore, less energy will be delivered to the rock sample. The dust, debris and cuttings present loss of energy in terms of specific energy (figure 4)

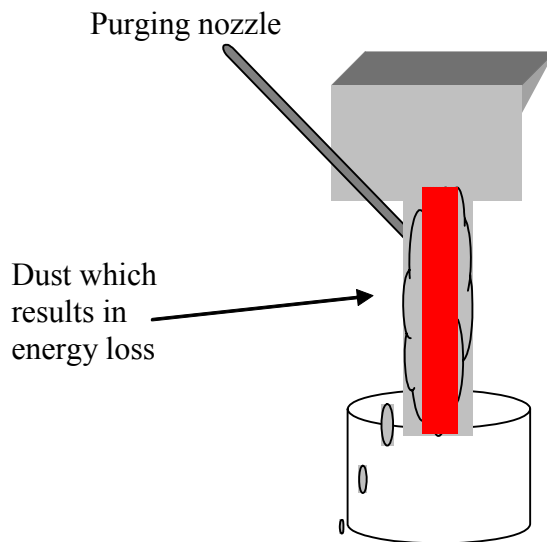


Figure 4. Schematic of purging mechanism

The purging methods was improved by adjusting the distance between the purging nozzle to the surface of the rock sample, the angle of the purge and the flow pressure (figure 5).

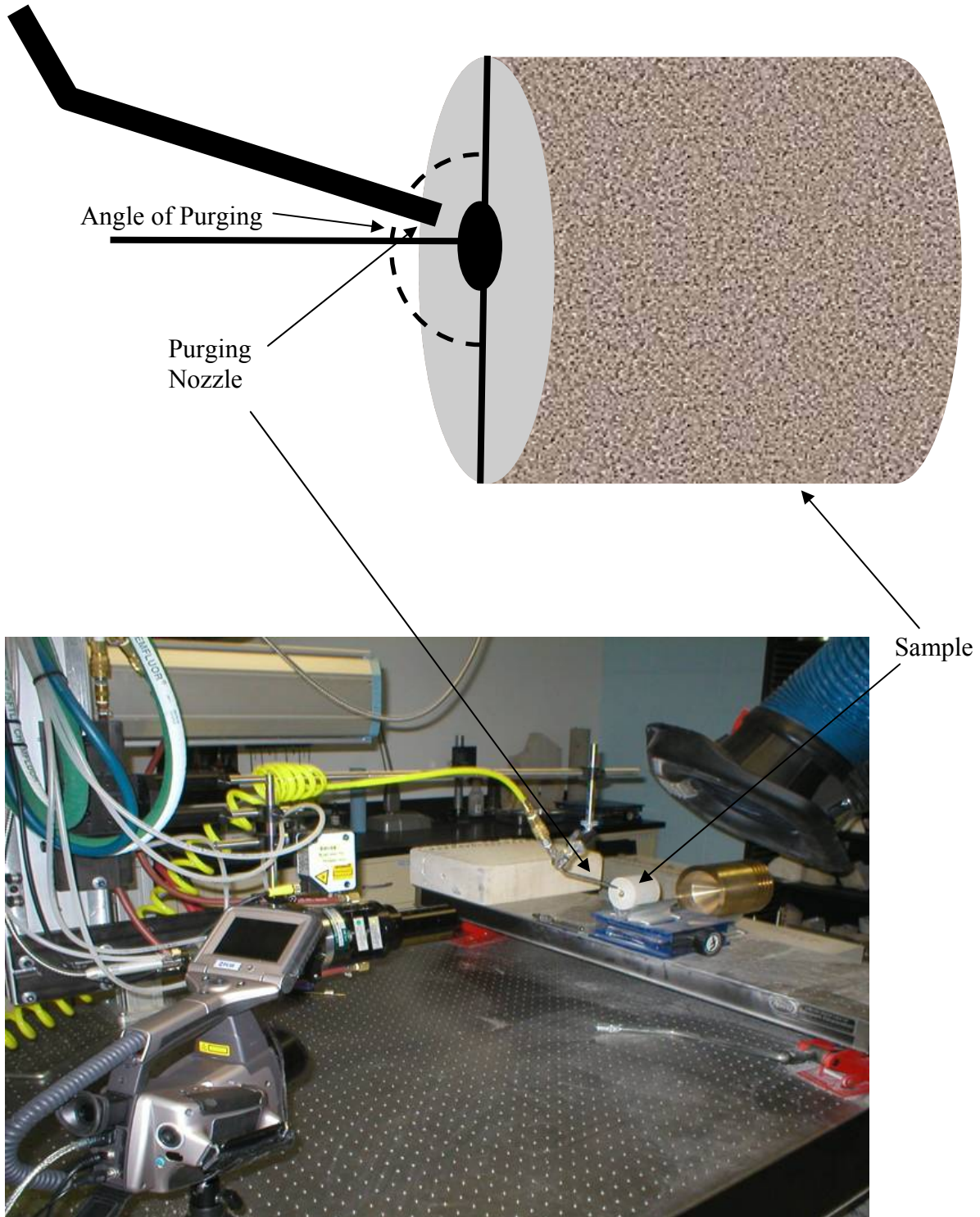


Figure 5. Experimental set up showing purge gas delivery system

The optimized angle was found to be 35° and the optimized distance from the target was one inch also the flow pressure was 75-100 PSI. The angle and the distance were the most efficient in removing the dust and debris which allow the energy to be delivered to the sample. Figure 6 (actual experiment) shows the purging set up while lasing.



Figure 6. Purging mechanism (while lasing)

Once the purging methods were optimized, two methods were used to calculate the specific energy, these are weight removed and geometry (dimensions). Weights removed is based on the weigh measured before lasing and after, while the geometry method is based on assuming that the hole created by the beam is a typical geometry of conical or cylindrical shape based on the shape of the beam. There was difference when between the two methods when the experiments were carried out as seen in figure 7 and figure 8.

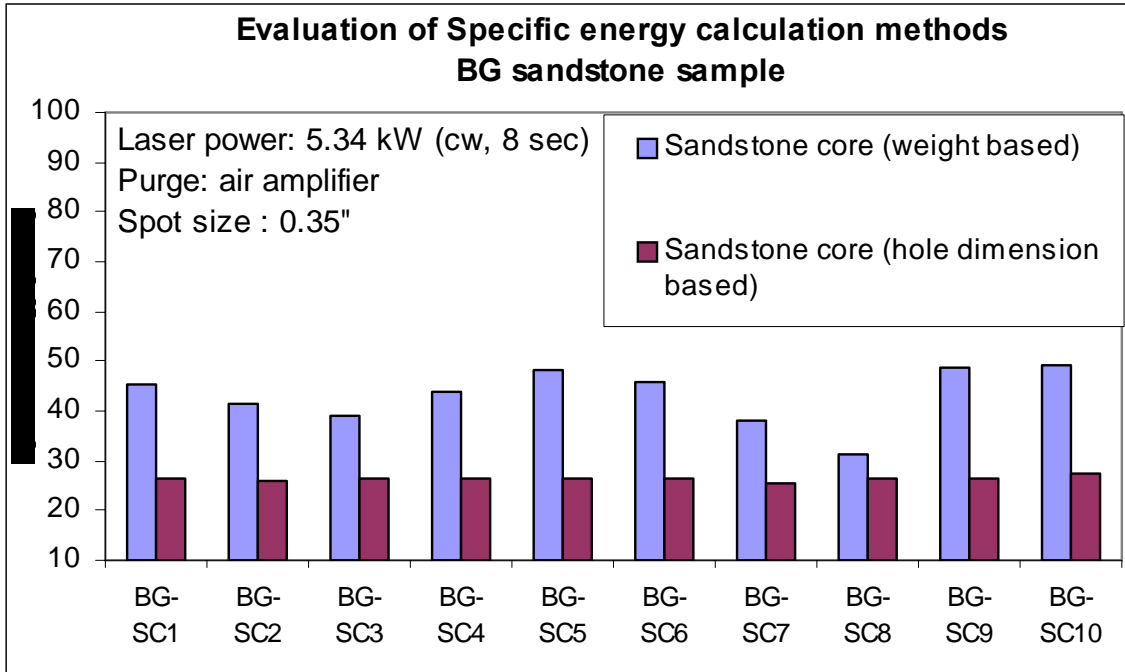


Figure 7. Comparison of specific energy calculation methods for sandstone sample

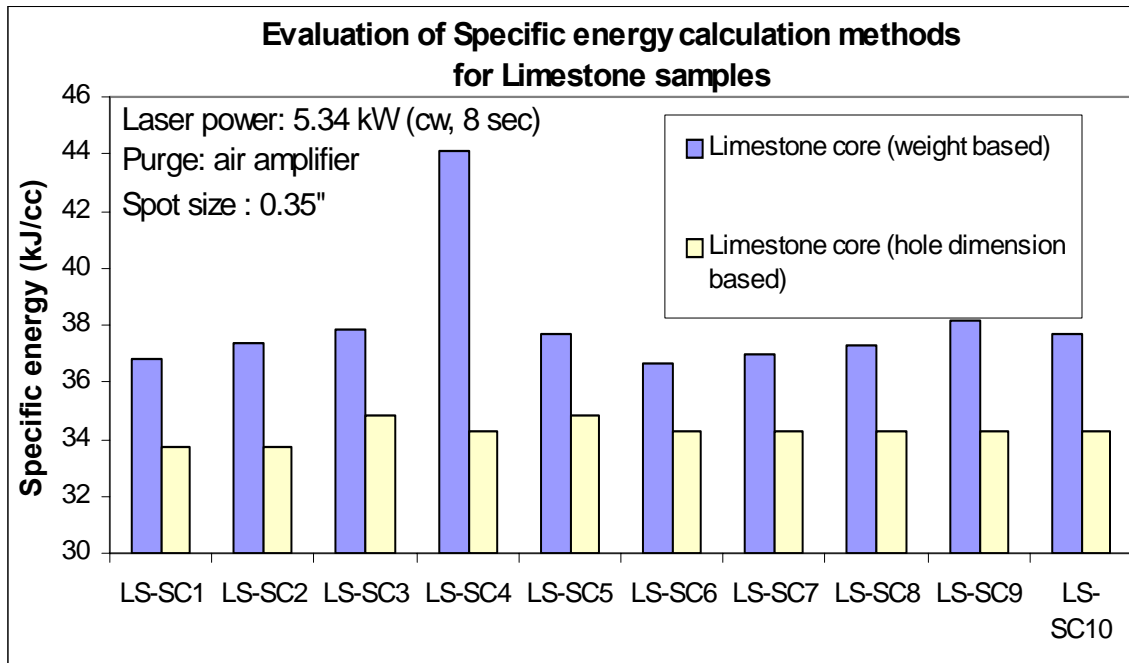


Figure 8. Comparison of specific energy calculation methods for sandstone sample

In ideal condition, if the purging is efficient, then the laser should create a typical hole identical to the shape of the beam, the hole created in the sample should match the shape of the beam, and from the mass removed the volume can be calculated as in equation (1)

$$SE = \frac{\text{Energy input}}{\text{Volume removed}} = \frac{P}{dV / dt}$$

$$= \frac{\left[\frac{kW}{cm^2} \right] \cdot \text{Time}}{cm} = \frac{kW}{cm^3 / sec} = \frac{kJ}{cm^3} + C \dots \dots \dots (1)$$

$$\rho = \frac{m}{v} \text{ g / cc}$$

By optimizing the purging, the SE values for both weight and geometry were very similar. This indicates that the purging was efficient and a clean hole was created with no melt (figure 9).

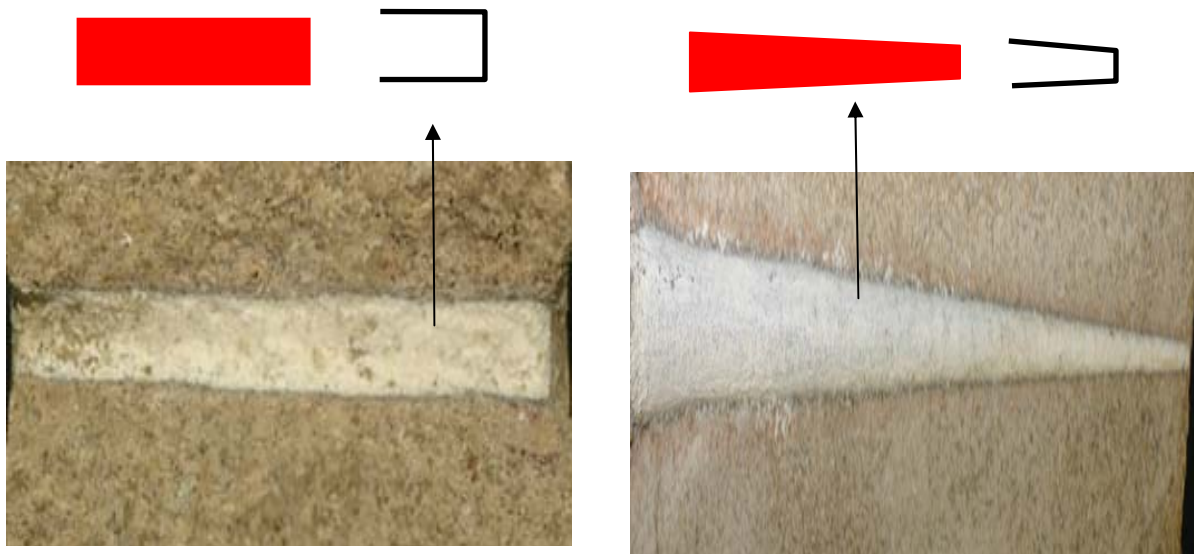


Figure 9. Effect of shape of the beam on resulting hole with various purge mechanism

Comparing the air amplifier methods with the nozzles is presented in figure 10. (Amplifier vs nozzles). The result shows that nozzles are more efficient than the amplifier, the nozzles for the gas to flows in narrower path and the debris and the dust to escape from sides of the hole.

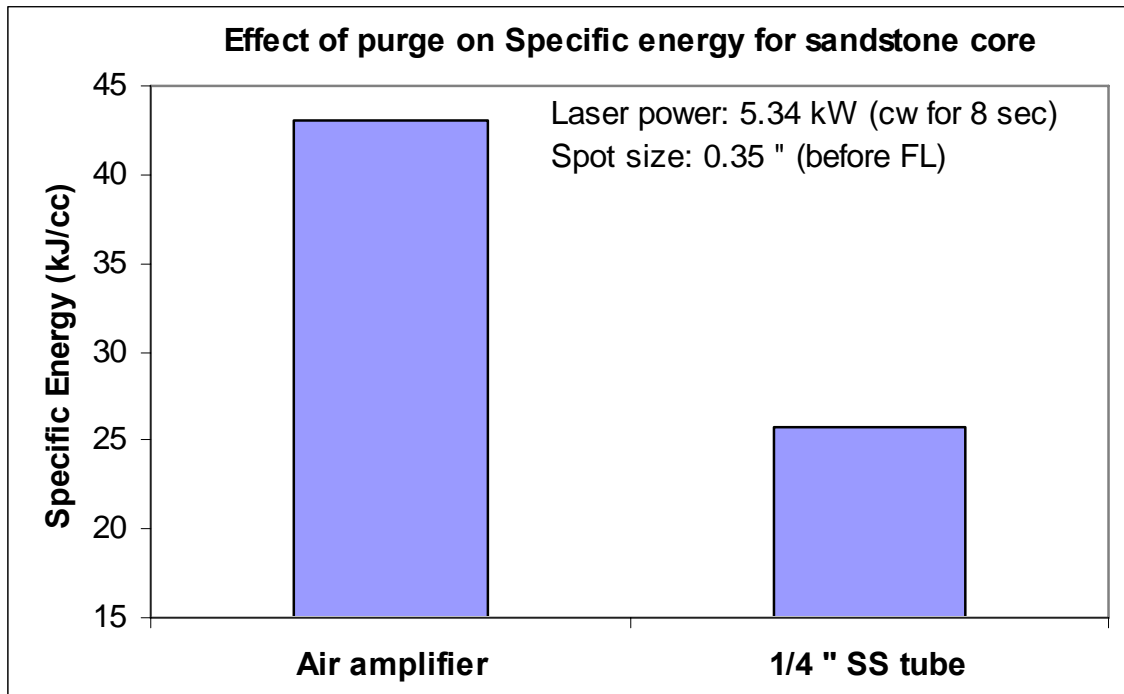


Figure 10. Effect of purge mechanism on specific energy for sandstone

Based on this result, blocks were used instead of core. The advantage of using block is that the boundary effect is reduced and coring is time consuming operation. Also more holes can be made using blocks that cores.

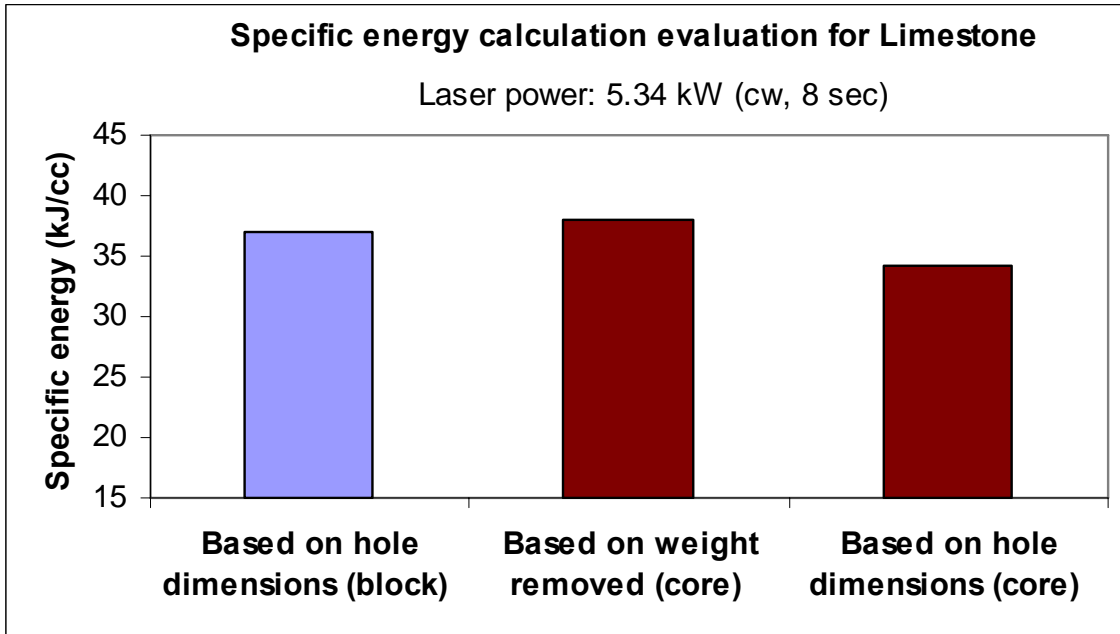


Figure 11. Comparison of specific energy calculation methods

3.3 Orientation Effect Test:

Objective:

To find the effect of deposition orientation (face and side) on limestone and sandstone material

Procedure:

A test was conducted to determine if a change in depositional orientation (face and side) of the rock would affect the specific energy when exposed to the beam. An identical exposure was targeted on all faces of 10x10x10 cm sandstone block and 5 x 5 x 5 cm limestone block with 5.34 kW continuous wave (CW) beam for 8 seconds. Gas nozzle in concentric position was used as purge system. Air was used as purge gas with 90 psia line pressure. Distance between purge and sample was about 1". Lens with 1000 mm focal length was used to focus 1" collimated beam. Spot size (penetrating laser beam diameter) was kept 0.35". Figure 12 shows the holes created on different faces and figure 13 and 14 graphs the specific energy for each face of sandstone and limestone sample respectively.

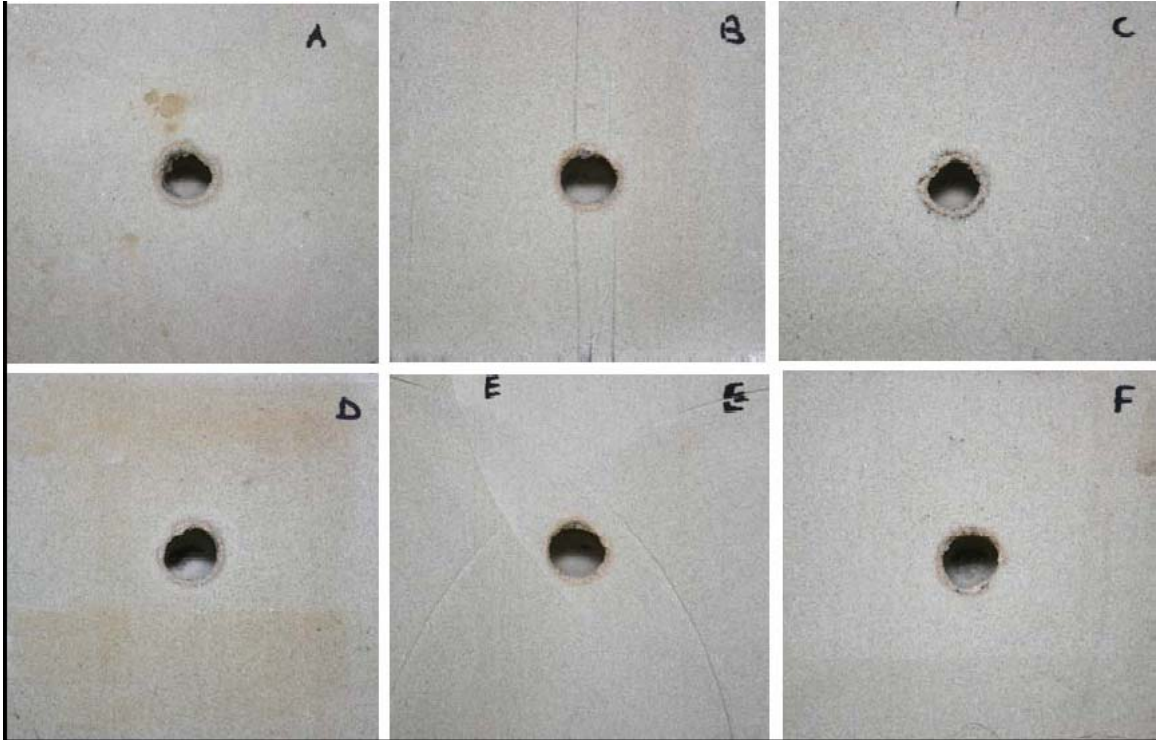


Figure 12. Six faces of sandstone block; lased at same power level and lasing time

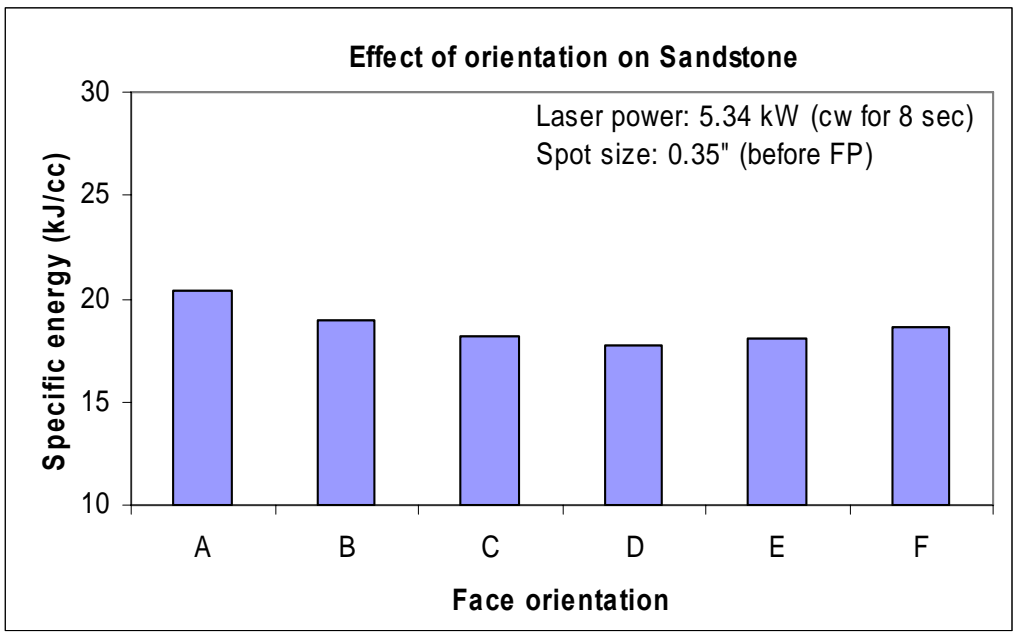


Figure 13. Effect of orientation on specific energy for sandstone

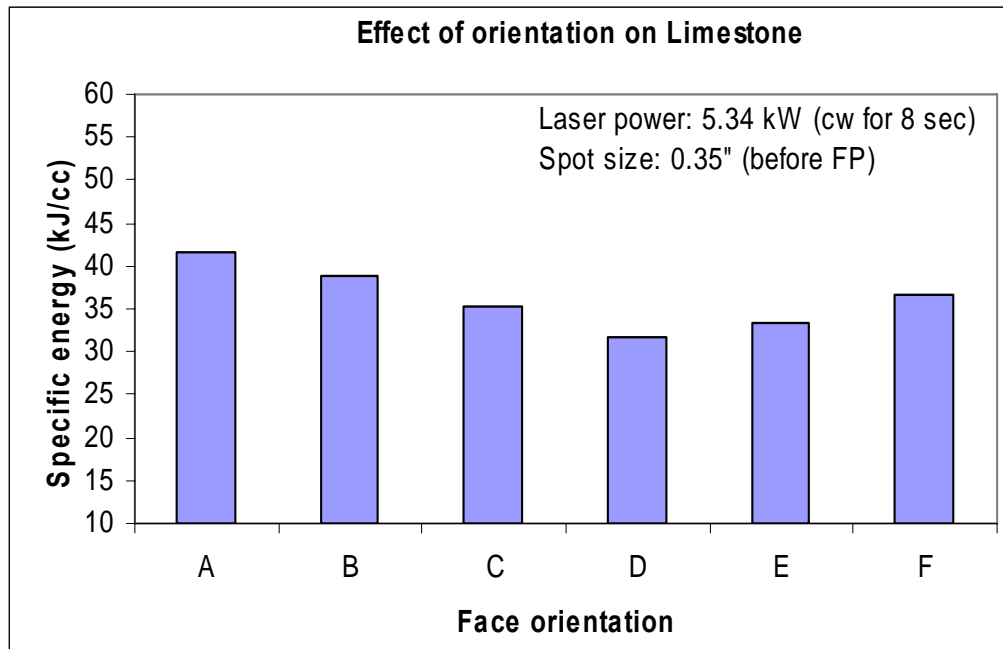


Figure 14. Effect of orientation on specific energy for limestone

As shown in the graph, deposition orientation is not an issue for lasing limestone and sandstone material used for this study. Specific energy required to create the hole in all faces of the block was almost the same.

3.4 Determination of Boundary Effect

Objective:

To determine the effect of sample size on specific energy.

Procedure:

A set of experiment was conducted to determine the effect of sample size on specific energy.

Sandstone/Limestone cores of diameter 0.75", 1", 2", 2.75", 3", 4" and 2" length were used for this experiment. Each experiment was repeated 3 times to check repeatability. Each core was lased for 4 second with a 5.34 kW focused laser beam. Gas nozzle in concentric position was used as purge system. Air was used as purge gas with 90 psia line pressure. Distance between purge and sample was about 1". Lens with 1000 mm focal length was used to focus 1" collimated beam. Spot size (penetrating laser beam diameter) was kept 0.35". Weight based method (explained in methods of calculating SE) was used to calculate specific energy.

Graph 15 and 16 show values of specific energy for sandstone and limestone samples as a function of core diameter. 4" core diameter shows no boundary effect as shown in graph.

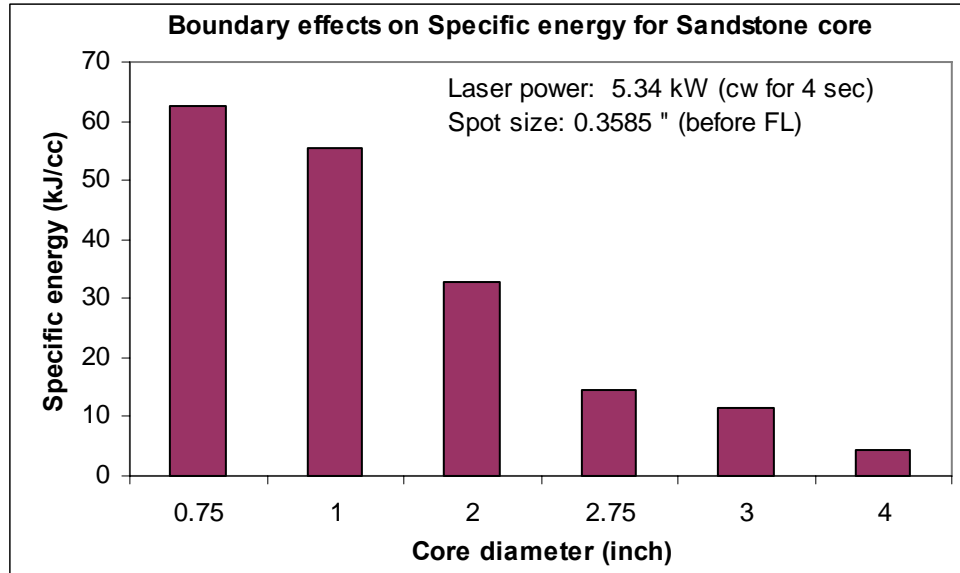


Figure 15. Effect of size of sample on specific energy for burea sandstone

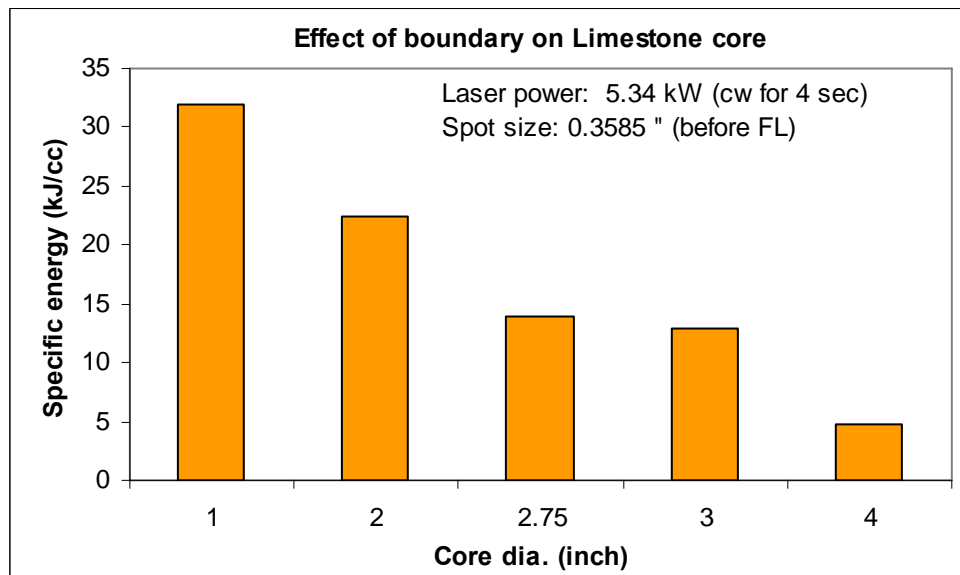


Figure 16. Effect of size of sample on specific energy for limestone

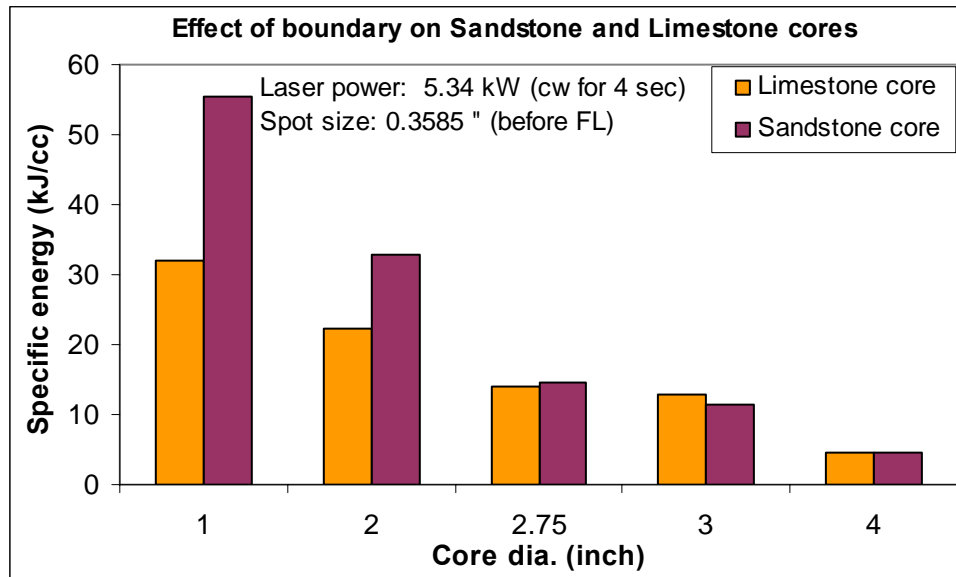


Figure 17. SE Comparison for sandstone and limestone for various sample sizes

Result and Analysis:

This test was designed basically for the high pressure perforation cell to know the size of the cell and how much the pressure core holder that without any boundary effect or secondary effect. The spot size was optimized in other test, and it was found to be 0.35 inches. The result shows that 4 inches diameter was the optimized diameter for 0.35 inches spot size. There was no test to confirm this relationship that shows relate the spot size and core size. It has been observed that at 4 inches diameter there was no fractures or cracks developed in the rock sample with minimum specific energy.

3.5 Effect of Beam Density on Specific Energy

Objective:

To determine the effect of beam intensity by lasing the sample with focused and diverged beam of same spot size

Procedure:

The shape of the laser beam and hence the lased hole in rock can be changed by using different types of lenses. A conical shape was obtained when samples were placed before the focal point while using a convex lens. Changing the distance

between the target sample and lens or using lenses with a different focal length can change the dimensions of this cone. Cylindrical hole was obtained by using a collimated beam. Controlling the shapes of the hole is significant in terms of fluid flow from the reservoir to the well. Figure 18 illustrates the resulting change to hole geometry by shaping the beam with different lenses.



Figure 18. Different hole geometry produced by shaping laser beam with different lenses

The same spot size can be achieved for both converging and diverging beams equidistant on either side of the focal point. To study the difference between energy required to remove same material for both cases, sandstone block (12" x 6" x 6") was lased at 5.34 kW (CW) power for 4 seconds with focused beam of 0.35" spot size.

The block was lased again with same parameter except with the diverging beam of 0.35" spot size. Gas nozzle with 90 psi line pressure was used as purge. Distance between sample and purge was fixed at about 1". Each experiment was repeated 5 times.

Specific energy achieved with sample placed before and after focal point was calculated for each case. Average values are presented in graph shown on Fig. 19. Less specific energy was required to create the same size hole on converging side of focal point as the intensity of the beam continues to increase and less material is removed per unit length as it nears the focal point.

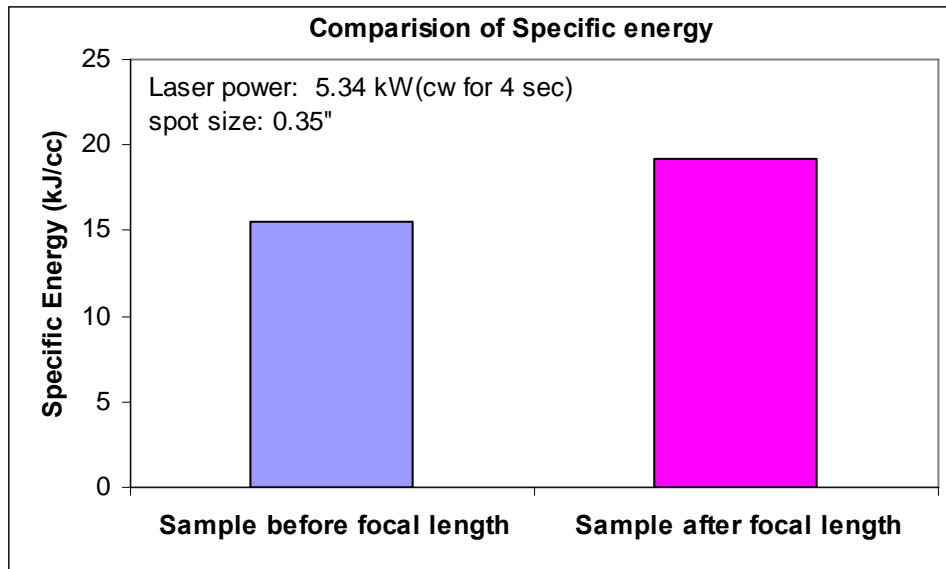


Figure 19. Comparison of SE at different beam density for sandstone

Result and Analysis:

Previous tests have been conducted using different high power lasers, including MIRAC, COIL, Nd:YAG, CO, Diodes laser and CO₂, using focused lenses. The samples were placed before the focal point and sometimes after the focal point (figure 20). For consistency and accuracy, this test was conducted to learn more about the difference between before and after the focal point.

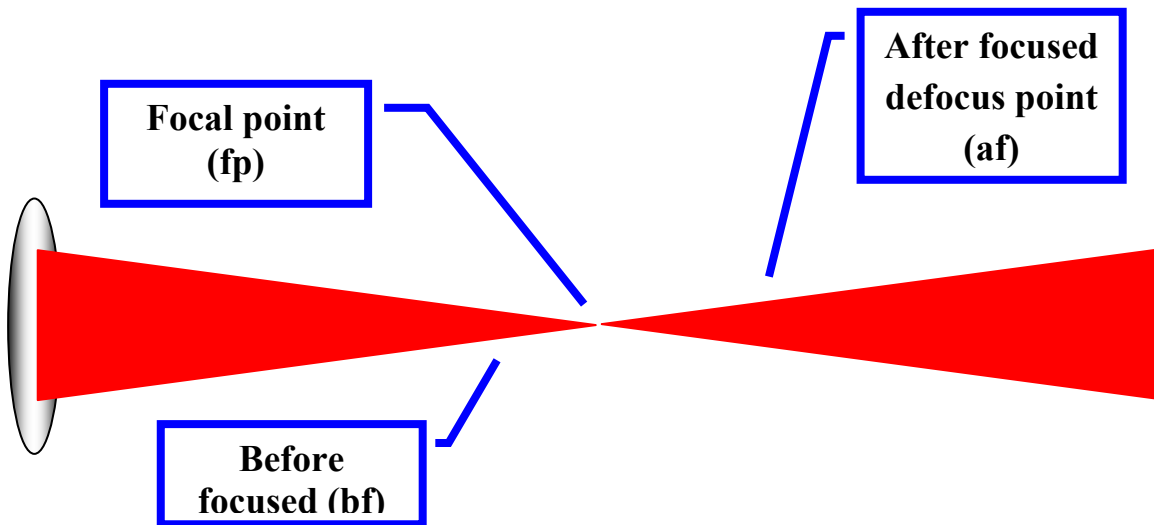


Figure 20. Schematic of laser beam producing same spot size before and after focal point of lens used

The difference between placing the sample before or after the focal point is the power intensity. The intensity is defined as the power applied over the area, equation 2

$$Intensity = \frac{Power}{Area} \dots\dots\dots(2)$$

If the samples placed before the focal point, and as the beam is on, keeping the power constant, the area will decrease according to the beam shape, therefore, the intensity will increase, and if the sample placed after the focal, then the area will decrease resulting in an increase in the intensity.

It should be taken into consideration when comparing SE values using different types of laser the position of the samples, whether it is placed before the focal point as in the case of using Nd:YAG (figure 21) or after the focal point as in the case of COIL (figure 22).

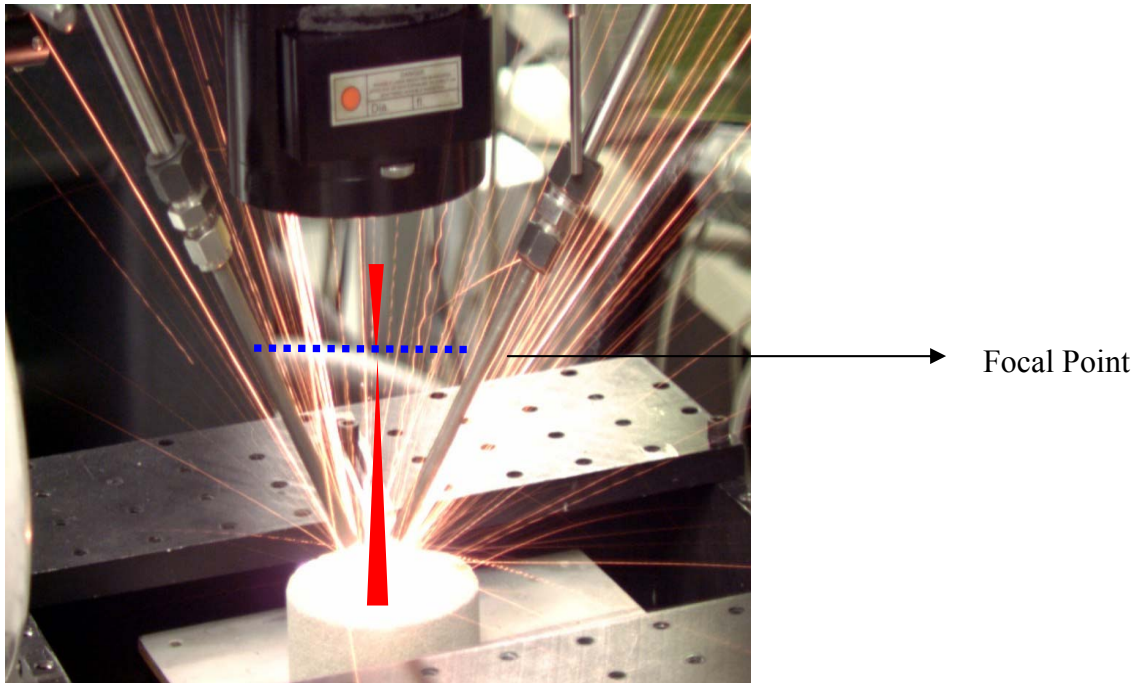


Figure 22. Sample placed after focal point

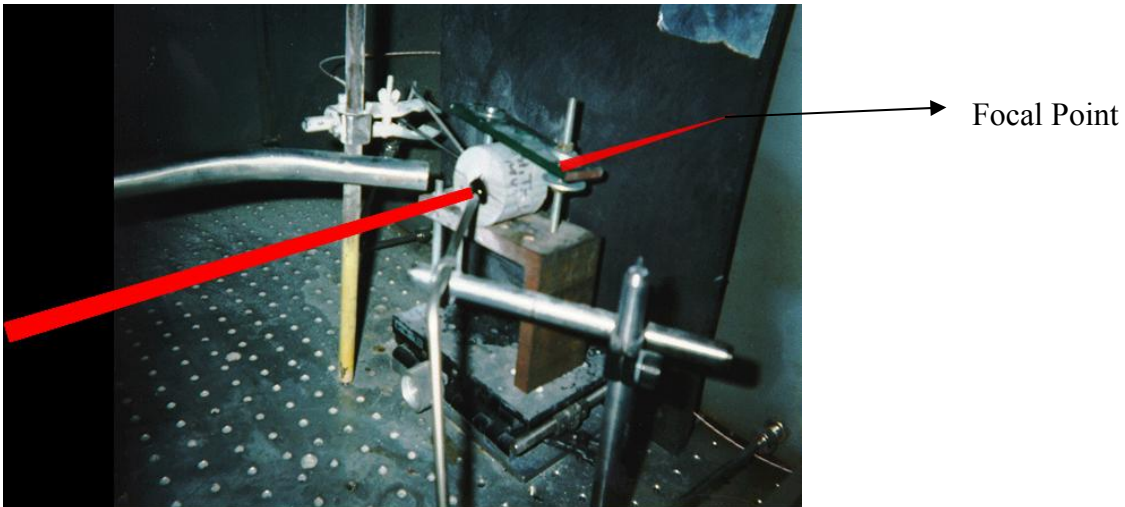


Figure 23. Sample placed before focal length

To understand how effective fiber lasers are in drilling and cutting rock, comparisons were made to results obtained from other lasers used in laser/rock interaction experiments. Figure 24 presents minimum SE values for Berea sandstone and limestone (a carbonate with little silica content), obtained using the fiber laser, as compared to those recorded using other high power lasers.

The experimental conditions for these reported SE values were not identical, and the methods employed were not consistent. However, each value represents a best attempt at determining optimal conditions of rock removal, thus providing a minimal SE value for the laser/rock combination presented.

To date, the SE values obtained for both sandstone and limestone with the fiber laser were the lowest achieved from reported laser/rock interaction data. Also, there was little difference in the best fiber laser SE values between sandstone and limestone; however there were distinctly higher SE values for limestone as compared to sandstone with the other laser types. Another comparison of SE values was made for each of the same lasers and is presented in Figure 25. In this case, comparisons were made between the average observed SE values obtained using the fiber laser with average SE values recorded using the COIL, CO₂, and Nd:YAG lasers.

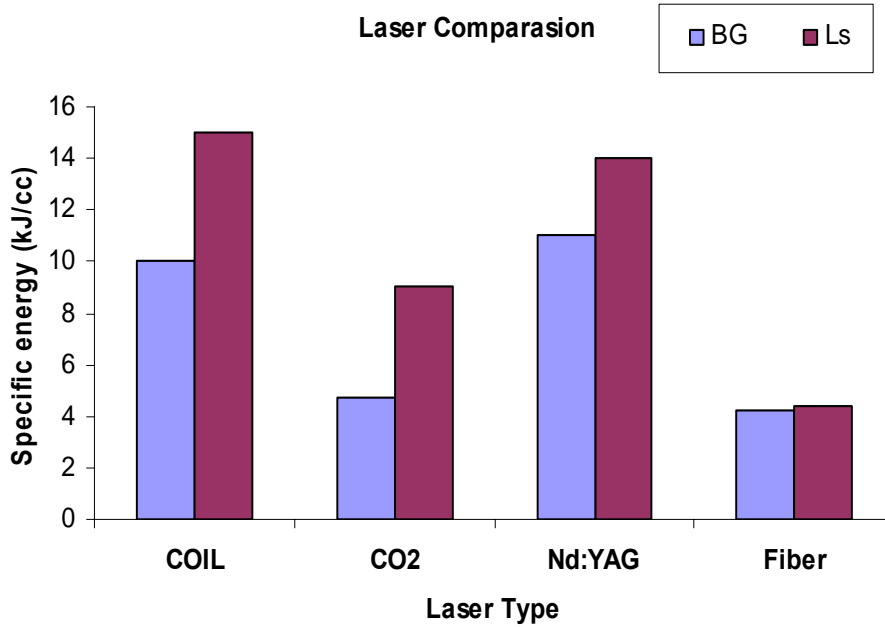


Figure 24. Lowest SE values obtained from laser/rock interaction experiments using COIL, CO₂, Nd:YAG and ytterbium fiber lasers on Berea sandstone (BG) and limestone (Ls) at lowest SE conditions.

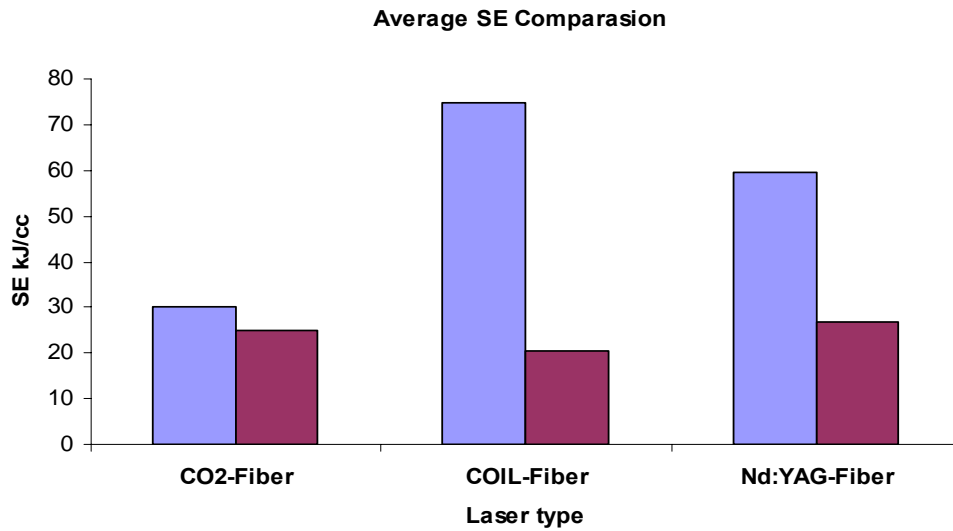


Figure 25. Average specific energy obtained from laser/rock interaction experiments using COIL, CO₂, Nd:YAG and ytterbium fiber lasers on Berea sandstone at identical conditions.

The fiber laser data was collected by repeating the experiments previously performed on Berea sandstone with other laser types under the same conditions (Table 2). The average SE values for all laser types were

Test Parameters	COIL	CO ₂	Nd:YAG
Average Power, kW	1.40 - 5.34	3.5 - 5.0	0.77 - 1.20
Rep Rate, pulse/sec	CW	CW	100 - 400
Beam Diameter, cm	1.61	0.71	0.15
Exposure Time, sec	8.0	3.0 - 6.9	0.5 - 1.5
Core Diameter, cm	5.08	5.08	2.54
Core Length, cm	5.0 - 10.6	5.00	2.54

Table 2. Test parameters per laser type used to experimentally determine comparative fiber laser data and average SE values for Berea sandstone samples.

much higher than the best values observed in Figure 24, since SE values at non-optimal conditions were included in the average, and hole diameters were the same as their respective beam diameters. Given these conditions, the fiber laser

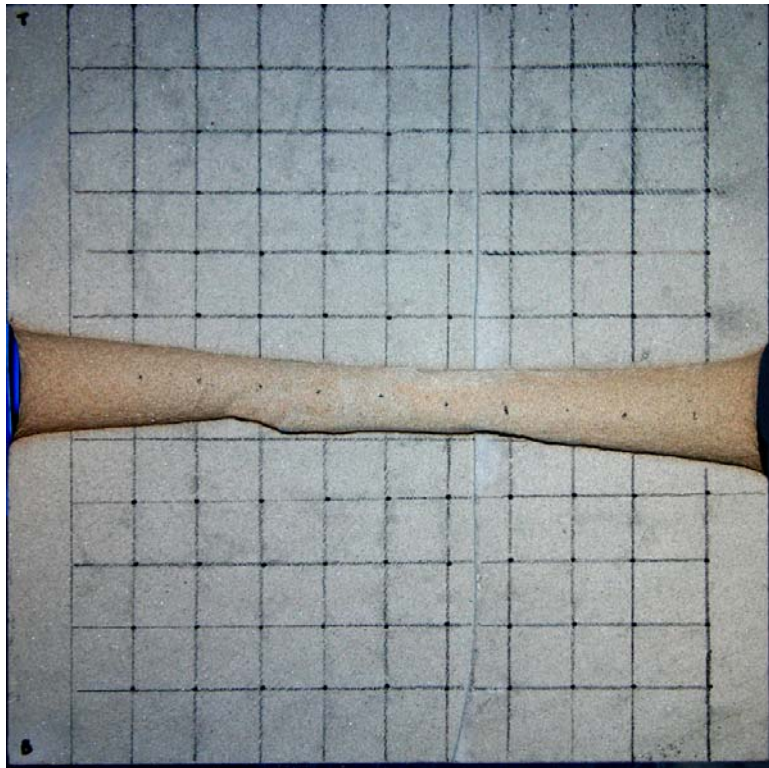


Figure 26. Post-laser cross-section through a cube of Berea sandstone (30.48 cm per side) formed by spallation with 3.2 kW fiber laser beam for 6 minutes. Tunnel diameter ranges between 2.8 and 5.1 cm.

performed slightly better than the CO₂ laser, and significantly better than the COIL and Nd:YAG lasers. Recently, a perforation-like tunnel was created under lab conditions in a cubic block of Berea sandstone measuring 30.48 cm (1 foot) per side using GTI's 5 kW ytterbium fiber laser (Figure 26). A borehole fully penetrated the block at an average diameter of 3 cm. A power level of 3.2 kW was applied to the block for a total of 6 minutes, and an SE was calculated at 5.5 kJ/cc [8]. This is the deepest and most energy efficient high power laser application in Berea sandstone reported to date.

3.6 Effect of laser power on Specific Energy (focused beam)

Objective: To determine the effect of laser power on limestone and sandstone material for optimized beam condition (0.35")

Procedure:

The purpose of this test is to study the effect of laser power by varying the laser power from 0.5 to 5 kW on limestone and sandstone samples and keeping the time constant (4 sec and 8 sec). Limestone and sandstone blocks of size 20 x 5 x 5 inch were used in this study. One of the 20 x 5 inch surfaces was divided into 1 x 1 inch grids as shown in the figure 27. Each grid was lased at different power level from

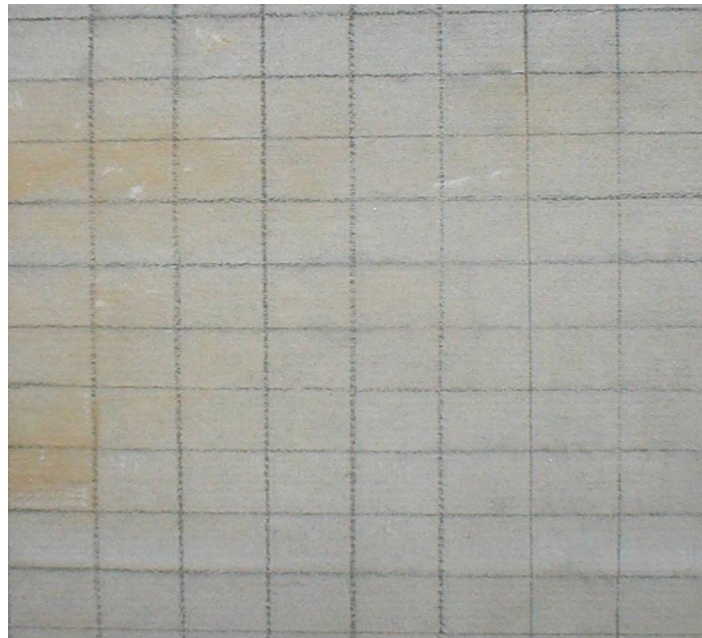


Figure 27. Test block showing grids

0.5 to 5 kW in 0.5 kW increment. The lasing time of each hole was kept constant at 4 seconds and 8 seconds for two sets of experiment. The beam was CW with

0.35” spot size. Gas nozzle in concentric position was used as purge system. Air was used as purge gas with 90 psia line pressure. Distance between purge and sample was about 1”. Lens with 1000 mm focal length was used to focus 1” collimated beam.

Result and Analysis:

When a high power laser beam strikes the surface of a rock, energy will be reflected, scattered and absorbed. The absorbed energy is that which is transferred to the sample, and is responsible for breaking and cutting rock. Depending on the sample composition and properties, absorbed energy will be consumed by various mechanisms, including dehydration, vaporization, grain expansion, melting, pore expansion, decomposition, and other factors (Equation 3). Each mechanism occurs within a specific temperature range.

$$E_{\text{Absorb}} = E_{\text{Dehy}} + E_{\text{Vap}} + E_{\text{GrainExp}} + E_{\text{Melt}} + E_{\text{PoreExp}} + E_{\text{Decomp}} + E_{\text{Other}} \quad (3)$$

Given this, there are energy absorption/thermal accumulation issues that may affect the laser’s cutting efficiency. For example, as high power lasers transfer energy to silica-based rocks, quartz mineral grains begin melting at 1900 °C. This phase change in the mineral results in a reduction in rock cutting capability as the melted material absorbs and reflects beam energy.

The power optimization test was conducted by calculating the SE and by visual observation of the hole, for perforation purposes and sand production issue, the hole is preferred to be clean without melt, debris or sand particles. The selection of the optimized SE was based on low SE value as well less melt and damage.

An example of visual observation is presented in figure 28, showing the results of lasing Sandstone sample at an increment of 10%. At the first lasing the power was only 10% which did not make any significant change in the rock as seen on the upper left frame of Fig. 28.

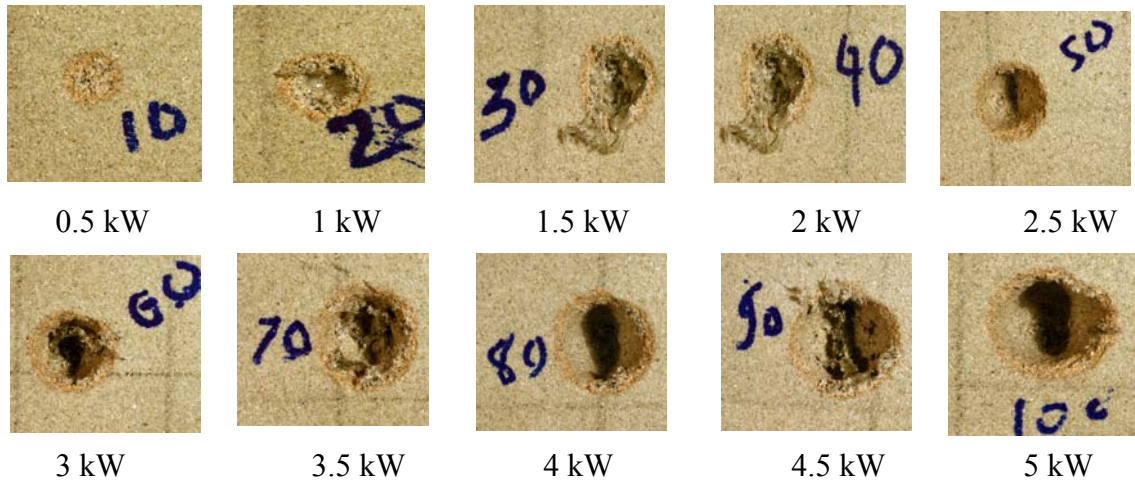


Figure 28. Sandstone sample lased by HPFL at different power level, the top left shows lowest power percentage

Berea sandstone was used as the primary rock type due to its relative homogeneous physical characteristics including higher silica content, common use in laboratory studies of rock, and extensive body of experimental data and literature. Berea sandstone is a sedimentary rock composed predominately of quartz grains (SiO_2) cemented together by material consisting of one or a combination of silica, iron, calcium carbonate or other materials. The first was test was conducted on the Berea sandstone for 8 second, at 0.35 inches beam spot size, the result is presented in figure 29.

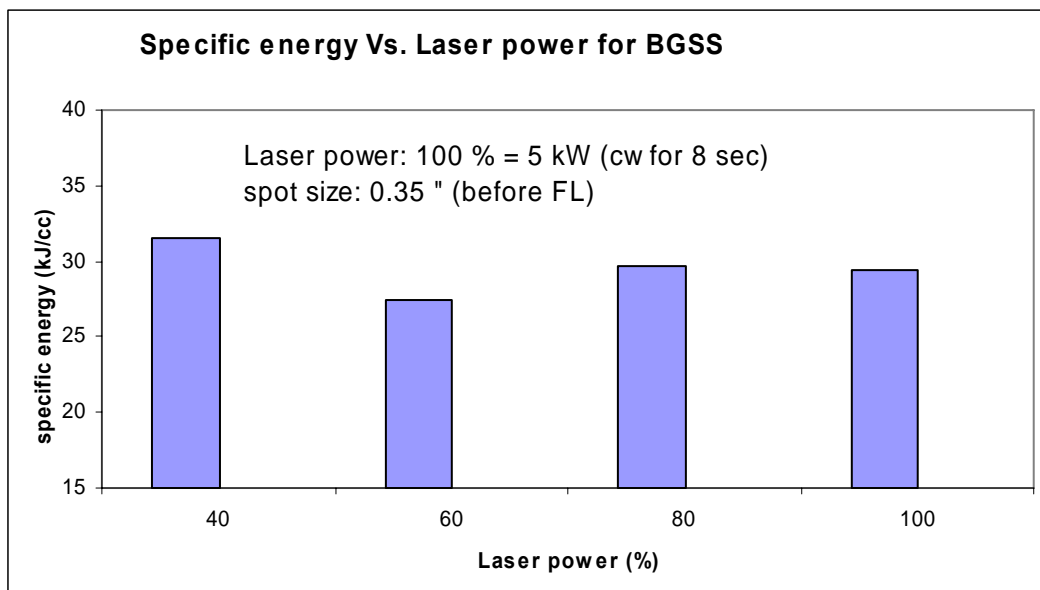


Figure 29. Laser optimization test showing SE value as the power increases of 20%, using HPFL for 8 seconds on Sandstone, Spot size was 0.35 inches.

These observations show that 60% power for 8 seconds was the optimized power for sandstone; the result was based on SE value as well as physical samples analysis.

It was observed that at this power (60%), spallation took place, where the grains spall from the matrix and broke free. In order to analyze this result and learn more about spallation mechanism, a test was designed to investigate more about spallation and the sample went through a series of analysis that include mineralogy, Infrared and thermal analysis.

3.6.1 Spallation Test:

The mineral composition of Berea sandstone was analyzed by thin section analysis under a high magnification optical microscope, Figure 30.

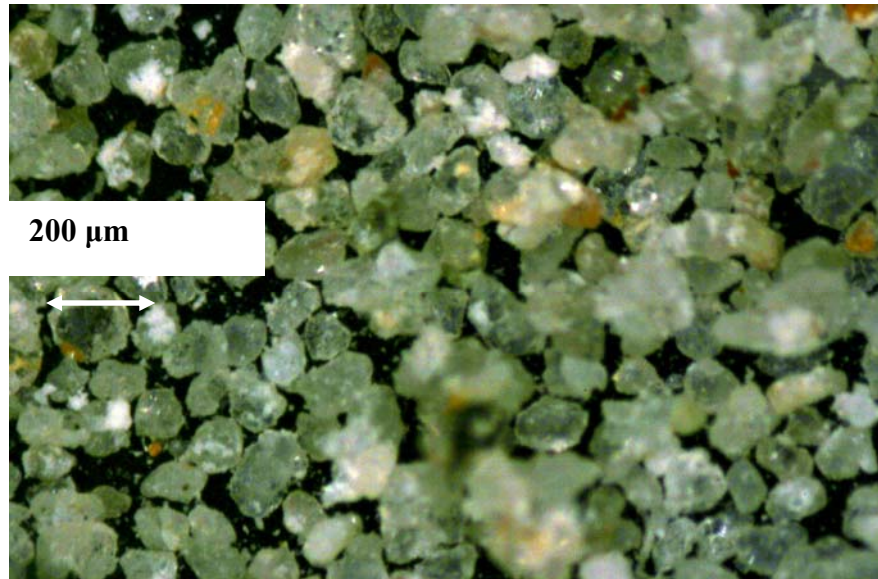


Figure 30. Thin section of sandstone sample showing mineralogy, cementation and grains.

The thermal behavior of the sample was obtained by using *thermogravimetric analysis* (TGA), measuring a change in mass as a function of temperature.

An infrared camera with a temperature detection range of minus 40°C to 2200°C was used to measure the temperature profile of the lased material.

An initial test firing of the laser system was made by exposing a Berea sample to a 2.54 cm diameter beam at 3 kW for 62 seconds. A hole with dimensions of 7.62 cm deep and 2.54 cm diameter at opening was created through spallation of the grains with no evidence of grain melt (Figure 31).

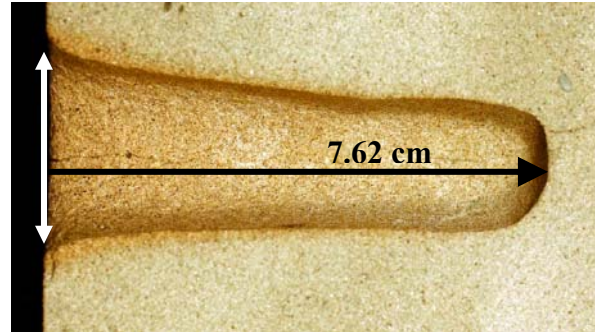


Figure 31. Post-laser cross-section of a hole in Berea sandstone formed by spallation with 3 kW for 62 seconds. Dimensions are 7.62 cm deep and 2.54 cm diameter at opening.

To investigate the conditions by which the Berea sandstone quartz grains begin to melt with the fiber laser, and thus the limit for efficient spallation conditions, a block of Berea sandstone was exposed to several beams where the laser power was increased from 1 kW to 5 kW at 0.5 kW increments. This was accomplished while holding all other variables constant, including beam duration and spot size at 4 seconds and 8.9 mm, respectively. As a result, beam intensity on the target ranged from 1607 to 8037 kW/sq. cm.

A single hole was created in the block for each exposure, and the results are presented in Figure 32. Given the conditions of the tests, a power level of about 3 kW provided a clean hole (no melted quartz grains) at a minimum SE value of 25 KJ/cc. Exposures at power levels less than 3 kW produced less rock at power

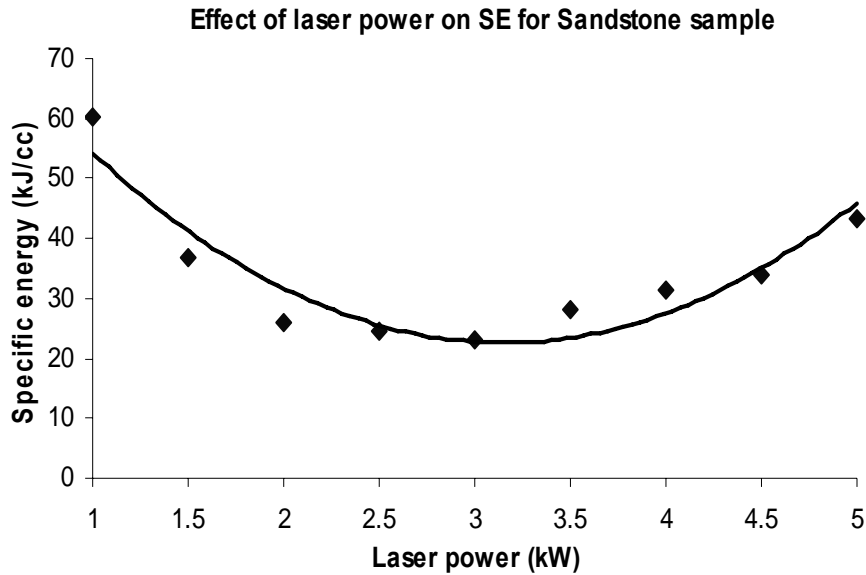


Figure 32. Laser power vs. specific energy for fiber laser exposed to Berea sandstone at constant beam duration and spot size.

levels at power levels less than 3 kW produced less rock volume removed and no evidence of mineral melt. However, exposures at power levels greater than 3 kW produced holes greater than 5 cm deep with accompanying mineral melt.

3.6.2 Thermal Effects on Berea Sample

Thin section, thermographic and thermogravimetric methods were used to evaluate and analyze the resulting data.

Thin Section Analysis: This analysis provides the physical properties and composition of the Berea sandstone sample. Mineral composition consists mainly of quartz (95%) with other constituents, including feldspars (5%) and traces of black organic material and fragments. The type of cementation that binds the grains together is silica (SiO₂).

Thermographical Analysis: Figure 50 illustrates the thermal behavior of rock when exposed to the beam as a function of time. The average temperature of the rock during lasing was about 1200 °C.

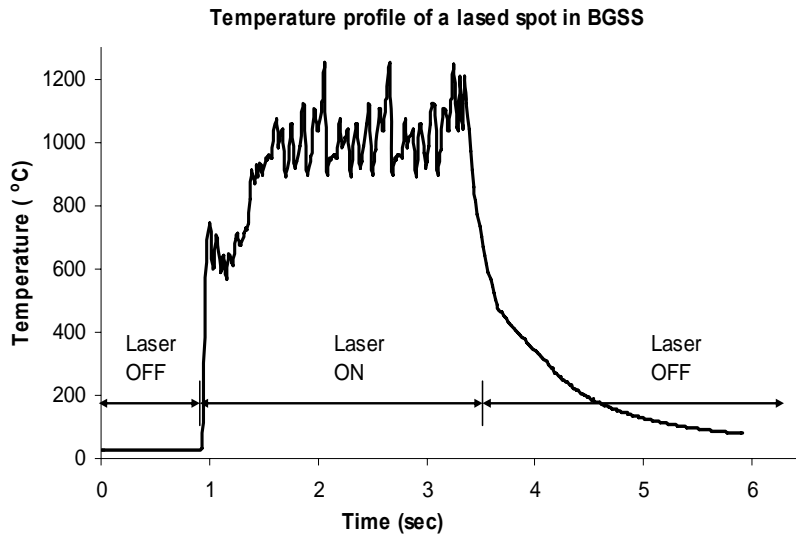


Figure 33. Temperature profile of fiber laser beam on Berea sandstone over time using 3 kW power beam and 8.9 mm beam diameter.

As seen from the Figure 33, there is a sharp rise in the temperature of the rock as the rate of absorbed energy from the beam greatly exceeds the rocks ability to dissipate heat away from the exposed area. The temperature range of the rock induced by a 3 kW beam with 8.9 mm diameter was sufficient to break the cementation material and cause dehydration, decomposition, vaporization and grain expansion that resulted in the spallation of the rock grains. With the help of assisted gas, spalled grains were quickly removed out of the hole and away from the beam.

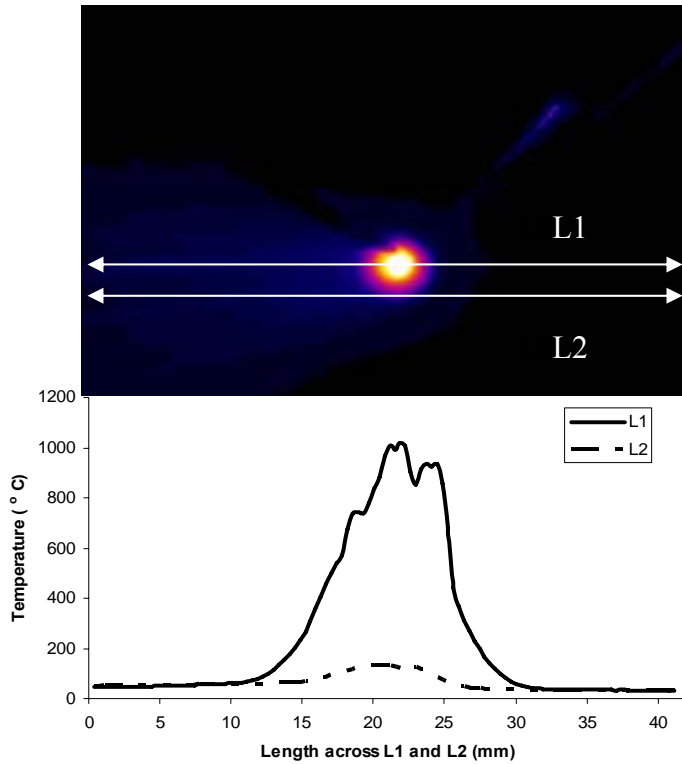


Figure 34. Infrared video capture during laser exposure on Berea sandstone with temperature profile across the laser contact point (line L1) and immediately below the laser contact point (line L2).

Figure 34 shows an image of the Berea sandstone block captured with an infrared camera while exposed to a 3 kW beam. Temperature profiles across lines L1 and L2 are presented below the image. Thermal stress produced by high temperature gradient and differential thermal expansion of minerals breaks the bonds between the grains without a thermal accumulation reaching the melting temperature of quartz (>1900 °C).

Since the temperature of the exposed rock sample remains below the melt temperature of the quartz grains, the primary rock removal method is spallation. The spallation temperatures in sandstone have been documented as ranging between 400 – 800 °C [6]. Should local temperatures rise and phase changes occur in the rock minerals, such as melting and vaporization, absorbed energy is redirected away from the rock cutting process.

There are physical and chemical changes occurring throughout this temperature range associated with the process of spallation. A primary physical change associated with spallation of the rock results from the thermal expansion of the grains. A sudden temperature increase in sandstone, as shown in Figure 7, results in the expansion of quartz and plagioclase grains.

The degree of expansion in each mineral is different. Table 3 presents the thermal expansion of the principal Berea sandstone minerals in one direction, as a percent of original size, at temperatures between 100°C and 600°C. As closely packed grains in the matrix expand with a rapid rise in temperature, they develop stress fractures and cracks within the grains, as well as break the cementation of adjacent grains. As a result, the affected grains will begin to break free from one another. A purge gas can assist in removing the loose grains away from the hole and the beam path.

Table 3: Single axis thermal expansion of sandstone minerals (as percent of original size) at different temperatures [5].

Mineral	100 °C	200 °C	400 °C	600 °C
Quartz	0.14	0.3	0.73	1.75
Plagioclase	0.09	0.14	0.22	0.83

The effects of differential thermal expansion can be seen by comparing the physical characteristics between pre- and post-lased grains. Figure 35a shows a magnified view (32X) of loose grains from Berea sandstone, carefully prepared and extracted from the rock sample before lasing. The grains observed in this sample are well sorted, and the shapes of the grains are round and sub-round. Figure 35b shows the same magnified view of sandstone grains collected following their spallation and ejection from the rock sample during lasing. Note the angular broken grains and poor sorting due to stresses imposed by thermal expansion and cooling.

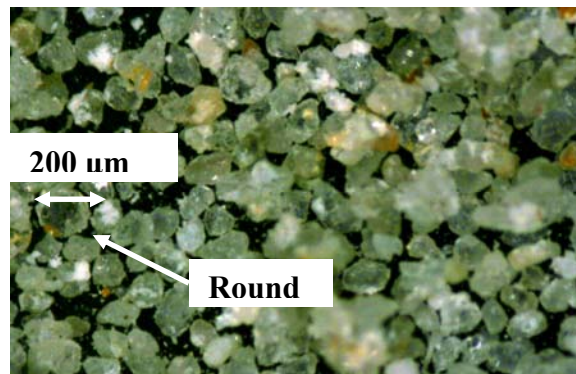


Figure 35a. Berea sandstone grains (pre-lase) at 32X.

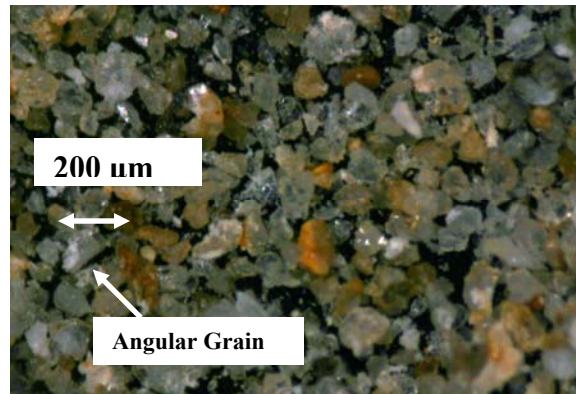


Figure 35b. Berea sandstone grains (post-lase) at 32X.

Chemical changes to the rock matrix occur as black organic material and other fragments present in the sandstone matrix dissociate, dehydrate, decompose and/or vaporize at temperatures lower than that required to melt quartz. The Berea sandstone sample was composed of less than 5% of these types of material by volume. As this material was altered or removed during lasing, adjacent mineral grains were allowed to break free from the matrix.

Thermogravimetric Analysis: The chemical changes that occur in rock over a temperature range can be observed using thermogravimetric analysis (TGA). A fragment of the Berea sandstone sample (about 31 mg) was heated from 50°C to 1200 °C at the rate of 200 °C/min to measure weight loss at elevated temperatures. Results confirmed the weight loss due to organics present in the matrix. Nearly 2 percent weight loss was observed as a function of temperature, and occurred as predicted between 400 – 800 °C.

Figure 10 shows the spallation temperatures at which the bonds between the grains weaken and break. It illustrates the thermal effects during a 3 kW beam exposure on Berea sandstone as temperatures increase from room temperature to 1200°C. Of note is the response in the 400-800°C range, where much of the rock's physical and chemical changes occur, confirming the spallation temperature zone as presented in the literature.

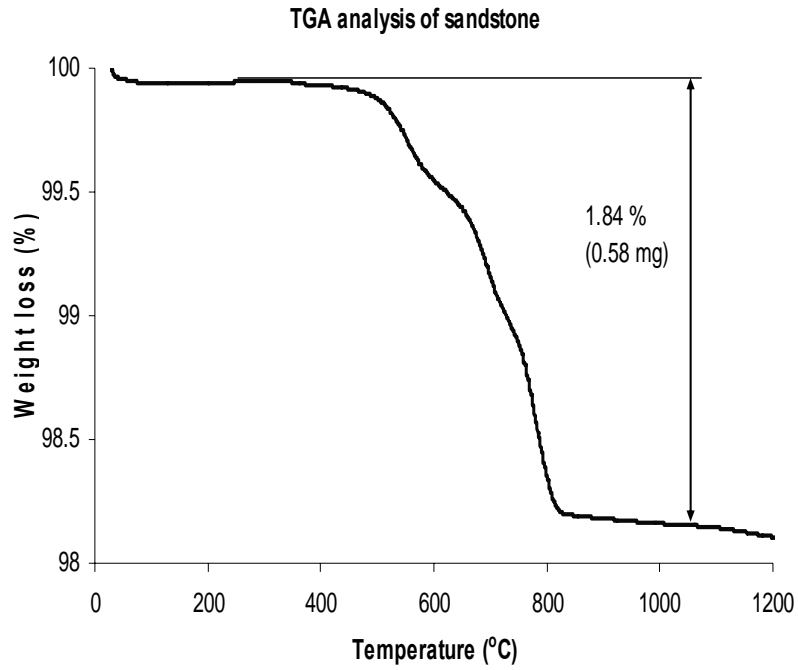


Figure 36. Weight loss as a function of temperature for Berea sandstone using Thermal Gravimeter Analysis (TGA).

At 60% power, the hole can be seen form 3-D image that the hole is clean and there is no melt or debris, Figure 37 a and b.

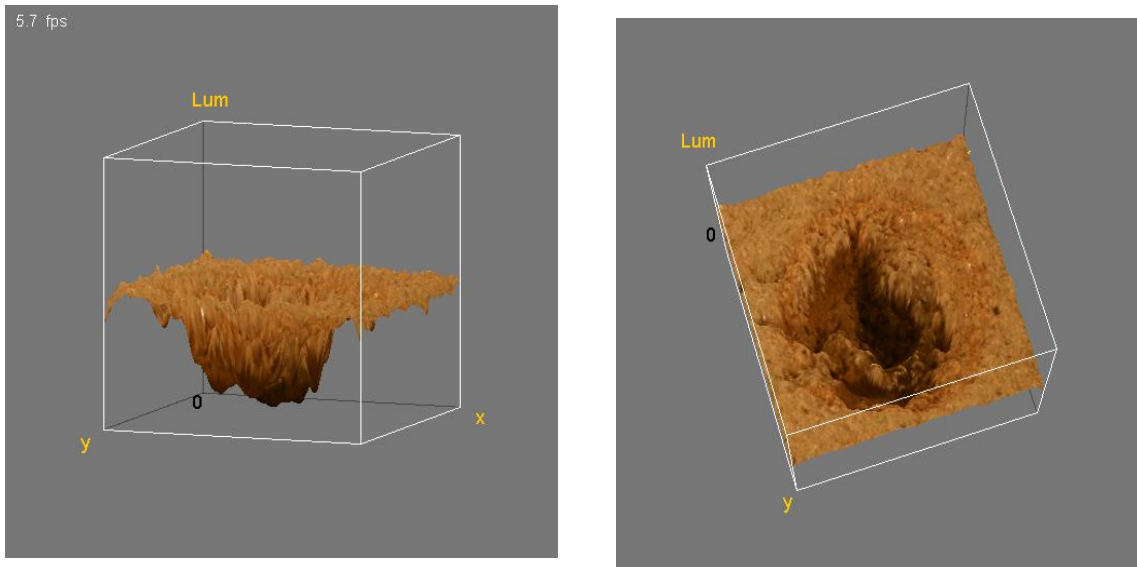


Figure 37a- 37b. Showing lased hole of Berea sandstone by HPFL at 60% power.

3.6.3 Thermal Effects on Limestone Sample

In the case of Limestone, the mechanism of laser rock interaction with Limestones is different from Sandstone. due to the chemical composition different. The physical and chemical changes in limestone were different due to mineralogy and chemical composition. Thermal dissociation takes place when limestone interacts with the laser, producing carbon dioxide (CO₂), (Equation 2). No melting was observed in limestone, due to the thermal dissociation of CaCO₃.

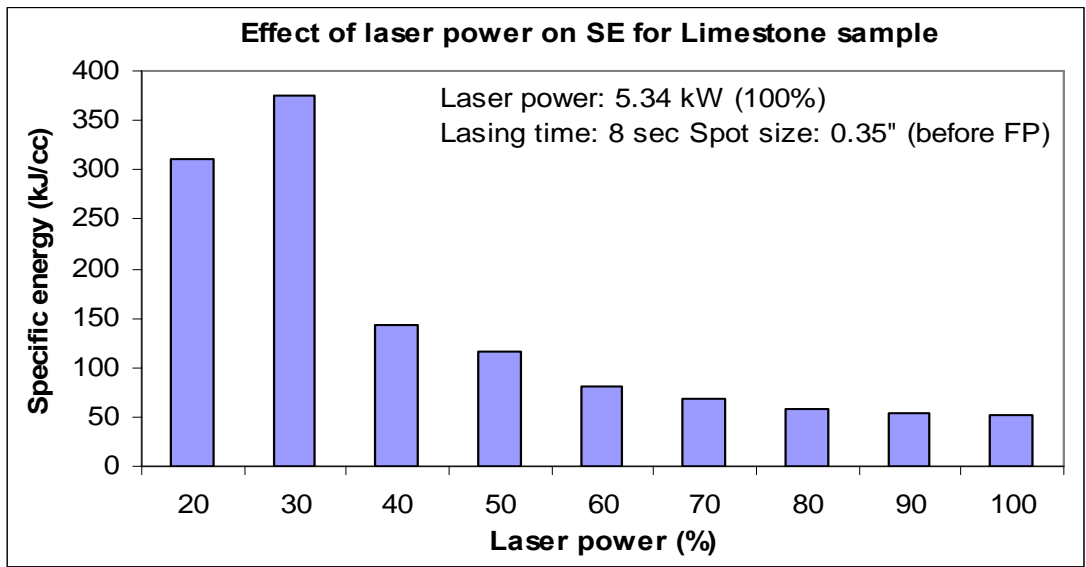
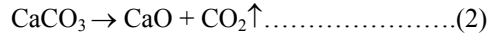


Figure 38. Laser optimization test showing SE value as the power increases of 10%, using HPFL for 8 seconds on limestone, Spot size was 0.35 inch.

The dissociation takes place at temperature less than 1200 °C, this can be seen from the analysis conducted by DTA, Figure36.

For limestone, the more power is required to obtain deeper tunnels, the more time and power the more dissociation takes place. For that reason, there was no picture taken for the Limestone when lasing at lower power percentage, there was no significant difference till the power reached 70% and up. But the SE value could be calculated because there was mass removed form the rock. Holes can be obtained in limestone at lower power by reducing the spot size which results in an increase in power intensity.

Effect of heating rate on weight loss for Limestone material

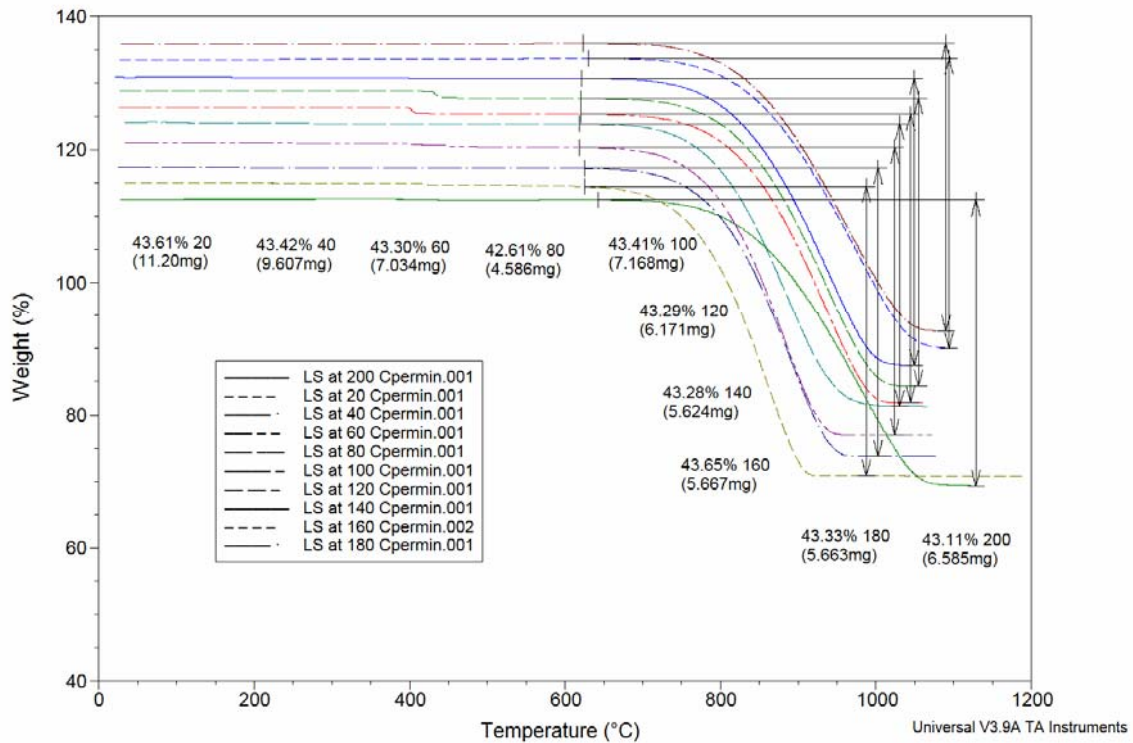


Figure 39. TGA analysis of limestone showing weight change as a function of temperature.

Effect of lasing time on Specific Energy (focused beam)

Objective: To find the effect of lasing time on limestone and sandstone material

Procedure:

The purpose of this test is to study the effect of beam duration exposed to the sample, varying the time from 1 to 20 seconds on limestone and sandstone samples. Limestone and sandstone blocks of size 20 x 5 x 5 inch were used in this study. One of the 20 x 5 inch surfaces was divided into 1 x 1 inch grids. Each grid was lased at 5.34 kW laser power. The lasing time of each hole was increased incrementally by one second starting from 1 second up to 20 seconds. The beam was CW and 8.9 mm spot size with 5.34 kW power. Gas nozzle in concentric position was used as purge system. Air was used as purge gas with 90 psia line pressure. Distance between purge and sample was about 1". Lens with 1000 mm focal length was used to focus 1" collimated beam. Specific energy values were calculated and are presented in figure below. An increase in the lasing time

resulted in increasing specific energy values and deeper holes were obtained. The result shows the same trend for sandstones, although less energy was consumed.

Result and Analysis:

The first test was conducted on a block of Berea sandstone and Limestone. One block for each rock type was used so that the rock properties will be constant. The laser power kept constant at full power, while varying the lasing time. Lasing times were increased from 1 to 20 seconds at an increment of 1 second. Figure 40 shows the results of sandstone,

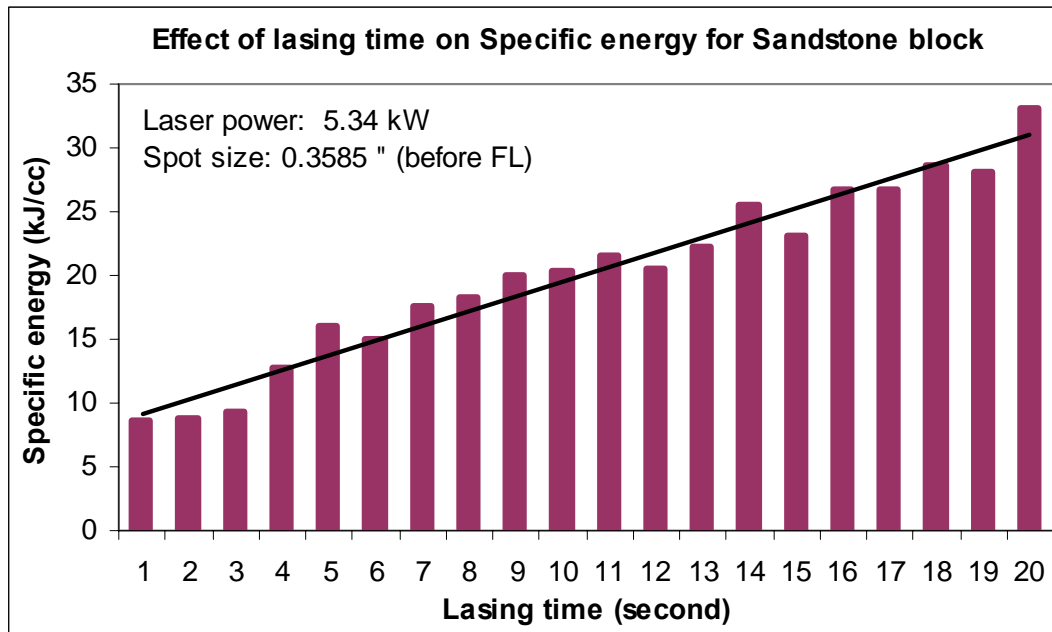


Figure 40. Relationship between lasing time and SE of Berea Sandstone, time was increased from 1 second to 20 seconds at 1 second increment

There was a trend between lasing time and SE. This indicates that more lasing time results in more penetration depth, because the more lasing time means more laser interaction with the rock sample (mineralogy variable is constant).

On the other hand, in term of SE, more lasing time means more plasma formation and gases in the lased hole, which result in more energy loss. The deeper the hole, the less the effect of purging.

Another test was conducted on a limestone sample, (Figure 41). The figure shows a relationship between SE and lasing time (more lasing time consumes more SE).

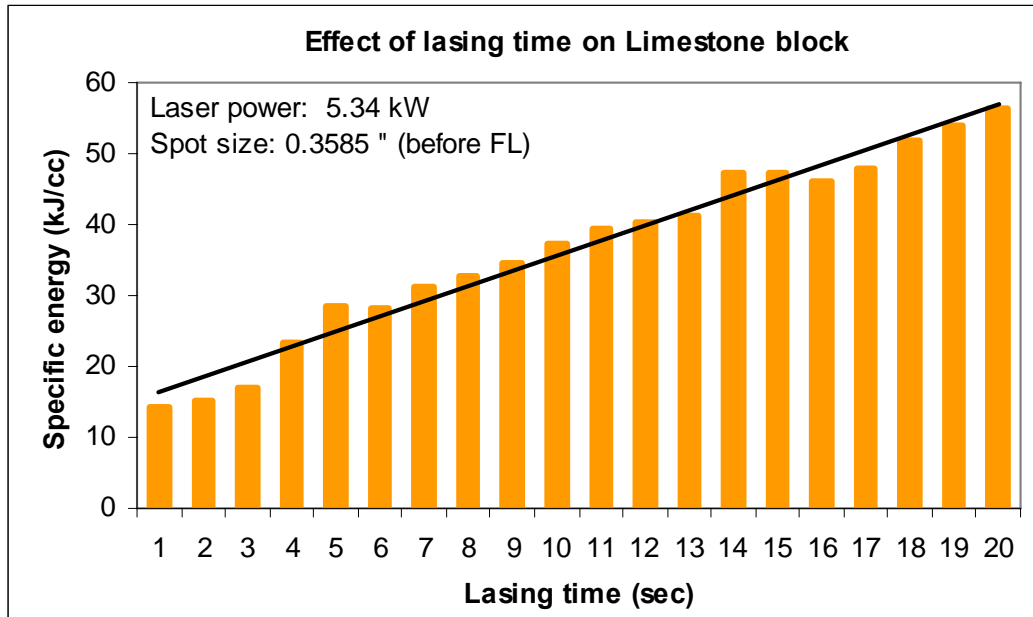


Figure 41. Relationship between lasing time and SE of Limestone, time was increased from 1 second to 20 seconds at 1 second increment.

Comparing both samples in one figure is presented in figure 42, where both the samples show the same trend as an increase in lasing time result in an increase in SE.

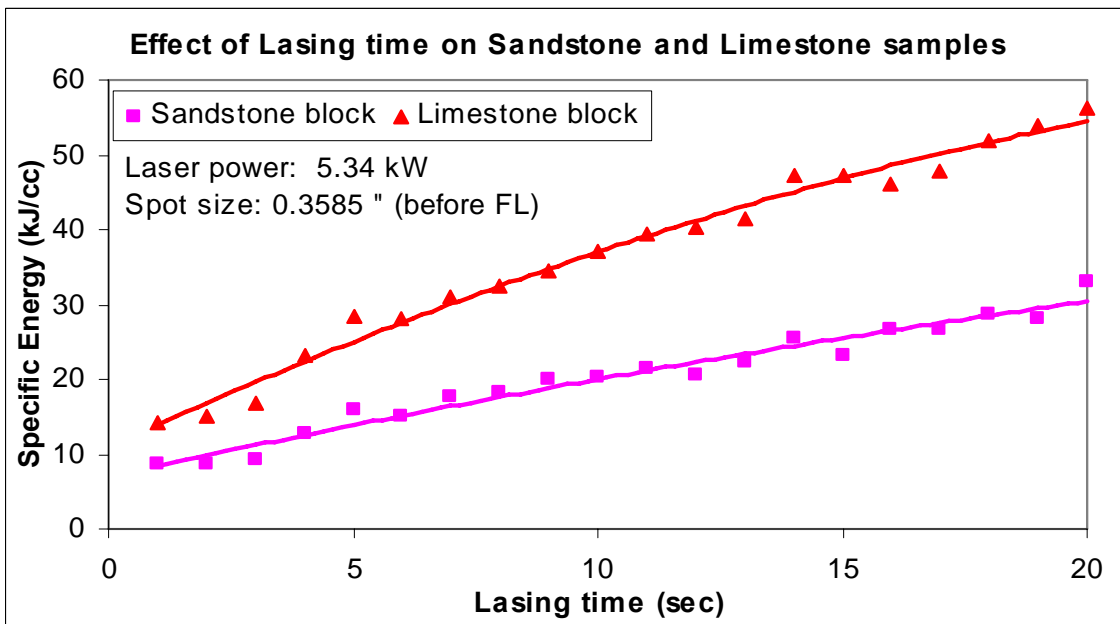


Figure 42. Relationship between lasing time and SE of Limestone and Berea Sandstone, time was increased from 1 second to 20 seconds at 1 second increment.

Frequency test procedure

Objective:

To study the effect of repetition rate on depth of penetration (& specific energy) for limestone and sandstone (focused beam)

Procedure:

A Block size 20 x 5 x 5 inch was used to study limestone material. One of the 20 x 5 inch surfaces was divided into 1 x 1 inch grids as shown in the figure 43. Sandstone block size 12 x 16 x 4 inch was used to study sandstone material. One of the 12 x 16 inch surfaces was divided into 1 x 1 inch grids as shown in the figure 1. Each grid was lased at 5.34 kW laser power for 8 seconds with frequency varying from 1 to 999 Hz (intervals are shown in graph).



Figure 43. Surface of limestone showing experiment grids

Experiment set up is shown in figure 44. Gas nozzle in concentric position was used as purge system. Air was used as purge gas with 90 psia line pressure. Distance between purge and sample was about 1". Lens with 1000 mm focal length was used to focus 1" collimated beam. Spot size (penetrating laser beam diameter) was kept 0.35". PLC pulsar (Omron CPM2C) was used to control the repetition rate of laser exposure. It can control the laser beam frequency from 0.1 Hz to 999.9 Hz. PLC can also control the amount of

laser on time for each frequency cycle. All experiments were done with 50 % and 99 % laser on time for a cycle (duty cycle: 50 % and 99 %).

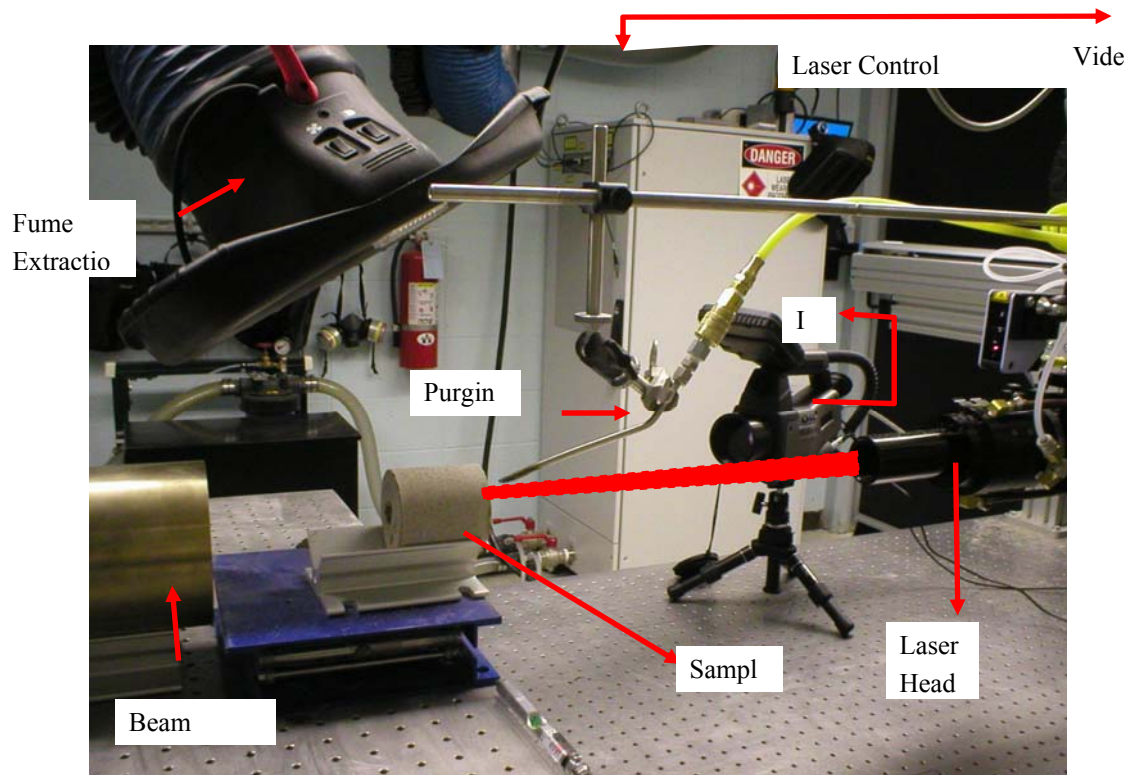


Figure 44. Experimental set up for frequency test

Result and Analysis:

Two sets of experiments were conducted to evaluate the effect of frequency on the SE, the first set was done by changing the frequency from 1 to 10 pulses per second at an increment of 1 pulse/second for both sandstone and limestone sample. The second set is by changing the frequency from 10 to 999 at 10 pulses/second increment.

The result was mainly based on the SE, the observations from the pictures of the sample did not add to the analysis due to the fact that there was no significant change in terms of melt or damage. The melt was form only at the edge of the sample due to the boundary effect. (Figure 45)

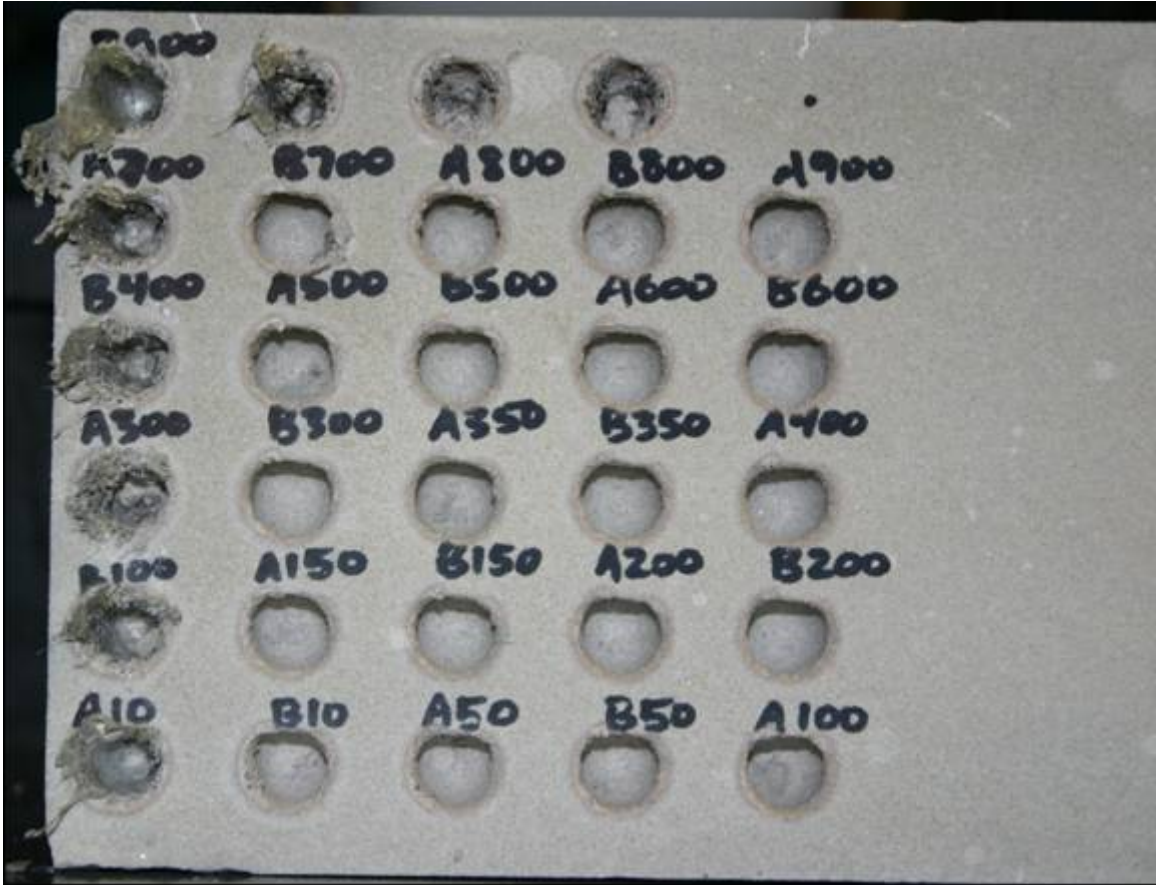


Figure 45 . Berea sandstone showing holes by changing the frequencies from 10 to 999Hz.

The results of lasing sandstone from 1 to 10 hz I presented in figure 63. There was a not significant change from 1 to 9 hz, but the changes is significant at 10 hz.

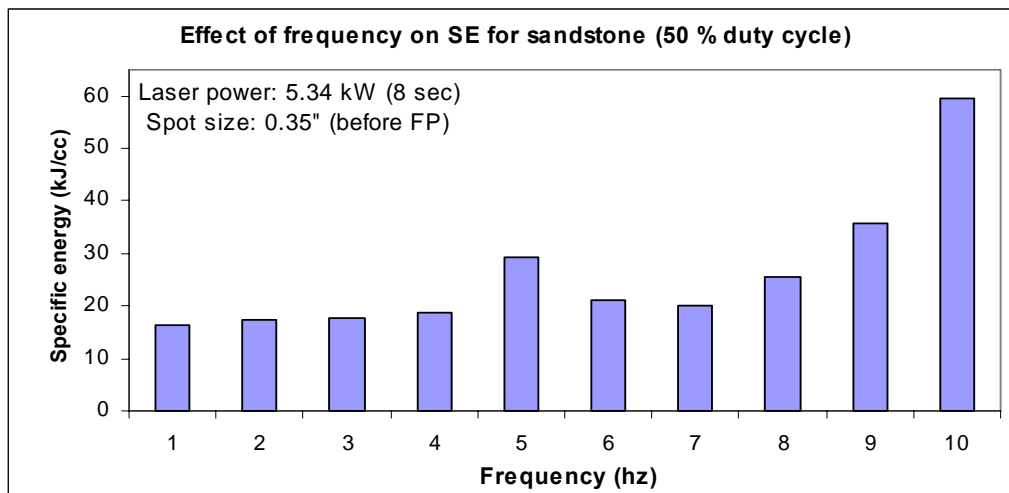


Figure 46. Pulsation from 1 to 10 hz for sandstone at 50% duty cycle.

The result indicates that frequency less than 10 shows less SE values, pulsing laser beam allows it to intermittently interact with the rock sample. Because the purge was continuous when the beam was not on the sample, pulsing allowed the dust and gas plume to clear. Dust and plume absorb energy from the laser and reduces the amount of energy transferred into the rock. When increasing the frequency from 10 to 999, laser beam is almost continuous for frequencies more than 10 Hz. Figure 47.

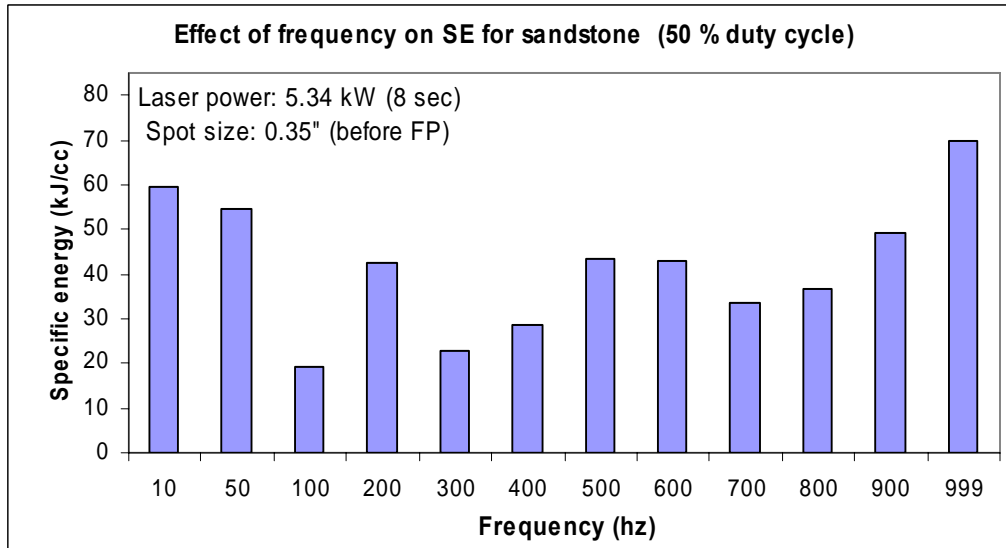


Figure 47. Pulsation from 10 to 999 hz for sandstone at 50% duty cycle.

Limestone showed the same trend as an increase in the frequency results in an increase in SE, the beam tend to be continues wave(Figure 48). Limestone requires more energy and more laser beam on the sample for disassociation to take place.

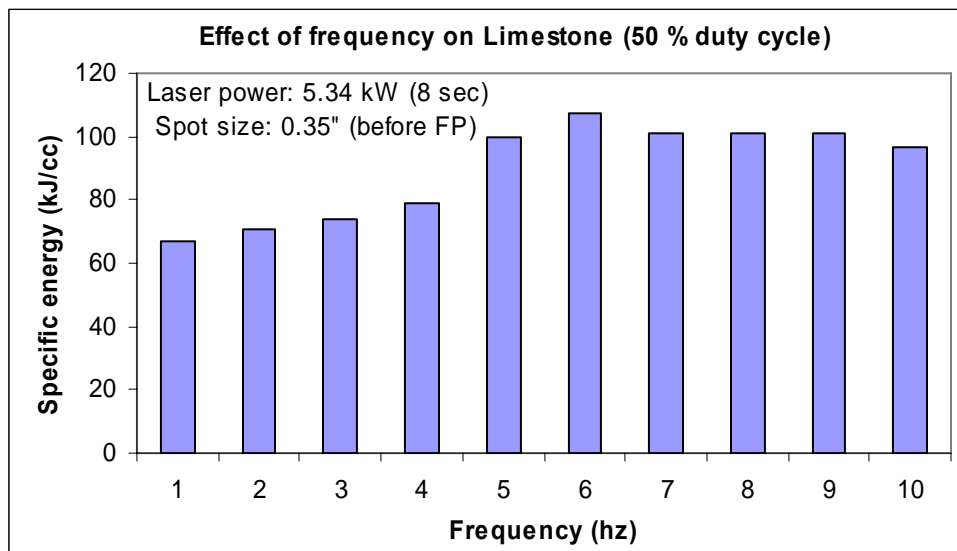


Figure 48. Pulsation from 1 to 10 hz for limestone at 50% duty cycle.

Effect of saturation and purge gases on specific energy

Objective:

To study the effect of saturation on specific energy for limestone and sandstone.

Procedure:

The laser-rock-fluid interaction test was conducted on Berea gray sandstone and limestone. The purpose of this test was to determine whether the interaction of fluids and laser radiation would have a significant effect on penetration and specific energy.

Sandstone and limestone cores (2" dia. x 2" depth) were placed in vacuum environment for about 6 hrs and then saturated separately with water, brine and oil for at least 24 hours. The samples were saturated with brine, fresh water and oil.

The composition of the brine used for saturating the rocks was potassium chloride (KCl) and sodium chloride (NaCl). The mixture consisted of 25,000 ppm of NaCl and 25,000 ppm of KCl in 1,000 ml of water. The density of the brine was 1.039 gm/cc. The crude oil used in testing had a density of 0.841 gm/cc.

Each sample was placed in Plexiglas chamber specially design to contain debris and harmful vapor as shown in figure 49. Each saturated sample was lased for 8 seconds with 5.34 kW (CW) laser power. Lens with 1000 mm focal length was used to focus 1" collimated beam. Spot size was kept constant at 0.35" before focal point. Gas nozzle in concentric position was used as purge system. Air, Argon, Nitrogen and Helium were used one by one on sandstone and limestone samples saturated with water, brine and oil to see the effect of purge gas on specific energy. This test was conducted to analyze the effect of the purge gas on SE. The reason for using the purging gas was to simulate reservoir conditions (an oxygen-free environment), remove rock debris and vapor, and safety consideration.

Line pressure for purge gas was kept constant at 90 psi. Distance between purge and sample was kept about 1". Specific energy was calculated based on weight removal and hole geometry. Results are presented in graph below for sandstone and limestone material.

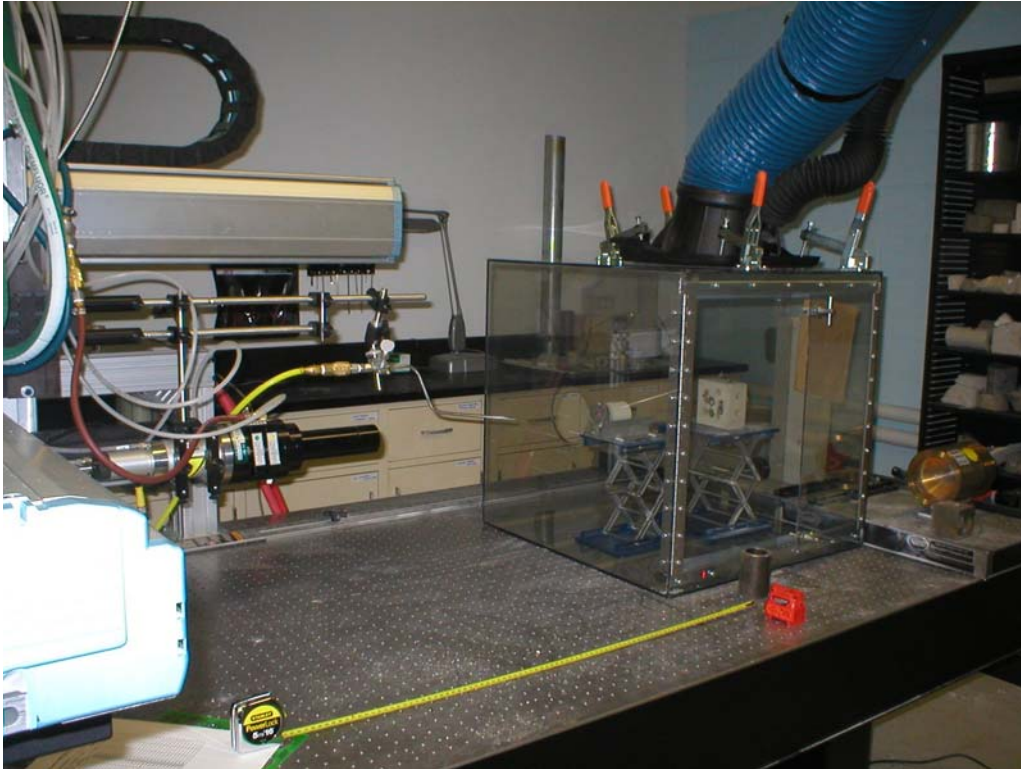


Figure 49. Experimental set up showing Plexiglas chamber to contain hazardous fumes

Results and Analysis

Purging gas:

The test was performed to determine if a change in the gas atmosphere near the hole during lasing affected Specific energy. Four types of gas were used; nitrogen, Air, argon and helium. The purge gas was used to simulate reservoir conditions (oxygen-free environment), clean the lased hole and for safety reasons. The test was performed on Berea gray sandstones and limestone.

For sandstone, there was not much significant difference when using helium, argon and nitrogen, on the other hand, air consumes more SE. This result is encouraging for the reason that air will not be used downhole due oxygen content. In the case of limestone, Nitrogen consumes less SE than the other three gases.

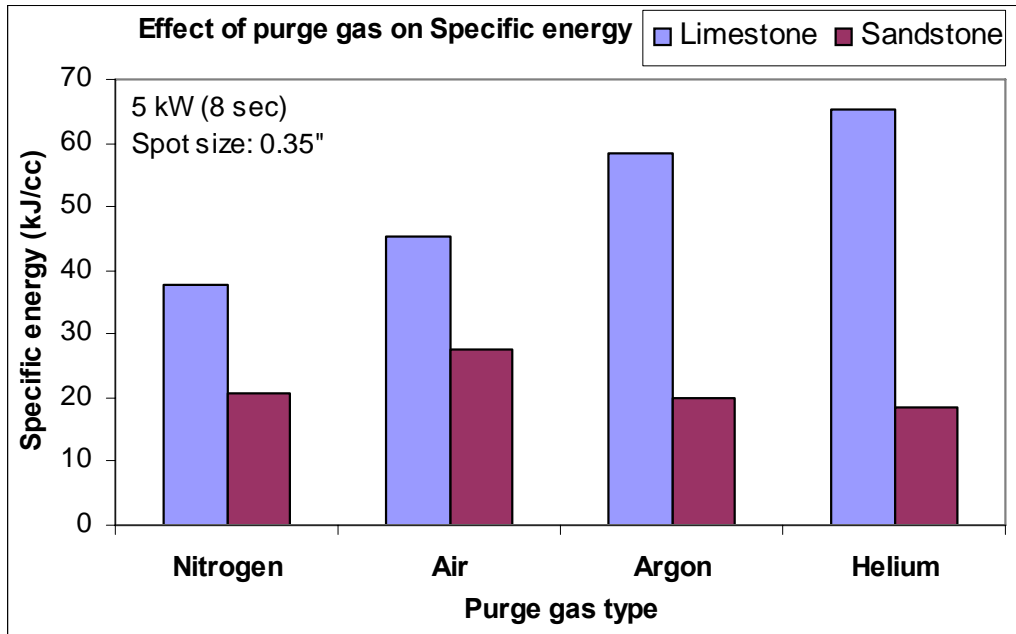


Figure 50. Effect of purge gas type on specific energy for limestone and sandstone

Purging gasses with Saturated Samples:

The test showed that saturated samples in general resulted in higher values of specific energy (SE) than unsaturated samples. The presence of liquids in the rocks consumed more energy since it takes more energy to heat liquids than air. Also the presence of liquid in the core results in producing vapor when subjected to laser radiation. This vapor or gases will absorb the energy and result in energy loss, therefore, less energy will be delivered to the rock sample and hence consumes more SE. Oil saturated samples consumed the highest SE values. More research needs to be conducted to determine how gas composition effects SE while lasing saturated samples. Figure51 can be used as guide or correlation when using gasses on saturated samples.

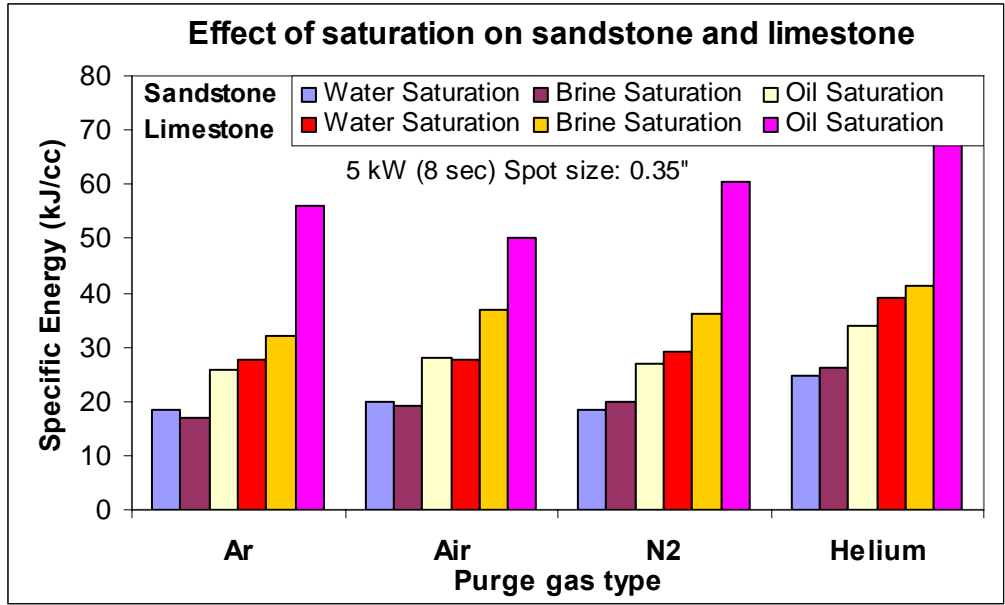


Figure 51. Effect of saturation media on specific energy for sandstone and limestone

Time of penetration test

Objective:

To find the time of penetration of GTI's Ytterbium fiber laser from various thickness (up to 1 inch) of steel, cement and clad of steel, cement and limestone/sandstone.

1. Time of penetration for steel samples:

Steel plates of various thicknesses (0.25", 0.35", 0.4", 0.5", 0.6", 0.75" and 1") were cut from 2" diameter steel rod. Each steel plate was lased at 5.34 kW power (CW) and time was measured for focused laser beam to penetrate through. Gas nozzle in concentric position was used as purge system. Air was used as purge gas with 90 psia line pressure. Distance between purge and sample was about 1". Lens with 1000 mm focal length was used to focus 1" collimated beam. Spot size (penetrating laser beam diameter) was kept 0.35". Same experiments were repeated with N₂ as purge gas to study the effect of purge gas on time of penetration.

Two methods were evaluated for steel cutting; the first method is by exposing the sample directly to one beam without moving the robot, figure 52.

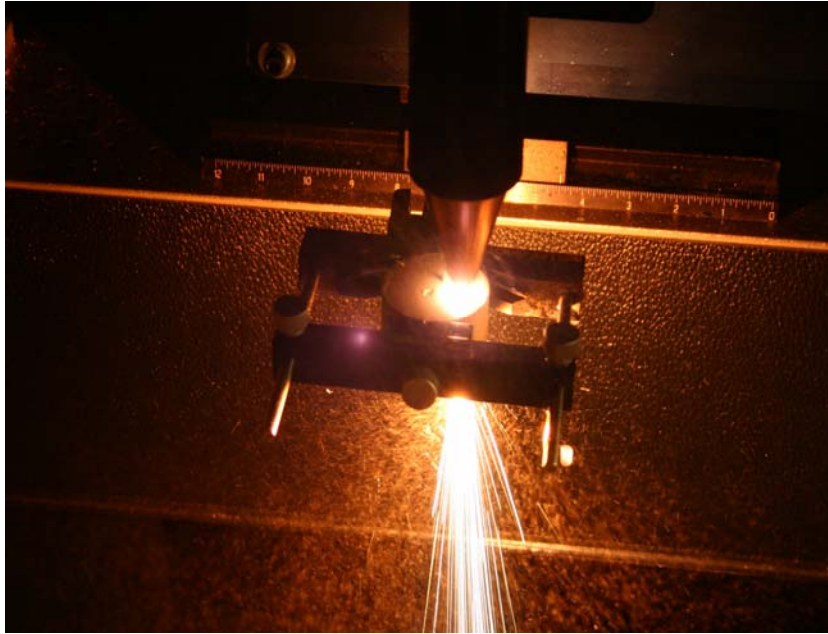


Figure 52. Steel drilling when the laser is at fixed position.

Samples pictures were taken before and after lasing as shown in figure 53 and 54 respectively.

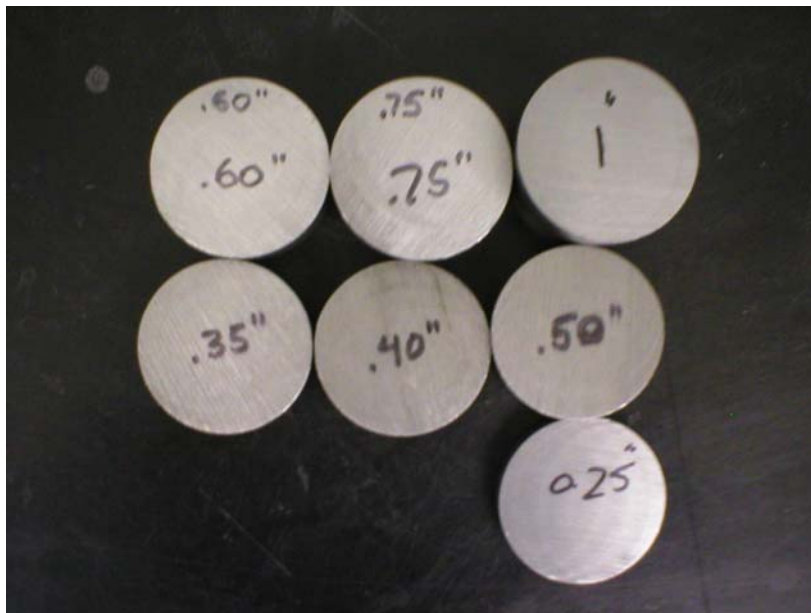


Figure 53. Steel sample at different thicknesses before lasing



Figure 54. Steel sample at different thicknesses after lasing
The second methods was by moving the robot in a circular motion to cut a circle as shown in figure 55.

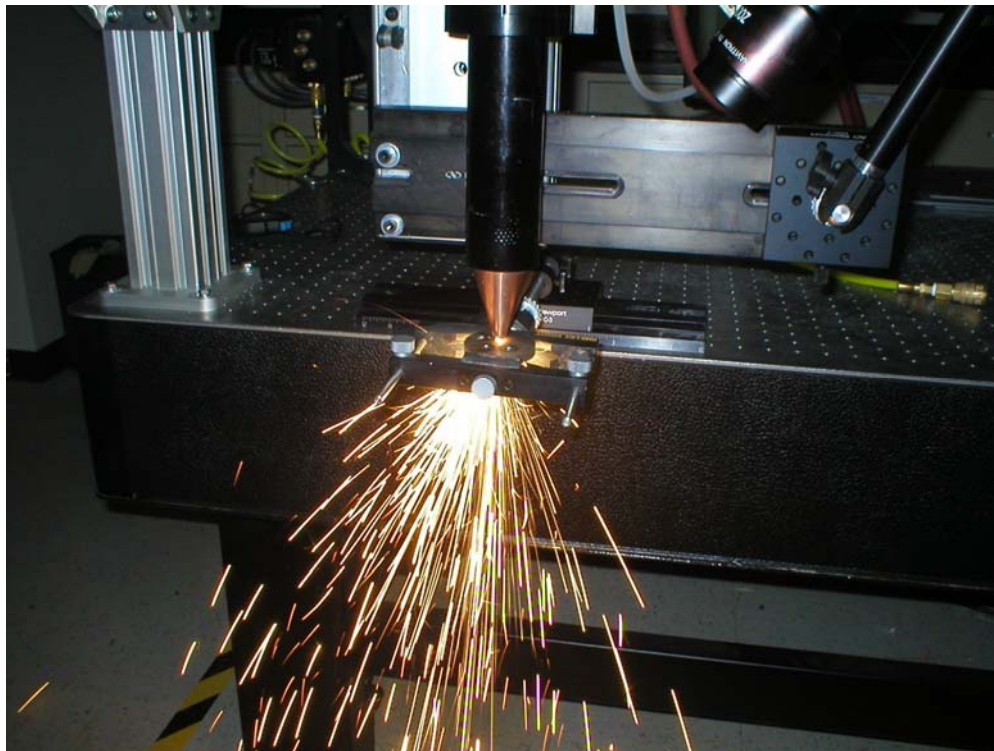


Figure 55. Steel cutting by moving the robot in a circular motion.

The methods followed for all the experiment is by keeping the robot steady without motion. This is more effect and closer to down hole conditions because the complexity of moving the robot down hole.

The result of using air vs nitrogen for different thicknesses of the steel is shown in figure 56.

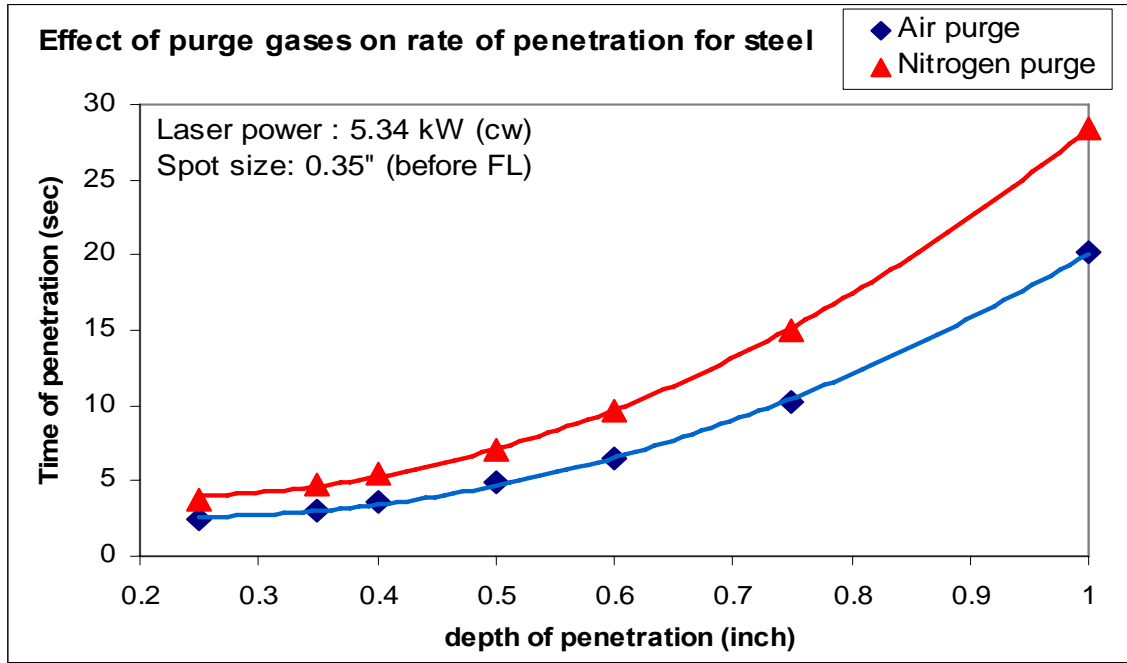


Figure 56. Time of penetration Vs. depth of penetration for steel using air and nitrogen purge.

Time of penetration increases with a trend shown in graph below, with increase in steel plate thickness. Time required to penetrate through the same thickness of steel is lesser with air as purge gas then Nitrogen.

2. Time of penetration for cement samples:

Quikrete anchoring cement was used for this study. It is rapid settling and pourable cement. Three different types of this cement, namely, Class A, Class G and YS 250 used most widely for related work were tested. Molds of cement plates with various thicknesses (0.25", 0.35", 0.4", 0.5", 0.6", 0.75" and 1") and 2" diameter were made with 2" ID Teflon tube and they were cured for 24 hrs. Each sample (cement plate) was lased at 5.34 kW power (CW) and time was measured for focused laser beam to penetrate through. Gas nozzle in concentric position was used as purge system. Air was used as purge gas with 90 psia line pressure. Distance between purge and sample was about 1". Lens with 1000 mm focal length was used to focus 1" collimated beam. Spot size (penetrating laser beam diameter) was kept 0.35". Time of penetration increases with increase in cement layer thickness.

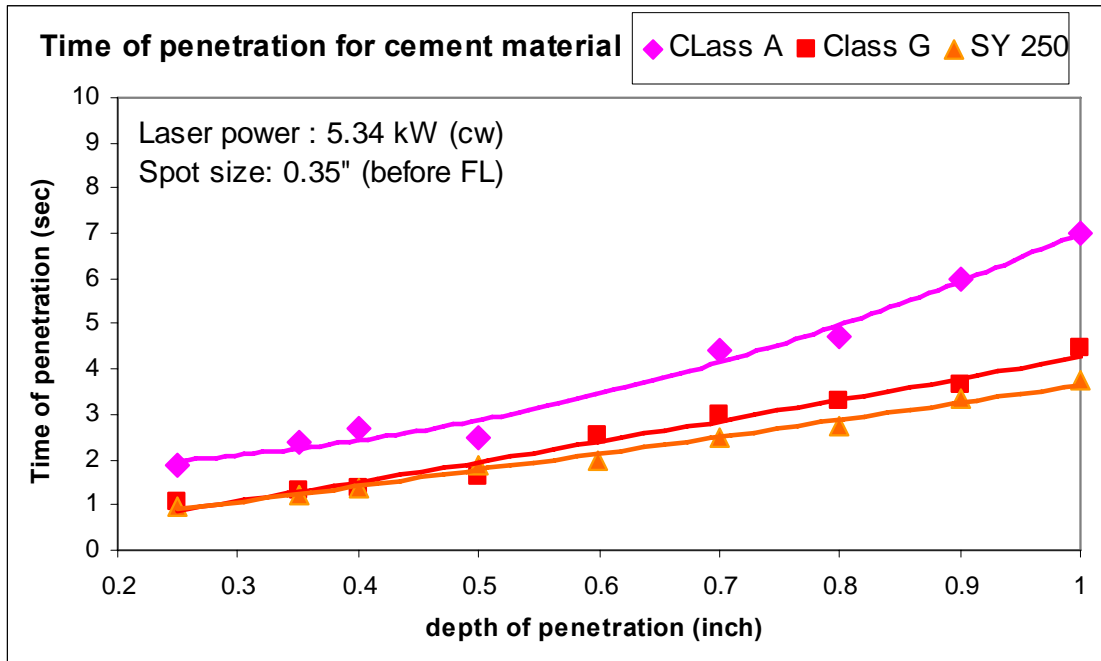


Figure 57. Time of penetration Vs. depth of penetration for various cement materials commonly used in industry

3. Time of penetration for clad samples:

Clad samples were made with various thicknesses (0.25”, 0.35”, 0.4”, 0.5”, 0.6”, 0.75” and 1”) of cement material sandwiched between 0.25 “ thick steel plate and 2 “ thick core of limestone or sandstone. The diameter of all plates and cores was 2”.

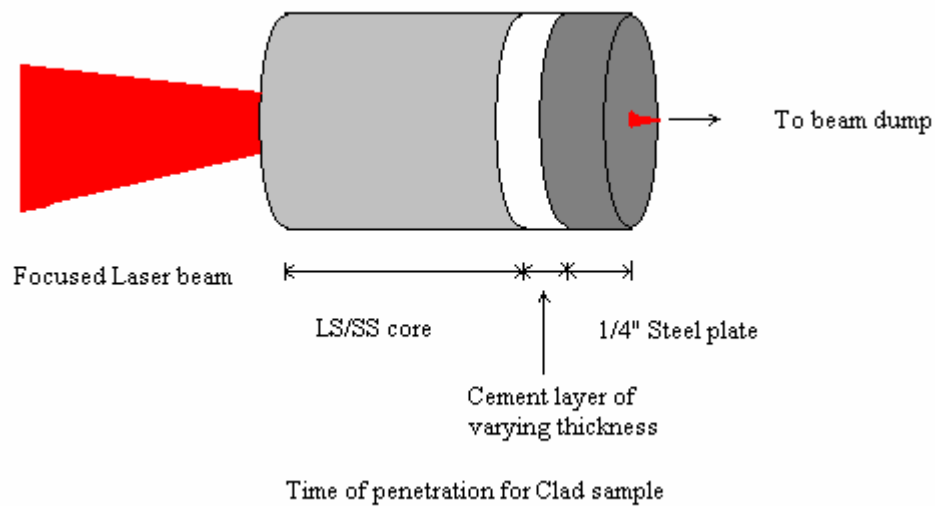


Figure 58. Schematic showing time of penetration concept for clad (casing) material

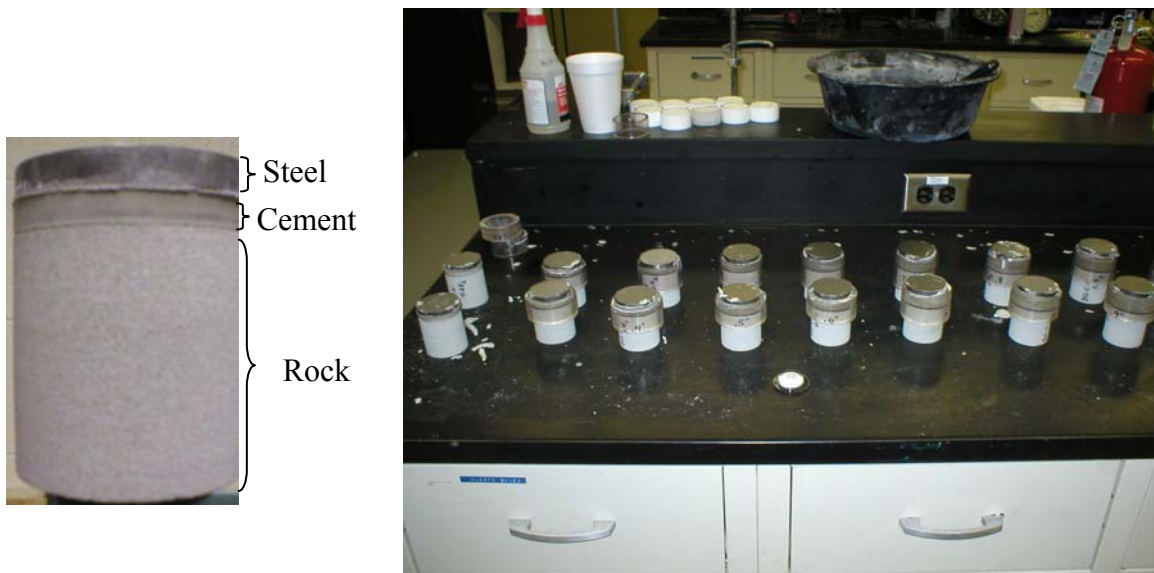


Figure 59. Preparation of the clad samples (steel, cement and core) in the lab.

Each clad sample was lased at 5.34 kW power (CW) and time was measured for focused laser beam to penetrate through. Gas nozzle in concentric position was used as purge system. Air was used as purge gas with 90 psia line pressure. Distance between purge and sample was about 1". Lens with 1000 mm focal length was used to focus 1" collimated beam. Spot size (penetrating laser beam diameter) was kept 0.35". Time of penetration was also measured for 2" thick cores of limestone and sandstone to compare time of

penetration for clad sample with sum of individual material (cement, steel and LS/SS) as shown in figure 60 and figure 61.

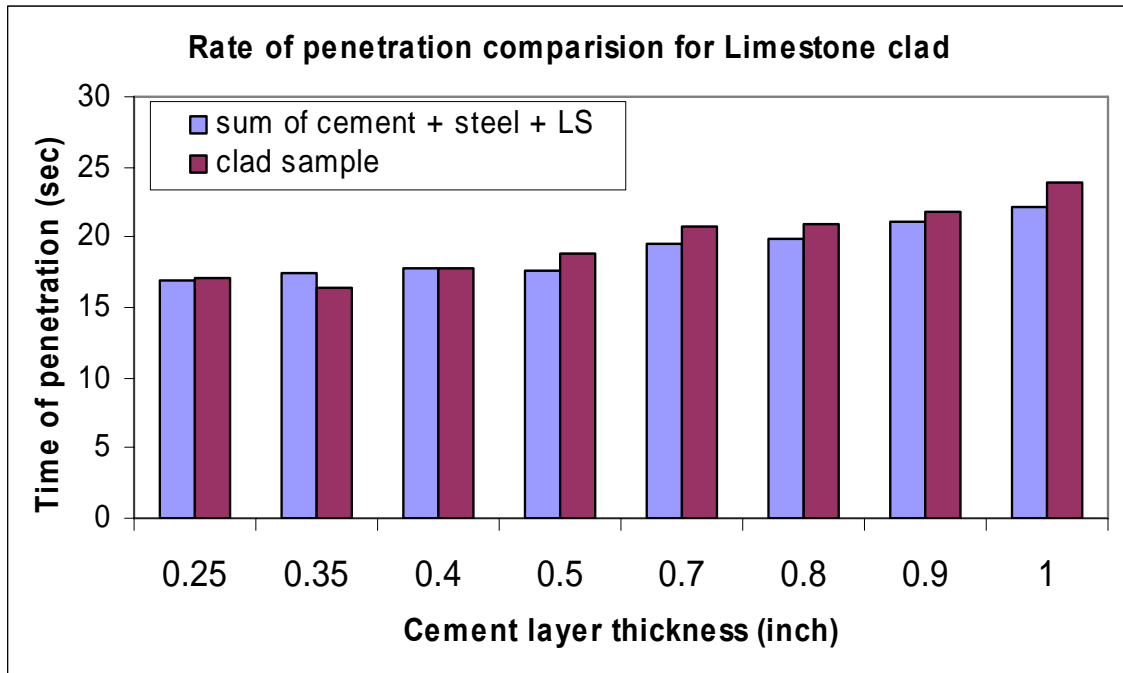


Figure 60. Rate of penetration for limestone clad sample

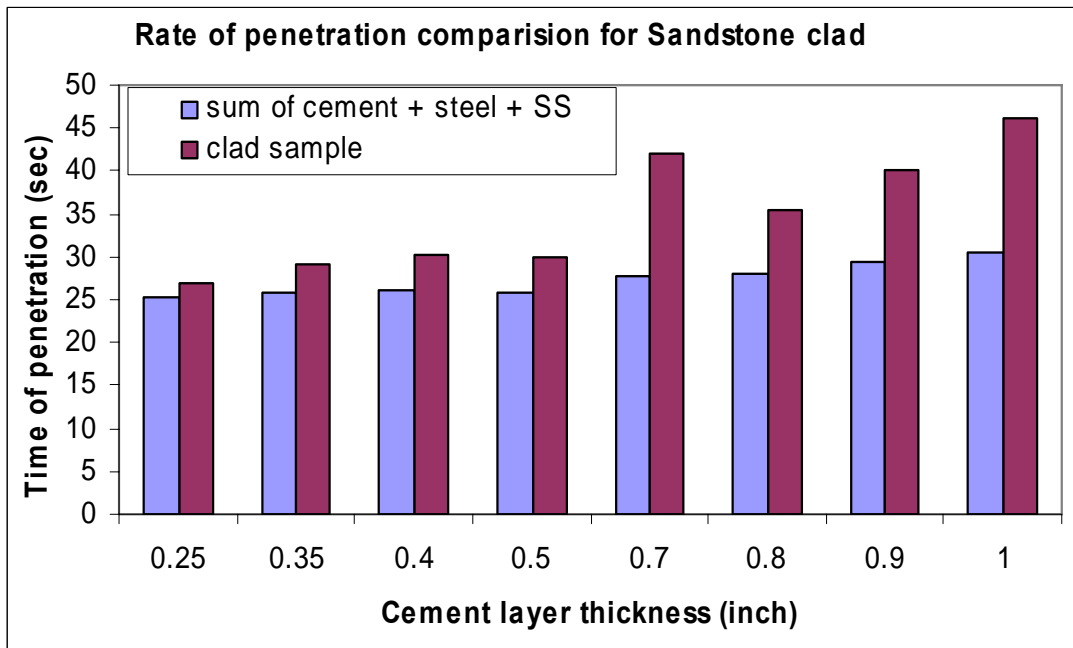


Figure 61. Rate of penetration for limestone clad sample

The result was used for the high pressure cell to know how long it will take the laser to penetrate different steel thickness and cement so the laser can be programmed to be on for sufficient time to penetrate rock.

Fluid transmission test:

Objective:

- To study the transmission of laser power through varying depth of Halocarbon fluids

Experimental setup:

30 cm long cylindrical plastic tube (43 mm ID) was glued at one end with 50.8 mm diameter (4 mm thickness) cover glass to make a fluid container. RTB silicon sealant was used as glue and it was cured for 24 hrs. 5 kW ytterbium fiber laser head was positioned vertically on the top of fluid container, aligned with fluid container and laser power meter at the bottom as shown in figure 62. Fluid container was kept about 30 cm apart from laser power meter. Laser power meter was used to measure the amount of power transmitted from fluid.

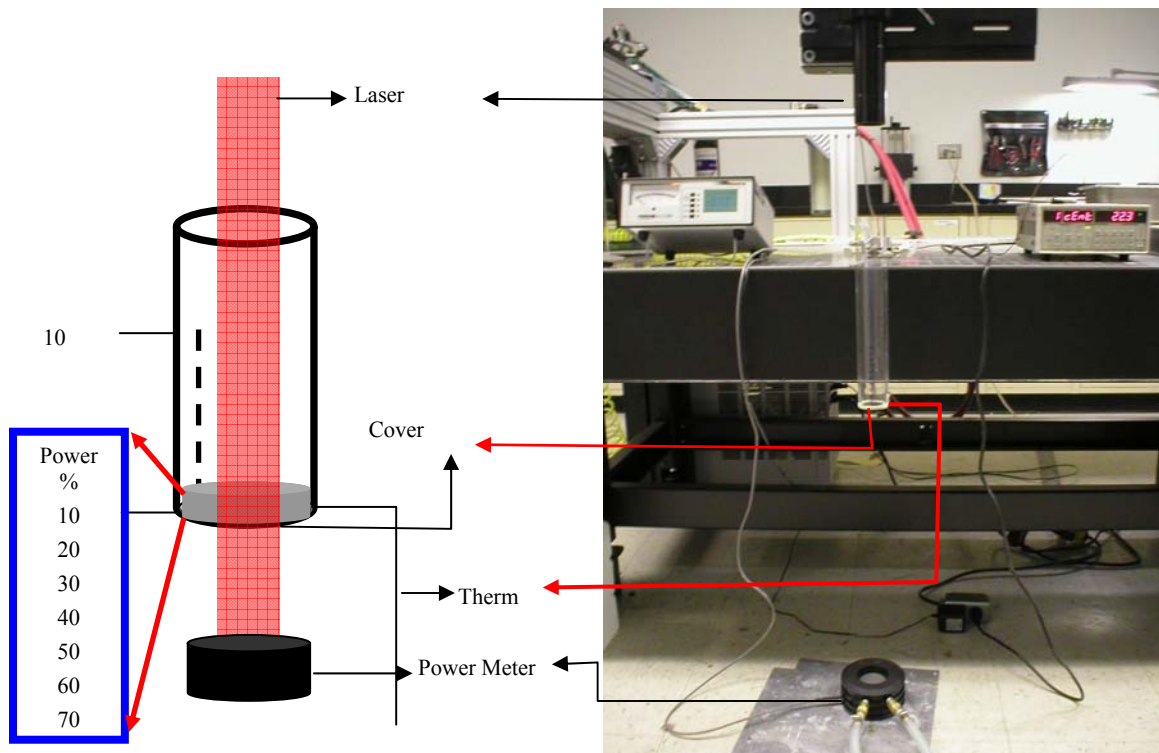


Figure 62. Experimental set up for fluid transmission test

K type thermocouple was attached at wall of fluid container to monitor temperature with change of laser power.

Procedure:

First, fluid container was kept empty and lased at 10 to 100 % power level in increments of 10 %. Power meter reading was recorded for each shot. This was a baseline test for measuring effect of fluid on laser transmission. Then, halocarbon fluids with different viscosity (0.8, 95, 200, 400, 1000 N) were studied for laser transmission consecutively. Depth of Halocarbon 0.85 N fluid was changed from 1 cm to 10 cm in increments of 1 cm. For each fluid depth laser power was varied from 10 % to 100 % in increments of 10 %. Lasing time was kept constant at 60 seconds. Based on results achieved, all other fluids were lased from 10 % to 100 % laser power in increments of 10 % for 1, 5 and 10 cm depths. Transmitted power was recorded with Laser power meter. Wall temperature and time of response for Laser power meter were also recorded. After each lasing shot, time was allowed for fluid temperature to reach ambient temperature. For higher viscous fluids temperature stabilization time after lasing was about 5 to 7 minutes were as less viscous fluid took lesser time to stabilize.

Observation and Result:

As shown in the following graphs, for fluid with low viscosities (0.85 to 200 N) increase in fluid depth does not have any major effect on power transmission. For 1000 N fluid, transmitted laser power decreased with increasing percentage laser power and fluid depth. For 1000 N fluid 13 % decrease of laser power was noted at 10 cm depth and 100 % laser power.

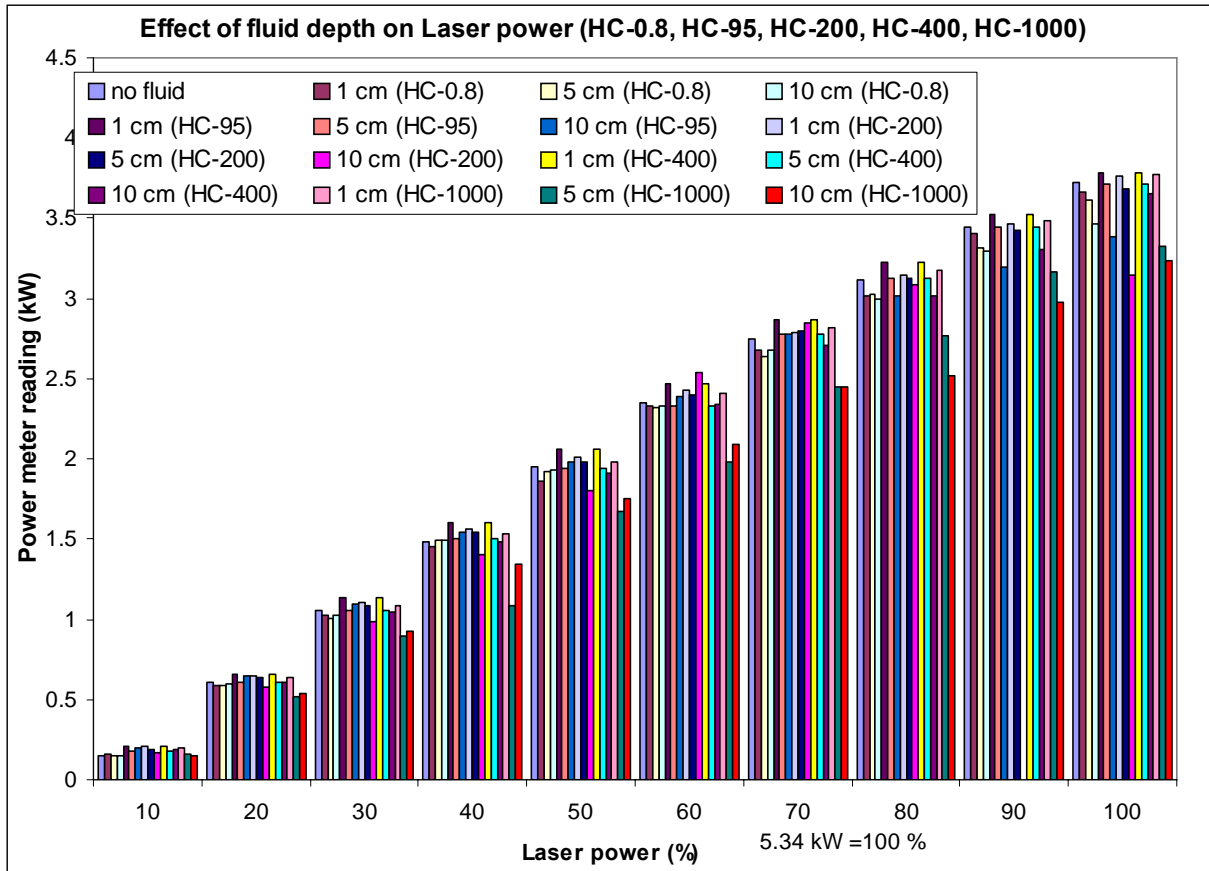


Figure 63. Loss in laser power as a function of fluid depth for various halocarbon fluids

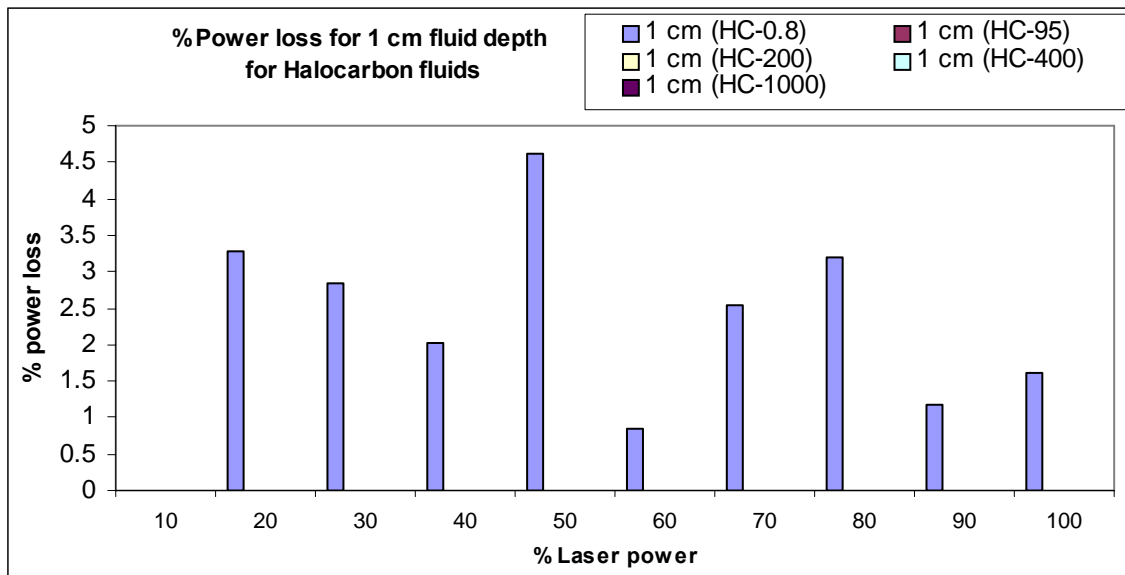


Figure 64. Percentage Loss in laser power for 1 cm fluid depth for various halocarbon fluids

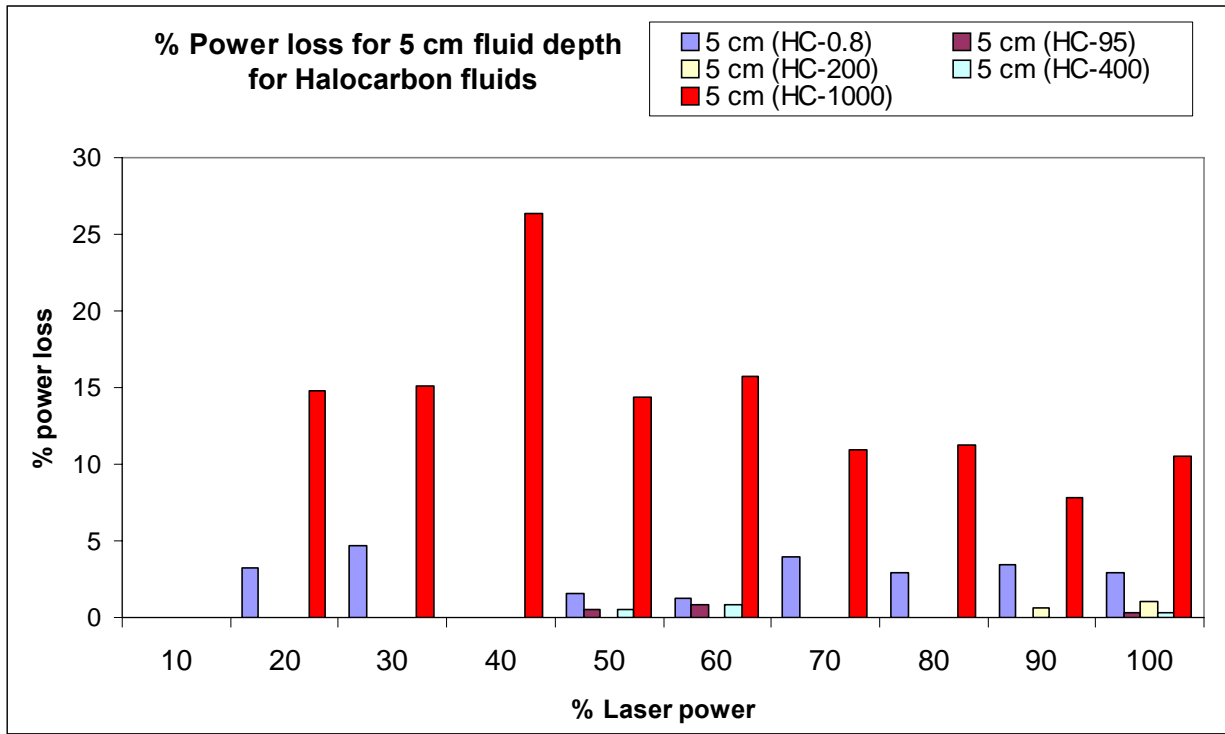


Figure 65. Percentage Loss in laser power for 5 cm fluid depth for various halocarbon fluids

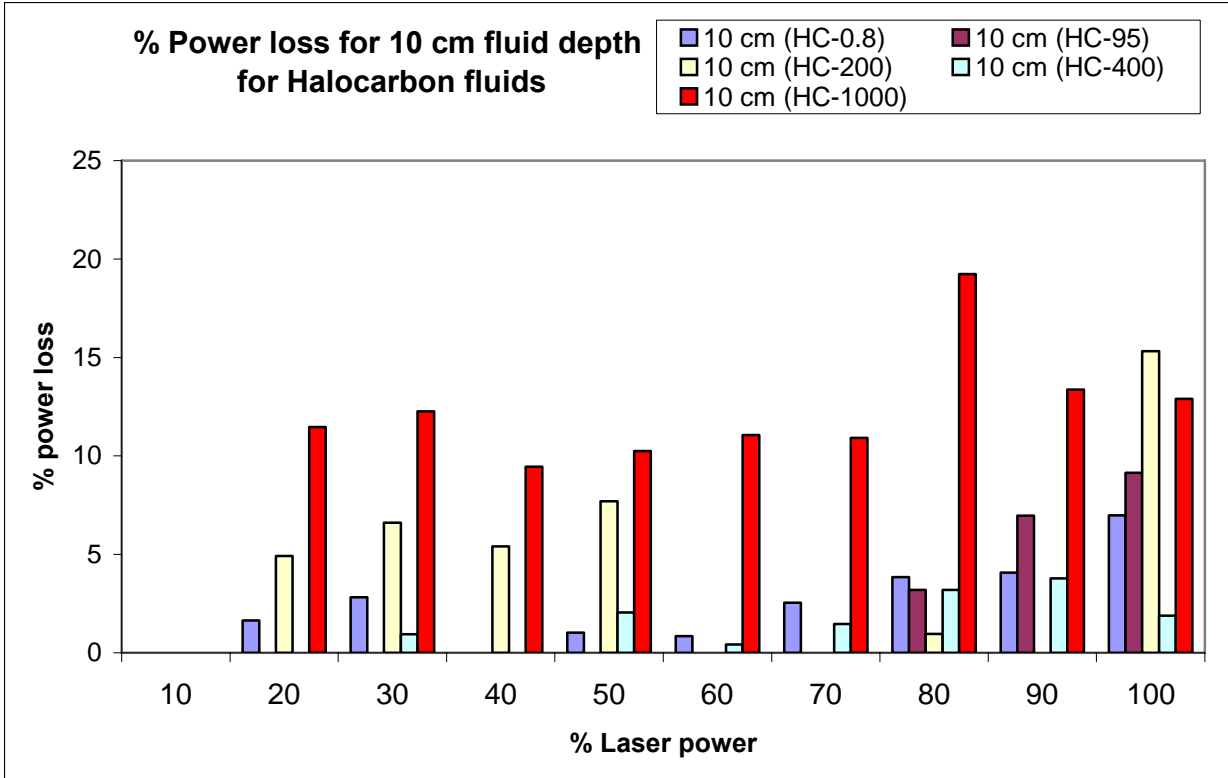


Figure 66. Percentage Loss in laser power for 10 cm fluid depth for various halocarbon fluids

Liquid purge test:

Objective: To investigate the effect of various liquid purge medium (water, anti freeze, optical fluid) on deep hole penetration using high power laser.

Overview:

In previous tasks, effect of using different gaseous medium as purge had already been studied on deep hole penetration in sandstone and limestone. Air, Nitrogen, Argon and Helium had been used as purging media for these studies. Effect of using liquid instead of gas purge was studied with water purging as a starting point. Anti freeze liquid was also tried.

Experimental set up:

As shown in figure 67, a tank made of Plexiglas was used with a mechanism to recycle liquid. Liquid pump was used the purge liquid to the rock being lased. Different shapes of nozzles (fig. 67) were tried to achieve better purging mechanism.

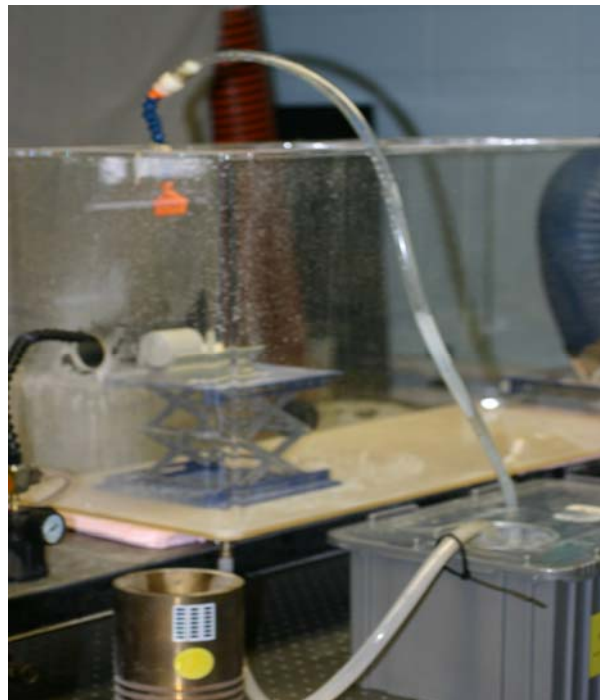


Figure 67. Experimental set up for liquid purge test

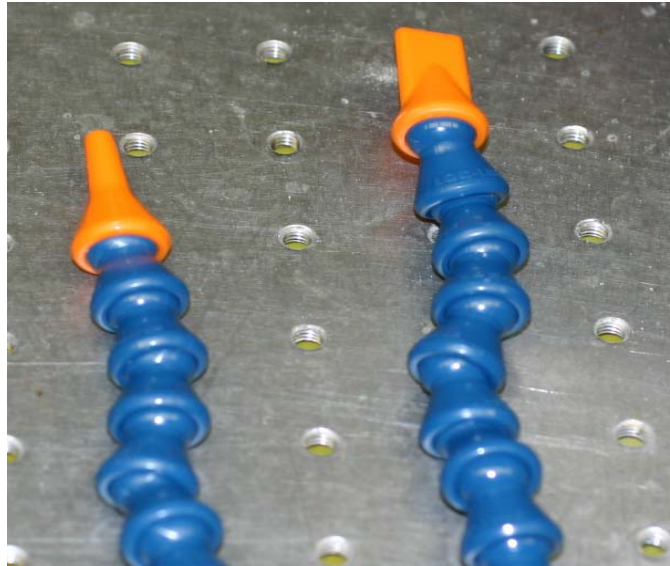


Figure 68. Various nozzle shapes tried for liquid purging

Rock samples (sandstone or limestone) were placed in the tank and water was purged using the nozzle. Focused (0.35" spot size) and collimated beams were tried with 5 kW laser power for up to 10 second lasing time. The purging was coinciding with laser beam at the target. In other set of experiments, purging direction was made perpendicular to beam, where the beam penetrated the liquid flow and went to rock.

Observations:

- Water absorbed the energy from laser beam and raised its temperature to form vapor. No sizeable penetration was achieved for rock samples in any experiment.
- Anti freeze also absorbed energy from laser beam to reach to its flash point. No considerable penetration was achieved for this experiment.

Effect of lasing time and power on Specific energy (Optical fluid as purge)

Objective:

To determine the effect of lasing time and laser power level on sandstone/limestone material (optical fluid as purging media)

Procedure:

As shown in figure 69, a tank made of Plexiglas was used with a mechanism to recycle liquid. Liquid pump was used the purge liquid to the rock being lased. Rock samples

(sandstone or limestone) were placed in the tank and water was purged using the nozzle. Focused laser beam with 0.35" spot size was applied on sandstone/limestone with 5.34 kW laser power from 4 to 10 seconds in 2 second increment. The purging was coinciding with laser beam at the target.

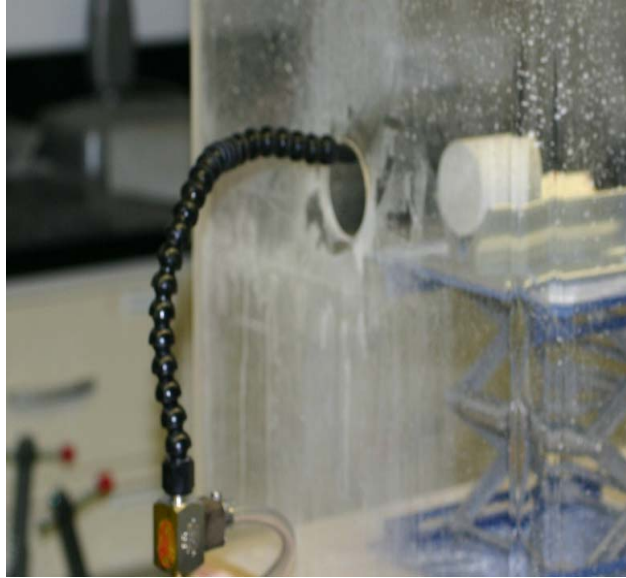


Figure 69. experimental set up for liquid purge test

Graph below shows the values of specific energy as function of lasing time for sandstone and limestone samples. SE values are high compared to air purge as can be seen from the comparison graphs. One of the reasons was the available pump capacity was not enough to purge liquid with similar force as in case of air purge (90 psi line pressure)

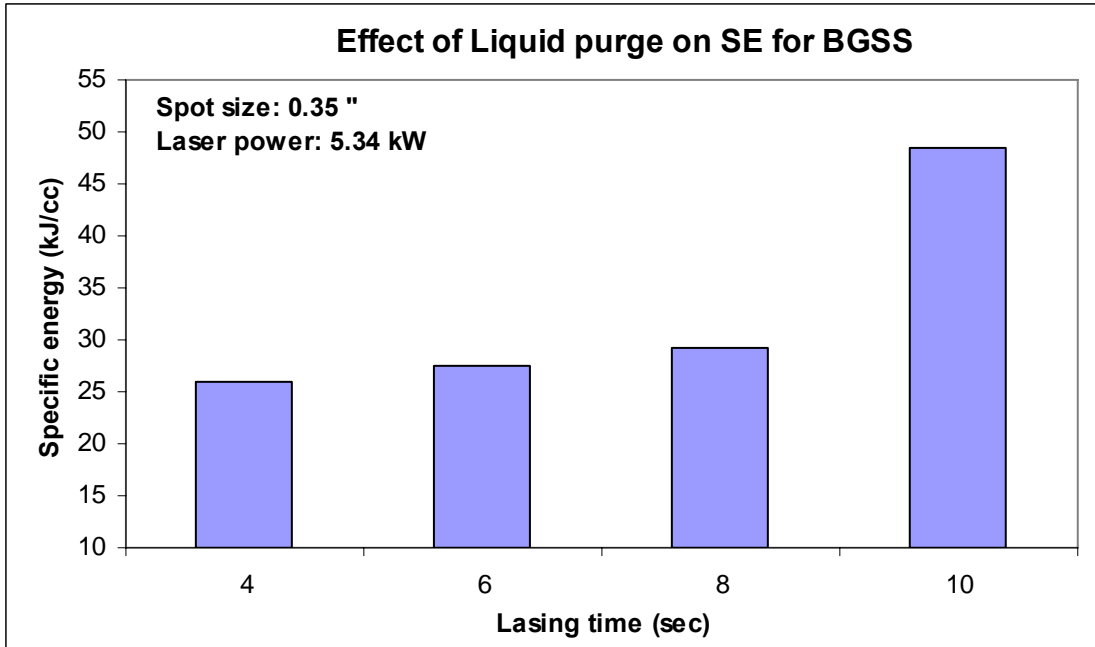


Figure 70. Effect of liquid purge as a function of time on SE for sandstone

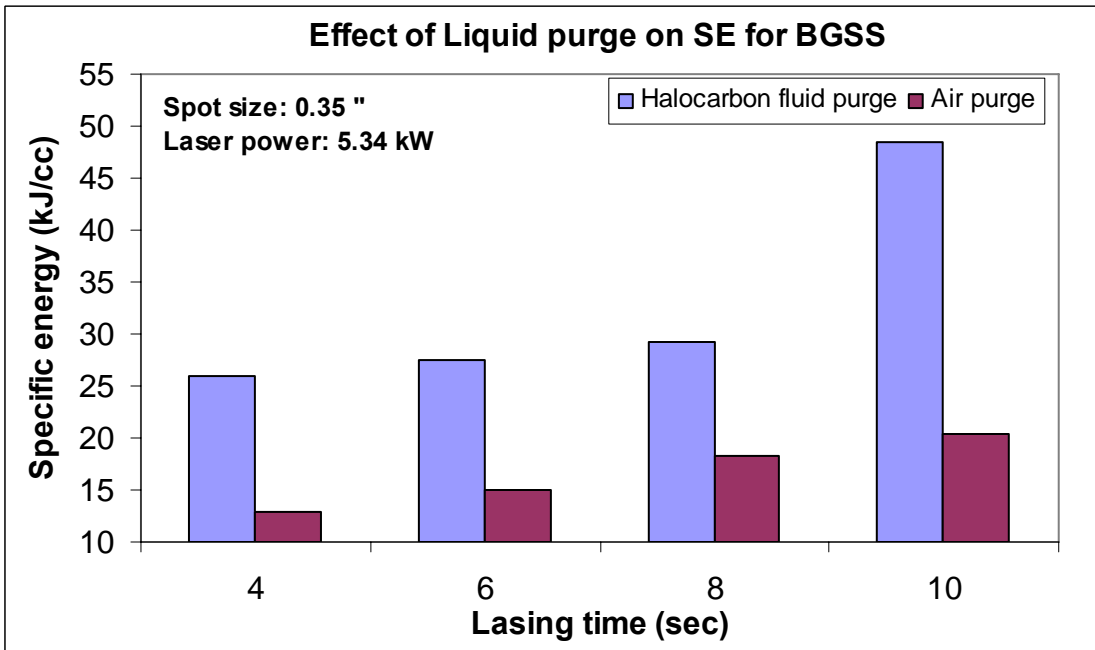


Figure 71. Comparison of air and liquid purge system as a function of time for sandstone

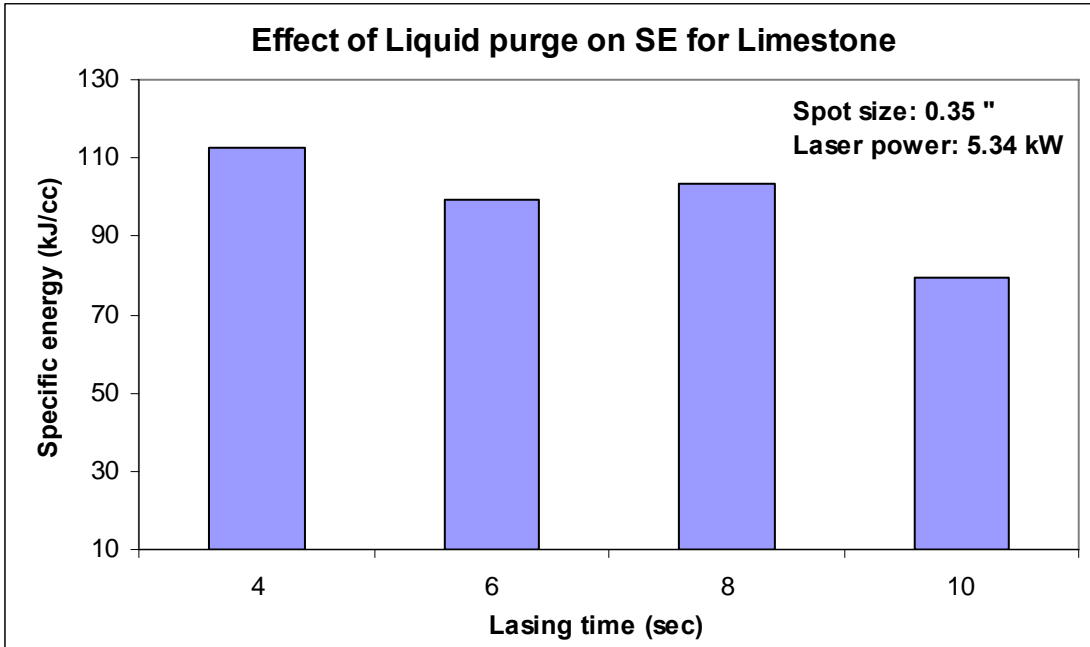


Figure 72. Effect of liquid purge on specific energy as a function of time for limestone

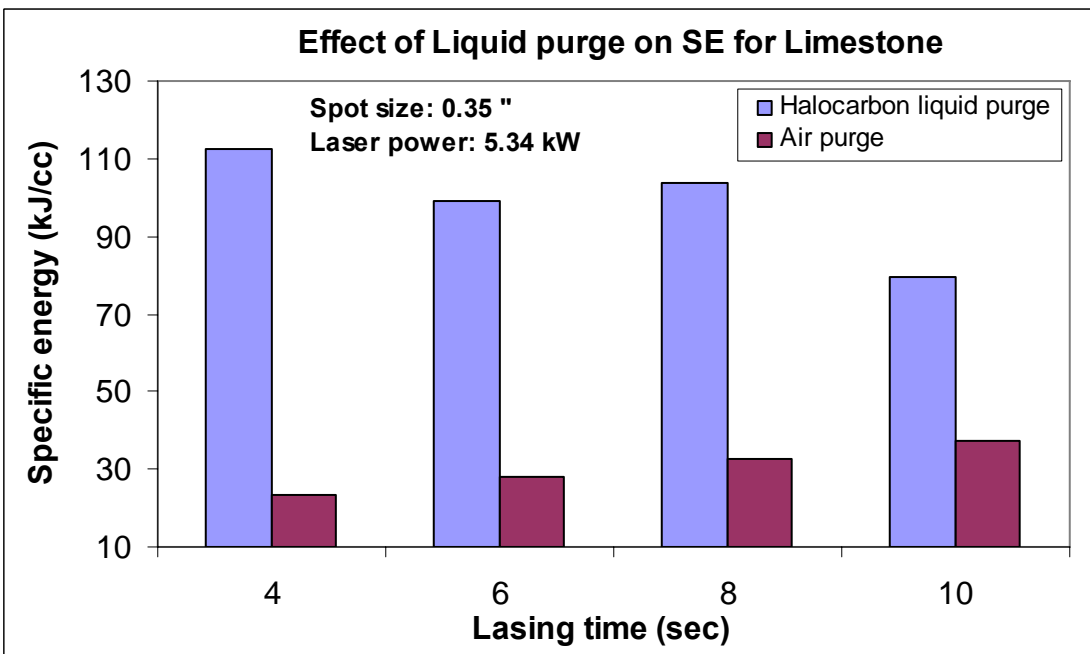


Figure 73. Comparison of air and liquid purge system as a function of time for limestone

Another set of experiment was conducted on sandstone/limestone material with same set up but by changing laser power level from 2 kW to 5 kW in increment of 1 kW. (40% to 100 % in increment of 20%) Focused laser beam with 0.35'' (8.9 mm) spot size was applied. Lasing time was kept constant at 4 seconds.

Graph shows the values of specific energy as a function of laser power level. Specific energy follows the same trend for liquid purge as air purge system. The values of specific energy are higher in case of liquid purge than air purge.

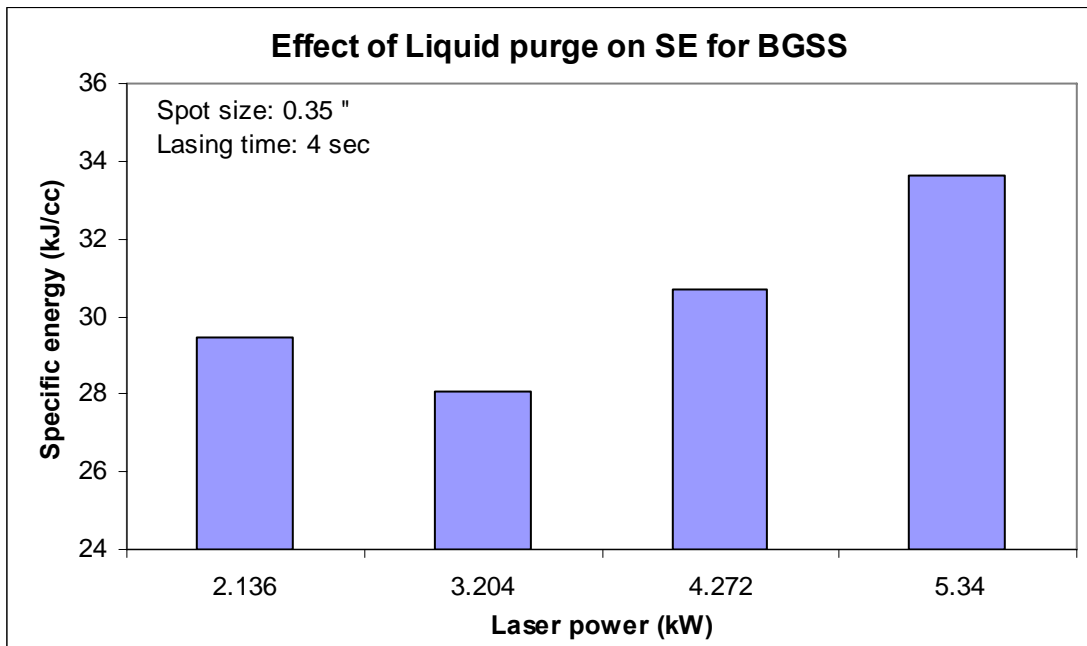


Figure 74. Effect of liquid purge on specific energy as a function of laser power for sandstone

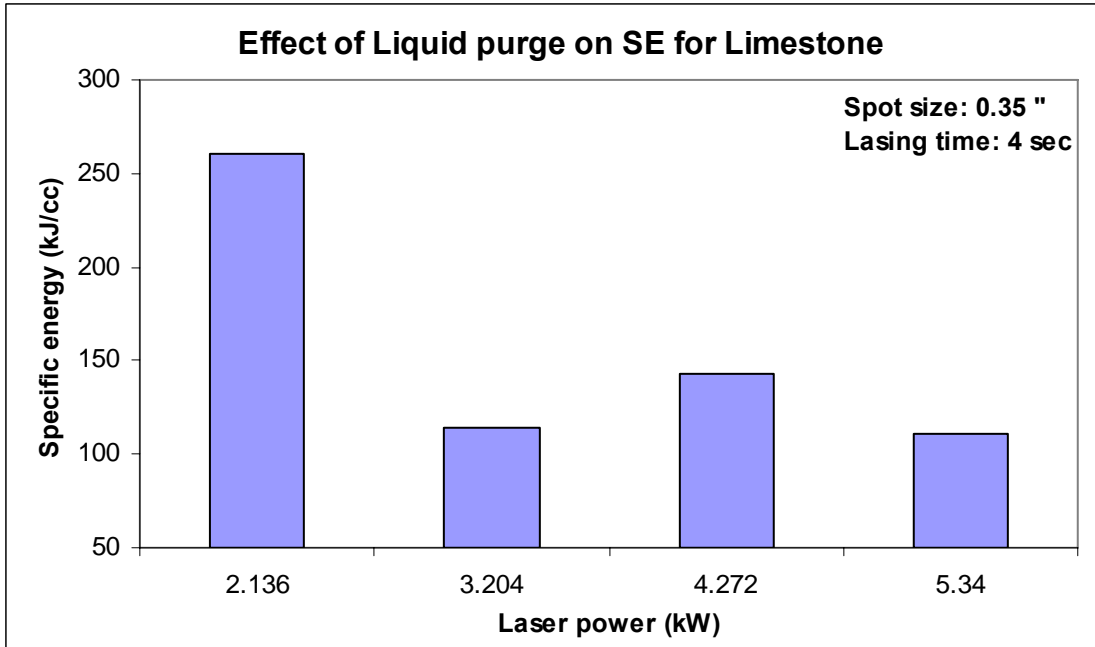


Figure 75. Effect of liquid purge on specific energy as a function of laser power for limestone

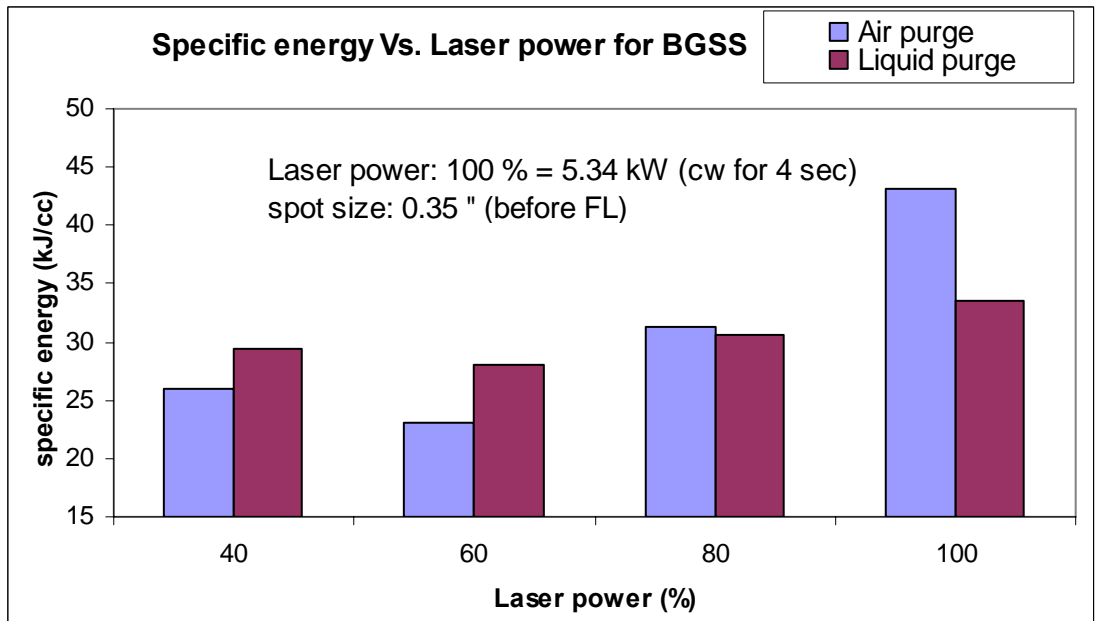


Figure 76. Comparison of air and liquid purge system as a function of laser power for sandstone

Result and Analysis:

Halocarbon fluid is toxic when exposed to high temperature (300 °F, safety sheet of halocarbon). Special design should be applied to handle this hazard fumes and fluids. The primary test was conducted as shown in the figures above to confirm the ability of laser to penetrate fluid and interact with the laser.

Future design in the second phase will be design to allow all the experiments to be conducted in the fluid environment without any risk.

Effect of laser power on Specific Energy (Collimated beam)

Objective: To determine the effect of laser power on limestone and sandstone material for collimated beam (0.35")

Procedure:

The purpose of this test is to study the effect of laser power with collimated beam by varying the laser power from 0.5 to 5 kW on limestone and sandstone samples and keeping the time constant (4 sec and 8 sec). Limestone and sandstone blocks of size 20 x 6 x 6 inch were used in this study. One of the 20 x 6 inch surfaces was divided into 1 x 1 inch grids. Each grid was lased at different power level from 0.5 to 5 kW in 0.5 kW increment. The lasing time of each hole was kept constant at 4 seconds and 8 seconds for two sets of experiment. Collimator lens assembly was used to deliver 0.35" collimated beam (CW). Sample was placed in waste area (Highest intensity for given collimation) of beam. Gas nozzle in concentric position was used as purge system. Air was used as purge gas with 90 psi line pressure. Distance between purge and sample was about 1". Specific energy values were calculated and are presented in figure below.

Observation: For limestone, collimated beam did not create any perforation up to 2 kW power level for both 4 and 8 seconds lasing time. Sandstone surface was affected above 1 kW power level for both 4 and 8 second cases. Graph below (figure 79) shows comparison of specific energy for focused and collimated beam for 8 second lasing time in case of sandstone and limestone.

Result and Analysis:

Knowing that Limestone dissociate and there is no quartz or very less quantity of quartz in lime stone, the more power results in more dissociation. Comparing the lasing time when collimated beam was used, the 8 seconds consumes less SE due to the direct relationship of energy on the sample and mass removed for Limestone.

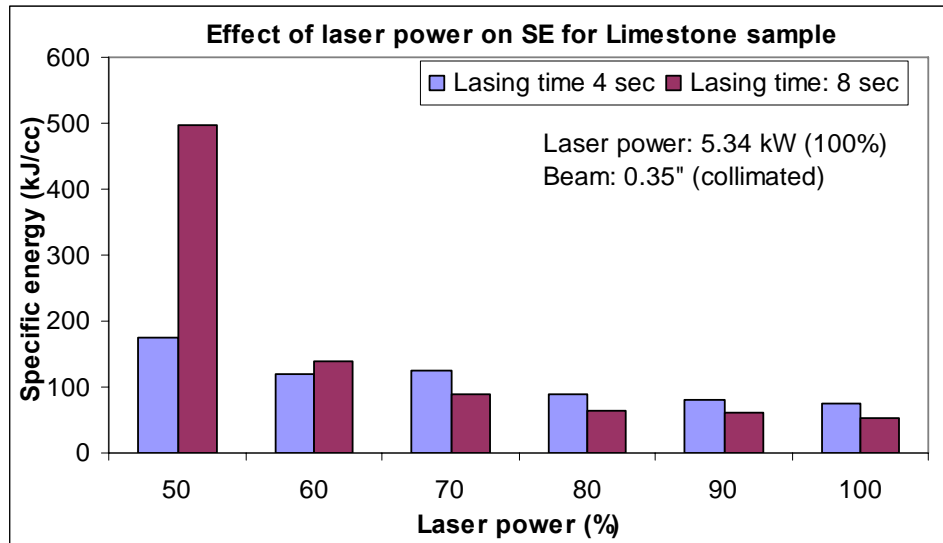


Figure 79. Comparison of 4 second and 8 seconds when using collimated beam for Limestone and increasing the power from 50 to 100% at an increment of 10%

When comparing the effect of focused beam vs collimated on Limestone, the result show that collimated consumed more SE due to the less intensity and therefore less energy delivered to the sample. The result is presented in Figure 80. At full power, the more intensity is created and the SE value of both focused and collimated is similar.

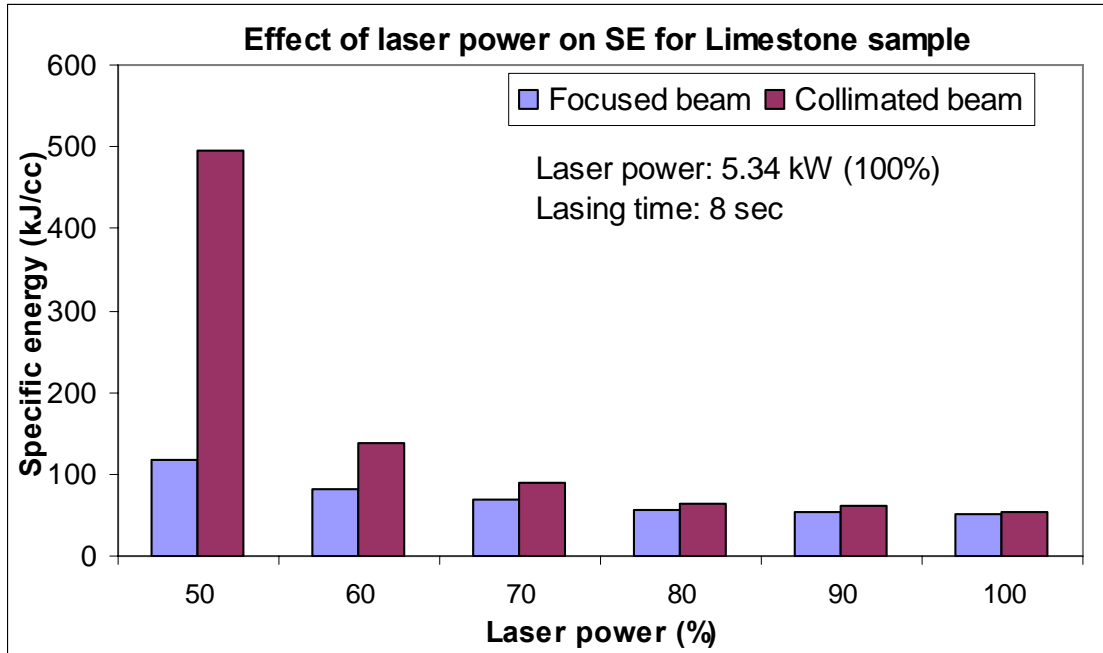


Figure 80. Comparison of collimated and focused beam for 8 seconds for Limestone and increasing the power from 50 to 100% at an increment of 10%

When comparing 8 seconds and 4 seconds lasing time for Sandstone using collimated beam, the result showed that 8 seconds consumes more SE because the more lasing time on the samples result in more heat and melting of the quartz. The result is presented in figure 81.

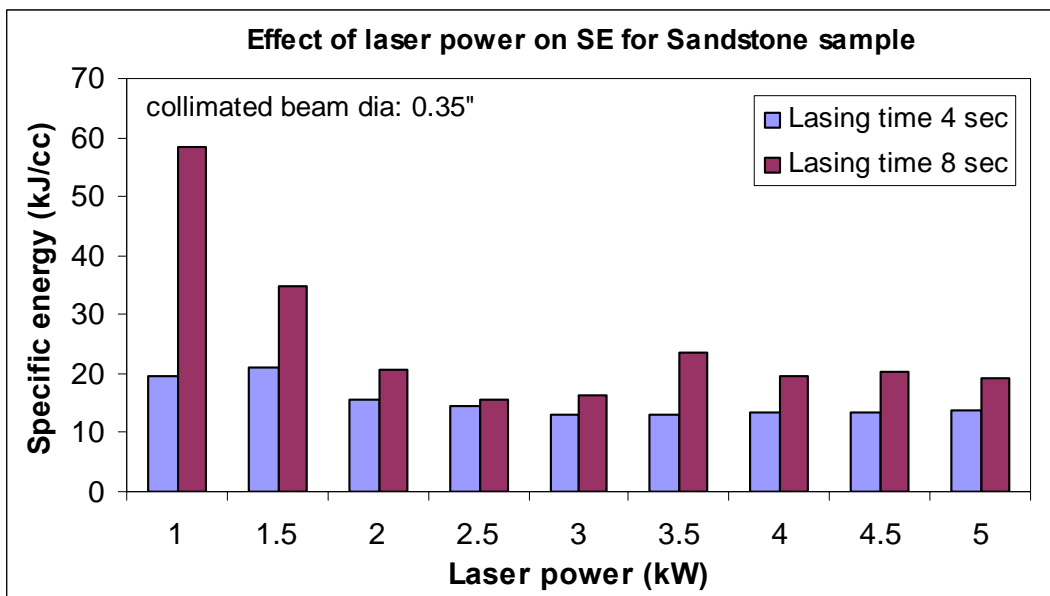


Figure 81. Comparison of 4 second and 8 seconds when using collimated beam for Sandstone and increasing the power from 1 to 5 kW at an increment of 0.5 kW.

Comparing collimated and focused beam can be seen in figure 82. The result show that focused beam has higher values than collimated, the unlike the focused beam, the collimated beam distribute the beam uniformly on the sample, therefore less intensity and the melt is avoided.

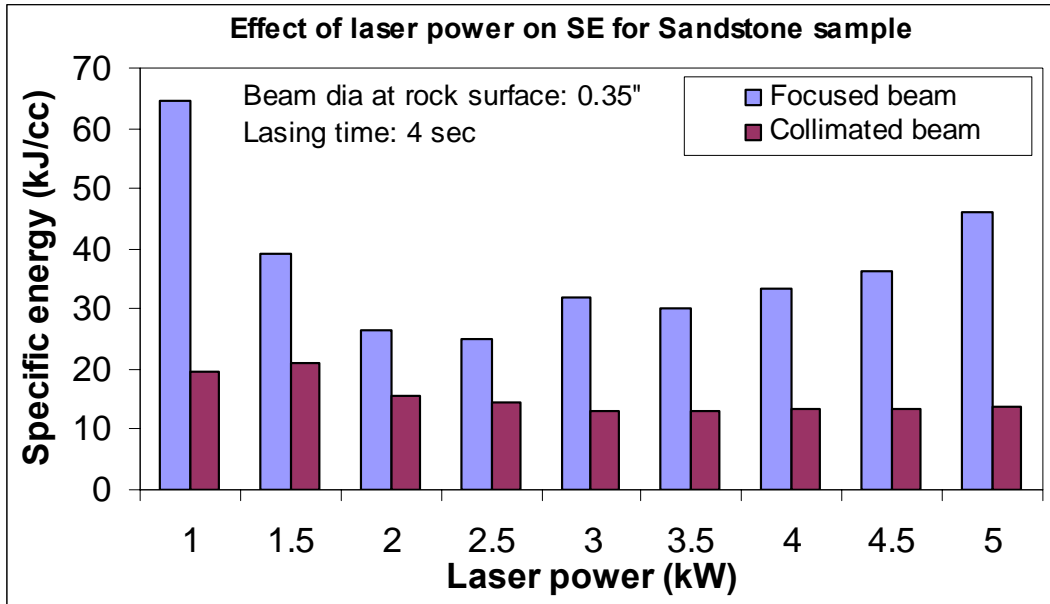


Figure 82. Comparison of collimated and focused beam for 4 seconds for Sandstone and increasing the power from 1 to 5 kW at an increment of 0.5kW.

The beam shape can be seen in figure 83, where the beam shows flat surface which indicates uniform distribution of the energy.

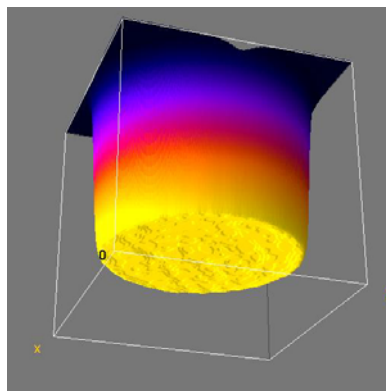


Figure 83. Collimated laser beam showing uniform energy distribution of HPFL.

Effect of lasing time on Specific Energy (collimated beam)

Objective: To find the effect of lasing time on limestone and sandstone material with collimated beam (0.35" diameter)

Procedure:

The purpose of this test is to study the effect of beam duration exposed to the sample, varying the time from 1 to 20 seconds on limestone and sandstone samples. Limestone and sandstone blocks of size 20 x 6 x 6 inch were used in this study. One of the 20 x 6 inch surfaces was divided into 1 x 1 inch grids. Each grid was lased at 5.34 kW laser power. The lasing time of each hole was increased incrementally by two second starting from 2 second up to 20 seconds. Collimator lens assembly as figure 84 was used to deliver 0.35" collimated beam. Gas nozzle in concentric position was used as purge system. Air was used as purge gas with 90 psi line pressure. Distance between purge and sample was about 1". Lens with 1000 mm focal length was used to focus 1" collimated beam. Same set of experiments were repeated for sandstone with 3 kW power level. Specific energy values were calculated and are presented in figure below.

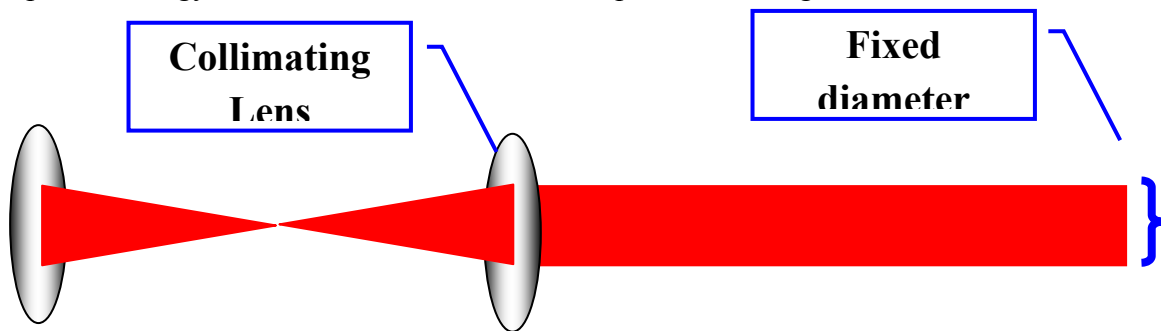


Figure 84. Collimator for HPFL collimates beam from 0.25" to 1"

An increase in the lasing time resulted in increasing specific energy values and deeper holes were obtained. The result shows the same trend for sandstones, although less energy was consumed.

Result and Analysis:

The difference between the focused beam and the collimated is the shape of the beam, the focused beam has a conical shape while the collimated beam is a cylindrical shape and the beam size and waste does not change in theory. Figure 85 presents the result of lasing using 0.35" collimated beam at two powers, at 3 and 5 kW. The trend shows that at 3 kW consumes less SE.

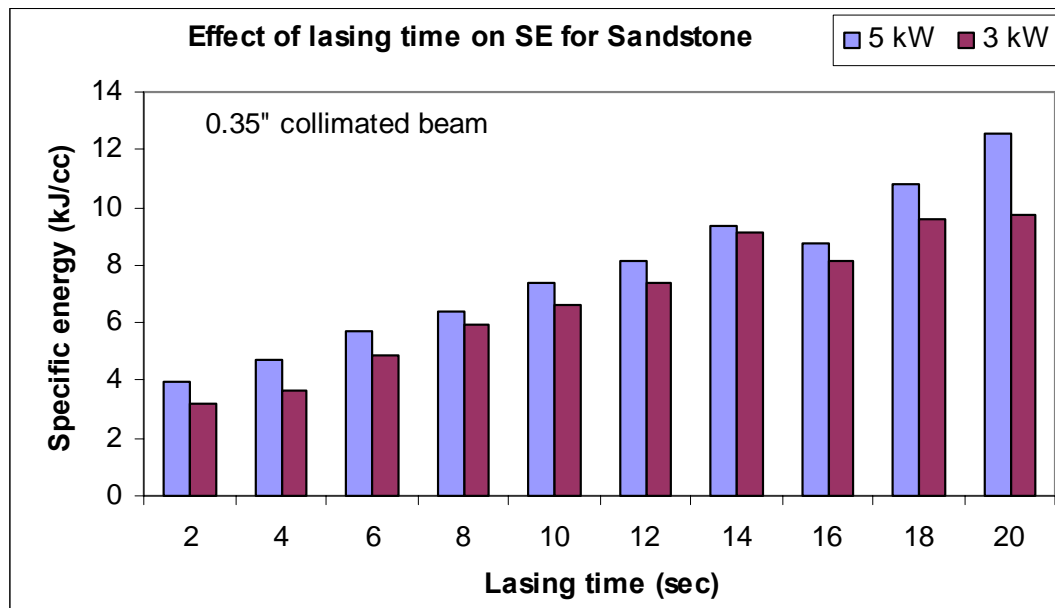


Figure 85. Collimated beam of Sandstone sample lased at 3 and 5 kW using HPFL.

The result shows that there is an increase in power result in an increase in SE due to the directly proportional relationship between SE and power. Also as the time increases, the SE increased as well. Sandstone spall at lower energy and melt a higher energy, if spallation takes place, the particles will break off the matrix and with the help of the purging system, they will be carried out the hole and absorb energy from the laser. When comparing both collimated and focused beam regarding SE values, the result is presented in Figure 86.

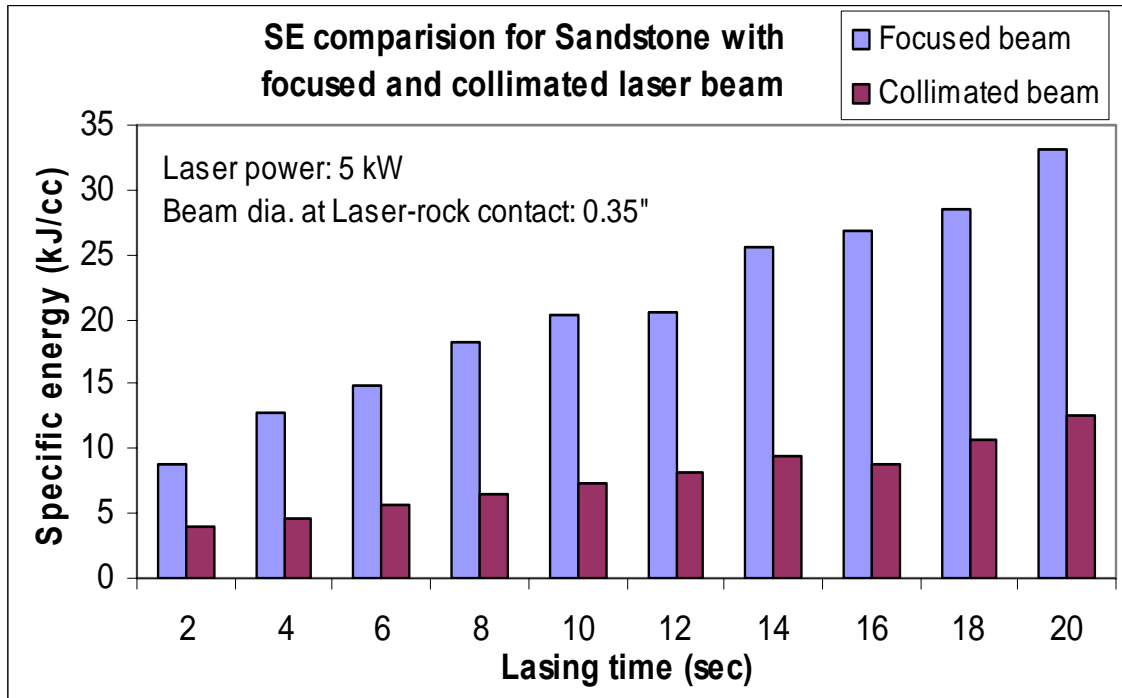


Figure 86. Comparison of focused and collimated beam when increasing the time from 1 to 20 seconds at an increment of 1 second.

The results shows that as time of lasing increases, the SE values for collimated beam is less than the focused beam, this is due to the shape of the beam, the focused beam is a conical shape which leads to maximum power at the tip of the beam due to an increase of beam intensity. Figure 87.

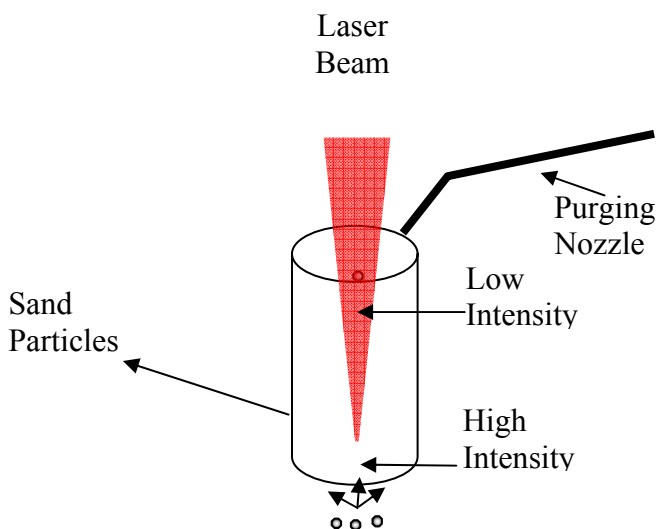


Figure 87. Focused beam shape of HPFL showing higher intensity at the tip of the beam.

The high intensity of the beam when interact with Sandstone result in melting the quartz and forming melt materials that absorbed the energy.

The second experiment was conducted on Limestone at 5 kW, the limestone requires more energy in order to dissociate, the result shows that an increase in lasing time result in decrease in SE because more time in the case of Limestone means more material removed and dissociate. Figure 88.

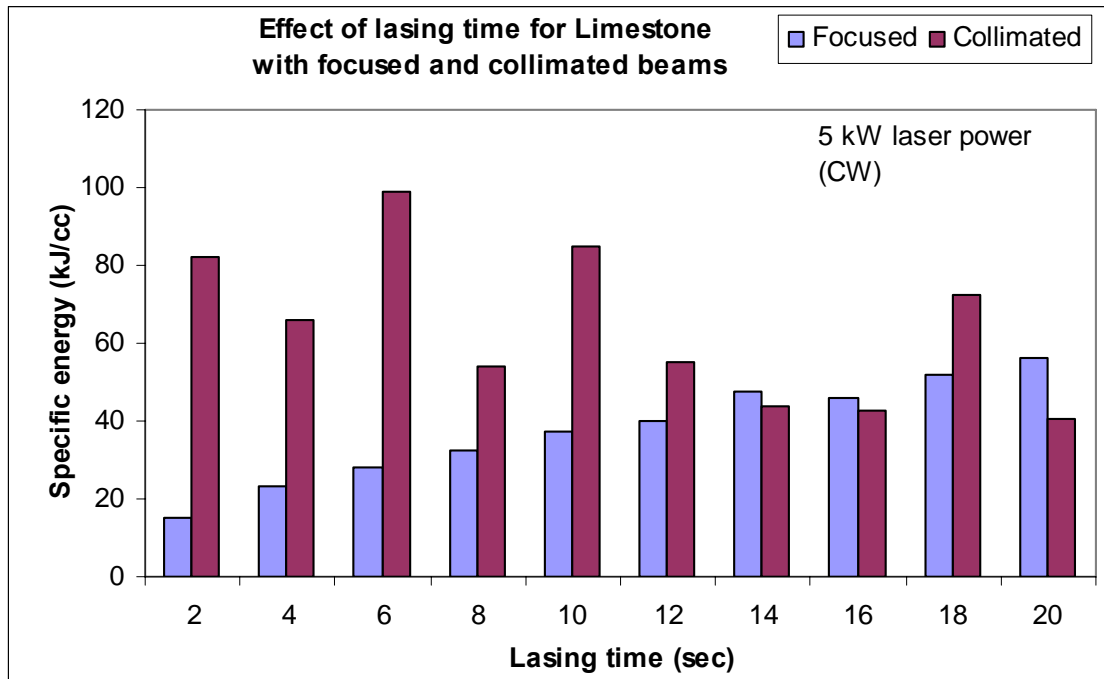


Figure 88. Comparison of focused and collimated beam when increasing the time from 1 to 20 seconds at an increment of 1 second

High pressure perforation:

Objective:

To simulate perforation under down hole conditions by applying axial, pore and confining pressures on sandstone and limestone core samples.

Background:

Concept of high pressure perforation cell had been developed at gti and tested several time before it was built.

Concept testing included

- Simultaneous application of axial, confining and pore pressure
- Testing of effective purge system under confined volume at high pressure (Removing debris from confined volume at high pressure was a major issue)

- Lasing core inside a cell at high pressure with minimum temperature rise of cell parts (safety issue)

All assembly parts are as shown in figure. This cell is rated for 3000 psi pressure and had been tested for 4500 psi pressure by manufacturer.

Spare o-rings, spacers and handling tools were ordered.

Pressure transducers for confining, axial and pore pressure ports were calibrated, connected to cell assembly and tested for tri-axially (confining and axial) pressurized conditions.

High Pressure Cell Design and Development:

When designing the high pressure perforation, the following concerns were encountered due to the unique application and complexity of the operation.

- 1- Safety
- 2- Pore Pressure flexibility
- 3- Purging with tri axial
- 4- Lenses clearance

Dealing with high pressure perforation cell under high pressure condition and with high power laser beam to interact is a serious safety issue. Also the ability to apply pore pressure, purging with tri axial stress and keeping the lens clean was a challenge that required a careful design, keeping in mind that the system is closed system and the beam required to access the sample so the laser perforation can take place. The original design for the high pressure was a conventional tri axial cell that is used for flow measurement. Figure 89. Evaluation of this cell and the idea to modify it to accommodate high the laser was discussed in detail and declined.

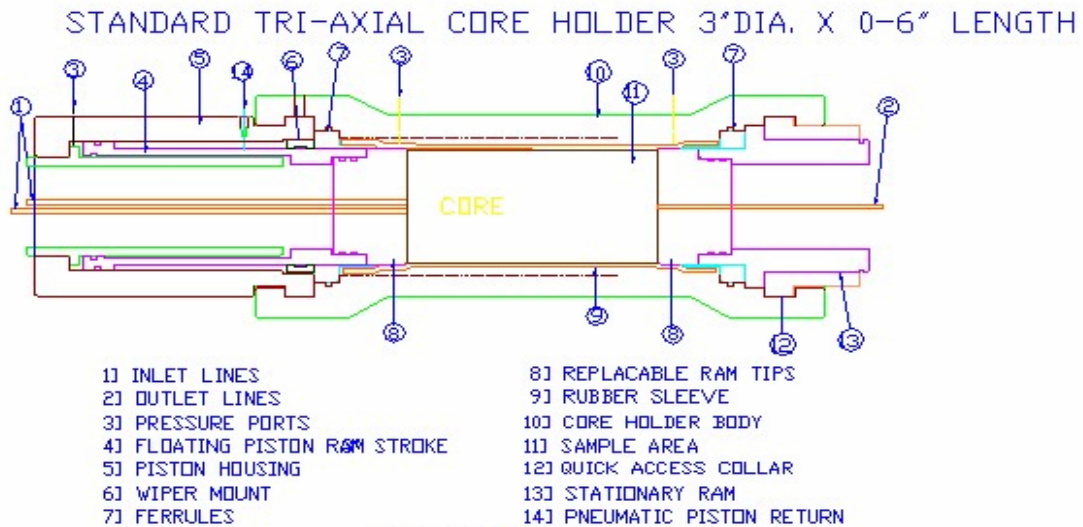


Figure 89. The original design of high pressure perforation cell that was not suitable for high power laser perforation.

For safety, the following steps were taken:

- 1- Prove of concept
- 2- Add Compartment to the cell
- 3- Relief valve

Prove of concepts experiments were design and tested by building a tube that has cover lens to see if the cover lens will accumulate dust and block the beam. Figure 90. The experiment took place by placing the sample inside the tube and aiming the beam on the sample through the cover window. There are ventilations holes for the particles to escape as seen in figure 1. The result was as expected, the dust accumulated on the cover lens and blocks the beam to pass through the cover windows, which resulted in heating up the glass and broke it. Figure 91 shows the lens before and the lens after lasing which is damaged.

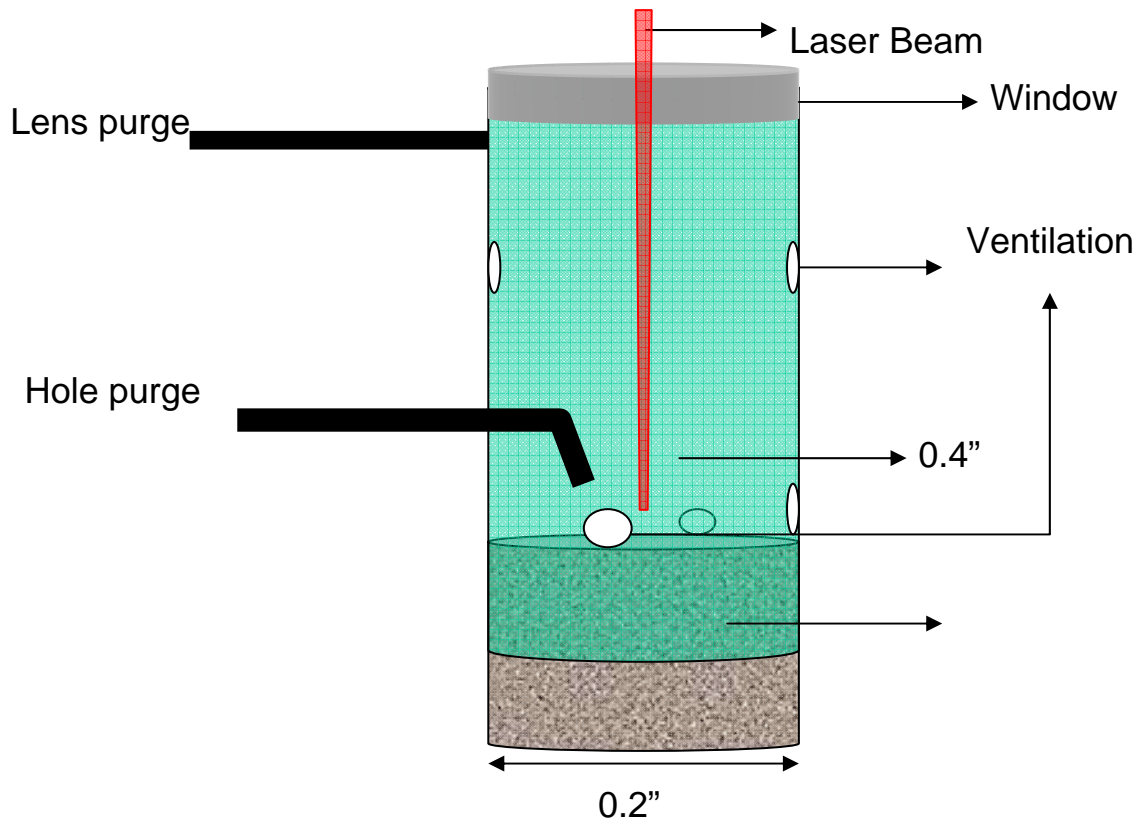


Figure 90. High pressure perforation cell prove of concept tube with a cover lens.

Before lasing

After lasing

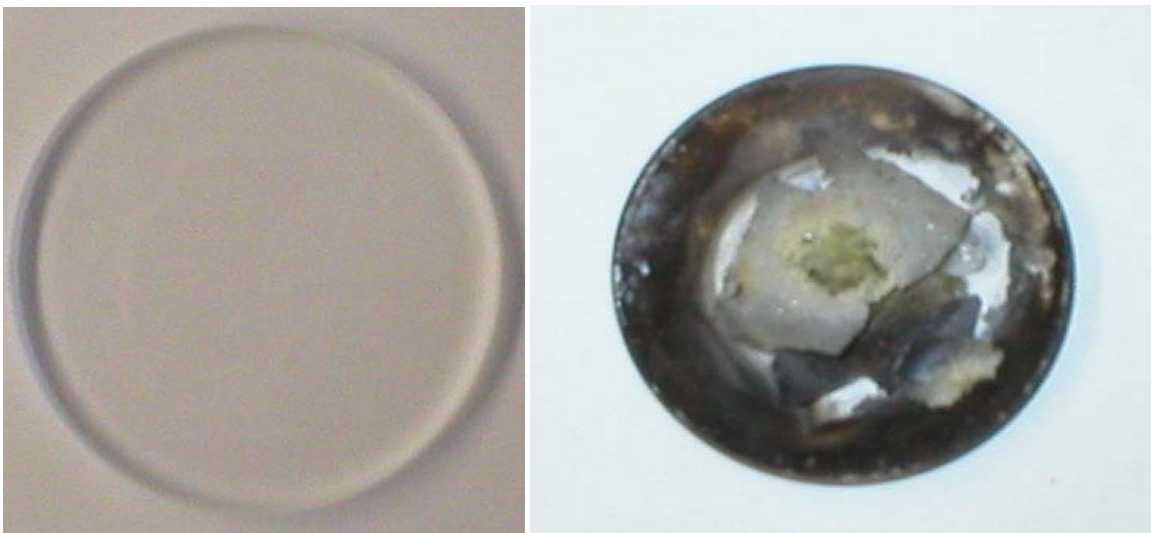


Figure 91. High pressure perforation cell cover lenses before and after lasing for prove of concept experiment.

Since lasing through tube will result in dust accumulation and blocking the beam, the cone structure was the another idea needed to be evaluated and investigated, the same tube was set again with a cone inserted in it, and a cover lens from one end and the sample from the other end. The purging tube was inserted on top where beneath the cover lens above the tube, this way the cone will direct the flow through the opening of the cone co axial with the beam directly to the sample. Figure 92.

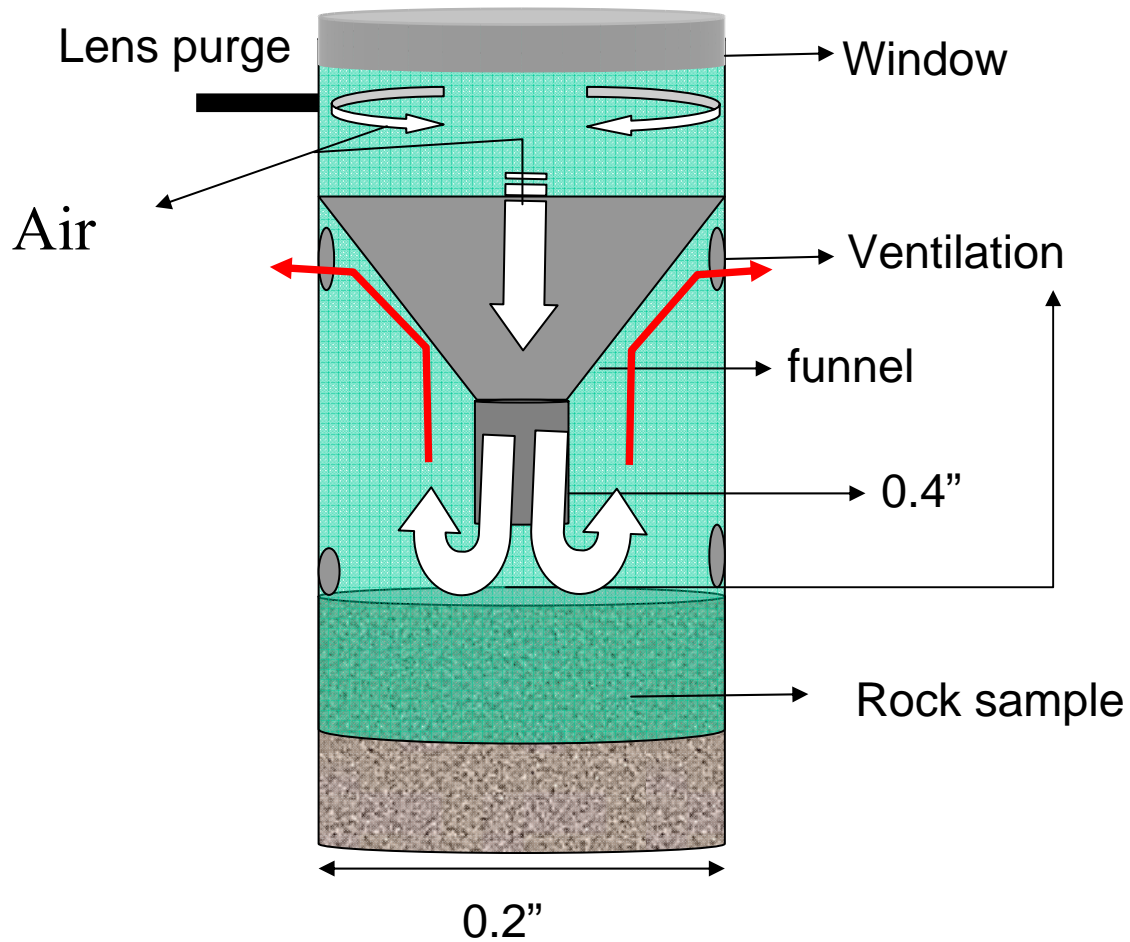


Figure 92. High pressure perforation cell prove of concept tube, cone and a cover lens.

There are ventilation placed on around the tube beneath the cone which will allow the dust and the particles to clear out. Also the shape of the cone act as restricted path for the beam and the air to go through it and block the particles to flow against the air flow due to the small surface area. Figure 93 shows the actual set up for the cone structure. And figure 94 shows the chamber when the laser is on.

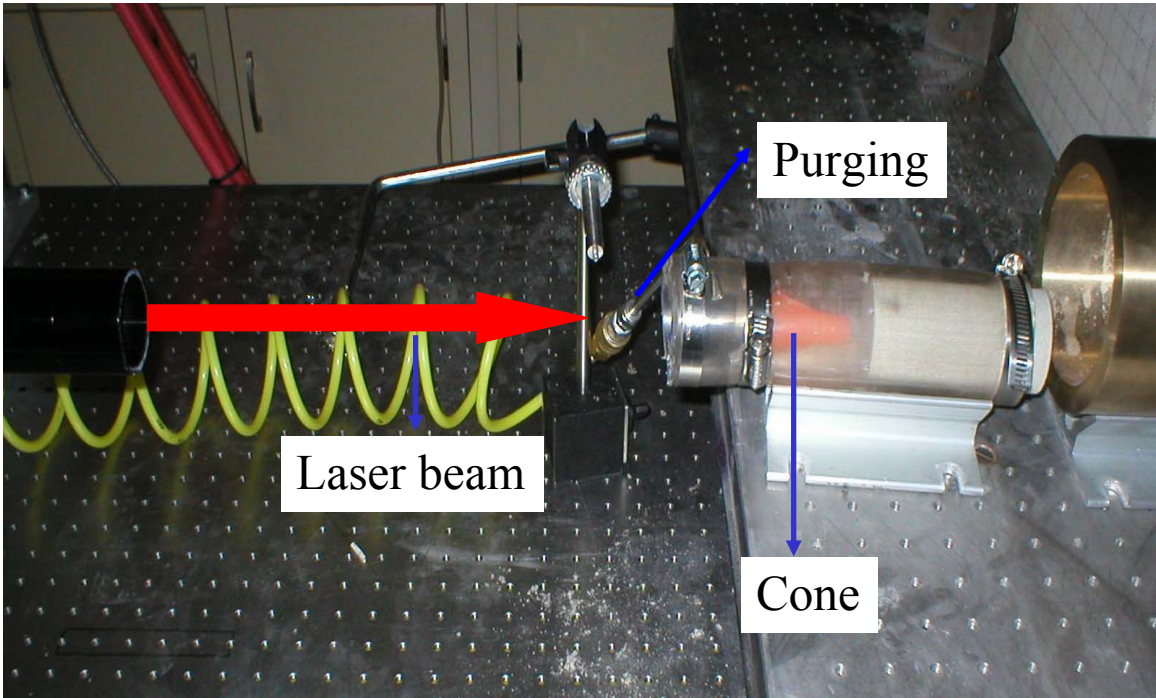


Figure 93 shows the actual set up for the cone structure

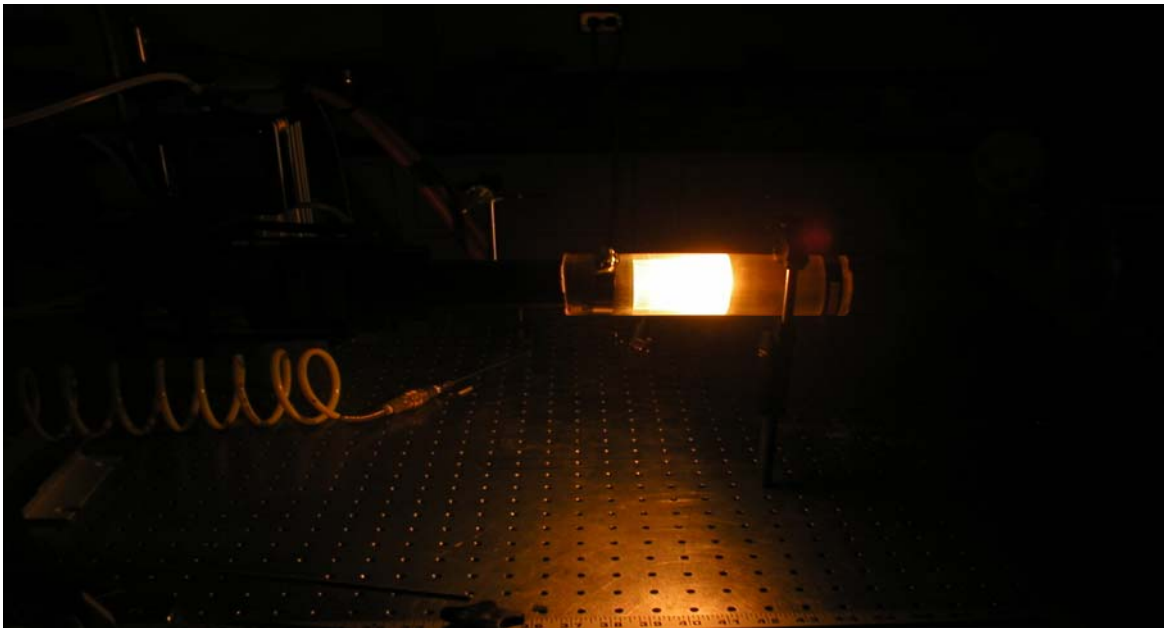
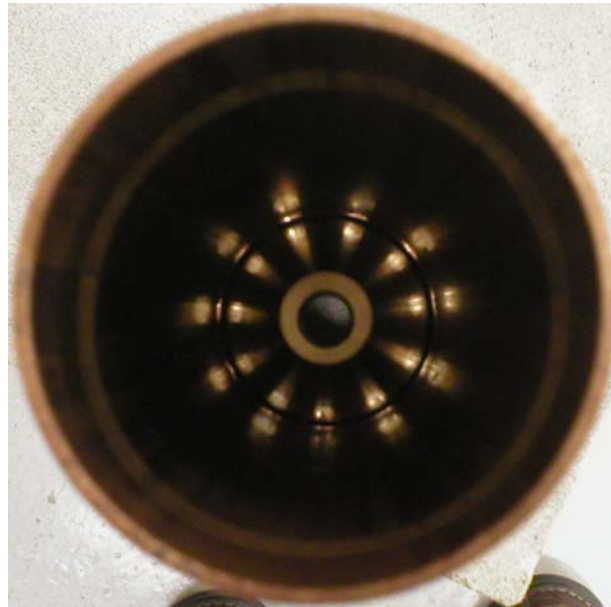


figure 94 shows the chamber when the laser is on.

The cone was inserted in a transparent tube for visibility purposes and monitoring the particles and dust behavior in the tube for improvement and modification purposes if they needed. The last design which includes the distance between the cover lens and the surface of the sample, the purging angle and ventilation opening size was decided and known, a metal tube was design and tested using the optimized dimensions, Figure 95 A and B. In the figure A, the outside of the tube showing the ventilation holes, and in B the inside structure showing the cone and the ventilations..



A



B

Figure 95. Cone structure in metal for the high pressure cell, A shows the outside and B is the inside showing the cone and the ventilation structure.

Figure 96 shows the connection of the tube with the purging system ready for the laser beam. And figure 97 shows the tube in the dust chamber before lasing.

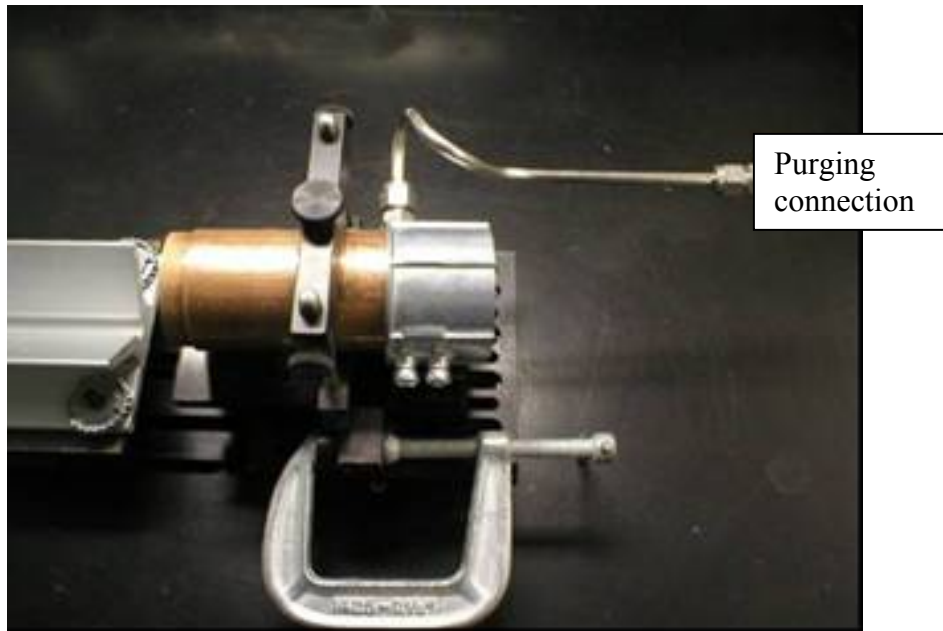


Figure 96. Metal tube with the purging connection.

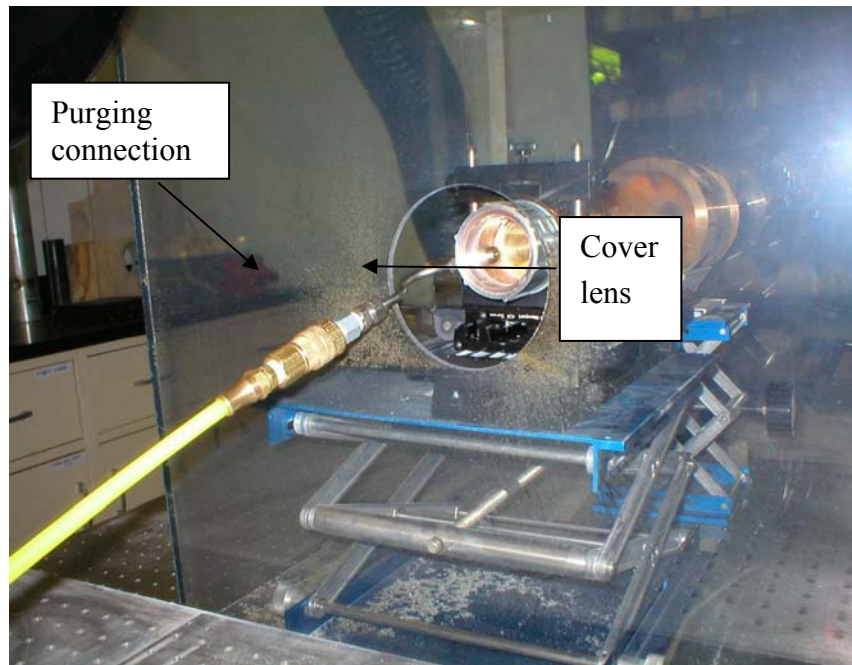


Figure 97. Metal tube with the sample, purging and cover lens in the dust chamber ready for the laser.

The design at this point should consist of cone structure in the chamber, chambers for safety; relieve valves, tri axial, pore pressure and purging capability as seen in figure 98.

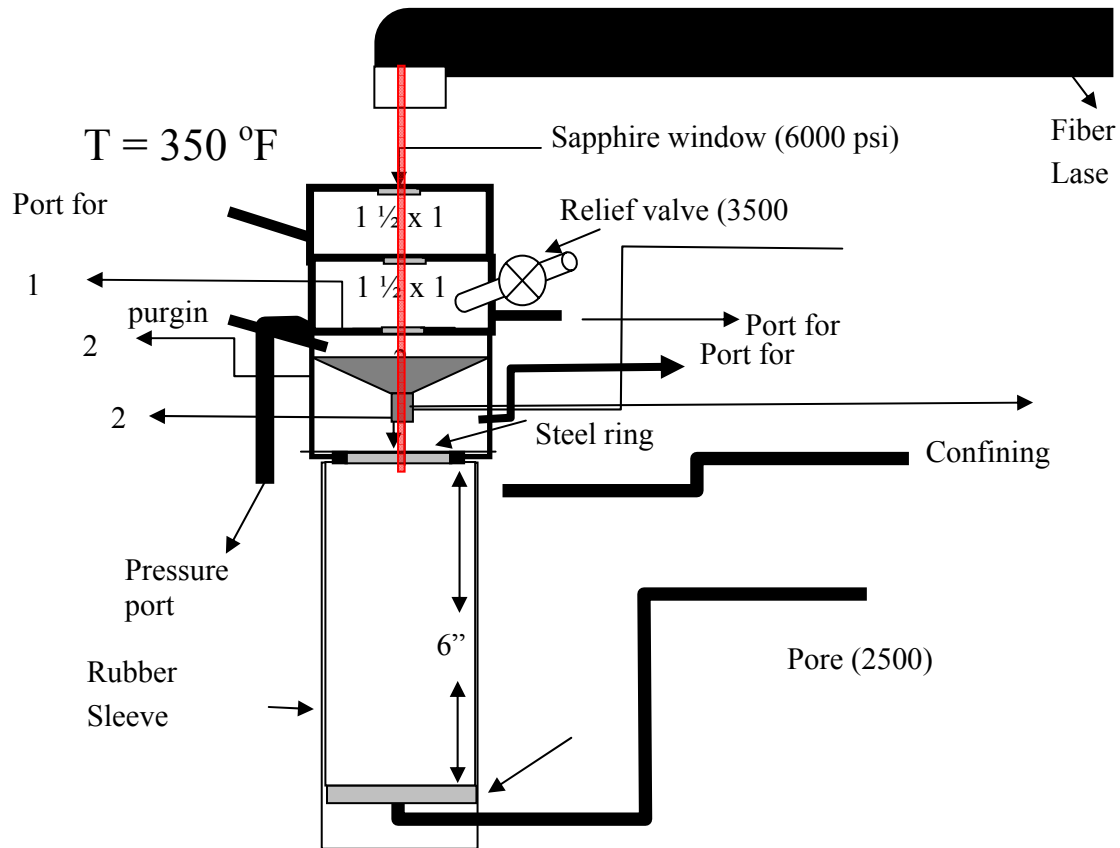


Figure 98. High pressure perforation cell tri axial, pore pressure, under and over balance conditions.

The High pressure perforation cell has the flexibility to

1. Perforate under or over balance up to 3000 psi
2. Pore pressure, tri axial conditions
3. Purge with fluid or gas
4. Samples up to 4" in diameter with 6" length
5. Clad samples (Rock, cement and casing)

The 3 chambers and for applying wellbore pressure for over balance and for safety concerns, there are sapphire windows between each chambers that can handle up to 6000

psi. The second and third chamber is for safety incase the sapphire windows breaks. Also there are relief valves to allow access pressure to exit the cell.

The final design of the high pressure is presented in figure 99. The actual cell can be seen in figure 100 where the high pressure cell is fully operational in the lab.

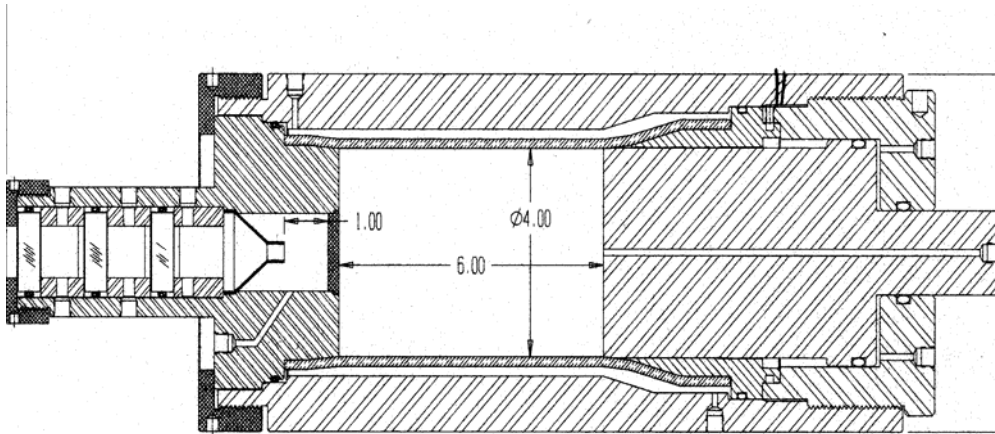


Figure 99. High pressure perforation cell tri axial, pore pressure, under and over balance conditions final design.

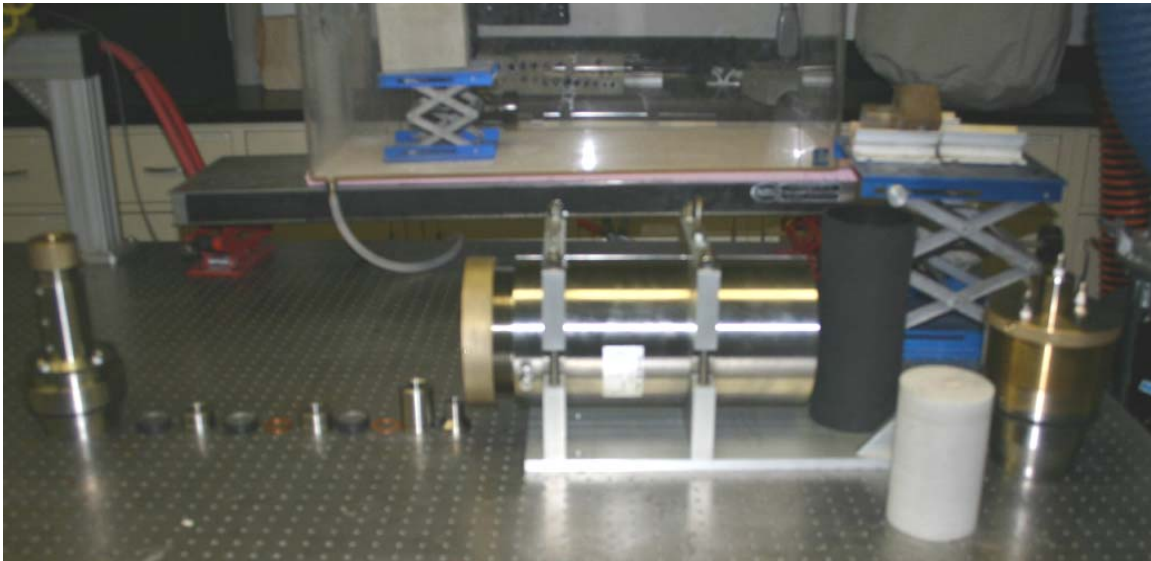


Figure 100. High pressure perforation cell tri axial, pore pressure, under and over balance conditions actual cell in the lab.

Procedure:

Boundary effect experiments on sandstone and limestone confirmed no periphery effect for 0.35" spot size on 4" diameter cores. Hence, High pressure cell was designed for core samples of size 4" in diameter 6" in height. For all the experiments, spot size, lasing time and power level were kept constant at 0.35", 8 seconds and 5.34 kW respectively.

Sandstone/Limestone core sample (4" diameter X 6" height) was placed in high pressure perforation cell. Cell was pressurized for confining and axial pressures up to 2000 psi for first set of experiments. Second set of experiment was done by applying confining, axial and pore pressures up to 2000 psi. Gas nozzle with 90 psi line pressure was used as purge in first case whereas there was no purge used in second case as pore pressure was enough to drive the debris out.

Figure 102 shows the experimental set up and figure 102 shows the high pressure cell when the laser is on. Focused laser beam at 5.34 kW power was applied to the sample for 8 seconds. Spot size was kept 0.35". Calculated specific energy for this shot was 7.78 kJ/cc. Also the hole created was clean with no cracks or melt formation. Similar shots at ambient pressure had shown this value to be 18.2 kJ/cc.

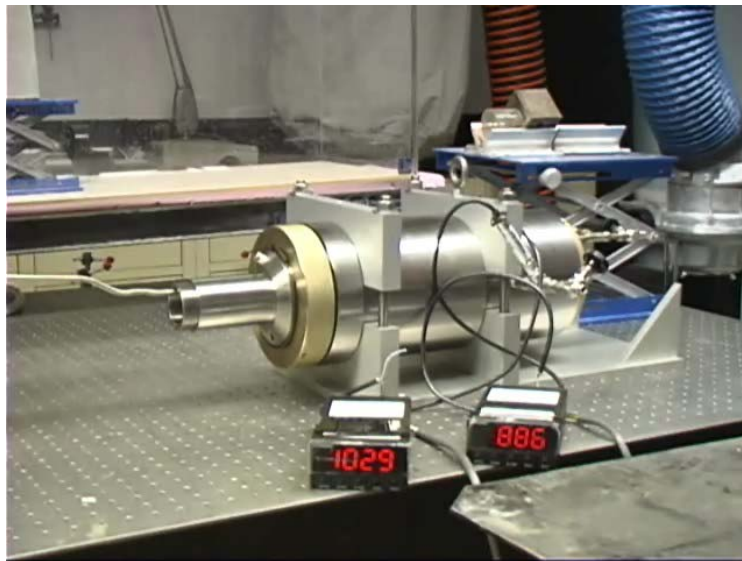


Figure 101. Experimental set up for perforation test in high pressure perforation cell

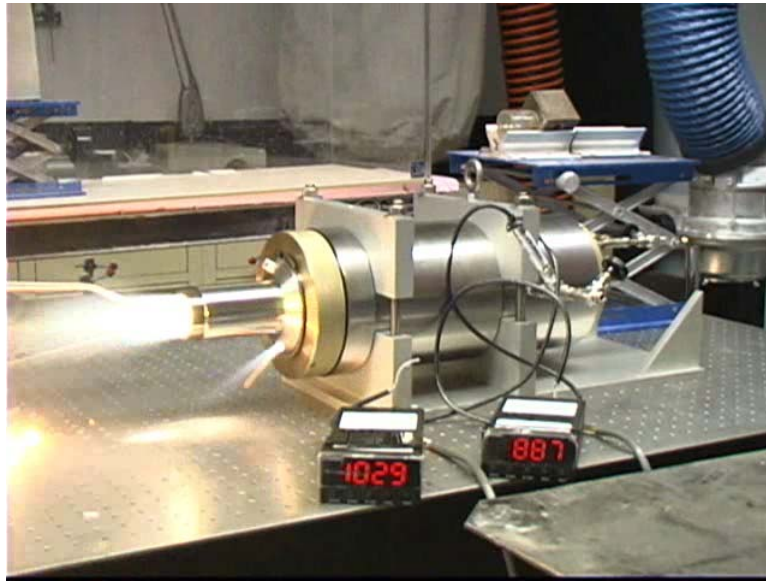


Figure 102. Perforation test in progress

Result and Analysis:

Figure 103 and figure 104 respectively presents sandstone and limestone at different lasing conditions, No pressure indicates the lasing conditions in the high pressure cell without any pressure or stress, the reason for that is for consistency when comparison is made so the all the measurements and the data are taken from the same core holder under identical condition in terms of purging system, core position and size. The test was conducted at different conditions, the No pressure indicates to the test and ambient condition, P_c indicates confining stress, P_a for axial pressure and P_p for pore pressure.

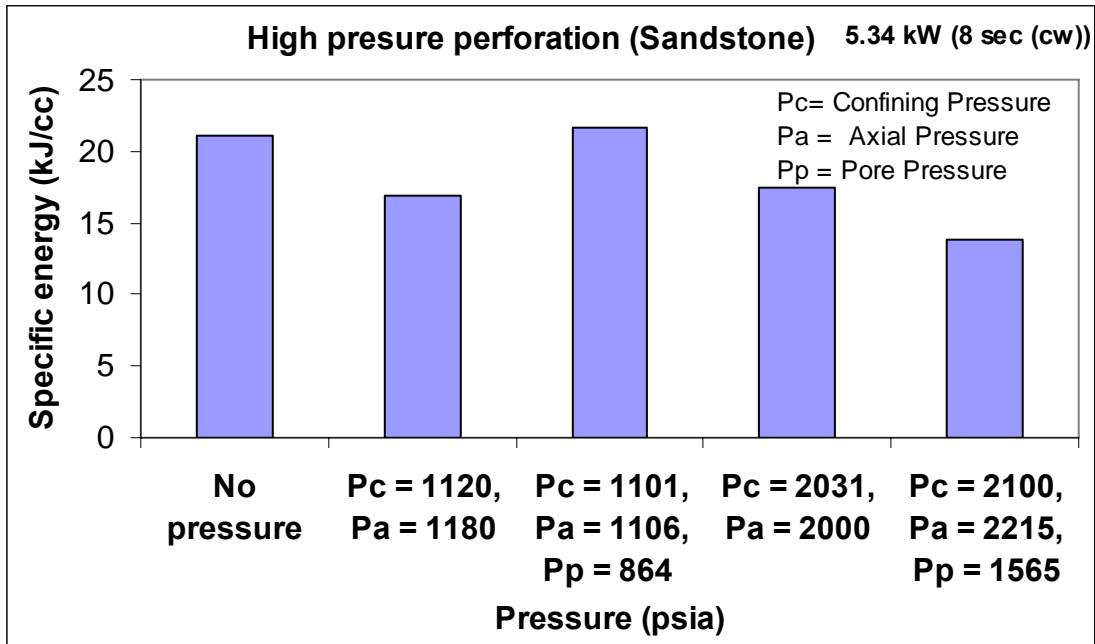


Figure 103. Comparison of Sandstone sample in the high pressure perforation cell at ambient conditions, confining pressure, axial and pore pressure.

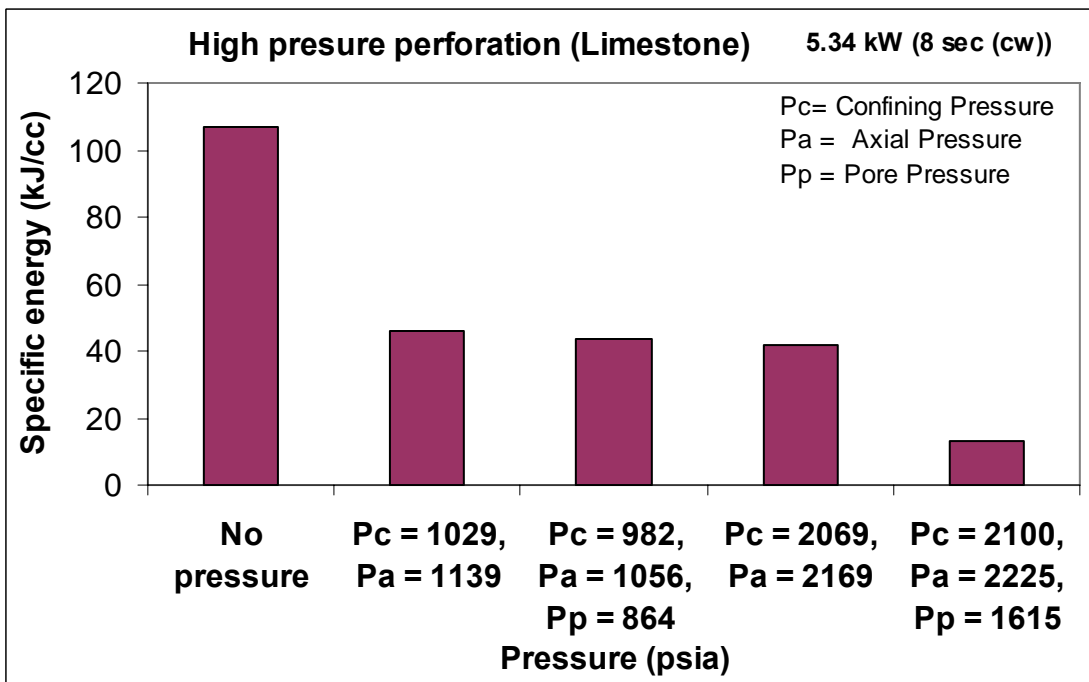


Figure 104. Comparison of limestone sample in the high pressure perforation cell at ambient conditions, confining pressure, axial and pore pressure.

For comparison, figure 103 and figure 104 are combined in figure 105, as seen below.

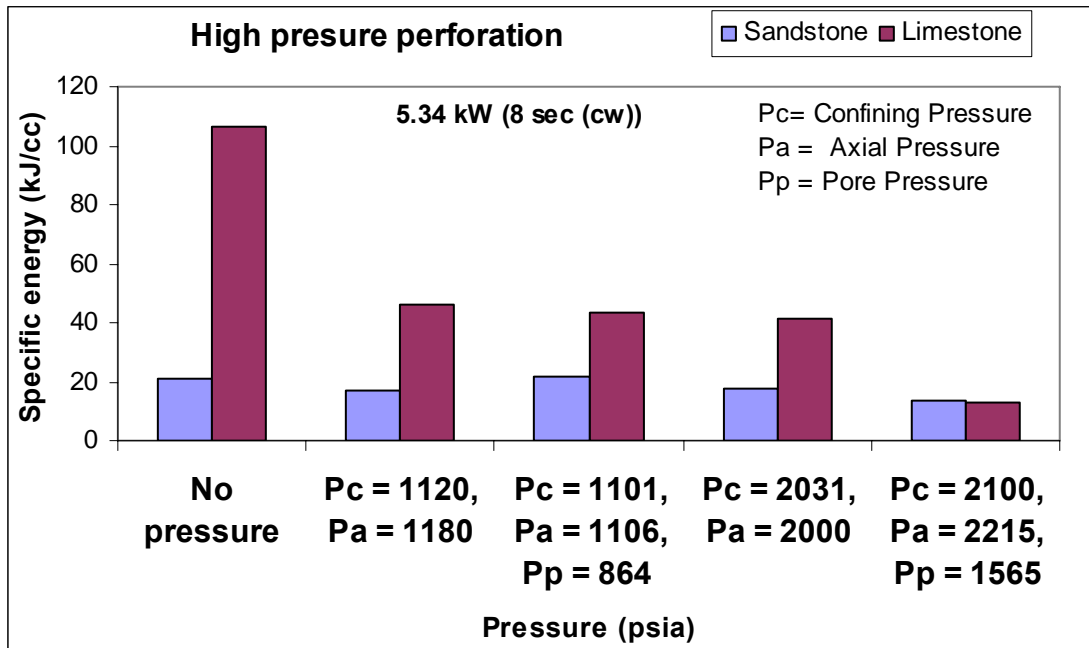


Figure 105. Comparison of Sandstone and limestone samples in the high pressure perforation cell at ambient conditions, confining pressure, axial and pore pressure.

When applying stress on rocks, the rock deforms and compact, depends on the elastic properties of the sample and the strength of the sample, in the case of the limestone that was used in this research is a quarry limestone which was at the surface and was not under any stress or over burden natural stress because of it was at a shallow depth, therefore, the sample are weak, figure 106 shows a fracture developed in limestone when high stress is applied (which was 2215 psia), while in the case of sandstone, there is no fractures are observed when applying the same stress, Figure 107. Applying stress can on those types of rocks can cause failure when stress exceeds the strength of the rock, stress allows the grains to come closer and the contact between the grains will closer. As described in rock analysis, sandstone consists of grains that are bounded by cementation. Sandstone has a high porosity and permeability, when high power laser the beam interact with the sample, the heat transfer takes place within the solid by conduction, and with in the void space as convection as seen in figure 107. When applying stress on Limestone, the sample gets more compacted and the solids grains gets closer and more heat will transfer. Limestone shows response when applying stress as the SE decreases. In the case of sandstone, the sample is stronger and applying stress did not show much change.

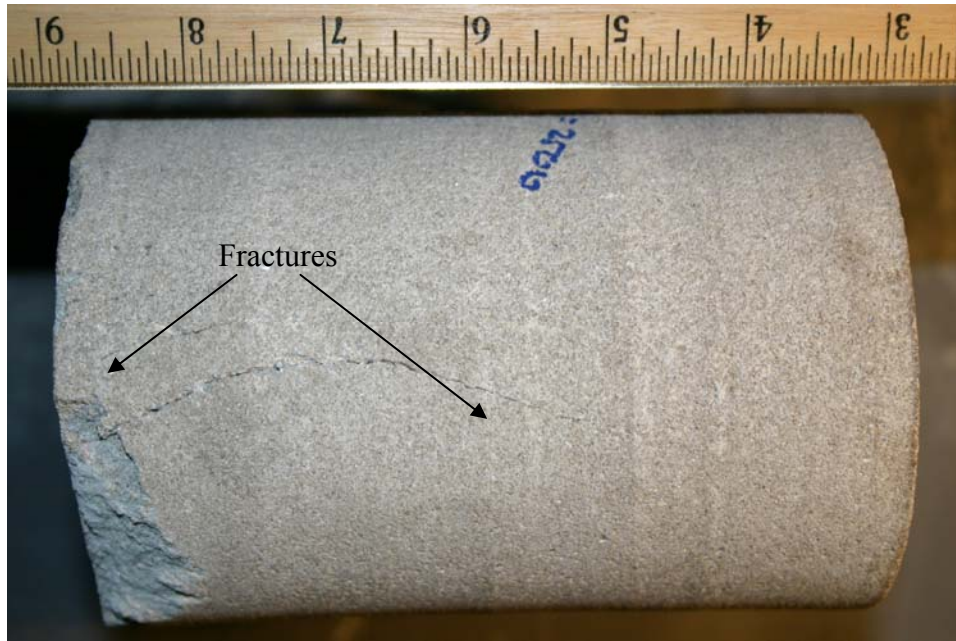


Figure 106. Fracture developed in limestone sample when stress was applied



Figure 107. Sandstone samples shows no fractures development when high stress is applied.

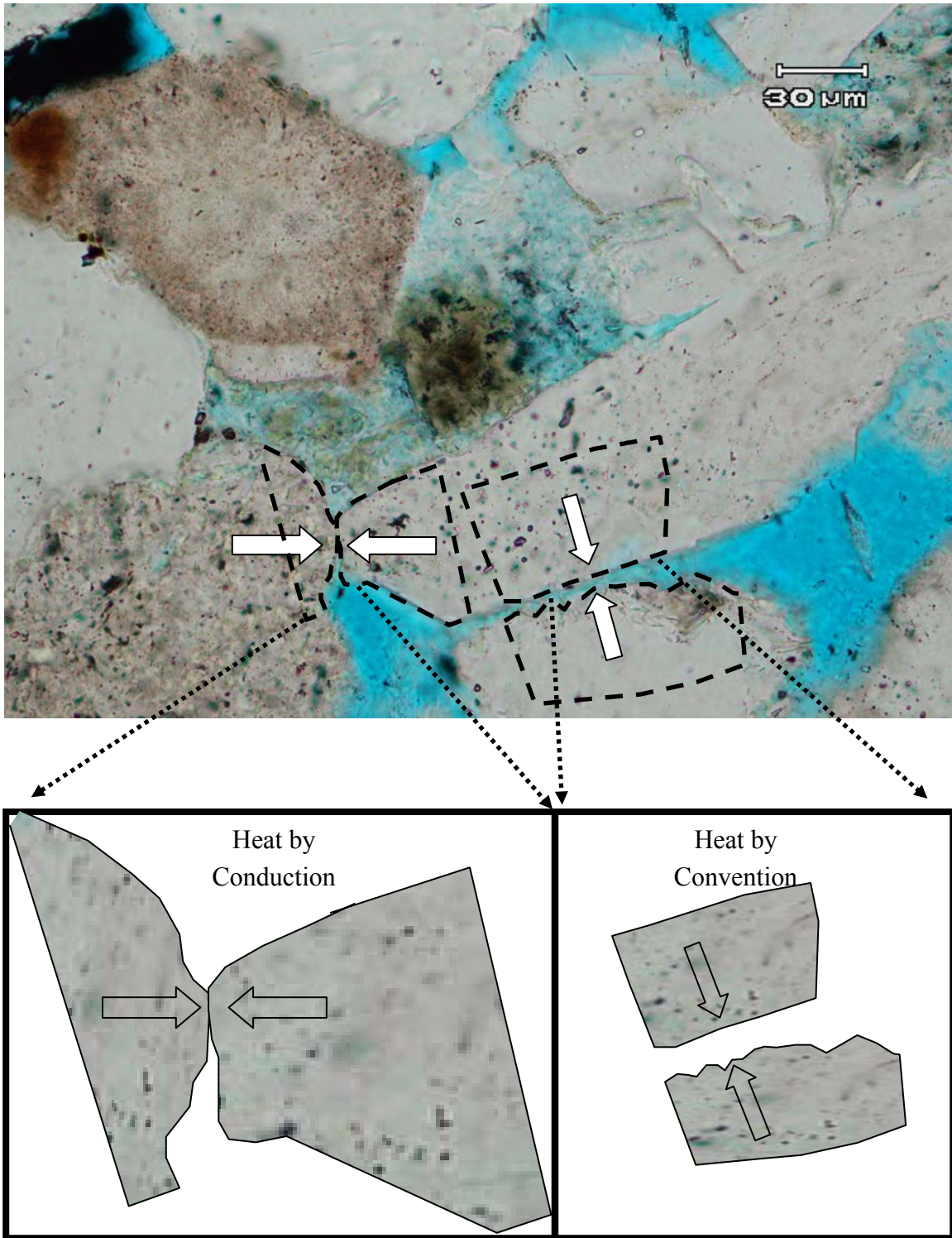


Figure 108. Heat transfer in Sandstone by conduction (solid to solid) and convection (solid to air).

Figure 108 shows that the maximum SE value was for the sample with no stress or pressure applied, because the sample is at the original condition where the gap between the grain are not forced to come closer, therefore large percentage of the heat will be transfer by convection. When stress is applied, the grain get closer and heat transfer will be more effective. The lowest value of SE is when increasing the confining, axial and pore pressure. The pore pressure present under balance conditions where the debris and grains will be carried out of the tunnel to the well bore.

In the case of limestone, the void space is much less than the sandstone, if the void space is connected, then this will increase the porosity and permeability, and limestone has low permeability and porosity. The heat transfer is more effective because it is by conduction. Figure 109.

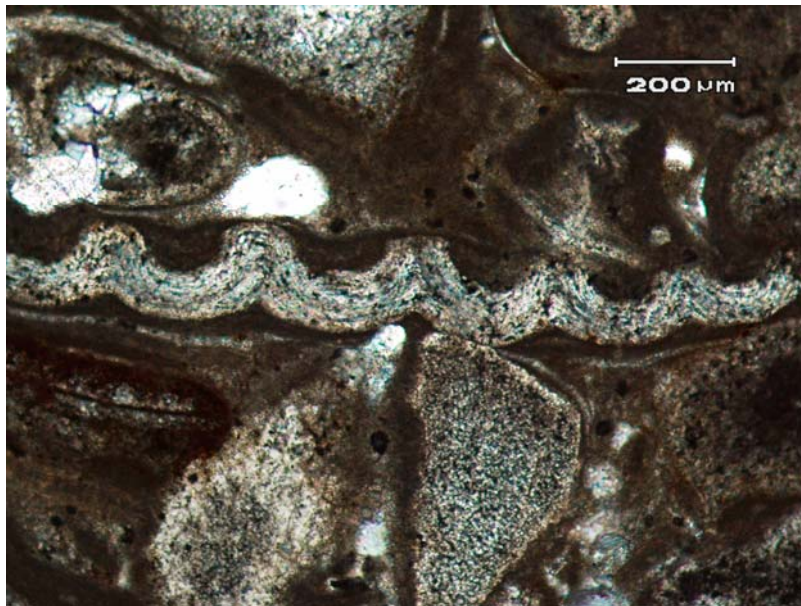


Figure109. Thin section shows quarry limestone with low porosity and permeability, high grain contact.

Perforation of saturated cores under well bore condition

Objective:

To simulate perforation under down hole conditions by applying axial and confining pressures (tri-axial load) on sandstone and limestone saturated core samples.

Procedure:

Sandstone and limestone cores (4" dia x 6" depth) were placed in vacuum environment for about 6 hrs and then saturated with brine and oil for at least 24 hours. Water with 50 ppm Sodium Chloride was used as brine water. Each sample was placed in cell and it was pressurized for confining and axial pressures up to 2000 psi. Each saturated sample was lased for 8 seconds with 5.34 kW laser power. Spot size was kept constant at 0.35". Pore pressure was not applied in this case as the pores were saturated with oil/brine.

Results for both the rock types are shown in graph below to compare specific energy values with unsaturated samples. Figures of each sample before and after lasing are shown in appendix.

Result and Analysis:

As explained previously, the stress because grains to get closer there for more heat transfer. In figure 110 and 111 the graphs show sandstone and limestone under confined, axial and saturation conditions.

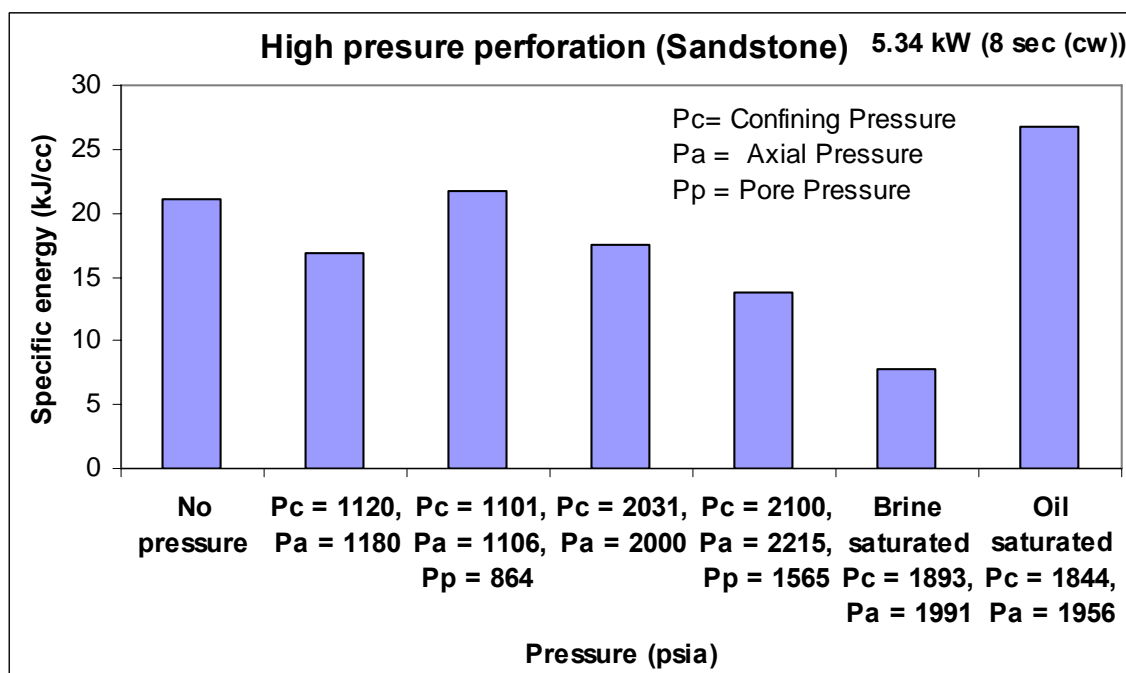


Figure 110. sandstone sample in the high pressure perforation cell at ambient conditions, confining pressure, axial and pore pressure.

The figure shows that sample saturated with oil present the high SE value. Then lasing with oil saturation, the oil consumes energy to heat up and the vapor and the product of lasing is like a dark cloud with blocks the beam from reaching the sample. In the case of brine, the water evaporates and the sample path gets clear for the beam.

For limestone the same trend was observed where the Oil saturated sample shows more SE than the brine, but for limestone the SE value oil is still less than dry with no stress because there void space is very small in limestone, therefore the amount of the oil injected in the sample is very small or even insignificant.

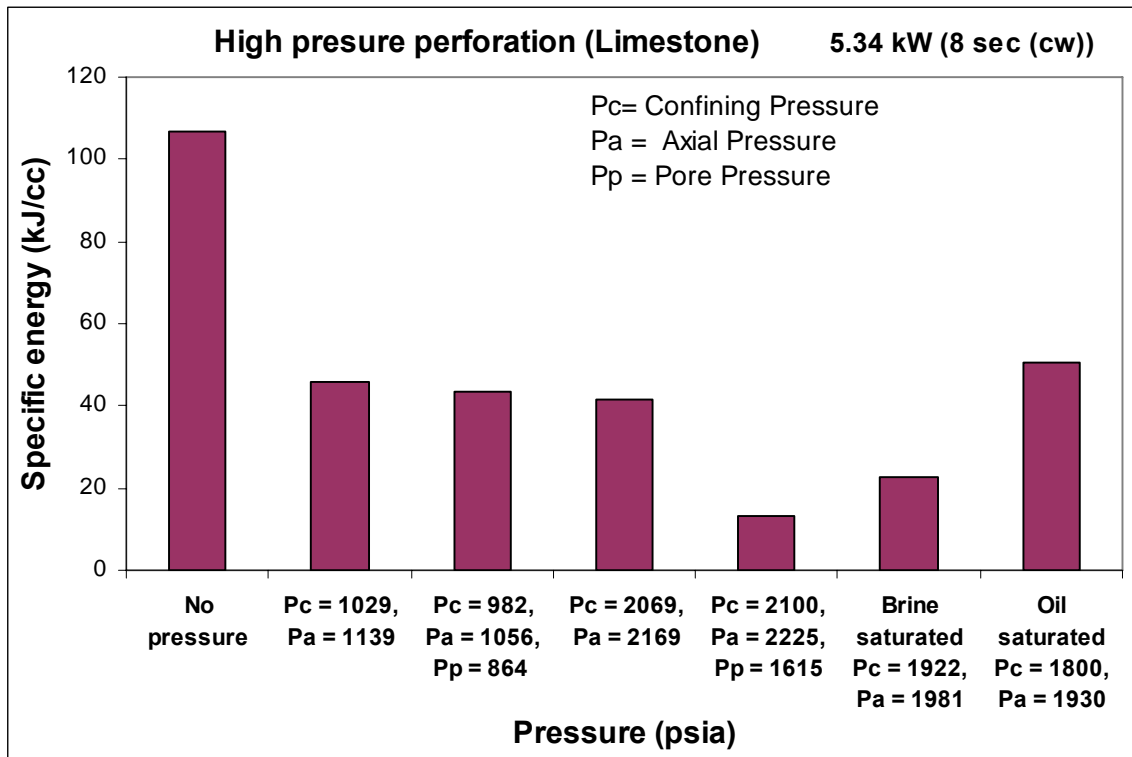


Figure 111. Limestone sample in the high pressure perforation cell at ambient conditions, confining pressure, axial and pore pressure

Perforation of clad samples under well bore condition

Objective:

To estimate the perforation depth for clad samples under tri-axial pressure condition

Sample Preparation and Concerns:

When preparing the clad sample for high pressure perforation and if the samples were prepared as in figure 112, some concerns were raised as:

1. The heat generated will melt the sleeve
2. Melted steel might get attached to the upper side part of the cell.

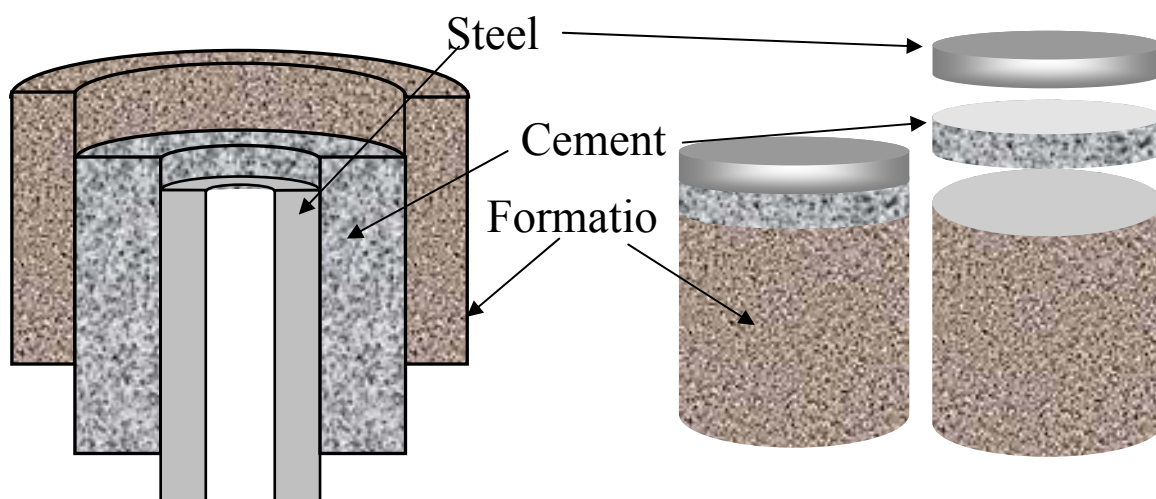


Figure 112. Clad samples where used for time of penetration measurements.

Procedure:

Clad samples were prepared by drilling 2" diameter x 2" hole inside 4" x 6" core sample. Figure 113 shows the schematic of prepared clad sample. Previous experiments on three widely used cement type showed minimum time of penetration for given depth in Y250 cement type. Hence this cement was used to prepare these samples. Previous penetration

experiments on steel plate and clad sample were used to estimate the depth of penetration for given lasing time. Several laser shots were also tried before actual experiment to determine optimum lasing time and purging. Each clad sample was placed in high pressure cell. Applied axial and confining pressures were 2100 psi and 2030 psi respectively for sandstone whereas 2074 psi and 1966 psi for limestone. Laser was kept on for a total of 90 seconds. Relaxation time of 20 seconds was allowed after each 30 second continuous shot as a precaution to overheat the cell assembly.

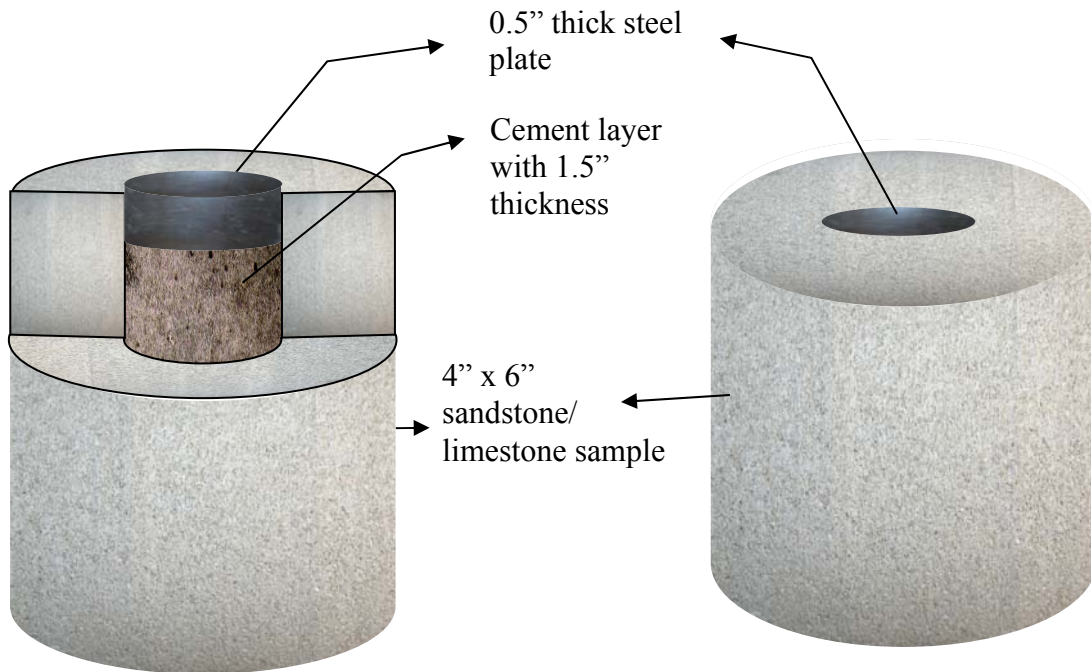


Figure 113. Clad sample for the high pressure cell, modified design for melting issues.

The purpose of this test to evaluate the performance of the high pressure cell in perforating clad test, the time to penetrate the steel and cement was testing before. The result of the test for sandstone and limestone is:

Depth of penetration:

Limestone: 4.5" (2.5" beyond steel and cement layer)

Sandstone: 2.5" (0.5" beyond steel and cement layer)

The depth of penetration and the shape was also monitored by CT images as shown in figure 114.

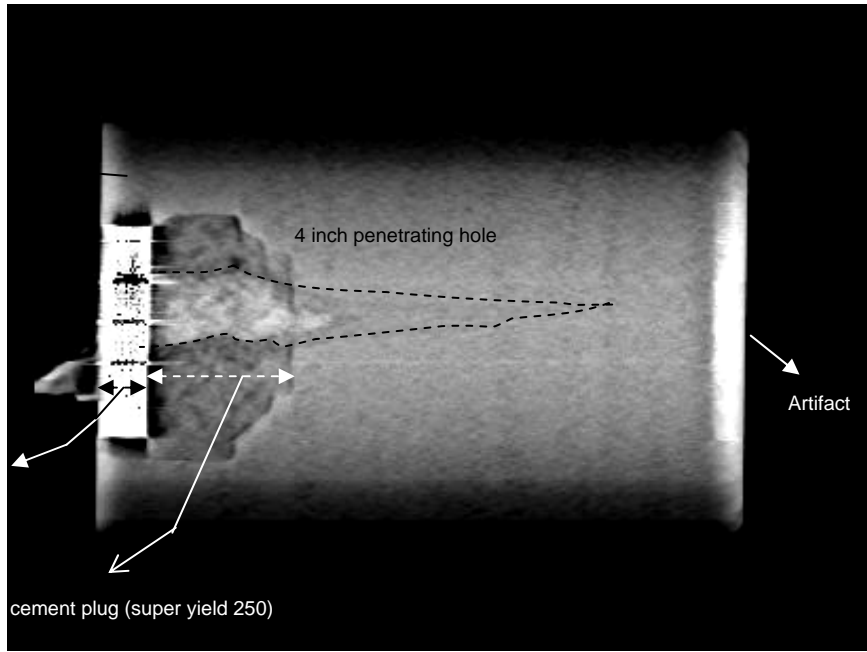


Figure 114. Perspective view of X-ray CT scan image of laser perforated limestone core sample

Conclusions

Laser technology applied to well completion operations has the potential to reduce time, eliminate the damage in the well bore and improve well performance through improved perforation operations. However, there are also potential tradeoffs in using laser technology to complete oil and gas wells. How much energy is required? What are the optimized laser parameters for perforating specific rock type? Can fluid be used instead of gas? Can an experiment be conducted at down hole conditions to compare high power lasers perforation with shape charge perforation?

This experimental research was conducted to answer the specific research questions listed above. In this research a 5.34 kW ytterbium-doped multicladd fiber laser with an emission wavelength of 1.07 microns.

The conclusions determined from this research are summarized below according to the specific research questions asked.

Purging Optimization:

The purging is important for cuttings removals and clear the path for the beam to deliver to the rock. Dust, debris and cuttings will absorb the beam and therefore, less energy will be delivered to the rock sample. The dust, debris and cuttings present loss of energy in terms of specific energy, the test was conducted to calibrate and evaluate different nozzles like Air amplifier and different shapes purging nozzles. By improving the purge system, blocks were used instead of core, this allow to save time and material (rocks) and eliminate boundary effect. The optimization was done by adjusting the flow, distance between the nozzles and the surface of the rock, the angle of the purge. Different holes were obtained with damage and melt (figure 115), then clean holes without melt were obtained, the variables like the distance of the purge, angle and flow were noted and used through the experiment.

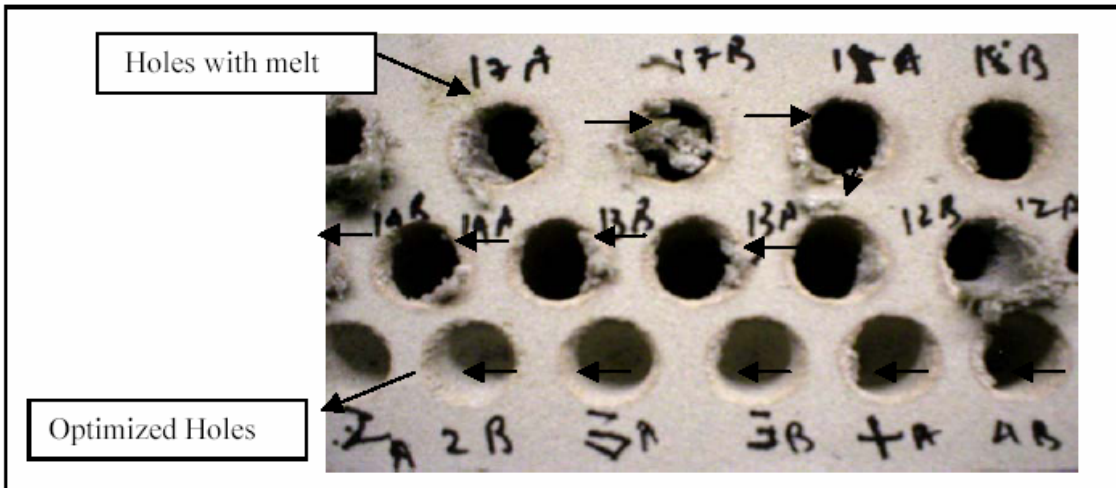


Figure 115. Purging optimization showing the improvement of holes

- For focused beam the best purging system is using focused nozzles, the distance between the nozzles and the surface is 1” and the angle of the purge was 35°.
- For collimated beam, the air amplifier can be used instead of nozzles.
- With optimized purging system, block can be used instead of cores.
- The efficiency of the purging system can be measured by SE value, high SE indicates poor purging system

Effect of laser power on Specific Energy (focused beam):

- The power optimization test was conducted by calculating the SE and by visual observation of the hole, for perforation purposes and sand production issue, the hole is preferred to be clean without melt, debris or sand particles. The selection of the optimized SE was based on low SE value as well less melt and damage.
- The power increased from 10 to 100% at 10% increment, in the case of sandstone, the first reading the power was only 10% which did not make any significant change in the rock, this can be seen from figure 116 at 10% power.



Figure 116. Power optimization for Berea sandstone at 10%.

The optimized power for Berea sandstone is 60%.

- At 60% power, spallation takes place that is breaking of sand grain from the matrix. The mechanism of spallation was monitored by IR camera, during the process of lasing; the temperature was shown to be less than 1200 oC, and that corresponds with the literature. Thin section showed the trace of the spallation where the grains shapes changed from rounded to angular. Figure 117.

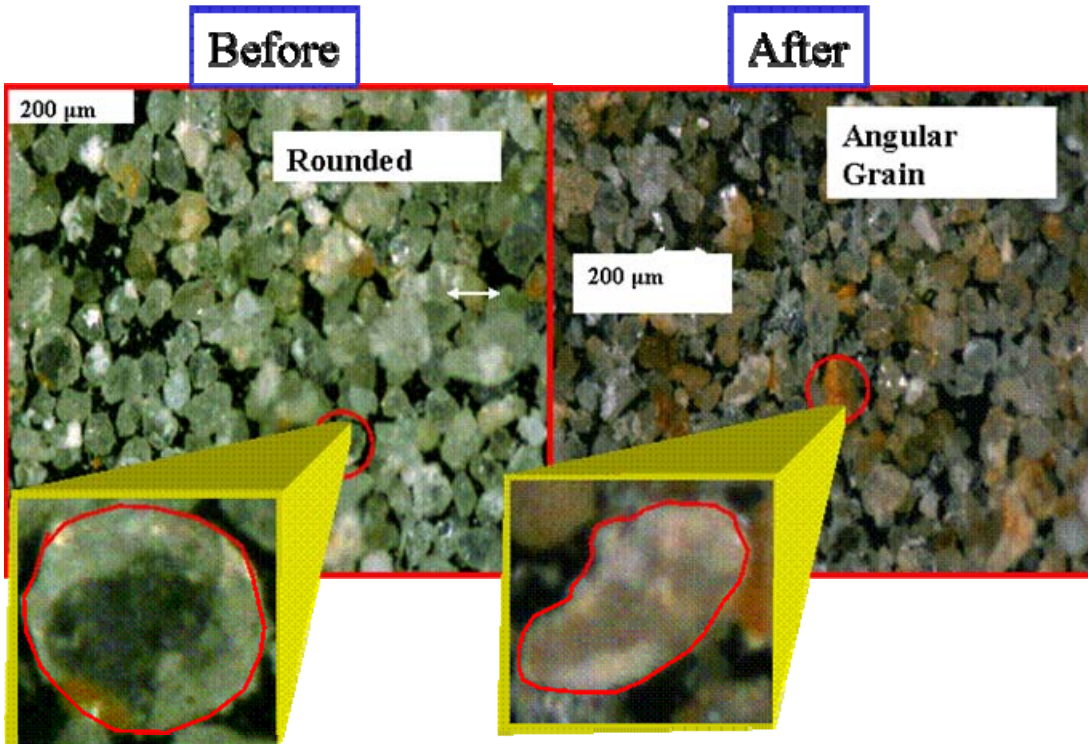
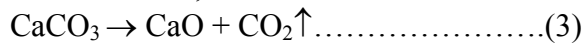


Figure 117. Thin-section shows comparison of grain shape before and after laser due to spallation, the grains changed shape from rounded to angular.

- In the case of Limestone, the mechanism of laser rock interaction with Limestone is different from Sandston due to the chemical composition different. The physical and chemical changes in limestone were different due to mineralogy and chemical composition. Thermal dissociation takes place when limestone interacts with the laser, producing carbon dioxide (CO₂), (Equation 3). No melting was observed in limestone, due to the thermal dissociation of CaCO₃.



For limestone, the more power is required to obtain deeper tunnels, the more time and power the more dissociation takes place. For that reason, there was no picture taken for the Limestone when lasing at lower power percentage, there was no significant difference till the power reached 70% and up. But the SE value could be calculated because there was mass removed form the rock. Holes can be obtained in limestone at lower power by reducing the spot size which results in an increase in power intensity.

Effect of laser power on Specific Energy (Collimated beam)

- When comparing the effect of focused beam vs collimated on Limestone for 8 seconds (no data were gathered at 4 seconds, there was no significant change), the result show that collimated consumed more SE due to the less intensity and therefore less energy delivered to the sample.
- When comparing 8 seconds and 4 seconds lasing time for Sandstone using collimated beam, the result showed that 8 seconds consumes more SE because the more lasing time on the samples result in more heat and melting of the quartz
- Comparing collimated and focused beam can be seen in figure 4. The result show that focused beam has higher values than collimated, the unlike the focused beam, the collimated beam distribute the beam uniformly on the sample, therefore less intensity and the melt is avoided.

Effect of lasing time on Specific Energy (focused beam)

- For Sandstone, the result of increasing the time while keeping the power constant show a trend between lasing time and SE. This indicates that more lasing time results in more penetration depth; because the more lasing time means more laser interaction with the rock sample (mineralogy variable is constant). On the other hand, in term of SE, more lasing time means more plasma formation and gases in the lased hole, which result in more energy loss. The deeper the hole, the less the effect of purging.

Comparing samples, sandstone and limestone, there result indicates that the same trend as an increase in lasing time result in an increase in SE.

Effect of lasing time on Specific Energy (collimated beam)

- The difference between the focused beam and the collimated is the shape of the beam, the focused beam has a conical shape while the collimated beam is a cylindrical shape and the beam size and waste does not change in theory. the result of lasing using 0.35” collimated beam at two powers, at 3 and 5 kW. The trend shows that at 3 kW consumes less SE. There is an increase in power result in an increase in SE due to the directly proportional relationship between SE and power. Also as the time increases, the SE increased as well. Sandstone spall at lower energy and melt a higher energy, if spallation takes place, the particles will break off the matrix and with the help of the purging system, they will be carried out the hole and absorb energy from the laser. Increasing the time, allows more particles to be ejected and more energy absorption. .
- When comparing both collimated and focused beam regarding SE values, The results shows that as time of lasing increases, the SE values for collimated beam

is less than the focused beam, this is due to the shape of the beam, the focused beam is a conical shape which leads to maximum power at the tip of the beam due to an increase of beam intensity. The high intensity of the beam when interact with Sandstone result in melting the quartz and forming melt materials that absorbed the energy.

- The second experiment was conducted on Limestone at 5 kW, the limestone requires more energy in order to dissociate, the result shows that an increase in lasing time result in decrease in SE because more time in the case of Limestone means more material removed and dissociate

Effect of saturation and purge gases on specific energy

The samples were saturated with brine, fresh water and oil. Four types of gas were used; nitrogen, Air, argon and helium.

This test was conducted to analyze the effect of the purge gas on SE and types of gases on saturated rocks types. The reason for using the purging gas was to simulate reservoir conditions (an oxygen-free environment), remove rock debris and vapor, and safety consideration.

- Purging gases on dry rocks: for sandstone, the result showed not much significant difference when using helium, argon and nitrogen, on the other hand, air consumes more SE. This result is encouraging for the reason that air will not be used downhole due oxygen content. In the case of limestone, Nitrogen consumes less SE than the other three gases.
- Purging different gases on saturated rocks: The test showed that saturated samples in general resulted in higher values of specific energy (SE) than unsaturated samples. The presence of liquids in the rocks consumed more energy since it takes more energy to heat liquids than air. Also the presence of liquid in the core results in producing vapor when subjected to laser radiation. This vapor or gases will absorb the energy and result in energy loss, therefore, less energy will be delivered to the rock sample and hence consumes more SE. Oil saturated samples consumed the highest SE values. More research needs to be conducted to determine how gas composition effects SE while lasing saturated samples. The figure (below) can be used as guide or correlation when using gasses on saturated samples

Deep hole penetration at ambient conditions

- Deep holes for sandstone can be obtained by spallation mechanism, the power is 60% was found to both optimized power, and purging with nozzles should be used when the holes gets deeper.

The deepest hole created in sandstone was 12” deep with a 1” in diameter. Figure 118.



Figure 118. Deep hole in sandstone by spallation, the hole was clean without melt or debris and SE of 4 kJ/cc, Diameter of 1 inch with 12 inches long

- For limestone, more power needed to create deeper hole due to the composition of the limestone. Calcium carbonate dissociations. The deepest hole obtained was shown in figure 119.



Figure 119. Deep hole in limestone of 12 inches deep.

The reason for limiting the length in this test is that there are no rocks available in the lab deeper or longer than those. The limitation was the sample size.

Frequency test

Two sets of experiments were conducted to evaluate the effect of frequency on the SE, the first set was done by changing the frequency from 1 to 10 pulses per second at an increment of 1 pulse/second for both sandstone and limestone sample. The second set is by changing the frequency from 10 to 999 at 10 pulses/second increment.

The result was mainly based on the SE, the observations from the pictures of the sample did not add to the analysis due to the fact that there was no significant change in terms of melt or damage. The melt was form only at the edge of the sample due to the boundary effect.

- The results of lasing sandstone from 1 to 10 Hz. I did not show a significant change from 1 to 9 Hz, but the changes are significant at 10 Hz.
The result indicates that frequency less than 10 shows less SE values, pulsing the laser beam allows the laser to intermittently interact with the rock sample. Because the purge was continuous when the beam was not on the sample, pulsing allowed the dust and gas plume to clear. Dust and plume absorb energy from the laser and reduces the amount of energy transferred into the rock. When increasing the frequency from 10 to 999, laser beam is almost continuous for frequencies more than 10 Hz.
- Limestone showed the same trend as an increase in the frequency results in an increase in SE, the beam tend to be continues wave.
Limestone requires more energy and more laser beam on the sample for disassociation to take place.

Liquid Purging Test:

Halocarbon fluid is toxic when exposed to high temperature (300 °F, safety sheet of halocarbon). Special design should be applied to handle this hazard fumes and fluids. The primary test was conducted as shown in the figures above to confirm the ability of laser to penetrate fluid and interact with the laser.

Future design in the second phase will be design to allow all the experiments to be conducted in the fluid environment without any risk.

- The result of the experiments of purging with fluids indicates that, the behavior of the rocks under fluid is the same trend as gas.

Time of Penetration test:

Two methods were evaluated for steel cutting; the first method is by exposing the sample directly to one beam without moving the robot. The second methods were by moving the robot in a circular motion to cut a circle.

- The methods used for all the experiment for steel drilling is by keeping the robot steady without motion. This is more effect and closer to down hole conditions because the complexity of moving the robot down hole.
- The result of penetration time of steel and cement was used for the high pressure cell to know how long it will take the laser to penetrate different steel thickness

and cement so the laser can be programmed to be on for sufficient time allowing time for rock penetration.

Orientation effect test:

The test was design to study effect of lamination or deposition on the experiment.

- Deposition orientation is not an issue for lasing limestone and sandstone material used for this study. Specific energy required to drill the hole in all faces of the block was almost the same.

Boundary Effect determination for Limestone and Sandstone:

This test was designed basically for the high pressure perforation cell to know the size of the cell and how much the pressure core holder that without any boundary effect or secondary effect. The spot size was optimized in other test, and it was found to be 0.35 inches.

- The result shows that 4 inches diameter was the optimized diameter for 0.35 inches spot size. There was no test to confirm this relationship that shows relate the spot size and core size. It has been observed that at 4 inches diameter there was no fractures or cracks developed in the rock sample.

High pressure perforation

When designing the high pressure perforation, the following concerns where encountered due to the unique application and complexity if the operation.

- 5- Safety
- 6- Pore Pressure flexibility
- 7- Purging with tri axial
- 8- Lenses clearance
- The original design of the high pressure cell was evaluated and was not suitable for high pressure laser perforation, a new design was generated.
- For safety, the following features were added to the high pressure perforation cell:
 - i. Three compartments
 - ii. Relief valves
 - iii. Back pressure regulator
- The High pressure perforation cell has the flexibility to
6. Perforate under or over balance up to 3000 psi
7. Pore pressure, tri axial conditions
8. Purge with fluid or gas
9. Samples up to 4" in diameter with 6" length
10. Clad samples (Rock, cement and casing)

- Developments and prove of concept has been evaluated and modification has been made by adding cone structure inside chamber one. The cone allows the purging to be co axial with the bam and block the opposite direction from the core to the lenses (sapphire windows)
- Comparison between limestone and sandstone, dry conditions, under different conditions show that an increase in pressure or stress result in decrease in SE value for limestone due to the mechanical properties of sandstone. More stress result in closer contact of the matrix and more heat transfer to the rock sample. Keeping in mind that limestone is quarry stone and it is weak compare to sandstone, means it deforms more when stress is applied.
- For sandstone, the same trend was noticed, but the deformation was less than the limestone.

Perforation of saturated cores under well bore condition

- The result of lasing sandstone sample with Oil and Brine show that sample saturated with oil present the high SE value. When lasing with oil saturated samples, the oil consumes energy to heat up, and forms dark cloud vapor which blocks the beam from reaching the sample. In the case of brine, the water evaporates and the sample path gets clear for the beam.
- For limestone the same trend as in sandstone was observed where the Oil saturated sample shows more SE than the brine.

Perforation of clad samples under well bore condition

Sample Preparation and Concerns:

When preparing the clad sample for high pressure perforation some concerns were raised as the heat generated would melt the sleeve and melted sleeve might get attached to the upper side part of the cell.

The purpose of this test was to evaluate the performance of the high pressure cell in perforating clad test, the time to penetrate the steel and cement was tested before. The result of the test for sandstone and limestone is:

- Depth of penetration:
Limestone: 4.5” (2.5” beyond steel and cement layer)
Sandstone: 2.5” (0.5” beyond steel and cement layer)

3.7 Laser Drilling Systems

3.7.1 Nd:YAG System

Most of the tests reported here were conducted with a laser drilling system that consisted of a 1.6 kW pulsed Nd:YAG laser with fiber-optic beam delivery, five-axis CNC workstation and coaxial purging gas unit (Figure 7). The fact that the beam is delivered by an optical fiber is particularly attractive because of its inherent flexibility and the possibility that this will be the method used to deliver and aim the high power beam down in a well. A 12.5-cm transmissive focusing lens was used producing a collimated beam diameter of 985 μm . A constant nitrogen flow of 189 liter/min (400 ft³/hour) was coaxially delivered to the rock by a nozzle 6 cm in diameter.

The Nd:YAG laser is attractive for this work not only because of the optical fiber delivery system, but because the wavelength is in the range where water is very nearly transparent and minimal power is lost during transmission through water. Also, the system is relatively compact and portable. Disadvantages include the low efficiency of the laser generation system, about 10 percent.

New developments are taking place in Nd:YAG technology, with higher power lasers now available. Lumonics, a laser manufacturer has a 4kW average power laser in their development laboratory.

3.7.2 Nuvonyx Diode System

The diode laser at NA Technologies is used primarily for metal-forming research. It has few of the advanced sample handling capabilities of the ANL facility, such as the programmable movable stage and the coaxial gas purge nozzle. The system consists of the laser head, which is roughly an 8" cube, the electronic control console, and the cooling water chiller, both of which are about two feet by two feet by three feet high.

3.8 Saturated and Submerged Tests

3.8.1 Saturated

Due to the difficulty of saturating the dense limestone and shale samples available for these tests, the saturated tests were done exclusively on Berea Gray samples. At the end of the May tests, samples resting in water-filled dishes with only the top surface exposed were exposed to the laser. The purge gas disturbed the water, and reliable results were not possible. It was decided to saturate the sandstone samples and set the wet samples on the stage with all other parameters (purge and lens distance, for instance). The disks were kept in water up to the moment of the tests, so very little was lost to evaporation.

3.8.2 Submerged

To truly test the behavior of the laser through water or other fluid and onto a sample would require the design and fabrication of a system beyond the scope of this feasibility study. A series of tests were undertaken to prepare for such a study, to be part of Phase Two. The first problem is to inject the laser beam into the water directly, so that surface instability and reflections could be avoided. Since the Nd:YAG beam is conveyed by an optical fiber, the end of the fiber could be placed, unprotected, into the water without damaging any of the optics. Zach Xu calculated that beam dispersion out of the fiber would be about 4 degrees, which was within the range needed to get a good beam diameter without having excessive distance between the fiber end and the sample.

First task was to confirm experimentally the value given in the literature of about 3 per cent energy absorption per centimeter of water thickness. A container was modified so that the bottom consisted of a glass disk as is used in the Nd:YAG optical system. A known thickness of water was placed in the container and the average power measuring instrument was placed below it. The power measured was close to what was expected, and it could be seen visually (from the heated spot) that the beam was a good shape and quite consistent across the area covered. The sample was then placed in a container and the fiber placed into the water above it.

4 Results and Discussion

4.1 Data Analysis

The data from all of the tests are contained in Excel spreadsheets, which are included as appendices to this report and as Acrobat Reader files.

For each sample, the laser parameters and the change in weight before and after lasing were recorded. The raw data model has the following headings:

- Sample no. (rock, specimen and spot numbers)
- Laser “Schedule” (ERL shorthand)
- Measured average power (P_{av})
- Pulse width (W_p)
- Repetition rate (R)
- Time beam was on (t)
- Spot diameter (d)
- Weight before
- Weight after

Calculated fields include:

- Delta weight
- Spot area (A)
- Total Energy (TE, $P_{av} * t$)
- Total Energy Density (TE/A)
- Specific Energy (SE, $(P_{av} * t) / (w / \text{density})$)

The data has been plotted using the Excel graphing capability, primarily in the x-y (scattered) type of graph. Symbols and colors of the data points in the graphs allow categorization of the data to examine any trends and relationships that may be present. Selected graphs are in the sections discussing particular tests, below.

4.2 Important Rock Parameters

At the beginning of the GRI study, it was felt that porosity would be an important factor in efficiency of cutting rock, as high porosity rocks would have narrower grain contacts to be broken. It was feared that shale, being non-granular, with no discernable porosity, would not cut well, or at all. The GRI study showed that the shale spalled in a manner similar to granular rocks. All lithologies were shown to

have similar measured SE. The behavior of shale is important, as approximately 70 per cent of rock encountered in today's wells is shale.

Parameters that are probably important, and will be studied further, include:

- Thermal conductivity
- Reflectance
- Color (Albedo)

The physical characteristics of the rocks undoubtedly have a role in how they are affected by laser energy, such as:

- Porosity
- Permeability
- Mineralogy
- Degree of Cementation
- Compressive Strength
- Tensile Strength

Unfortunately, the size of the sample has been revealed to be a secondary effect. Often cracking from the hole to the edge was observed and, when present, affected the SE. Changes in the thickness of the sample also affected the SE. The mechanisms causing these changes are not known.

4.3 Spallation and Melting Zones Identified

For this series of tests, the aim was to identify the laser parameters in the spalling zone, and then identify the onset of melting. Conditions were identified under which the laser energy will break and remove rock without significantly melting, given the parameters used in this experiment for this set of samples.

The zone change of the rock depends on the laser parameters and the melting temperature of the minerals in the sample. The melting temperature of the rock sample increases with the percentage of quartz in the rock. As the melting temperature of the whole rock increases, rock destruction decreases. Applying this concept to SE, the higher the percentage of quartz, the higher the energy consumed in melting and vaporizing. That concept is particularly applicable when drilling "deep" holes (depth greater than width). In the case of shallow holes with a good purging system, other parameters compete with quartz concentration for control of onset of significant melting. Those parameters are surface roughness, color, grain cementation, vugs and fractures, in addition to the thermal properties like conductivity, heat capacity and diffusivity. The values of those parameters for sandstone, shale, and limestone test samples are listed in Table 4.

An example of zone changes as a function of rock type and SE is presented in Figure 10. The sample used was shale. The laser power was increased from 0.2 to 1.2 kW. All other parameters remained the same for this series. In this plot there are two mechanisms clearly observed: the zone on the left is a spalling zone, which occurs at a lower average power, and a melting zone is on the right. A transition zone identifies a region between average powers of 0.534 kW and 0.62 kW where the spalling zone changes to a melting zone. We observed that the lowest specific energy is obtained in the spalling zone just prior to the onset of melting. A possible sequence is that at low laser powers, a considerable fraction of the energy is consumed by thermal expansion, fracture formation and mineral and gas decomposition, leaving little energy left to effectively remove rock material. As the average power increases, heat transfer and additional reactions occur, removing material more effectively. As the average power increased further, the minerals begin to melt, energy is used for melting instead of removing material and higher SE values resulted. Once melting occurred, secondary effects began to consume additional energy, and SE values increased further.

Based on the linear track results, test parameter matrixes were selected for conditions that produced thermal spallation up to a slight melting zone. This is the area where the team expected to find the lowest SE values. The matrixes included three energy per pulse levels (4, 8, and 16 J/pulse), each with specific pulse width and repetition rate. The pulse width was either 1 or 2 ms, whereas the repetition rate varied between 50 and 400 pulse/second.

The test parameter matrix was performed on the samples. The beam diameters on the rock surface were 1.27 and 0.95 cm. The beam exposure time was controlled at 0.5 and 1.0 or 1.5 seconds to only produce a shallow hole so that the secondary effects could be avoided. To determine the material removed by the laser, the rock sample was precisely weighed pre- and post-lasing using a Mettler AT 261 balance with maximum 205g/62g and resolution 0.1mg/0.01mg. The removed volume was then calculated based on the rock bulk density.

4.4 Spallation Tests with Dry Samples

As a result of the long sample linear tests described in the Experimental Procedures section, a matrix for each lithology, sandstone, shale and limestone, was created (Appendix B). The parameters identified above were varied in a pre-planned manner, according to how difficult it was to set up new parameters. In general, for each matrix, the E, L, R and t values were set, then the focusing lens distance (spot size). One or more samples would be exposed (three spots per sample for sandstones, one or more for shale and several for limestone, see pictures of the samples in Appendix A), then the distance changed and more samples tested. Then a new set of E, L, R and t values would be programmed and

the procedure performed again. This was done for 30 sandstone samples, 24 shales and eight limestones at the Argonne laser facility and five sandstones, three shales and two limestones at Native American Technologies.

In general, specific energy values increased with the exposure time since, at the beginning of lasing, the laser radiation interacts with the surface only. At this time, the secondary effects, such as deposits of melted material are at a minimum. In this case, the laser beam can directly reach the solid rock and remove matter from it. However, as the exposure time increased the interaction region heats up, secondary effects including melted material begin to form consuming additional laser energy, but not removing material. Furthermore, this melt acts as a barrier, preventing the laser beam from fully interacting with the solid rock beneath. Also, longer laser beam exposure times mean more heat will be dissipated in the sample, and that heat will be used in thermal expansion, fracture formation and mineral decomposition. All these effects combined result in measured specific energy values increasing with longer exposure times. These results are in agreement with the CW COIL experiments, where a similar trend was observed for the specific energy values.

4.4.1 Lithology Samples

4.4.1.1 Sandstone

Most of the samples exposed to the laser were the Berea gray sandstone, because the physical properties of this quarry rock are so consistent, and it is readily available. However, the behavior of the rock is not straightforward. The long linear tests demonstrated that there are five discernable zones as power density increased:

1. Threshold scorching
2. Slight grain removal
3. Cutting with grain rounding but no grain-to-grain attachments
4. Light, loose melt
5. Heavy attached melting.

These five zones were all demonstrated by the individual samples, with the added complication of cracking from the spot to the edge of the sample in some samples. Sometimes the crack developed after the first and sometimes after the second spot in a sample. Even if cracks are not visible to the naked eye, they can be detected by the separation of the individual spot data when plotted Total Energy Density vs Weight (Figure 11).

4.4.1.2 Shale

The long linear test identified three zones on the shale sample. Spallation started almost immediately and continued over a greater range of power density values before melting started. The shale samples gave the best indication that the

secondary mechanisms had seriously affected the GRI deep hole samples. The SE calculation for the shale samples dropped by an order of magnitude from the GRI results. The shale samples also show a definite SE jump when the rock starts melting (Figure 10), and the gradient of the SE changes with power is different in the melting zone compared to the spallation zone.

4.4.1.3 Limestone

Limestone SE values were higher than shale, however we can only speculate at this time that it may be due to the relative reflective properties of the rocks. The lighter color of the limestone used in the present experiments may have reflected a larger percentage of the laser beam energy, resulting in less energy absorption and therefore, in weaker coupling efficiency. Another possible mechanism for limestone is that the laser energy disassociates the calcium carbonate in to calcium oxide and carbon dioxide, rather than melting or vaporizing the carbonate molecule. The energy required to do this could be more than the breaking energy of sandstone and shale spallation. However, there is something going on that is not yet understood. Figure 13 shows results of laser energy on dry limestone. The two curves are two different hole sizes, 1/8 in and 5/16 in. There is no clearcut relationship with any other laser parameter, and the fact that the larger hole is exhibiting more efficient cutting indicates a change in mechanism between the two energy densities.

4.4.2 Specific Energy as Power Increases: Non-melt vs. Melt

Figure 10 shows the SE for shale samples as a function of laser power under fixed beam spot size of 0.5 inches and exposure time of 0.5 seconds. The SE results were grouped together by thermal spalling and melting identified by the physical reaction observed on the rock samples. Thermal spalling produced a clear hole, and melting left deposits in the hole. At very low beam power (200 W), the energy absorbed was only enough to heat up a small amount of rock and thermally fractured it; therefore, the SE value is very high. As the power was increased, a larger volume of rock heated up and fractured, resulting in smaller SE values. This trend continues until the melting of rock started at beam power over 600 W. There is a sharp increase of SE (from 0.5 to 2.2 kJ/cm³) when transition occurred from thermal spallation zone to melting zone. The SE decreased slightly in the melting zone as the laser power increased. This is due to a reduction of the viscosity of the melt at higher temperature induced by higher beam power, and the less viscous liquid was more easily removed from the hole by the purging gas.

4.4.3 Effects of Pulse Width and Repetition Rate

A second set of experiments studied the behavior of the pulse width on specific energy. The results obtained with the sandstone for pulse widths of 1 and 2 ms found that SE decreases as the pulse width increases for similar peak intensities. This behavior has been explained in terms of the amount of energy deposited in the sample per unit time and the length of the cooling time between pulses. At a

given intensity, the amount of energy deposited on the rock per unit area doubles for pulse widths of 2 ms than for 1 ms, therefore, putting more heat into the rock. Also, the longer the pulse, the less time there is for the rock to cool down and therefore the thermal stresses are reduced, as was previously discussed. These two effects combine to reduce SE when long pulse widths are used.

Another parameter that was explored was the effect of the repetition rate on SE. The repetition rate was varied from 50 to 400 pulses/sec while keeping the other laser parameters constant, resulting in a decrease in SE as the pulse repetition rate increases. This behavior was observed for different values of pulse width, exposure time, and peak intensity in each of the rock types. The result can be attributed to the fact that a pulsed discharge creates a cyclic heating and cooling of the rock sample, resulting in thermal stresses that can generate micro fissures. At a low repetition rate, the cooling time between pulses is long enough so that each new pulse generates a drastic change in temperature conducive to the formation of micro fissures. In the case of a high repetition rate, the time between pulses is short and the sample does not have time to cool as much, reducing the micro fissures. In this last case, the rock temperature increases more steadily.

Although Figure 12 indicates that the specific energy decreases with an increase in pulse repetition rate, these results are valid as long as the pulse width is kept constant or slightly varying. The effects of pulse width on the specific energy are dominant over the repetition rate. This property is shown when a pulse width of 2 ms was used, it lowers the specific energy regardless of the fact that the pulse repetition rate was increased from 50 to 400 pulses/sec. It has been observed that the lowest specific energy was obtained from a pulse width of 2 ms.

The effects of repetition rate and energy per pulse on SE values are shown in Figure 12. The group of 8 J/pulse contains the lowest SE values. With a high energy per pulse (e.g. 16 J/pulse) the minerals in the rock melted, and therefore a higher SE value was observed. With a low energy per pulse (e.g., 4 J/pulse), a small volume of rock was removed through spallation, also leading to a high SE value. By holding energy per pulse constant at either 4 or 8 J/pulse, an increase in repetition rate reduced the SE values first in thermal spallation zone, then increased the SE was observed as the local mineral temperatures increased above their respective melting points. After melting started, the SE value decreased slightly as repetition rate increased.

It is very interesting to note that the SE data produced at a constant calculated laser power of 1.6 kW, as shown by the point SH13, SH2 and SH15 in Figure 12, were the same with the following combinations of energy per pulse and repetition rate: high energy per pulse and low repetition rate (SH13, 16 J/pulse, 100 1/s); medium energy per pulse and repetition rate (SH2, 8 J/pulse, 200 1/s); and low energy per pulse and high repetition rate (SH15, 4 J/pulse, 400 1/s). In other

words, the same penetration rate could be achieved by differing these laser parameter combinations under the same average power.

4.4.4 Temperature Factors

Two major factors that control the material removal rate are the maximum temperature (T_{max}) and temperature cycling frequency (T_f) in the thermal spalling dominant zone. T_{max} , largely controlled by the applied energy per pulse, determines the temperature difference (ΔT) in the rock, which in turn determines the thermal stress in the rock that is proportional to ΔT . When the thermal stress reached the static rupture strength of the rock, fracture of rock occurred.

Fracture of rock could also occur at a stress that is lower than the rupture strength of the rock, but cyclic from tension to compression. Increase of repetition rate of the laser beam would increase the cyclic frequency of the thermal stress and enhance the fracture. When overall effect of T_{max} and T_f was constant, the same SE results were expected. More systematic studies need to be done in the future to quantitatively characterize the laser-induced temperature and thermal stress field in the rock.

Another contributor to the material removal is the laser-driven shock wave, which was detected by many researchers^{8,9} and also by the current study. By increasing the repetition rate, a resulting increase in the intensity of the shock wave was induced, therefore, causing a reduction in the observed specific energy values.

4.4.5 Spallation Tests with Saturated Samples

The saturated samples were processed after a saturated linear test was done, similar to those done for the dry samples. It was decided that only the sandstone would be used, as the shale and limestone are not nearly as porous and saturation could not be ensured. After the linear test was done, a matrix was created and samples were exposed to the laser (Figures 15, 16, 17)

The results are very encouraging, if not totally understood. Having water in the pores could potentially have had two possible effects. The first was that the water would explosively turn to steam, helping the breaking process. The other was that the increased thermal conductivity would cause the heat to flow away from the working face and the cutting action would be diminished.

⁸ A.H. Clauer, B.P. Fairand, and J. Holbrook, 1981.

⁹ Y. Sano, M. Mukai, K. Okazaki, and M. Obata, 1997.

The results are positive, for a combination of reasons, if our understanding is correct. There were no obvious steam explosions, although there was steam. The thermal conductivity increase may have actually helped decrease the SE by delaying the onset of melting, allowing more energy to be put into the rock and increasing the cutting action.

4.4.6 Submerged Sample Test

The submerged sample test demonstrated that the mechanisms inherent within these experiments are not totally understood (Figure 18). The preliminary tests described in the Experimental Procedures section showed that about 3 per cent of the beam energy was lost per centimeter of water over the sample and that the beam coming directly out of the raw fiber spread by the predicted 4 degrees. When the experiment was set up to get the desired spot size and the power parameters set on the laser, no material was removed from the sample. The laser obviously reached the sample surface, but was not able to put enough energy into the rock to spall it. The water probably carried off the heat too quickly.

When the fiber was moved much closer to the sample, decreasing the spot size and increasing the power density, the energy put into the sample went directly into the melting zone. The positive result is that a hole was put into the sample (Figure 19). Unfortunately, trying to repeat the experiment and find out more about this process resulted in the fiber end being damaged, and it was decided that the possibility of damaging the laser was too great to continue.

A table of the results can be seen in Appendix C.

4.4.7 Diode Laser Tests with Dry Samples

While the team was assembled at ANL for the May tests, a representative from Nuvonyx, a diode laser manufacturer, presented the team with information on a new diode laser. The specifications of this laser can be seen in the Experimental Procedures section. The laser is small, portable and capable of many configurations. A company near CSM was identified, Native American Technologies Company, in Golden, Colorado, that uses a 4 kW Nuvonyx laser for metal reforming.

NA Tech was very cooperative in allowing the team to test the laser on several rock samples. The results are very encouraging, but the beam configuration (being a rectangle) needs work. Figure 14 shows a shale sample that exhibits the characteristic beam profile of the diode laser. The four bars that together create the 4 kW of power each cut a line in the sample. The combination of the four lines creates a sizable hole.

A table of the results can be seen in Appendix F.

5 Conclusions

The results of this study are an extension of the GRI-funded work in two ways:

1. The test plan was developed to measure the amount of energy required to remove material under various laser conditions, and not how quickly a hole could be made into a rock sample (penetration rate). Focus is on trying to minimize the secondary effects that absorb so much of the laser power.
2. By focusing on establishing an absolute specific energy for each sample, it became clear that there is a measurable difference in this value for the different lithologies, sometimes by an order of magnitude. The GRI study did not show this difference conclusively.

Instead of making deep, narrow holes in the samples, the hole diameters created by the laser beam were larger than the depth. This, in combination with a coaxial purge gas nozzle, meant that the exsolved gases and spalled particles, the cause of much of the energy robbing secondary effects, were removed quickly enough such that the laser beam was continuously hitting newly exposed rock surface. The results may not provide perfect measures of the absolute specific energy, but we are confident that the SE's determined in this study are very close to the intrinsic SE for each sample.

The plan for this study included a series of tests with CW laser beams to determine the absolute SE under the same conditions of the GRI study. It became clear that the CO₂ laser at Argonne National Laboratory, under CW conditions, went from merely scorching the rock to melting it without a discernable spalling zone. Based on these preliminary tests, the experiment plan was modified to focus on the pulsing capabilities of the ND:YAG laser. A series of linear tests were done where the power density was changed along the length of the sample. The tests were performed on the Berea gray sandstone, a shale and a limestone. For each combination of peak power, pulse width and repetition rate, a spalling-only zone was clearly visible. The power density of that zone was used as the starting point of the test matrix developed for each lithology.

Limestone is the only lithology the absolute SE of which is practically the same as the SE range determined in the GRI study (20-50 kJ/cc). It appears that the hole is made by thermal degradation (CaCO₃ to CaO and CO₂) instead of breaking bonds between grains or within mineral crystals as is seen in sands and shales, so there is no melting and no secondary effects to cloud the results.

Reservoir rocks can be removed using a high power laser beam through thermal spalling, melting, or vaporizing. Thermal spallation is the most efficient rock removal mechanism requiring the lowest specific energy. The laser beam

irradiance required for producing the thermal spallation zones are around 920 W/cm² for Berea gray sandstone and 784 W/cm² for shale.

The absolute SE required for laser removal of rock material was obtained in this study by carefully controlling the laser beam irradiance and exposure time and avoiding most of the secondary effects. As laser power increased, two rock removal zones, spallation and melting, were identified. In the sample data the lowest SE occurred at the point just prior to melting.

Increasing beam repetition rate within the same material removal mechanism zone would increase the material removal rate due to an increase of the maximum temperature, thermal cycling frequency, and intensity of laser-driven shock wave within the rock.

In this paper we have presented studies of the effects of the various Nd:YAG laser parameters on the specific energy for samples of shale, limestone, and sandstone. The major observation can be stated as follows:

- Measured SE increases very quickly with the beam exposure time indicating the effects of energy consuming secondary processes.
- Shale samples recorded the lowest specific energy values as compared with limestone and sandstone samples.
- As both pulse repetition rate and pulse width increase, the specific energy decreases, however, pulse width is a more dominant mechanism for reducing the specific energy than the pulse repetition rate.
- Two rock removal zones, spallation and melting, were identified in the shale sample data with the least required SE occurring at the point prior to melting.
- Each rock type has a set of optimal laser parameters to minimize SE as observed in the linear track tests.
- Rates of heat diffusion in rocks are easily and quickly overrun by absorbed energy transfer rates from the laser beam to the rock. As absorbed energy outpaces heat diffusion by the rock matrix, local temperatures rise to the minerals' melting points and quickly increase SE values.
- Sandstones saturated with water cut faster with more power able to be applied before melting commenced.
- The laser is able to spall and melt rock through water.

6 Recommendations

6.1 Phase 2 Research Plan

6.1.1 Additional Fundamental Research

To continue this work, the end has to be defined. The goal for the three-year period originally proposed was to have the design for a field prototype completed, ready to be constructed and tested. This implies many steps that have to be undertaken. The prototype equipment can be separated into systems, each of which has design specifications to be created, potential problems identified and solutions worked out. In this section, the systems will be identified and a work plan outlined.

1. More detailed determination of the spallation/melting zone interfaces should be identified in sandstone, shale and limestone samples to determine their respective minimum SE values. The existence of such a boundary was demonstrated by this study, but its position can be determined with more accuracy.
2. The GRI study, as recorded in S. Batarseh's dissertation, gave strong indication that the rock immediately around the lased hole exhibits increased permeability due to the formation of micro-fractures and the destruction of grain-grain contacts. A follow-up analysis should be conducted to determine the effects of the laser rock interaction on permeability.
3. The shale results were quite surprising. The SE for this lithology is not only about an order of magnitude lower than the sandstone and limestone, but show a clear division between the spalling zone and the melting zone. The SE decreases rapidly to a minimum value, and then jumps up as melting starts. The gradient in the melting zone has a very different value than the gradient in the spalling zone. This result needs to be extended to other shales, since shale characteristics can be extremely varied.
4. One possible mechanism for applying the results of this work to the drilling of deep wells is to alternate the lasing of many spots to create a hole of the desired size. In order to estimate the number of spots required for a given hole, the amount of overlap necessary to create a smooth work face has to be determined. Also, the amount of "relaxation" time necessary to cool a given spot and prevent the accumulation of melted material needs to be measured.

6.1.1.1 In-situ conditions

The laser/rock interaction at atmospheric pressure in air, inert gas and water environments is fairly well understood, due to the GRI study and this Phase 1 DOE study. Mechanical methods of breaking rock are known to change behavior radically when the environment changes to the elevated pressures found at depth

in wells. Phase 2 of the DOE study includes the development of a suitable pressure vessel that will simulate downhole confining stresses and pore pressures. The experiments will start using water as the fluid, and then will involve one or more common drilling fluids.

6.1.2 Modeling and Theoretical Studies

The empirical results from the GRI study and this phase of the DOE project have created a huge body of data. In order to understand and make the best use of this data, a theoretical understanding must be developed. In Phase 2, computer models will assist in creating a theoretical framework for the data.

6.1.3 Engineering Studies

6.1.3.1 Cutting schemes

The research team has discussed several possible designs for bottomhole assemblies. Most involve using optical fiber to bring the energy to the wellbore floor, but whether the energy will be combined into one beam or applied as a number of smaller beams, is yet to be determined. The work planned for fundamental portion of Phase 2 and the other engineering studies will help make this determination.

6.1.3.2 Laser System

The remaining fundamental work to be done in Phase 2 will have as one of its goals to determine the specific laser to be used for the prototype. Candidates at this time include the Nd:YAG, the COIL, a new diode laser and possibly the free electron laser. It should be noted that these lasers are all toward the shorter wavelengths within the infrared frequency band. The Nd:YAG is 1.06 microns, the COIL is 1.31 microns, the diode laser is 0.8 microns, and the free electron is tunable over a fairly wide wavelength range. In contrast, the MIRACL is 3.15 microns and the CO₂ is 10.6 microns.

6.1.3.3 Energy Delivery System

Optical fibers seem to have the characteristics necessary for sending large amounts of power down a hole. However, the diode laser head is so small that, properly reconfigured, it may be possible lower the laser head down into the wellbore. As part of the Phase 2 work, a literature review and summary of optical fibers will be performed.

6.1.3.4 Drill String and Bottom Hole Assembly Systems

Laser drilling will differ from current technology in that no weight on bit is necessary; therefore there is no need for the tensile and compressive strength of steel in the drill string. Also, if optical fiber is used to send the energy down hole, sectional tubing will complicate the deployment of the fiber. A composite coiled tubing system seems like it would perform admirably, as long as pressure

differentials between annulus and tubing interior do not exceed the tubing collapse strength.

Also, since there will be a minimum of abrasive activity around the drill head containing the fiber end effectors and fluid nozzles, there is no need for a heavy steel “bit”. A composite matrix, easily shapeable and millable should work fine.

6.1.3.5 Drilling Fluid and Solids Control Systems

It is our vision that these systems will remain much the same as is being used for the rotary drilling rigs today. Some adaptation will be needed for use in composite tubing.

6.1.3.6 Additional Systems

At some time, a pressure control system will have to be adopted for deeper wells, but for the purposes of the prototype, will not be needed.

7 References

- [1] Economides, M.J., Hill, A.D. & Ehlig-Economides, C. (1994) Petroleum Production Systems, Pearson Education, 624 pp.
- [2] Walters, W.P. & Zukas, J.A. (1998) Fundamentals of Shaped Charges, John Wiley and Sons, 407pp.
- [3] Batarseh, S.I. (2001) Application of laser technology in the oil and gas industry: an analysis of high power laser-rock interaction and its effect on altering rock properties and behavior, PhD thesis, Colorado School of Mines, USA.
- [4] Maurer, W.C. (1968) Novel Drilling Techniques, Pergamon Press, 114pp.
- [5] Batarseh, S.I., Gahan, B.C., Sharma, B.C. & Gowelly, S.I. (2004) Deep hole penetration of rock for oil production using ytterbium fiber laser, in Proceedings of the SPIE International Symposium High-Power Laser Ablation 2004, Taos, NM, USA.
- [6] Somerton, W.H. (1968) Thermal properties and temperature-related behavior of rock/fluid systems, Elsevier Publishing, 258pp.
- [7] Reed, C.B., Xu, Z., Parker, R.A., Gahan, B.C., Batarseh, S.I., Graves, R.M., Figueroa, H., & Deeg, W. (2003) Application of high powered lasers to drilling and completing deep wells, U. S Department of Energy Topical Report ANL/TD/TM03-02.
- [8] Gahan, B.C., Batarseh, S., Sharma, B., Gowelly, S. (2004) Analysis of efficient high-power fiber lasers for well perforation, in Proceedings of the 2004 SPE Annual Technical Conference and Exhibition, Houston, TX, USA.

1. DeGolyer and MacNaughton, One Energy Square, Dallas, Texas, 2000.
2. Andersen, et al, "Deep Drilling Basic Research: Volume 2 - Deep Drilling," GRI 90/0265.2, June 1990, 78p.
3. W.C. Maurer, Novel Drilling Techniques, Pergamon Press, 1968.
4. W.C. Maurer, Advanced Drilling Techniques, Petroleum Publishing, 1980.
5. R.M. Graves and D.G. O'Brien, "Star Wars Laser Technology Applied to Drilling and Completing Gas wells," SPE 49259, 1998.
6. O'Brien, D. and R. Graves, "Targeted Literature Review: Determining the Benefits of StarWars Laser Technology for Drilling and Completing Natural Gas Wells," GRI Topical Report GRI-98/0163, 1998.
7. Batarseh, S., "Application of Laser Technology in the Oil and Gas Industry: An Analysis of High Power Laser-Rock Interaction and Its Effect on Altering Rock Properties and Behavior," PhD Thesis T-5492, Colorado School of Mines, Petroleum Engineering Department, 2001.
8. R.M. Graves and S. Batarseh, "Rock Parameters that Effect Laser-Rock Interaction: Determining the Benefits of Applying Star Wars Laser Technology for Drilling and Completing Oil and Natural Gas Wells," GRI Topical Report GRI-01/0080, 2001a.
9. R.M. Graves and S. Batarseh, "Laser Parameters that Effect Laser-Rock Interaction: Determining the Benefits of Applying Star Wars Laser Technology

- for Drilling and Completing Oil and Natural Gas Wells,” GRI Topical Report GRI-01/0079
10. R.M. Graves and S. Batarseh, “Determining the Benefits of Applying Star Wars Laser Technology for Drilling and Completing Oil and Natural Gas Wells,” GRI Final Report GRI-01/0078
 11. B.C. Gahan, R. A. Parker, S. Batarseh, H. Figueroa, C.B. Reed and Z. Xu, " Laser Drilling: Determination of Energy Required to Remove Rock," SPE 71466, 2001.
 12. J.F. Ready, D. F. Farson, LIA Handbook of Laser Materials Processing, Laser Institute of America, 2001.
 13. W.T. Silfvast, Laser Fundamentals, Cambridge, 1996.
 14. J. Hecht, The Laser Guidebook, McGraw-Hill, 1992.
 15. W.H. Somerton, Thermal Properties and Temperature-related Behavior of Rock/Fluid System. University of California, Development in Petroleum Science. Elsevier, Amsterdam-London-New York-Tokyo, 1992.
 16. B.V. Hunter, K.H. Leong, C.B. Miller, J.F. Golden, R.D. Glesias and P. J. Laverty, "Understanding high-power fiber-optic laser beam delivery," J. Laser Applications, 8, 1996: 307-16.
 17. A. Kuhn, P. French, D.P. Hand, I.J. Blewett, M. Richmond, and J.D.C. Jones, "Preparation of fiber optics for the delivery of high-energy high-beam-quality Nd:YAG laser pulses," Applied Optics, vol. 39, No. 33, 20 November 2000: 6136-43.
 18. Frank M. White, Fluid Mechanics, Third Edition, New York, McGraw-Hill, Inc., 1994:699.
 19. A.H. Clauer, B.P. Fairand, and J. Holbrook, Shock Waves and High Strain Phenomena in Metals, vol. III, Plenum Press, New York, 1981:675-91.
 20. Y. Sano, M. Mukai, K. Okazaki, and M. Obata, Nucl. Instr. And Meth. In Phys. Res. B, vol. 121, 1997:432-39.
 21. J. Johnson, J. Am. Chem. Soc. 32 (1910), p.938.
 22. J. Mitchell, J. Am. Chem. Soc. 123 (1923), p.1055.
 23. Z. Brill, Anorg. Chem., 45 (1905), p. 279.
 24. Z. Brill, Anorg. Chem., 57 (1907), p. 721.
 25. K. W. Ray and F. C. Mathers, I. & E. Chem. 20 (1928), pp. 415-419.
 26. R. Doman, J. Barr and A. Alper, J. Am. Ceram. Soc., 46 (1963), p. 313.

8 Appendix: A-F

A: GTI Laser Applications Bibliography

1. Gahan, B.C., Batarseh, S. 2004. "An Overview of High Power Laser Applications Research from Well Construction and Completion," 2004 International Gas Research Conference (IGRC), Vancouver, BC, November 1-4.
2. Batarseh, S., Gahan, B.C., Sharma, B., Gowelly, S. 2004. "Evaluation of High Power Ytterbium Fiber Lasers for Rock Cutting and Removal Applications," Paper 1402, 23rd International Congress on Applications of Lasers and Electronics, San Francisco, CA, October 4-7.
3. Gahan, B.C., Batarseh, S., Reilly II, J.F., Wilcox, B.H. 2004. "Geological Investigation of the Lunar and Martian Surface and Subsurface Using High Power Lasers," AIAA-2004-6046, American Institute of Aeronautics and Astronautics (AIAA) Space 2004 Conference and Exhibit, San Diego, CA, September 28-30.
4. Gahan, B.C., Batarseh, S., Sharma, B., Gowelly, S. 2004. "Analysis of Efficient High-Power Fiber Lasers for Well Perforation," SPE Paper 90661, SPE Annual Technical Conference and Exhibition, Houston, TX, September 26-29.
5. Batarseh, S., Gahan, B.C. 2004. "Deep Hole Penetration of Rock for Oil Production Using Ytterbium Fiber Laser," SPIE Poster 5448-98, SPIE High-Power Laser Ablation V, Taos, NM, April 25-30.
6. Gahan, B.C., Shiner, B. 2004. "New High-Power Fiber Laser Enables Cutting-Edge Research" GTI Document No. GTI-03/0207, GasTIPS 10(2004): 29-31.
7. Gahan, B.C., Batarseh, S., Parker, R.A. 2003. "Lasers May Offer Alternative to Conventional Wellbore Perforation Techniques" GTI Document No. GTI-03/0153, GasTIPS 9(2003): 25-29.
8. Batarseh, S., Gahan, B.C., Parker, R., Graves, R. 2003. "Rock Phase Control by Using High Power Laser for Production Enhancements," Paper 505, 22nd International Congress on Applications of Lasers and Electronics, Jacksonville, FL, October 13-16.
9. Parker, R., Xu, Z., Reed, C., Graves, S., Gahan, B.C., Batarseh, S. 2003. "Drilling Large Diameter Holes in Rocks Using Multiple Laser Beams," Paper 504, 22nd International Congress on Applications of Lasers and Electronics, Jacksonville, FL, October 13-16.
10. Reed, C., Xu, Z., Parker, R., Graves, S., Gahan, B.C., Batarseh, S., Deeg, W. 2003 "Laser Rock Drilling for Oil and Gas Wells," 2003 AAPG Mid-Continent Section Meeting, Tulsa, OK, October 12-14.

11. Batarseh, S.; Gahan, B.C.; Graves, R.M.; Parker, R.A. 2003. "Well Perforation Using High-Power Lasers," SPE Paper 84418, SPE Annual Technical Conference and Exhibition, Denver, CO, October 5-8.
12. Parker, R.A.; Gahan, B.C.; Graves, R.M.; Batarseh, S.; Xu, Z.; Reed, C.B. 2003. "Laser Drilling: Effects of Beam Application Methods on Improving Rock Removal," SPE Paper 84353, SPE Annual Technical Conference and Exhibition, Denver, CO, October 5-8.
13. Xu, Z., Reed, C., Parker, R., Gahan, B., Batarseh, S., Graves, R., Figueroa, H., W. Deeg. 2003. "Application of High Powered Lasers to Drilling and Completing Deep Wells," Topical Report ANL/TD/TM03-02, DOE/NGOTP Contract Number 49066.
14. Xu, Z., Reed, C., Kornecki, G., Gahan, B., Parker, R., Batarseh, S., Graves, R., Figueroa, H., Skinner, N., 2002. "Specific Energy for Pulsed Laser Rock Drilling," Journal of Laser Applications 15(2003):25-30.
15. Graves, R., Batarseh, S., Parker, R., Gahan, B. 2002. "Temperatures Induced by High Power Lasers: Effects on Reservoir Rock Strength and Mechanical Properties," SPE/ISRM Paper 78154, SPE/ISRM Rock Mechanics Conference, Irving, Texas, October 20-23.
16. Xu, Z., Reed, C., Gahan, B., Parker, R., Batarseh, S., Graves, R., Figueroa, H. 2002. "Laser Rock Drilling by a Super-pulsed CO₂ Laser Beam," 21st International Congress on Applications of Lasers and Electronics, Scottsdale, AZ, October 14-17.
17. Graves, R., Araya, A., Gahan, B., Parker, R. 2002. SPE, "Comparison of Specific Energy Between Drilling With High Power Lasers and Other Drilling Methods," SPE Paper 77627, Annual Technical Conference and Exhibition of the Society of Petroleum Engineers, San Antonio, Texas, September 29 – October 2.
18. Gahan, B.C., Batarseh, S, Siegfried, R.W. 2002. "Improving Gas Well Drilling And Completion With High Energy Lasers," GTI Annual Conference and Exhibition on Natural Gas Technologies, Orlando, FL, September 30 - October 2.
19. Figueroa, H.G., LeGreca, A., Gahan, B.C., Parker, R.A., Graves, R.M., Batarseh, S., Skinner, N., Reed, C.B., Xu, Z. 2002. "Rock Removal Using High Power Lasers For Petroleum Exploitation Purposes," SPIE paper 4760-89, International Society for Optical Engineering's International Symposium on High-Power Laser Ablation 2002, Taos, NM, April 21-26.

20. Gahan, B.C. 2002. "Laser Drilling: Understanding Laser/Rock Interaction Fundamentals." GasTIPS 8(2002):4-8.
21. Gahan, B., Parker, R.A., Graves, R., Batarseh, S., Reed, C.B., Xu, Z., Figueroa, H., Skinner, N. 2001. "Laser Drilling: Drilling with the Power of Light, Phase 1: Feasibility Study," DOE Topical Report, Cooperative Agreement No. DE-FC26-00NT40917.
22. Gahan, B.C., Parker, R.A., Batarseh, S., Figueroa, H., Reed, C.B., Xu, Z. 2001. "Laser Drilling: Determination of Energy Required to Remove Rock," SPE paper 71466, Annual Technical Conference and Exhibition of the Society of Petroleum Engineers, New Orleans, LA September 30-October 3.
23. Xu, Z., Reed, C.B., Parker, R.A., Gahan, B.C., Graves, R., Figueroa, H. 2001. "Specific Energy for Laser Removal and Destruction of Rocks," 20th International Congress on Applications of Lasers and Electronics, Jacksonville, FL October 15-18.

B: Tables of Results

Experiment: Methods of calculating Specific energy

Sample Name	Core dia. (cm)	Core length (cm)	Weight before lasing (gm)	Weight after lasing (gm)	Weight removed by lasing (gm)	Calculated spot size (inch)	Laser power (kW)	Lasing time (sec)	Density (gm/cc)	Volume removed (cc)	Specific Energy based on weight removed (kJ/cc)	hole dia (cm)	depth of penetration (cm)	Specific Energy based on hole dimensions (kJ/cc)
BG-SC2	5.005	5.298	217.9	212.8	5.1	0.3585	5.34	8	2.1	2.4	17.5	1.621	3.03	20.5
BG-SC3	5.004	5.422	222.1	216.7	5.4	0.3585	5.34	8	2.1	2.6	16.5	1.764	2.95	17.8
BG-SC4	5.004	5.342	221.8	216.9	4.9	0.3585	5.34	8	2.1	2.3	18.4	1.71	2.974	18.8
BG-SC5	5.008	5.361	221.9	217	4.9	0.3585	5.34	8	2.1	2.3	18.3	1.671	3.004	19.5
BG-SC6	5.009	5.354	221.1	216.8	4.3	0.3585	5.34	8	2.1	2.1	20.8	1.69	3.048	18.7
BG-SC7	5.004	5.419	223.2	219	4.2	0.3585	5.34	8	2.1	2.0	21.3	1.697	2.95	19.2
BG-SC8	5.003	5.313	219.9	215.9	4	0.3585	5.34	8	2.1	1.9	22.5	1.748	3.026	17.6
BG-SC9	5.004	5.403	223	218.8	4.2	0.3585	5.34	8	2.1	2.0	21.3	1.617	2.958	21.1
BG-SC10	5.004	5.398	222.7	218	4.7	0.3585	5.34	8	2.1	2.2	19.1	1.76	2.938	17.9
Average											19.5			19.0

Experiment: Effect of orientation (of structure of formation to laser) on specific energy

Material: Limestone

Face Side	Calculated spot size (inch)	Inside hole diameter (cm)	Outside hole diameter (cm)	Hole depth (cm)	Laser power (kW)	Lasing time (sec)	Specific Energy (kJ/cc)
A	0.3585	1.1	1.5	3.24	5.34	8	41.6
B	0.3585	1.1	1.4	3.49	5.34	8	38.9
C	0.3585	1.1	1.3	3.63	5.34	8	35.2
D	0.3585	1.2	1.4	3.73	5.34	8	31.8
E	0.3585	1.2	1.4	3.65	5.34	8	33.3
F	0.3585	1.1	1.5	3.54	5.34	8	36.5

Material: Sandstone

Face Side	Calculated spot size (inch)	Hole diameter (cm)	Hole depth (cm)	Laser power (kW)	Lasing time (sec)	Specific Energy (kJ/cc)
A	0.3585	1.6	3.2	5.34	8	20.4
B	0.3585	1.6	3.5	5.34	8	18.9
C	0.3585	1.6	3.6	5.34	8	18.2
D	0.3585	1.6	3.7	5.34	8	17.7
E	0.3585	1.6	3.6	5.34	8	18.1
F	0.3585	1.6	3.5	5.34	8	18.6

Experiment: Effect of boundary (heat flow) on specific energy

Material: Sandstone

Spot size: 0.35”

Sample Name	Core dia. (cm)	Core length (cm)	Weight before lasing (gm)	Weight after lasing (gm)	Weight removed by lasing (gm)	Calculated spot size (inch)	Laser power (kW)	Lasing time (sec)	Density (gm /cc)	Volume removed (cc)	Specific Energy based on weight removed (kJ/cc)	Avg. Specific Energy based on weight removed (kJ/cc)
BGSS-C-B1	10.1	5.4	919.7	908.6	11.1	0.3585	5.34	4	2.10	5.27	4.05	4.49
BBSS-C-B2	10.1	5.3	881.3	872.6	8.7	0.3585	5.34	4	2.07	4.21	5.08	
BGSS-C-B3	10.1	5.6	934.3	924	10.3	0.3585	5.34	4	2.10	4.91	4.35	
BBSS-C-B4	7.5	5.4	499.6	495.3	4.3	0.3585	5.34	4	2.09	2.06	10.37	11.51
BGSS-C-B5	7.5	5.4	504	500	4	0.3585	5.34	4	2.09	1.92	11.14	
BBSS-C-B6	7.6	5.4	501.4	498	3.4	0.3585	5.34	4	2.07	1.64	13.03	
BGSS-C-B7	6.9	5.3	415.3	412.5	2.8	0.3585	5.34	4	2.10	1.33	16.01	14.65
BBSS-C-B8	6.9	5.4	421.4	418.4	3	0.3585	5.34	4	2.09	1.43	14.91	
BGSS-C-B9	6.9	5.3	417.5	414.1	3.4	0.3585	5.34	4	2.07	1.64	13.02	
BBSS-C-B10	5.1	5.4	222.7	221.4	1.3	0.3585	5.34	4	2.07	0.63	33.94	32.88
BGSS-C-B11	5.0	5.3	219.8	218.4	1.4	0.3585	5.34	4	2.09	0.67	31.82	
BBSS-C-B12	5.0	4.5	188.8	186.4	2.4	0.3585	5.34	4	2.08	1.15	18.54	
BGSS-C-B13	2.5	5.3	53.1	52.3	0.8	0.3585	5.34	4	2.08	0.39	55.44	55.34
BBSS-C-B14	2.5	5.3	52.7	51.9	0.8	0.3585	5.34	4	2.07	0.39	55.24	
BGSS-C-B15	2.5	5.3	52.1	51.5	0.6	0.3585	5.34	4	2.06	0.29	73.19	
BBSS-C-B16	1.9	5.3	30.9	30.2	0.7	0.3585	5.34	4	2.03	0.35	61.83	62.51
BGSS-C-B17	1.9	5.3	31.9	31.2	0.7	0.3585	5.34	4	2.07	0.34	63.20	
BBSS-C-B18	1.9	5.3	31.4	31	0.4	0.3585	5.34	4	2.08	0.19	111.06	

Experiment: Effect of boundary (heat flow) on specific energy

Material: Limestone

Spot size: 0.35”

Sample Name	Core dia. (cm)	Core length (cm)	Weight before lasing (gm)	Weight after lasing (gm)	Weight removed by lasing (gm)	Calculated spot size (inch)	Laser power (kW)	Lasing time (sec)	Density (gm /cc)	Volume removed (cc)	Specific Energy based on weight removed (kJ/cc)	Avg. Specific Energy based on weight removed (kJ/cc)
LS-C-B1	10.1	5.4	981.3	970.5	10.8	0.3585	5.34	4	2.27	4.76	4.48	4.67
LS-C-B2	10.1	5.4	967.6	956.9	10.7	0.3585	5.34	4	2.26	4.74	4.50	
LS-C-B3	10.1	5.2	963.2	953.4	9.8	0.3585	5.34	4	2.31	4.24	5.04	
LS-C-B4	7.5	5.3	533.7	530.8	2.9	0.3585	5.34	4	2.23	1.30	16.42	12.87
LS-C-B5	7.6	5.6	559.6	555	4.6	0.3585	5.34	4	2.23	2.06	10.37	
LS-C-B6	7.5	5.2	532.1	528	4.1	0.3585	5.34	4	2.27	1.81	11.82	
LS-C-B8	6.9	5.4	455.5	451.6	3.9	0.3585	5.34	4	2.26	1.73	12.35	14.00
LS-C-B9	6.9	5.4	462.3	459.2	3.1	0.3585	5.34	4	2.27	1.37	15.64	
LS-C-B10	5.0	5.3	236.3	234.1	2.2	0.3585	5.34	4	2.25	0.98	21.82	
LS-C-B11	5.0	5.3	235.7	233.3	2.4	0.3585	5.34	4	2.24	1.07	19.97	22.38
LS-C-B12	5.0	5.3	238	236.1	1.9	0.3585	5.34	4	2.25	0.84	25.34	
LS-C-B13	2.4	5.4	52.4	51.1	1.3	0.3585	5.34	4	2.20	0.59	36.15	
LS-C-B14	2.5	5.3	56.5	55	1.5	0.3585	5.34	4	2.24	0.67	31.85	31.90
LS-C-B15	2.5	5.3	55.1	53.4	1.7	0.3585	5.34	4	2.20	0.77	27.68	

Experiment: Effect of beam density on specific energy (spot size before and after focal point)

Distance between Lens and sample: 641.5 mm for before FL exp
 1358 mm for before FL exp

	Sample name	Avg. Laser power (kW)	Exposure time (sec)	Spot size (inch)	Measured horizontal dia. (cm)	Measured vertical dia. (cm)	Average Dia. (cm)	Depth of penetration (cm)	SE based on dimensions kJ/cc (cone)	Average specific energy (kJ/cc)
Sample before focal point	BF1	5.34	4	0.35	1.667	1.777	1.722	1.804	15.25211	15.51723
	BF2	5.34	4	0.35	1.651	1.739	1.695	1.761	16.12627	
	BF3	5.34	4	0.35	1.721	1.722	1.7215	1.752	15.71392	
	BF4	5.34	4	0.35	1.621	1.784	1.7025	1.809	15.56037	
	BF5	5.34	4	0.35	1.711	1.726	1.7185	1.85	14.93351	
Sample after focal point	AF1	5.34	4	0.35	1.329	1.371	1.35	2.202	20.33049	19.19076
	AF2	5.34	4	0.35	1.37	1.371	1.3705	2.205	19.69999	
	AF3	5.34	4	0.35	1.458	1.333	1.3955	2.287	18.31921	
	AF4	5.34	4	0.35	1.307	1.495	1.401	2.297	18.09653	
	AF5	5.34	4	0.35	1.339	1.4	1.3695	2.23	19.50759	

Experiment: Effect of laser power on specific energy

Material: Limestone

Spot size: 0.35"

Percentage laser power (%)	Percentage laser power (kW)	lasing time (sec)	Inside hole diameter (cm)	Outside hole diameter (cm)	Hole depth (cm)	Specific energy (kJ/cc)
10	0.53	8	0.00	0.00	0.00	-
20	1.07	8	1.03	1.49	0.10	310.03
30	1.60	8	1.14	1.49	0.10	375.36
40	2.14	8	0.97	1.49	0.49	143.63
50	2.67	8	0.96	1.48	0.77	116.21
60	3.20	8	1.00	1.66	1.21	80.65
70	3.74	8	1.03	1.66	1.58	68.36
80	4.27	8	1.03	1.66	2.15	57.15
90	4.81	8	1.03	1.66	2.56	53.99
100	5.34	8	1.03	1.66	2.94	52.26

Experiment: Effect of laser power on specific energy

Material: Sandstone

Spot size: 0.35”

Percentage laser power (%)	Percentage laser power (kW)	lasing time (sec)	Vertical hole diameter (cm)	Horizontal hole diameter (cm)	Hole depth (cm)	Specific energy (kJ/cc)
20	1.07	4	0.91	1.17	0.30	64.39
30	1.60	4	1.05	1.35	0.56	39.34
40	2.14	4	1.09	1.39	1.03	26.60
50	2.67	4	1.19	1.39	1.15	24.99
60	3.20	4	1.11	1.40	1.25	31.91
70	3.74	4	1.16	1.37	1.41	30.08
80	4.27	4	1.18	1.57	1.40	33.39
90	4.81	4	1.17	1.43	1.47	36.39
100	5.34	4	1.16	1.29	1.31	46.14

Experiment: Effect of lasing time on specific energy (Samples 1-20)

Material: Limestone

Spot size: 0.35”

Sample name	Avg. Laser power (kW)	Exposure time (sec)	Spot size (inch)	Measured horizontal dia. (cm)	Depth of penetration (cm)	SE based on dimensions kJ/cc (cone)	Average SE based on dimensions kJ/cc (cone)
1	5.34	1	0.3585	1.29	0.86	14.38	
2	5.34	1	0.3585	1.29	0.86	14.26	14.32
3	5.34	2	0.3585	1.27	1.68	15.05	
4	5.34	2	0.3585	1.27	1.68	15.08	15.06
5	5.34	3	0.3585	1.26	2.28	16.85	
6	5.34	3	0.3585	1.26	2.29	16.89	16.87
7	5.34	4	0.3585	1.26	2.22	23.24	
8	5.34	4	0.3585	1.26	2.22	23.22	23.23
9	5.34	5	0.3585	1.26	2.27	28.36	
10	5.34	5	0.3585	1.26	2.25	28.59	28.48
11	5.34	6	0.3585	1.26	2.75	28.17	
12	5.34	6	0.3585	1.26	2.77	27.91	28.04
13	5.34	7	0.3585	1.26	2.91	30.96	
14	5.34	7	0.3585	1.26	2.88	31.35	31.15
15	5.34	8	0.3585	1.26	3.34	30.86	
16	5.34	8	0.3585	1.26	3.01	34.29	32.58
17	5.34	9	0.3585	1.26	3.37	34.38	
18	5.34	9	0.3585	1.26	3.35	34.59	34.48
19	5.34	10	0.3585	1.26	3.47	37.12	
20	5.34	10	0.3585	1.26	3.46	37.27	37.20

Experiment: Effect of lasing time on specific energy (Samples 21-40)

Material: Limestone

Spot size: 0.35”

Sample name	Avg. Laser power (kW)	Exposure time (sec)	Spot size (inch)	Measured horizontal dia. (cm)	Depth of penetration (cm)	SE based on dimensions kJ/cc (cone)	Average SE based on dimensions kJ/cc (cone)
22	5.34	11	0.3585	1.26	3.60	39.40	39.30
23	5.34	12	0.3585	1.26	3.64	42.49	
24	5.34	12	0.3585	1.26	4.07	38.03	40.26
25	5.34	13	0.3585	1.26	4.15	40.37	
26	5.34	13	0.3585	1.26	3.97	42.24	41.31
27	5.34	14	0.3585	1.26	3.77	47.81	
28	5.34	14	0.3585	1.26	3.84	46.97	47.39
29	5.34	15	0.3585	1.26	4.41	43.82	
30	5.34	15	0.3585	1.26	3.79	50.96	47.39
31	5.34	16	0.3585	1.26	4.58	45.07	
32	5.34	16	0.3585	1.26	4.40	46.87	45.97
33	5.34	17	0.3585	1.26	4.30	50.96	
34	5.34	17	0.3585	1.26	4.92	44.57	47.76
35	5.34	18	0.3585	1.26	4.49	51.68	
36	5.34	18	0.3585	1.26	4.45	52.10	51.89
37	5.34	19	0.3585	1.26	4.18	58.60	
38	5.34	19	0.3585	1.26	4.95	49.44	54.02
39	5.34	20	0.3585	1.26	4.70	54.83	
40	5.34	20	0.3585	1.26	4.46	57.77	56.30

Experiment: Effect of lasing time on specific energy (Samples 1-20)

Material: Sandstone Spot size: 0.35”

Sample name	Avg. Laser power (kW)	Exposure time (sec)	Spot size (inch)	Measured horizontal dia. (cm)	Measured vertical dia. (cm)	Average Dia. (cm)	Depth of penetration (cm)	SE based on dimensions kJ/cc (cone)	Average SE based on dimensions kJ/cc (cone)
1	5.34	1	0.3585	1.66	1.66	1.66	0.86	8.64	
2	5.34	1	0.3585	1.66	1.66	1.66	0.86	8.58	8.61
3	5.34	2	0.3585	1.66	1.66	1.66	1.68	8.75	
4	5.34	2	0.3585	1.66	1.66	1.66	1.68	8.75	8.75
5	5.34	3	0.3585	1.68	1.72	1.70	2.28	9.26	
6	5.34	3	0.3585	1.68	1.72	1.70	2.29	9.24	9.25
7	5.34	4	0.3585	1.65	1.72	1.69	2.22	12.97	
8	5.34	4	0.3585	1.68	1.72	1.70	2.22	12.72	12.84
9	5.34	5	0.3585	1.63	1.71	1.67	2.27	16.15	
10	5.34	5	0.3585	1.64	1.73	1.68	2.25	15.99	16.07
11	5.34	6	0.3585	1.69	1.76	1.72	2.75	15.04	
12	5.34	6	0.3585	1.69	1.76	1.72	2.77	14.88	14.96
13	5.34	7	0.3585	1.62	1.74	1.68	2.91	17.38	
14	5.34	7	0.3585	1.60	1.75	1.67	2.88	17.78	17.58
15	5.34	8	0.3585	1.70	1.70	1.70	3.34	17.00	
16	5.34	8	0.3585	1.71	1.63	1.67	3.01	19.48	18.24
17	5.34	9	0.3585	1.59	1.71	1.65	3.37	19.95	
18	5.34	9	0.3585	1.59	1.69	1.64	3.35	20.30	19.95
19	5.34	10	0.3585	1.68	1.74	1.71	3.47	20.09	
20	5.34	10	0.3585	1.64	1.74	1.69	3.46	20.62	20.35

Experiment: Effect of lasing time on specific energy (Samples 21-40)

Material: Sandstone

Spot size: 0.35”

Sample name	Avg. Laser power (kW)	Exposure time (sec)	Spot size (inch)	Measured horizontal dia. (cm)	Measured vertical dia. (cm)	Average Dia. (cm)	Depth of penetration (cm)	SE based on dimensions kJ/cc (cone)	Average SE based on dimensions kJ/cc (cone)
21	5.34	11	0.3585	1.66	1.77	1.72	3.62	21.08	
22	5.34	11	0.3585	1.60	1.77	1.69	3.60	21.96	21.52
23	5.34	12	0.3585	1.61	1.44	1.53	3.64	28.91	
24	5.34	12	0.3585	1.64	1.79	1.71	4.07	20.52	20.52
25	5.34	13	0.3585	1.62	1.79	1.70	4.15	22.02	
26	5.34	13	0.3585	1.67	1.78	1.72	3.97	22.55	22.29
27	5.34	14	0.3585	1.65	1.75	1.70	3.77	26.21	
28	5.34	14	0.3585	1.68	1.77	1.73	3.84	24.95	25.58
29	5.34	15	0.3585	1.67	1.79	1.73	4.41	23.16	
30	5.34	15	0.3585	1.54	1.54	1.54	3.79	34.18	23.16
31	5.34	16	0.3585	1.64	1.79	1.72	4.58	24.22	
32	5.34	16	0.3585	1.59	1.59	1.59	4.40	29.34	26.78
33	5.34	17	0.3585	1.57	1.75	1.66	4.30	29.26	
34	5.34	17	0.3585	1.61	1.80	1.70	4.92	24.31	26.79
35	5.34	18	0.3585	1.61	1.80	1.70	4.49	28.17	
36	5.34	18	0.3585	1.60	1.78	1.69	4.45	28.94	28.55
37	5.34	19	0.3585	1.40	1.68	1.54	4.18	39.00	
38	5.34	19	0.3585	1.57	1.77	1.67	4.95	28.04	28.04
39	5.34	20	0.3585	1.59	1.80	1.70	4.70	30.20	
40	5.34	20	0.3585	1.52	1.67	1.60	4.46	35.89	33.05

Experiment: Effect of pulsation on specific energy

Material: Limestone

Spot size: 0.35”

Duty cycle: 99 %

Experiment Name	Frequency (hz)	Inside hole diameter (cm)	Outside hole diameter (cm)	Hole depth (cm)	Laser power (kW)	Lasing time (sec)	Specific energy (kJ/cc)	Average specific energy (kJ/cc)
A10	10	1.06	1.66	0.94	5.34	4	76.27	
B10	10	0.99	1.60	1.10	5.34	4	75.26	75.77
A50	50	0.99	1.64	0.96	5.34	4	84.80	
B50	50	1.05	1.65	1.03	5.34	4	71.33	78.07
A100	100	1.04	1.63	1.00	5.34	4	74.48	
B100	100	1.04	1.64	0.81	5.34	4	91.92	83.20
A150	150	1.02	1.62	0.96	5.34	4	81.67	
B150	150	1.04	1.60	0.97	5.34	4	76.39	79.03
A200	200	1.00	1.65	1.03	5.34	4	78.03	
B200	200	1.03	1.63	1.04	5.34	4	74.07	76.05
A300	300	1.09	1.65	0.97	5.34	4	70.06	
B300	300	1.01	1.66	0.98	5.34	4	80.55	75.30
A350	350	0.99	1.65	1.02	5.34	4	80.23	
B350	350	1.03	1.62	1.04	5.34	4	72.36	76.30

Experiment: Effect of pulsation on specific energy (continued)

Material: Limestone

Spot size: 0.35”

Duty cycle: 99 %

Experiment Name	Frequency (hz)	Inside hole diameter (cm)	Outside hole diameter (cm)	Hole depth (cm)	Laser power (kW)	Lasing time (sec)	Specific energy (kJ/cc)	Average specific energy (kJ/cc)
A400	400	1.01	1.65	1.00	5.34	4	79.89	
B400	400	1.02	1.62	1.02	5.34	4	76.34	78.12
A500	500	1.05	1.67	1.03	5.34	4	71.27	
B500	500	1.03	1.70	1.04	5.34	4	73.21	72.24
A600	600	1.01	1.66	1.03	5.34	4	76.64	
B600	600	0.97	1.66	1.15	5.34	4	74.10	75.37
A700	700	0.96	1.64	1.00	5.34	4	87.11	
B700	700	1.08	1.66	0.99	5.34	4	69.62	78.36
A800	800	1.02	1.68	0.99	5.34	4	78.12	
B800	800	1.09	1.69	0.95	5.34	4	71.34	74.73
A900	900	1.03	1.67	0.93	5.34	4	81.96	
B900	900	1.02	1.66	1.10	5.34	4	70.85	76.40

Experiment: Effect of pulsation on specific energy

Material: Limestone

Spot size: 0.35”

Duty cycle: 50 %

Frequency (hz)	Inside hole diameter (cm)	Outside hole diameter (cm)	Hole depth (cm)	Laser power (kW)	Lasing time (sec)	Specific energy (kJ/cc)
10	1.25	-	0.30	5.34	4	86.45
50	1.28	-	0.29	5.34	4	86.76
100	1.3	-	0.29	5.34	4	84.40
200	0.98	-	0.16	5.34	4	265.48
300	0.398	-	0.14	5.34	4	1839.54
400	1.05	-	0.01	5.34	4	7400.38
500	no hole	-		5.34	4	
600	no hole	-		5.34	4	
700	no hole	-		5.34	4	
800	no hole	-		5.34	4	
900	no hole	-		5.34	4	
cw	1.253	1.42	1.00	5.34	4	51.97

Experiment: Effect of pulsation on specific energy

Material: Limestone

Spot size: 0.35”

Duty cycle: 50 %

Frequency (hz)	Inside hole diameter (cm)	Outside hole diameter (cm)	Hole depth (cm)	Laser power (kW)	Lasing time (sec)	Specific energy (kJ/cc)
1	1.09	1.40	1.03	5.34	8	67.00
2	1.09	1.40	0.97	5.34	8	70.80
3	1.09	1.40	0.93	5.34	8	73.84
4	1.09	1.40	0.87	5.34	8	78.93
5	1.09	1.40	0.69	5.34	8	99.52
6	1.09	1.40	0.64	5.34	8	107.30
7	1.09	1.40	0.68	5.34	8	100.99
8	1.09	1.40	0.68	5.34	8	100.99
9	1.09	1.40	0.68	5.34	8	100.99
10	1.09	1.40	0.71	5.34	8	96.72

Experiment: Effect of pulsation on specific energy

Material: Sandstone

Spot size: 0.35”

Duty cycle: 99 %

Experiment Name	Frequency (hz)	Hole diameter (horizontal)(cm)	Hole diameter (vertical)(cm)	Average hole diameter (cm)	Hole depth (cm)	Laser power (kW)	Lasing time (sec)	Specific energy (kJ/cc)	Average specific energy (kJ/cc)
A10	10	1.42	1.60	1.51	1.69	5.34	4	20.99	
B10	10	1.42	1.61	1.51	2.12	5.34	4	16.65	18.82
A50	50	1.42	1.56	1.49	2.20	5.34	4	16.54	
B50	50	1.42	1.56	1.49	2.23	5.34	4	16.34	16.44
A100	100	1.42	1.56	1.49	2.24	5.34	4	16.26	
B100	100	1.42	1.56	1.49	1.78	5.34	4	20.49	18.37
A150	150	1.42	1.56	1.49	2.24	5.34	4	16.26	
B150	150	1.42	1.56	1.49	2.28	5.34	4	15.99	16.12
A200	200	1.42	1.56	1.49	2.29	5.34	4	15.89	
B200	200	1.42	1.56	1.49	2.34	5.34	4	15.57	15.73
A300	300	1.42	1.56	1.49	1.87	5.34	4	19.45	
B300	300	1.42	1.56	1.49	2.24	5.34	4	16.28	17.86
A350	250	1.42	1.56	1.49	2.23	5.34	4	16.29	
B350	350	1.42	1.56	1.49	2.29	5.34	4	15.92	16.10

Experiment: Effect of pulsation on specific energy (continued)

Material: Sandstone

Spot size: 0.35”

Duty cycle: 99 %

Experiment Name	Frequency (hz)	Hole diameter (horizontal)(cm)	Hole diameter (vertical)(cm)	Average hole diameter (cm)	Hole depth (cm)	Laser power (kW)	Lasing time (sec)	Specific energy (kJ/cc)	Average specific energy (kJ/cc)
B400	400	1.42	1.56	1.49	1.70	5.34	4	21.38	18.50
A500	500	1.42	1.56	1.49	2.20	5.34	4	16.52	
B500	500	1.42	1.56	1.49	2.25	5.34	4	16.16	16.34
A600	600	1.42	1.56	1.49	2.25	5.34	4	16.17	
B600	600	1.42	1.56	1.49	2.26	5.34	4	16.13	16.15
A700	700	1.42	1.56	1.49	1.66	5.34	4	21.92	
B700	700	1.42	1.56	1.49	2.19	5.34	4	16.64	19.28
A800	800	1.42	1.56	1.49	2.23	5.34	4	16.34	
B800	800	1.42	1.56	1.49	2.22	5.34	4	16.37	16.35
A900	900	1.42	1.56	1.49	2.22	5.34	4	16.41	
B900	900	1.42	1.56	1.49	1.65	5.34	4	22.12	19.26
A999	999	1.42	1.56	1.49	2.12	5.34	4	17.18	
B999	999	1.42	1.56	1.49	2.08	5.34	4	17.47	17.33

Experiment: Effect of pulsation on specific energy

Material: Sandstone

Spot size: 0.35”

Duty cycle: 50 %

Frequency (hz)	Horizontal hole diameter (cm)	Vertical hole diameter (cm)	Average hole diameter (cm)	Hole depth (cm)	Laser power (kW)	Lasing time (sec)	Specific energy (kJ/cc)
1	1.42	1.60	1.51	2.21	5.34	8	16.29
2	1.41	1.54	1.47	2.19	5.34	8	17.20
3	1.39	1.57	1.48	2.13	5.34	8	17.53
4	1.40	1.59	1.50	1.96	5.34	8	18.60
5	1.32	1.40	1.36	1.51	5.34	8	29.31
6	1.39	1.49	1.44	1.86	5.34	8	21.15
7	1.37	1.44	1.40	2.07	5.34	8	19.99
8	1.41	1.45	1.43	1.56	5.34	8	25.58
9	1.27	1.22	1.24	1.47	5.34	8	35.84
10	1.02	1.02	1.02	1.32	5.34	8	59.55
50	1.07	1.07	1.07	1.30	5.34	8	54.72
100	1.43	1.43	1.43	2.09	5.34	8	19.12
200	1.26	1.22	1.24	1.25	5.34	8	42.35
300	1.38	1.38	1.38	1.86	5.34	8	22.94
400	1.47	1.39	1.43	1.39	5.34	8	28.78
500	1.28	1.28	1.28	1.15	5.34	8	43.36
600	1.29	1.29	1.29	1.15	5.34	8	43.08
700	1.41	1.41	1.41	1.22	5.34	8	33.62
800	1.35	1.35	1.35	1.22	5.34	8	36.83
900	1.37	1.35	1.36	0.90	5.34	8	49.23
999	1.30	1.30	1.30	0.69	5.34	8	69.76

Experiment: Effect of purge gas and saturation on specific energy

Material: Sandstone

Spot size: 0.35”

Sample Name	Core dia. (mm)	Core length (mm)	Weight (dry) before lasing (gm)	Weight (wet) before lasing (gm)	Weight after lasing (gm)	Weight removed (gm)	Specific density (gm/cc)	Volume removed (cc)	SE (kJ/cc)	Average SE (kJ/cc)
BG-P-AR-SW1	50.48	51.68	221.9	240.4	235.8	4.6	2.15	2.18	18.37	18.50
BG-P-AR-SW2	50.48	51.62	220.7	239.3	234.7	4.6	2.14	2.18	18.37	
BG-P-AR-SW3	50.48	51.49	220.4	238.8	234.3	4.5	2.14	2.13	18.77	
BG-P-AR-SB1	50.53	52.2	221.6	240.1	235.3	4.8	2.12	2.27	17.60	17.14
BG-P-AR-SB2	50.5	51.46	220.9	239.4	234.3	5.1	2.14	2.41	16.56	
BG-P-AR-SB3	50.46	51.5	220.6	238.9	234	4.9	2.14	2.32	17.24	
BG-P-AR-SO1	50.71	51.89	221.7	237.9	234.7	3.2	2.12	1.52	26.40	25.87
BG-P-AR-SO2	50.54	52.1	221.8	237.9	234.6	3.3	2.12	1.56	25.60	
BG-P-AR-SO3	50.42	52	221.4	237.8	234.5	3.3	2.13	1.56	25.60	
BG-P-N-SB1	50.62	52.4	221.5	240.5	236.6	3.9	2.10	1.85	21.66	20.08
BG-P-N-SB2	50.49	52.38	221.4	240.8	236.7	4.1	2.11	1.94	20.60	
BG-P-N-SB3	50.49	52.11	220.4	240	235.3	4.7	2.11	2.23	17.97	
BG-P-N-SW1	50.48	52.5	221.1	240.6	236	4.6	2.10	2.18	18.37	18.27
BG-P-N-SW2	50.48	52.28	220.7	240.1	235.7	4.4	2.11	2.08	19.20	
BG-P-N-SW3	50.48	52.19	220.6	239.6	234.7	4.9	2.11	2.32	17.24	
BG-P-N-SO1	50.48	51.98	219.9	238.1	234.8	3.3	2.11	1.56	25.60	27.00
BG-P-N-SO2	50.51	52.67	220.9	239.1	236	3.1	2.09	1.47	27.25	
BG-P-N-SO3	50.44	51.79	221.5	236.8	233.8	3	2.14	1.42	28.16	

Nomenclature

BG: Burea sandstone B: Brine N: Nitrogen Ar: Argon P: Purge gas O: Oil A: Air S: Saturation W: water H: Helium

Experiment: Effect of purge gas and saturation on specific energy

Material: Sandstone

Spot size: 0.35”

Sample Name	Core dia. (mm)	Core length (mm)	Weight (dry) before lasing (gm)	Weight (wet) before lasing (gm)	Weight after lasing (gm)	Weight removed (gm)	Specific density (gm/cc)	Volume removed (cc)	SE (kJ/cc)	Average SE (kJ/cc)
BG-P-A-SB1	50.44	53.66	220.5	240.2	235.9	4.3	2.06	2.04	19.65	19.05
BG-P-A-SB2	50.48	51.96	220.9	240.6	236.5	4.1	2.12	1.94	20.60	
BG-P-A-SB3	50.42	51.88	214.3	235.3	230.3	5	2.07	2.37	16.90	
BG-P-A-SW1	50.49	51.96	220.6	240.1	236.3	3.8	2.12	1.80	22.23	19.93
BG-P-A-SW2	50.4	51.96	213.8	234.9	230.3	4.6	2.06	2.18	18.37	
BG-P-A-SW3	50.51	51.91	220.7	240.5	236.1	4.4	2.12	2.08	19.20	
BG-P-A-SO1	50.46	52	221.1	236.4	233.4	3	2.13	1.42	28.16	27.86
BG-P-A-SO2	50.43	51.95	223	237.6	234.6	3	2.15	1.42	28.16	
BG-P-A-SO3	50.51	52.66	220	237.3	234.2	3.1	2.08	1.47	27.25	
BG-P-H-SB1	50.5	51.82	219.7	239.2	235.2	4	2.12	1.89	21.12	26.15
BG-P-H-SB2	50.48	52.15	222.9	241.6	238.2	3.4	2.14	1.61	24.85	
BG-P-H-SB3	50.48	51.86	222.4	240	237.4	2.6	2.14	1.23	32.49	
BG-P-H-SW1	50.47	52.47	222.1	240	236.8	3.2	2.12	1.52	26.40	24.67
BG-P-H-SW2	50.48	51.78	219.9	238.9	235.4	3.5	2.12	1.66	24.14	
BG-P-H-SW3	50.55	51.35	221	238.9	235.3	3.6	2.14	1.70	23.47	
BG-P-H-SO1	50.48	52.14	223	238.6	236	2.6	2.14	1.23	32.49	33.83
BG-P-H-SO2	50.53	52.06	222.9	238.5	236	2.5	2.14	1.18	33.79	
BG-P-H-SO3	50.51	52.5	223.1	238.5	236.1	2.4	2.12	1.14	35.20	

Nomenclature:

BG: Burea sandstone B: Brine N: Nitrogen Ar: Argon P: Purge gas O: Oil A: Air S: Saturation W: water H: Helium

Experiment: Effect of purge gas and saturation on specific energy

Material: Sandstone

Spot size: 0.35”

Sample Name	Core dia. (mm)	Core length (mm)	Weight (dry) before lasing (gm)	Weight (wet) before lasing (gm)	Weight after lasing (gm)	Weight removed (gm)	Specific density (gm/cc)	Volume removed (cc)	SE (kJ/cc)	Average SE (kJ/cc)
BG-P-Ar1	50.47	49.91	209	209	204.2	4.8	2.09	2.27	17.60	19.77
BG-P-Ar2	50.48	49.86	209.8	209.8	205.7	4.1	2.10	1.94	20.60	
BG-P-Ar3	50.49	50	209.9	209.9	205.9	4	2.10	1.89	21.12	
BG-P-H1	50.45	49.41	207.9	207.9	204.2	3.7	2.10	1.75	22.83	18.51
BG-P-H2	50.52	49.86	210.9	210.9	206.1	4.8	2.11	2.27	17.60	
BG-P-H3	50.49	49.14	209.4	209.4	203.8	5.6	2.13	2.65	15.09	
BG-P-N1	50.47	49.98	209	209	205.6	3.4	2.09	1.61	24.85	20.82
BG-P-N2	50.5	49.85	211.8	211.8	206.5	5.3	2.12	2.51	15.94	
BG-P-N3	50.47	50.13	209.6	209.6	205.7	3.9	2.09	1.85	21.66	
BG-P-A1	50.49	49.95	209.8	209.8	206.7	3.1	2.10	1.47	27.25	27.55
BG-P-A2	50.49	49.76	207.3	207.3	204.3	3	2.08	1.42	28.16	
BG-P-A3	50.43	51.49	219.1	219.1	216	3.1	2.13	1.47	27.25	

Nomenclature:

BG: Burea sandstone B: Brine N: Nitrogen Ar: Argon P: Purge gas O: Oil A: Air S: Saturation W: water H: Helium

Experiment: Effect of purge gas and saturation on specific energy

Material: Limestone

Spot size: 0.35”

Sample Name	Core dia. (mm)	Core length (mm)	Weight (dry) before lasing (gm)	Weight (wet) before lasing (gm)	Weight after lasing (gm)	Weight Difference (gm)	Specific gravity (gm/cc)	Volume removed (cc)	Specific energy (kJ/cc)	Average SE (kJ/cc)
LS-P-AR-SW1	50.46	51.84	236.3	251.3	246	5.3	2.28	2.33	18.37	27.66
LS-P-AR-SW2	50.45	51.56	233	248.3	245.3	3	2.26	1.33	32.19	
LS-P-AR-SW3	50.48	51.35	234	249.1	246.1	3	2.28	1.32	32.42	
LS-P-AR-SB1	50.46	51.81	234.1	250	247	3	2.26	1.33	32.17	32.24
LS-P-AR-SB2	50.45	51.82	235.7	250.8	247.8	3	2.28	1.32	32.40	
LS-P-AR-SB3	50.47	51.74	233.6	249.2	246.2	3	2.26	1.33	32.14	
LS-P-AR-SO1	50.45	51.28	232.4	242.4	240.6	1.8	2.27	0.79	53.81	55.86
LS-P-AR-SO2	50.49	52.06	234.9	246.3	244.6	1.7	2.25	0.75	56.63	
LS-P-AR-SO3	50.43	51.45	233.7	243.8	242.1	1.7	2.27	0.75	57.15	
LS-P-N-SB1	50.48	51.66	233.5	249.1	246.4	2.7	2.26	1.20	35.73	36.27
LS-P-N-SB2	50.47	51.67	233.9	249.1	246.4	2.7	2.26	1.19	35.80	
LS-P-N-SB3	50.44	50.45	228.7	243.9	241.3	2.6	2.27	1.15	37.28	
LS-P-N-SW1	50.49	51.45	233.3	248.6	245.4	3.2	2.26	1.41	30.24	29.03
LS-P-N-SW2	50.44	51.6	232.5	247.9	244.5	3.4	2.25	1.51	28.33	
LS-P-N-SW3	50.47	51.75	235.1	250	246.6	3.4	2.27	1.50	28.53	
LS-P-N-SO1	50.46	51.62	234.1	244.3	242.7	1.6	2.27	0.71	60.55	60.44
LS-P-N-SO2	50.43	51.87	234.5	246.2	244.6	1.6	2.26	0.71	60.43	
LS-P-N-SO3	50.44	51.58	232.9	244.6	243	1.6	2.26	0.71	60.33	

Nomenclature:

BG: Burea sandstone B: Brine N: Nitrogen Ar: Argon P: Purge gas O: Oil A: Air S: Saturation W: water H: Helium

Experiment: Effect of purge gas and saturation on specific energy

Material: Limestone

Spot size: 0.35”

Sample Name	Core dia. (mm)	Core length (mm)	Weight (dry) before lasing (gm)	Weight (wet) before lasing (gm)	Weight after lasing (gm)	Weight Difference (gm)	Specific gravity (gm/cc)	Volume removed (cc)	Specific energy (kJ/cc)	Average SE (kJ/cc)
LS-P-A-SB1	50.44	51.76	233.9	248.2	245.6	2.6	2.26	1.15	37.16	36.98
LS-P-A-SB2	50.45	51.32	233.2	248.3	245.8	2.5	2.27	1.10	38.84	
LS-P-A-SB3	50.47	49.85	228.4	243.1	240.3	2.8	2.29	1.22	34.94	
LS-P-A-SW1	50.48	51.62	231.3	246.9	243.3	3.6	2.24	1.61	26.57	27.83
LS-P-A-SW2	50.43	51.71	236.3	250.4	246.8	3.6	2.29	1.57	27.15	
LS-P-A-SW3	50.43	51.53	236.7	251.2	247.9	3.3	2.30	1.43	29.77	
LS-P-A-SO1	50.48	51.81	235.8	247	245.1	1.9	2.27	0.84	51.13	50.14
LS-P-A-SO2	50.42	51.59	232.6	244.7	242.7	2	2.26	0.89	48.23	
LS-P-A-SO3	50.44	51.39	233.2	244.1	242.2	1.9	2.27	0.84	51.06	
LS-P-H-SB1	50.42	51.4	234.7	249.4	247.2	2.2	2.29	0.96	44.41	41.39
LS-P-H-SB2	50.44	49.8	225.1	240	237.7	2.3	2.26	1.02	42.02	
LS-P-H-SB3	50.42	49.65	227.7	242.8	240.2	2.6	2.30	1.13	37.74	
LS-P-H-SW1	50.43	51.69	231.5	247.1	244.6	2.5	2.24	1.11	38.31	39.05
LS-P-H-SW2	50.45	51.26	232.3	247.6	245.2	2.4	2.27	1.06	40.35	
LS-P-H-SW3	50.42	51.03	229.4	244.9	242.4	2.5	2.25	1.11	38.47	
LS-P-H-SO1	50.43	51.87	233.7	245.6	244.1	1.5	2.26	0.66	64.24	68.21
LS-P-H-SO2	50.43	51.28	230.7	243.6	242	1.6	2.25	0.71	60.14	
LS-P-H-SO3	50.43	51.62	232.4	244.8	243.6	1.2	2.25	0.53	80.24	

Nomenclature:

BG: Burea sandstone B: Brine N: Nitrogen Ar: Argon P: Purge gas O: Oil A: Air S: Saturation W: water H: Helium

Experiment: Effect of purge gas and saturation on specific energy

Material: Limestone

Spot size: 0.35”

Sample Name	Core dia. (mm)	Core length (mm)	Weight (dry) before lasing (gm)	Weight (wet) before lasing (gm)	Weight after lasing (gm)	Weight Difference (gm)	Specific gravity (gm/cc)	Volume removed (cc)	Specific energy (kJ/cc)	Average SE (kJ/cc)
LS-P-Ar1	50.39	49.44	228.1	225.6	224.1	1.5	2.31	0.65	65.89	58.49
LS-P-Ar2	50.44	49.66	228	225.5	223.9	1.6	2.30	0.70	61.35	
LS-P-Ar3	50.36	49.77	223.9	223.9	221.9	2	2.26	0.89	48.24	
LS-P-H1	50.44	49.34	227.6	227.6	226.1	1.5	2.31	0.65	65.75	65.28
LS-P-H2	50.42	49.81	224	224	222.5	1.5	2.25	0.67	64.15	
LS-P-H3	50.46	49.64	229.9	229.9	228.4	1.5	2.32	0.65	65.96	
LS-P-N1	50.35	49.87	227.6	227.6	225	2.6	2.29	1.13	37.66	37.75
LS-P-N2	50.48	49.88	223.8	223.8	221.3	2.5	2.24	1.12	38.31	
LS-P-N3	50.43	49.49	224.3	224.3	221.7	2.6	2.27	1.15	37.28	
LS-P-A1	50.37	47.83	213.5	213.5	211.6	1.9	2.24	0.85	50.37	45.42
LS-P-A2	50.45	49.27	222.3	222.3	219.9	2.4	2.26	1.06	40.18	
LS-P-A3	50.41	49.77	223.3	223.3	221.2	2.1	2.25	0.93	45.73	

Nomenclature:

BG: Burea sandstone B: Brine N: Nitrogen Ar: Argon P: Purge gas O: Oil A: Air S: Saturation W: water H: Helium

Experiment: Time of penetration for casing material

Material: steel

Spot size: 0.35”

Plate thickness (inch)	Laser power (kW)	Time of penetration Air-purge (sec)	Time of penetration N2-purge (sec)
0.25	5.34	2.45	3.81
0.35	5.34	3	4.72
0.4	5.34	3.59	5.53
0.5	5.34	4.91	7.1
0.6	5.34	6.43	9.69
0.75	5.34	10.27	15.01
1	5.34	20.21	28.46

Experiment: Time of penetration for casing material

Material: Cement (Class A)

Spot size: 0.35”

Plate thickness (inch)	Laser power (kW)	Time of penetration (sec)
0.25	5.34	1.86
0.35	5.34	2.37
0.4	5.34	2.69
0.5	5.34	2.5
0.7	5.34	4.43
0.8	5.34	4.73
0.9	5.34	6
1	5.34	7.03

Experiment: Time of penetration for casing material

Material: Cement (50-50)

Spot size: 0.35”

Plate thickness (inch)	Laser power (kW)	Time of penetration (sec)
0.25	5.34	1.09
0.35	5.34	1.3
0.4	5.34	1.35
0.5	5.34	1.6
0.6	5.34	2.52
0.7	5.34	2.98
0.8	5.34	3.3
0.9	5.34	3.65
1	5.34	4.46
2	5.34	9.49

Experiment: Time of penetration for casing material

Material: Cement (SY 250)

Spot size: 0.35”

Plate thickness (inch)	Laser power (kW)	Time of penetration (sec)
0.25	5.34	0.96
0.35	5.34	1.23
0.4	5.34	1.39
0.5	5.34	1.88
0.6	5.34	1.98
0.7	5.34	2.49
0.8	5.34	2.72
0.9	5.34	3.36
1	5.34	3.77
2	5.34	7.84

Experiment: Time of penetration for casing material

Material: Clad: 0.25" thick steel plate + varying cement layer + 2" thick sandstone core

Spot size: 0.35"

Sample name	cement layer thickness	Laser power (kW)	Time of penetration (sec)	Average time of penetration (sec)
BG-C-S-0.25-1	0.25	5.34	27.04	27.04
BG-C-S-0.35-1	0.35	5.34	29.2	
BG-C-S-0.35-2	0.35	5.34	27.01	28.11
BG-C-S-0.4-1	0.4	5.34	28.8	
BG-C-S-0.4-2	0.4	5.34	30.11	29.46
BG-C-S-0.5-1	0.5	5.34	26.86	
BG-C-S-0.5-2	0.5	5.34	29.95	28.41
BG-C-S-0.6-1	0.6	5.34	35.78	
BG-C-S-0.6-2	0.6	5.34	37.38	36.58
BG-C-S-0.7-1	0.7	5.34	36.06	
BG-C-S-0.7-2	0.7	5.34	47.76	41.91
BG-C-S-0.8-1	0.8	5.34	35.63	
BG-C-S-0.8-2	0.8	5.34	35.26	35.45
BG-C-S-0.9-1	0.9	5.34	40.08	
BG-C-S-0.9-2	0.9	5.34	30.13	35.11
BG-C-S-1-1	1	5.34	46.15	
BG-C-S-1-2	1	5.34	39.05	42.60

Experiment: Time of penetration for casing material

Material: Clad: 0.25" thick steel plate + varying cement layer + 2" thick limestone core

Spot size: 0.35"

Sample name	cement layer thickness (inch)	Laser power (kW)	Time of penetration (sec)	Average time of penetration (sec)
LS-C-S-0.25-1	0.25	5.34	17.11	
LS-C-S-0.25-2	0.25	5.34	17.04	17.08
LS-C-S-0.35-1	0.35	5.34	16.45	
LS-C-S-0.35-2	0.35	5.34	-	16.45
LS-C-S-0.4-1	0.4	5.34	17.75	
LS-C-S-0.4-2	0.4	5.34	17.8	17.78
LS-C-S-0.5-1	0.5	5.34	18.18	
LS-C-S-0.5-2	0.5	5.34	19.51	18.85
LS-C-S-0.6-1	0.6	5.34	20.65	
LS-C-S-0.6-2	0.6	5.34	19.9	20.28
LS-C-S-0.7-1	0.7	5.34	21.03	
LS-C-S-0.7-2	0.7	5.34	20.34	20.69
LS-C-S-0.8-1	0.8	5.34	20.53	
LS-C-S-0.8-2	0.8	5.34	21.59	21.06
LS-C-S-0.9-1	0.9	5.34	22.29	
LS-C-S-0.9-2	0.9	5.34	21.4	21.85
LS-C-S-1-1	1	5.34	23.8	
LS-C-S-1-2	1	5.34	23.98	23.89

Experiment: Transmission of laser power through liquid

Material: water

Fluids Type	Fluid Viscosity (cp)	Fluid Level (cm)	Laser power (kW)	Power meter reading (kW)	Response time (sec)	Wall temperature (deg C)
water	1	1	0.5	0.41	20	23
water	1	1	1	0.4	20	30
water	1	1	1.5	0.55	17	35
water	1	1	2.0	Water started boiling and high temperature broke seal within container		
water	1	1	2.5			

Experiment: Transmission of laser power through liquid

Material: Halocarbon (0.8)

Fluid Level (cm)	Laser power (kW)	Power meter reading (kW)	Wall temperature (deg C)
1	0.534	0.16	23.6
1	1.068	0.59	24
1	1.602	1.03	24.1
1	2.136	1.45	25.4
1	2.67	1.86	31
1	3.204	2.33	31.8
1	3.738	2.68	32.3
1	4.272	3.02	34.2
1	4.806	3.4	37
1	5.34	3.66	38.5
2	0.534	0.15	25.6
2	1.068	0.6	26.3
2	1.602	1.04	26.8
2	2.136	1.46	27.8
2	2.67	1.9	28.6
2	3.204	2.32	29.8
2	3.738	2.7	31
2	4.272	3.02	32.2
2	4.806	3.32	33
2	5.34	3.6	33.9

Experiment: Transmission of laser power through liquid

Material: Halocarbon (0.8)

Fluid Level (cm)	Laser power (kW)	Power meter reading (kW)	Wall temperature (deg C)
3	0.534	0.15	22.7
3	1.068	0.61	23.1
3	1.602	1.06	23.5
3	2.136	1.51	24.2
3	2.67	1.93	25
3	3.204	2.37	25.7
3	3.738	2.72	26.4
3	4.272	3.11	27.6
3	4.806	3.43	28.4
3	5.34	3.71	29.4
4	0.534	0.15	24.9
4	1.068	0.6	25.6
4	1.602	1.05	26.4
4	2.136	1.5	27.9
4	2.67	1.92	29.5
4	3.204	2.35	31.7
4	3.738	2.74	34
4	4.272	3.03	35.4
4	4.806	3.36	38.2
4	5.34	3.65	40.2

Experiment: Transmission of laser power through liquid

Material: Halocarbon (0.8)

Fluid Level (cm)	Laser power (kW)	Power meter reading (kW)	Wall temperature (deg C)
5	0.534	0.15	25.2
5	1.068	0.59	25.9
5	1.602	1.01	27
5	2.136	1.49	28.5
5	2.67	1.92	30.4
5	3.204	2.32	32.5
5	3.738	2.64	34.7
5	4.272	3.03	38.9
5	4.806	3.32	42
5	5.34	3.61	46.7
6	0.534	0.15	26
6	1.068	0.6	26
6	1.602	1.04	27
6	2.136	1.48	28.4
6	2.67	1.91	30.8
6	3.204	2.29	33.5
6	3.738	2.69	38
6	4.272	3	42
6	4.806	3.31	42.9
6	5.34	3.6	48.5

Experiment: Transmission of laser power through liquid

Material: Halocarbon (0.8)

Fluid Level (cm)	Laser power (kW)	Power meter reading (kW)	Wall temperature (deg C)
7	1.068	0.6	27.2
7	1.602	1.05	26.6
7	2.136	1.48	27.3
7	2.67	1.89	29
7	3.204	2.32	31.7
7	3.738	2.69	35.4
7	4.272	3.02	36.5
7	4.806	3.33	41.7
7	5.34	3.6	42.2
8	0.534	0.15	28.8
8	1.068	0.61	28.5
8	1.602	1.05	29.1
8	2.136	1.49	30.2
8	2.67	1.9	31.8
8	3.204	2.32	34.4
8	3.738	2.69	36.6
8	4.272	3.04	39.5
8	4.806	3.34	44.3
8	5.34	3.6	49.3

Experiment: Transmission of laser power through liquid

Material: Halocarbon (0.8)

Fluid Level (cm)	Laser power (kW)	Power meter reading (kW)	Wall temperature (deg C)
9	1.068	0.61	28.5
9	1.602	1.05	29.1
9	2.136	1.49	30.2
9	2.67	1.9	31.8
9	3.204	2.32	34.4
9	3.738	2.69	36.6
9	4.272	3.04	39.5
9	4.806	3.34	44.3
9	5.34	3.6	45.3
10	0.534	0.15	28.6
10	1.068	0.6	28.7
10	1.602	1.03	29.4
10	2.136	1.49	31.2
10	2.67	1.93	34.3
10	3.204	2.33	36
10	3.738	2.68	42.1
10	4.272	3	46.5
10	4.806	3.3	57.8
10	5.34	3.46	64

Experiment: Transmission of laser power through liquid

Material: Halocarbon (95)

Fluid Level (cm)	Laser power (kW)	Power meter reading (kW)	Wall temperature (deg C)	Fluid Level (cm)	Laser power (kW)	Power meter reading (kW)	Wall temperature (deg C)	Fluid Level (cm)	Laser power (kW)	Power meter reading (kW)	Wall temperature (deg C)
1	0.534	0.21	32.1	5	0.534	0.18	28.6	10	0.534	0.2	21.5
1	1.068	0.66	32.4	5	1.068	0.61	36.2	10	1.068	0.65	23.2
1	1.602	1.13	32.5	5	1.602	1.06	43.9	10	1.602	1.1	25.1
1	2.136	1.6	34.4	5	2.136	1.5	44.5	10	2.136	1.54	26.6
1	2.67	2.06	35.4	5	2.67	1.94	52.3	10	2.67	1.98	28.3
1	3.204	2.47	36.1	5	3.204	2.33	55.6	10	3.204	2.39	30.1
1	3.738	2.87	37	5	3.738	2.78	57.8	10	3.738	2.78	34.2
1	4.272	3.23	37.5	5	4.272	3.13	58.3	10	4.272	3.02	37.9
1	4.806	3.52	36.2	5	4.806	3.44	55.4	10	4.806	3.2	40.6
1	5.34	3.78	37	5	5.34	3.71	56.4	10	5.34	3.38	43.8

Experiment: Transmission of laser power through liquid

Material: Halocarbon (200)

Fluid Level (cm)	Laser power (kW)	Power meter reading (kW)	Wall temperature (deg C)	Fluid Level (cm)	Laser power (kW)	Power meter reading (kW)	Wall temperature (deg C)	Fluid Level (cm)	Laser power (kW)	Power meter reading (kW)	Wall temperature (deg C)
1	0.534	0.21	23.4	5	0.534	0.19	24.2	10	0.534	0.17	25
1	1.068	0.65	26.7	5	1.068	0.64	26.5	10	1.068	0.58	29.8
1	1.602	1.11	29.3	5	1.602	1.09	28.9	10	1.602	0.99	35.5
1	2.136	1.56	32.5	5	2.136	1.54	32.3	10	2.136	1.4	40
1	2.67	2.01	35.1	5	2.67	1.98	36.3	10	2.67	1.8	45.8
1	3.204	2.43	38.9	5	3.204	2.4	41.6	10	3.204	2.54	55
1	3.738	2.79	40.4	5	3.738	2.8	45.1	10	3.738	2.85	61.5
1	4.272	3.15	44.3	5	4.272	3.13	46.1	10	4.272	3.09	69.2
1	4.806	3.46	48	5	4.806	3.42	49	10	4.806	-	-
1	5.34	3.76	54	5	5.34	3.68	52.9	10	5.34	3.15	82.5

Experiment: Transmission of laser power through liquid

Material: Halocarbon (400)

Fluid Level (cm)	Laser power (kW)	Power meter reading (kW)	Wall temperature (deg C)	Fluid Level (cm)	Laser power (kW)	Power meter reading (kW)	Wall temperature (deg C)	Fluid Level (cm)	Laser power (kW)	Power meter reading (kW)	Wall temperature (deg C)
1	0.53	0.21	32.1	5	0.53	0.18	28.6	10	0.53	0.19	25.6
1	1.07	0.66	32.4	5	1.07	0.61	36.2	10	1.07	0.61	28.6
1	1.60	1.13	32.5	5	1.60	1.06	43.9	10	1.60	1.05	32.3
1	2.14	1.6	34.4	5	2.14	1.5	44.5	10	2.14	1.48	36.1
1	2.67	2.06	35.4	5	2.67	1.94	52.3	10	2.67	1.91	40
1	3.20	2.47	36.1	5	3.20	2.33	55.6	10	3.20	2.34	45.2
1	3.74	2.87	37	5	3.74	2.78	57.8	10	3.74	2.71	48.2
1	4.27	3.23	37.5	5	4.27	3.13	58.3	10	4.27	3.02	56.8
1	4.81	3.52	36.2	5	4.81	3.44	55.4	10	4.81	3.31	63.5
1	5.34	3.78	37	5	5.34	3.71	56.4	10	5.34	3.65	71.5

Experiment: Transmission of laser power through liquid

Material: Halocarbon (1000)

Fluid Level (cm)	Laser power (kW)	Power meter reading (kW)	Wall temperature (deg C)
2	0.53	0.17	23.7
2	1.07	0.61	27.1
2	1.60	1.03	31.5
2	2.14	1.4	37.4
2	2.67	1.83	42.7
2	3.20	2.29	47.8
2	3.74	2.52	52.8
2	4.27	3.09	53.5
2	4.81	3.32	59
2	5.34	3.6	62.2
4	0.53	0.18	23.6
4	1.07	0.63	25.6
4	1.60	1.04	28.5
4	2.14	1.26	35.1
4	2.67	1.55	45.3
4	3.20	2.12	48.9
4	3.74	2.56	45.6
4	4.27	2.87	51.2
4	4.81	3.14	56.2
4	5.34	3.46	54.6

Experiment: Transmission of laser power through liquid

Material: Halocarbon (1000)

Fluid Level (cm)	Laser power (kW)	Power meter reading (kW)	Wall temperature (deg C)
6	0.53	0.14	35.8
6	1.07	0.49	52.7
6	1.60	0.9	71
6	2.14	1.4	56.8
6	2.67	1.76	54.4
6	3.20	2.08	60
6	3.74	2.44	61.1
6	4.27	2.76	63
6	4.81	3.21	67.4
6	5.34	3.36	65.7
8	0.53	0.18	29.9
8	1.07	0.61	31.6
8	1.60	1.05	33.8
8	2.14	1.49	36.5
8	2.67	1.9	39.7
8	3.20	2.11	56.6
8	3.74	2.28	52.2
8	4.27	2.68	56.1
8	4.81	3.08	43.6
8	5.34	3.21	53.1

Experiment: Transmission of laser power through liquid

Material: Halocarbon (1000)

Fluid Level (cm)	Laser power (kW)	Power meter reading (kW)	Wall temperature (deg C)
10	1.07	0.54	46.6
10	1.60	0.93	56.9
10	2.14	1.34	60.4
10	2.67	1.75	57.8
10	3.20	2.09	59
10	3.74	2.45	56.5
10	4.27	2.52	66.1
10	4.81	2.98	65.1
10	5.34	3.24	65

Experiment: Effect of liquid purge (halocarbon 0.8) on specific energy (at varying power level)

Material: Limestone

Spot size: 0.35”

Percentage laser power (%)	laser power (kW)	lasing time (sec)	Vertical hole diameter (cm)	Hole depth (cm)	Specific energy (kJ/cc)
40	2.14	4	1.12	0.10	260.17
60	3.20	4	1.34	0.24	114.07
80	4.27	4	1.37	0.24	142.53
100	5.34	4	1.5	0.33	111.23
100	5.34	4	1.49	0.33	112.46
100	5.34	6	1.58	0.49	99.24
100	5.34	8	1.62	0.60	103.50
100	5.34	10	1.66	0.93	79.54

Experiment: Effect of liquid purge (halocarbon 0.8) on specific energy (at varying power level)

Material: Sandstone

Spot size: 0.35”

Percentage laser power (%)	laser power (kW)	lasing time (sec)	Vertical hole diameter (cm)	Hole depth (cm)	Specific energy (kJ/cc)
40	2.14	4	1.62	0.42	29.46
60	3.20	4	1.62	0.66	28.06
80	4.27	4	1.70	0.74	30.69
100	5.34	4	1.70	0.84	33.61
100	5.34	4	1.85	0.92	26.00
100	5.34	6	1.93	1.19	27.56
100	5.34	8	2.10	1.27	29.31
100	5.34	10	1.86	1.22	48.39

Experiment: Effect of laser power on specific energy (0.35” collimated beam)

Material: Sandstone

Percentage laser power (%)	laser power (kW)	lasing time (sec)	Vertical hole diameter (cm)	Horizontal hole diameter (cm)	Hole depth (cm)	Specific energy (kJ/cc)
20	1.07	4	1.24	1.14	0.51	20.81
30	1.60	4	1.33	1.22	0.62	22.32
40	2.14	4	1.36	1.32	1.06	16.65
50	2.67	4	1.41	1.33	1.34	15.31
60	3.20	4	1.44	1.37	1.67	14.14
70	3.74	4	1.51	1.39	1.8	13.92
80	4.27	4	1.53	1.47	1.96	14.23
90	4.81	4	1.54	1.46	2.14	14.47
100	5.34	4	1.53	1.53	2.34	14.89
10	0.53	8	0.8	0.86	0.12	
20	1.07	8	1.19	1.03	0.37	62.29
30	1.60	8	1.28	1.27	0.8	37.35
40	2.14	8	1.38	1.29	1.56	21.97
50	2.67	8	1.36	1.33	2.66	16.58
60	3.20	8	1.41	1.34	2.8	17.59
70	3.74	8	1.47	1.47	2.1	25.17
80	4.27	8	1.52	1.41	2.68	21.08
90	4.81	8	1.43	1.5	3.34	21.50
100	5.34	8	1.49	1.59	3.57	20.59

Experiment: Effect of laser power on specific energy (0.35” collimated beam)

Material: Limestone

Percentage laser power (%)	laser power (kW)	lasing time (sec)	Inside hole diameter (cm)	Outside hole diameter (cm)	Hole depth (cm)	Specific energy (kJ/cc)
10	0.53	4	0	0	0	-
20	1.07	4	0	0	0	-
30	1.60	4	0	0	0	-
40	2.14	4	0	0	0	-
50	2.67	4	1.05	1.44	0.20	185.94
60	3.20	4	1.05	1.55	0.35	127.23
70	3.74	4	1.05	1.55	0.38	134.90
80	4.27	4	1.12	1.70	0.54	95.83
90	4.81	4	1.13	1.69	0.68	85.50
100	5.34	4	1.13	1.75	0.79	81.37
10	0.53	8	0	0	0	-
20	1.07	8	0	0	0	-
30	1.60	8	0	0	0	-
40	2.14	8	0	0	0	-
50	2.67	8	0.68	1.43	0.34	529.80
60	3.20	8	0.86	1.59	0.89	147.39
70	3.74	8	0.99	1.69	1.24	94.41
80	4.27	8	1.06	1.74	1.68	69.19
90	4.81	8	1.05	1.76	2.06	64.78
100	5.34	8	1.09	1.78	2.42	57.17

Experiment: Effect of lasing time on specific energy (0.35” collimated beam)

Material: Sandstone

Sample name	Avg. Laser power (kW)	Exposure time (sec)	Spot size (inch)	Measured horizontal dia. (cm)	Measured vertical dia. (cm)	Average dia. (cm)	Depth of penetration (cm)	SE based on dimensions kJ/cc (cone)
1	5.34	2	0.35	1.47	1.56	1.52	1.40	4.23
2	5.34	4	0.35	1.53	1.5	1.52	2.36	5.02
3	5.34	6	0.35	1.48	1.51	1.50	3.00	6.08
4	5.34	8	0.35	1.5	1.5	1.50	3.54	6.83
5	5.34	10	0.35	1.53	1.5	1.52	3.77	7.86
6	5.34	12	0.35	1.5	1.49	1.50	4.21	8.67
7	5.34	14	0.35	1.52	1.53	1.53	4.08	10.03
8	5.34	16	0.35	1.49	1.67	1.58	4.68	9.31
9	5.34	18	0.35	1.53	1.69	1.61	4.10	11.52
10	5.34	20	0.35	1.5	1.6	1.55	4.21	13.44

Experiment: Effect of lasing time on specific energy (0.35” collimated beam)

Material: Sandstone

Sample name	Avg. Laser power (kW)	Exposure time (sec)	Spot size (inch)	Measured horizontal dia. (cm)	Measured vertical dia. (cm)	Average dia. (cm)	Depth of penetration (cm)	SE based on dimensions kJ/cc (cone)
1	3.20	2	0.35	1.6	1.27	1.44	1.17	3.39
2	3.20	4	0.35	1.55	1.28	1.42	2.07	3.94
3	3.20	6	0.35	1.42	1.17	1.30	2.81	5.19
4	3.20	8	0.35	1.32	1.22	1.27	3.18	6.36
5	3.20	10	0.35	1.37	1.25	1.31	3.35	7.10
6	3.20	12	0.35	1.34	1.35	1.35	3.43	7.89
7	3.20	14	0.35	1.37	1.25	1.31	3.41	9.76
8	3.20	16	0.35	1.46	1.43	1.45	3.60	8.68
9	3.20	18	0.35	1.49	1.63	1.56	2.94	10.26
10	3.20	20	0.35	1.37	1.44	1.41	3.98	10.38

Experiment: Effect of lasing time on specific energy (0.35” collimated beam)

Material: Limestone

Sample name	Laser power (kW)	Exposure time (sec)	Spot size (inch)	Measured inside dia. (cm)	Measured outside dia. (cm)	Depth of penetration (cm)	SE based on dimensions kJ/cc (cone)
1	5.34	2	0.35	0.92	1.38	0.55	87.63
2	5.34	4	0.35	0.88	1.49	1.5	70.24
3	5.34	6	0.35	0.91	1.61	1.4	105.56
4	5.34	8	0.35	0.94	1.63	3.21	57.53
5	5.34	10	0.35	0.69	1.86	4.74	90.38
6	5.34	12	0.35	0.98	1.83	4.34	58.72
7	5.34	14	0.35	1.08	1.83	5.23	46.81
8	5.34	16	0.35	1.1	1.82	5.91	45.64
9	5.34	18	0.35	0.97	1.84	5.05	77.27
10	5.34	20	0.35	1.2	1.9	6.58	43.05

Experiment: High pressure perforation

Material: Limestone

Laser power: 5.34 kW

Lasing time: 8 seconds

Spot size: 0.35”

Name	Conf. Pressure (psia)	Axial Pressure (psia)	Pore Pressure (psia)	Core dia. (cm)	Core length (cm)	Weight before lasing (gm)	Weight after lasing (gm)	Weight removed (gm)	Density (gm/cc)	Volume removed (cc)	Specific energy (kJ/cc)
1	0	-	-	10.105	13.80	2489.60	2488.70	0.90	2.25	0.40	106.77
2	1029	1139	-	10.106	15.39	2785.80	2783.70	2.10	2.26	0.93	45.92
3	2069	2169		10.11	15.56	2793.40	2791.20	2.20	2.24	0.98	43.43
4	982	1056	864	10.11	15.62	2814.80	2812.50	2.30	2.24	1.02	41.69
5	2100	2225	1625	10.11		2731.20	2723.90	7.30	2.24	3.26	13.11
Saturated-Brine	1922	1981	-		2800.70	2987.20	2983.00	4.20	2.24	1.87	22.78
Saturated-Oil	1800	1930	-		2778.20	2850.80	2848.90	1.90	2.24	0.85	50.36

Conditions Tested:

Bi axial load

Tri axial load

Perforation of saturated sample (brine, oil)

Experiment: High pressure perforation

Material: Sandstone

Laser power: 5.34 kW

Lasing time: 8 seconds Spot size: 0.35”

Name	Conf. Pressure (psia)	Axial Pressure (psia)	Pore Pressure (psia)	Core dia. (cm)	Core length (cm)	Weight before lasing (gm)	Weight after lasing (gm)	Weight removed (gm)	Density (gm/cc)	Volume removed (cc)	Specific energy (kJ/cc)
1	-	-	-	10.11	15.19	2589.30	2585.00	4.30	2.12	2.03	21.09
2	1120	1180		10.12	15.39	2638.60	2633.20	5.40	2.13	2.53	16.88
3	1101	1106	864	10.10	15.34	2622.00	2617.80	4.20	2.13	1.97	21.69
4	2031	2000				2616.90	2611.70	5.20	2.13	2.44	17.50
5	2100	2215	1565			2437.00	2430.40	6.60	2.13	3.10	13.79
Saturated-Brine	1893	1991	-		2632.50	2866.30	2854.70	11.60	2.13	5.45	7.84
Saturated-Oil	1844	1956	-		2588.10	2776.60	2773.20	3.40	2.13	1.60	26.76

Conditions Tested:

Bi axial load

Tri axial load

Perforation of saturated sample (brine, oil)

Experiment: High pressure perforation (sandstone)

- Perforation of clad samples (0.5” steel plate + 1.5” cement (SY 250) + 4”x 6” sandstone core)
Spot size: 0.35”

Name	Conf. Pressure (psia)	Axial Pressure (psia)	Pore Pressure (psia)	Core dia. (cm)	Core length (cm)	Lasing time (sec)	Depth of penetration (inch)
1	2030	2100	-	10.1	15.2	90 (On time) (30 sec on/20 sec off)	2.5

Experiment: High pressure perforation (limestone)

- Perforation of clad samples (0.5” steel plate + 1.5” cement (SY 250) + 4”x 6” limestone core)
Spot size: 0.35”

Name	Conf. Pressure (psia)	Axial Pressure (psia)	Pore Pressure (psia)	Core dia. (cm)	Core length (cm)	Lasing time (sec)	Depth of penetration (inch)
1	1966	2074	-	10.15	15.2	90 (On time) (30 sec on/20 sec off)	4.5

C: Glossary

Absorption: The ratio of the energy carried by absorbed wave to the energy carried by the original wave.

Beam duration: The amount of time a sample is exposed to the laser beam.

Beam intensity (Power density): The ratio of the power to the beam diameter measured in watts/cm^2 .

Beam size: The diameter of the laser beam; can vary from microns to inches.

Blackbody radiation: When the rock temperature increases, the rock itself turns into an intense source of radiation; decreases rock destruction.

CAT: Computer Assisted Tomography, used to monitor the interior structure of the core.

Chipping (Spalling): Splitting off rock fragments from the rock face.

CMS-300: Core Measurement System used for permeability, porosity and bulk compressibility under stress up to 5000 psi.

COIL: Chemical Oxygen Iodine Laser.

Continuous wave (CW): Uninterrupted transmission of beam laser.

Differential Thermal Analysis (DTA): Used to determine melting temperature of the rock samples.

Diffusivity: The ability of a material to conduct thermal energy compared to its ability to store energy.

Divergence: Defined as a ratio of unfocused laser radiation spot diameter (at far distance) to the distance from the laser.

Elastic moduli: Describe a material or a state of a material where strain or deformation is recoverable after a displacing stress is removed.

Electron-microprobe (EMP): Used to determine the chemical composition of the melted material and rocks.

Plume: Gaseous effluent formed between the laser and the rock face due to heating. Results in less rock destruction.

LASER: An acronym formed from Light Amplification by Stimulation Emission of Radiation.

Laser-rock interaction: The result of exposing a rock to laser energy. Depending on the wavelength, power and duration of the exposure, the rock may break, melt or vaporize.

MIRACL: An acronym for Mid-InfraRed Advanced Chemical Laser.

PDPK-200: Pressure-decay profile permeameter, used to measure point permeability.

Plasma: The creation of an ionized cloud on the surface of the rock. It is produced by vaporization of some of the opaque target surface and subsequent absorption of laser light in the vaporized materials. In this research plasma refers to as gaseous melted materials. Plasma disperses the beam, so less destruction.

Poisson's ratio: Specifies the rock's ability to deform laterally when stress is applied.

Power peak: is the pulse energy to pulse length ratio.

Pulsed lasers: Lasers that emit short, high power pulses of light.

Rate of Penetration (ROP): The speed at which the well is drilled, usually measured in feet per hour.

Reflectivity: The ratio of the energy carried by a reflected wave to the energy carried by the original wave. High reflectivity means less rock destruction.

Scattering: The irregular and diffuse dispersion of energy caused by inhomogeneities in the medium through which the energy is traveling.

SEM-EDS: Scanning electron microscope-electronic dispersive system, used create 3-D images of rocks.

Spalling (Chipping): Splitting off pieces from the rock face due to low power laser that causes the rock to break into fragments.

Specific Energy (SE): The amount of energy required to remove a volume of rock.

Thermal conductivity: Quantity of heat transmitted through a unit volume in a unit time. High thermal conductivity means high rock destruction.

Thermal stress: Stresses created within a rock due to the non-homogeneity of the thermal expansion of different minerals making up the rock.

X-ray diffraction (XRD): Used for identify clays mineralogy.

Young's modulus: A measure of the rock's resistance to deformation.

D: Nomenclature

A	= area
BG	= Berea gray sandstone
BY	= Berea yellow sandstone
C_p	= heat capacity
C	= celcius/centigrade
cal	= calorie
d	= diameter
E	= Young's modulus
E_{abs}	= absorbed energy
$E_{blackbody}$	= blackbody energy
E_{inc}	= incident electromagnetic wave
E_{ref}	= reflected enery
E_{sc}	= scattered energy
G	= shear modulus
g	= gram
H	= melting depth
I	= intensity (power density)
J	= joule
k	= permeability

K_b	= bulk modulus
K_f	= thermal conductivity
Hz	= hertz
L	= length
Ls	= limestone
md	= millidarcy (Permeability Unit)
P	= power
P_{av}	= average power
P_p	= peak power
p	= pressure
R	= repetition rate
s	= seconds
S	= shear wave.
T	= time interval between the beginning of the laser pulses
t	= time
TE	= total energy
Tmax	= maximum temperature
Tf	= temperature cycling frequency
t_p	= compressional wave travel time
W	= watt
Wp	= pulse width
ΔT	= temperature difference

ε = blackness coefficient

λ = wavelength

τ = laser pulse length

τ = shear stress

ν = Poisson's ratio

E: Petrophysical and Petrographic Studies

Petrophysical and Petrographic Studies

The rocks were initially characterized during the GRI-funded research and are discussed in detail in the related GRI reports.^{10,11,12} Microscopic properties, such as mineralogy, clay content, and microfractures, were determined using a scanning electron microscope with the energy dispersive system (SEM-EDS), x-ray diffraction (XRD), and thin sections. Melting temperatures of these rocks were measured using differential thermal analysis (DTA). Figures 1 through 17 are examples of photomicrographs prepared in these studies.

Core properties, such as porosity and permeability, were measured on representative samples using the Core Measurement System-300 (CMS-300). The CMS-300 measures porosity, permeability, bulk modulus, Klinkenberg slip factor, and the non-Darcy flow coefficient (Forchheimer) up to 5,000 psi. For this study, the porosity and permeability data from the CMS-300 were used to ensure consistency of samples for comparison to other laser studies performed on these rock types.

The Pressure Decay Profile Permeameter (PDPK) was used to characterize the rocks before and after lasing. The PDPK measures point permeability at ambient conditions, Klinkenberg slip factor and the non-Darcy flow coefficient (Forchheimer). The PDPK is reliable down to a permeability of 0.001 md and experience has shown it to be repeatable and accurate. This non-destructive, unsteady-state test can measure permeability on irregular shapes, therefore, it an excellent tool to analyze before and after lasing permeability. The maximum permeability is 444 md at 2.0 inches. The permeability one-half inch above is 338 md while the permeability one-half inch below is 379 md. The minimum permeability is 117 md at 8.5 inches. BG1 also shows considerable variation along the width of the core. The maximum variation is at 8.5 inches with permeabilities from 127 md to 414 md.

Even though Berea exhibits consistent properties when compared to reservoir rocks, and is considered the standard used by industry, the permeability variations along four-slabbed 2-inch diameter cores was measured. These were the same Berea used to investigate the correlation between the rock removal mechanisms and beam irradiance through the linear track method with simultaneous change of beam size on the surface.

¹⁰ Graves and Batarseh, 2001a

¹¹ Graves and Batarseh, 2001b

¹² Graves and Batarseh, 2001c

In BG2, the data taken at 0.5 inches from the top edge demonstrate the potential error that can occur near the edges of the samples. This enhanced permeability could be due to microcracking during preparation or testing, however low-power microscopic inspection did not indicate cracks. Another possibility is that the PDPK might have had a leak in the probe seal because of the proximity to the edge. All measured permeability results taken before and after lasing were visually compared to the core so anomalous data would not be used.

The curves in BG2 have a more similar shape than the curves in BG1. Since they are from the same core, it was anticipated that the two slabs would have comparable curve shapes. The data were taken in a square grid pattern so the arithmetic average of the permeabilities was used. The average permeability for BG1 is 301 md and for BG2 it is 337 md. These permeability data demonstrate that even though Berea sandstone is considered to be an excellent sample for laboratory measurements, there is still variation within the rock. Great care was taken when cutting, cleaning, marking, and shipping the rocks to insure that the preparation did not affect the test results. Also, the PDPK data was taken several times at a given point and averaged. During the analysis, if any data did not follow an expected trend, the permeability was re-measured to confirm the reliability of the initial measurements.

The GRI study shows clearly that the rock samples will crack due to thermal stress from the heat of the laser. What was not understood is how the formation of the cracks affects the SE. The analysis of the data indicated that cracking should be treated as an energy absorbing boundary affect and should be avoided. For this reason, several holes were cut into larger bulk samples of rock with a noticeable lack of sample fracturing due to thermal and boundary stresses. This method was used whenever possible, and a minimal number of holes were drilled into smaller core samples to avoid these artifacts.

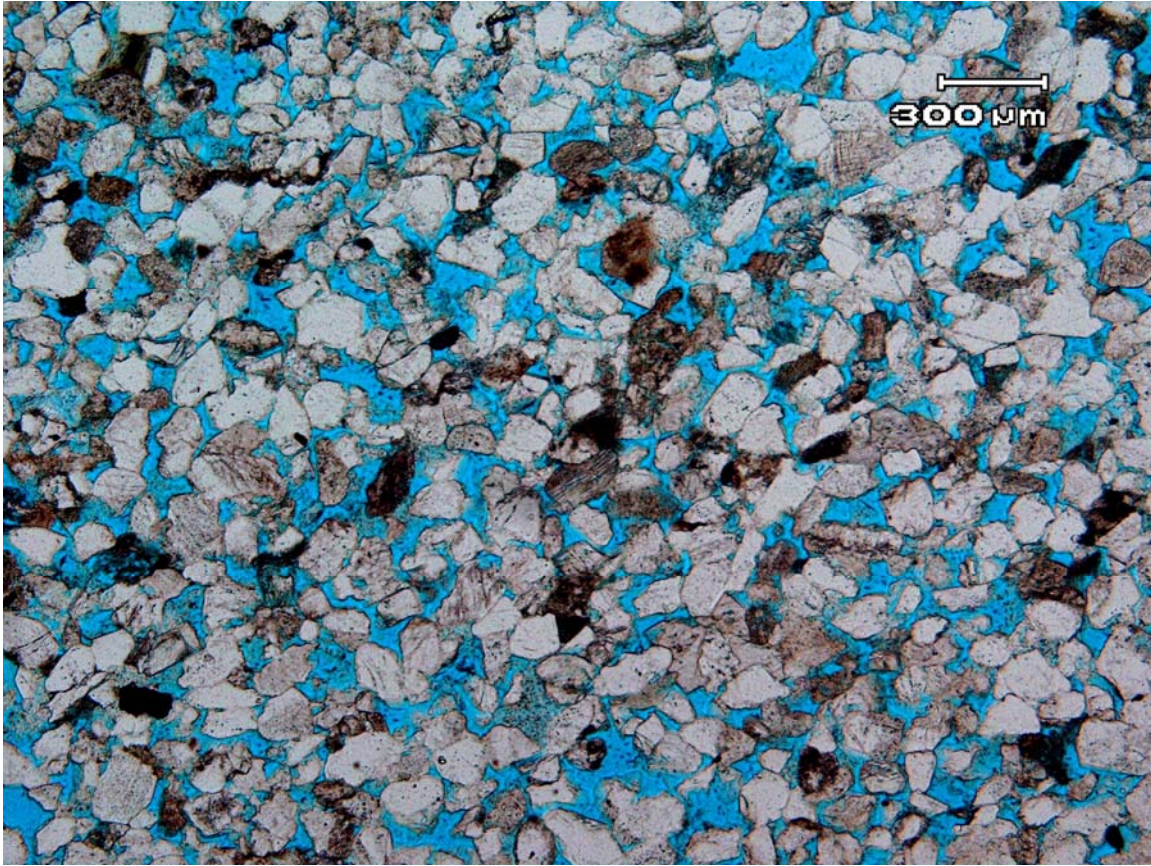


Figure 1 Low magnification view showing distribution of the framework grains, and porosity, and other trace minerals. The pore space (porosity) is stained with blue epoxy. Note the grains are subrounded to rounded grains occasionally subangular. Note the framework of the grains (well sorted to moderately sorted grains). Note the black organic matter dispersed throughout the thin section.

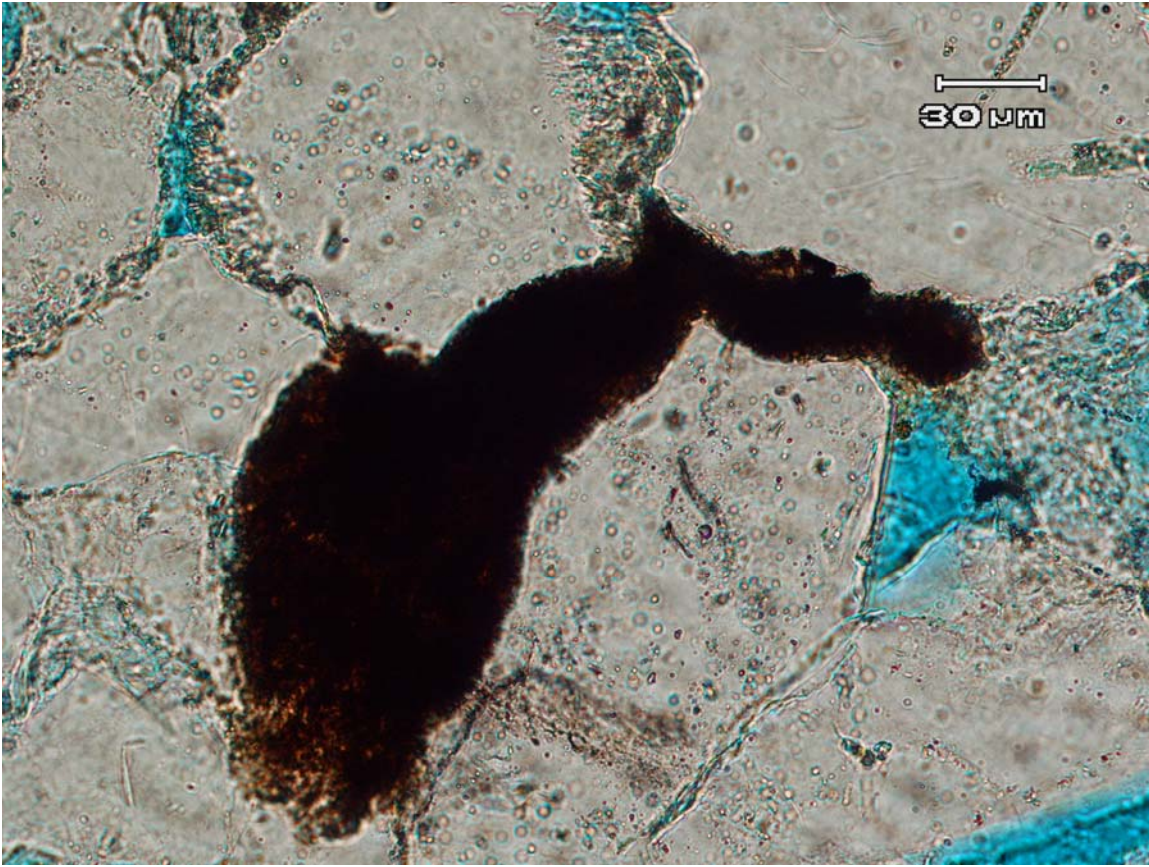


Figure 2 Detailed views of fabric elements. Intergranular pore filled with black organic matter.

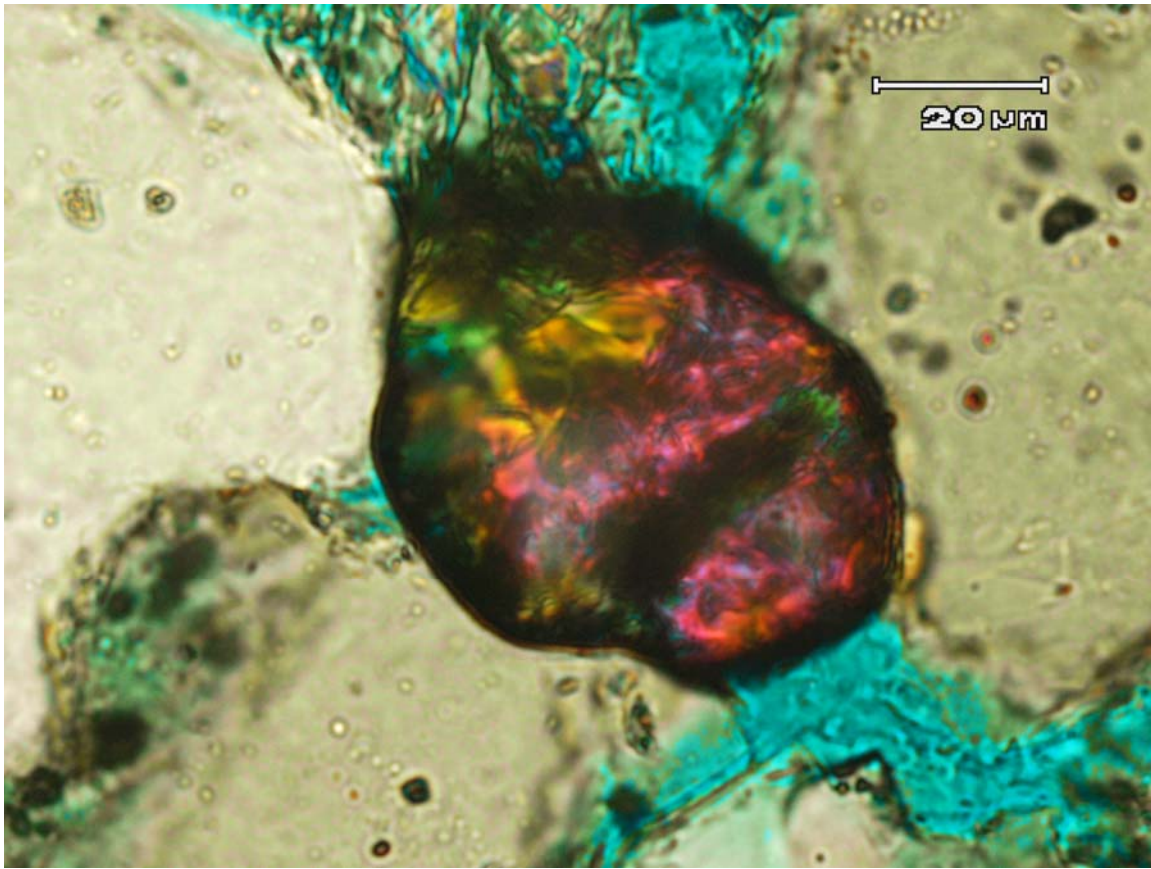


Figure 3 Under cross-polarized light zircon shows strong to extreme birefringence. Zircon is one of the trace minerals within the Brea sandstone.

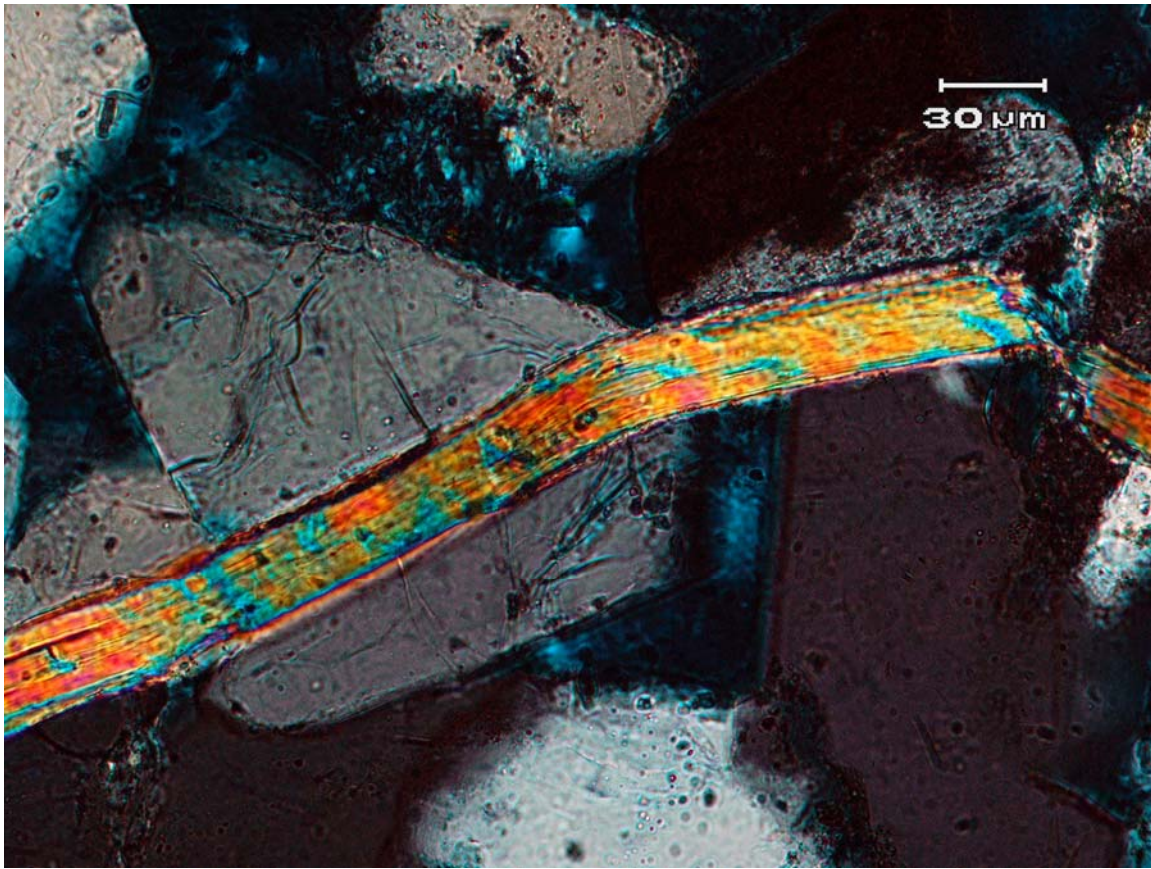


Figure 4 Cross polarized photo of detrital micas (muscovite). Note the grain deformation of the quartz grain which penetrated by the muscovite flake. The muscovite flake at the top was deformed at the top during major natural compaction. The compaction could account for porosity reduction in this sample.

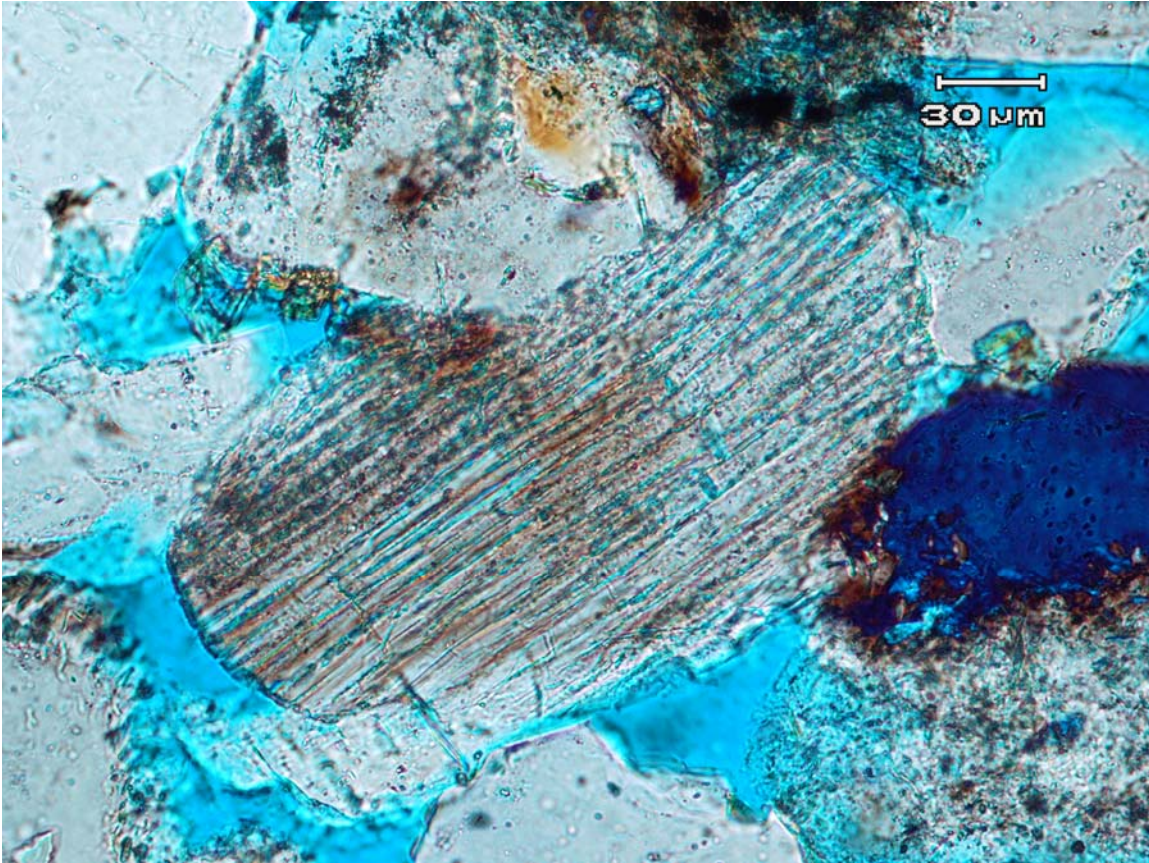


Figure 5 partially leached plagioclase feldspar. Secondary porosity has resulted from partial stages of dissolution of the feldspar. Note the quartz overgrowth cementation.

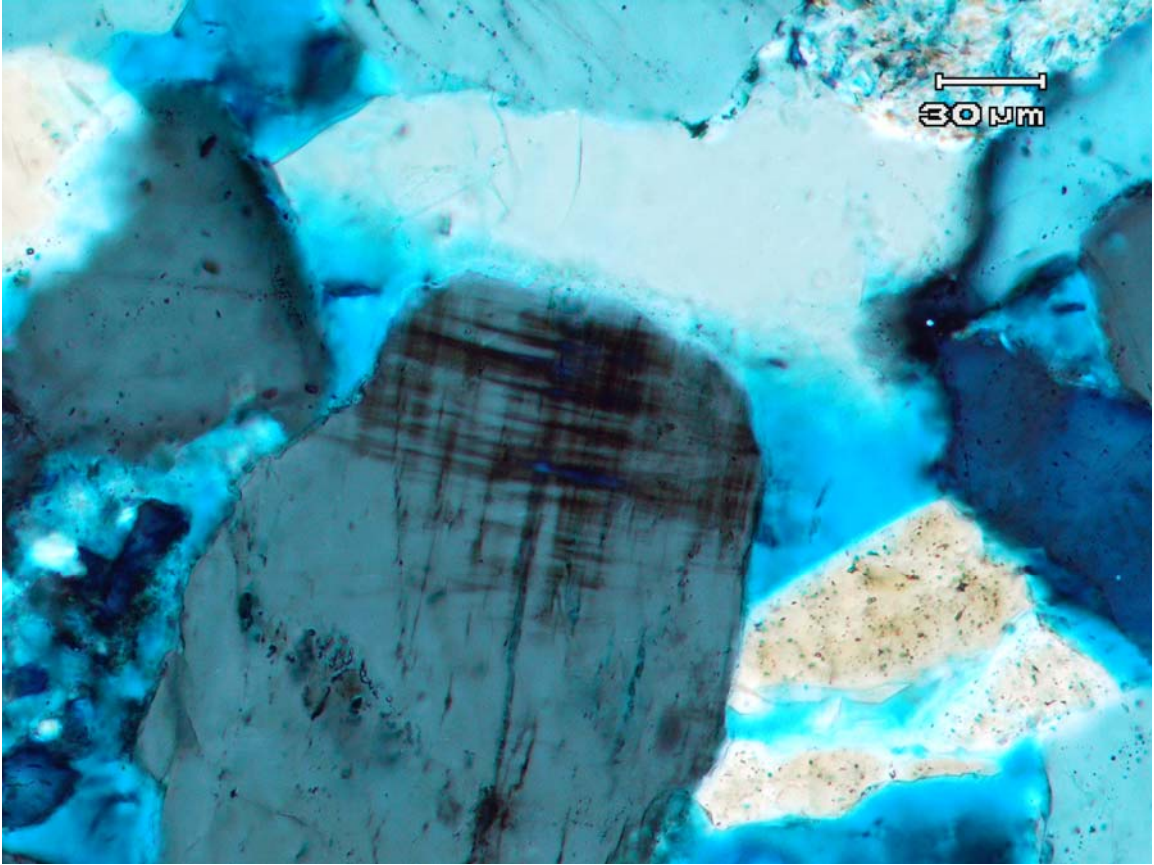


Figure 6 Microcline feldspar, with typical microcline grid twinning.

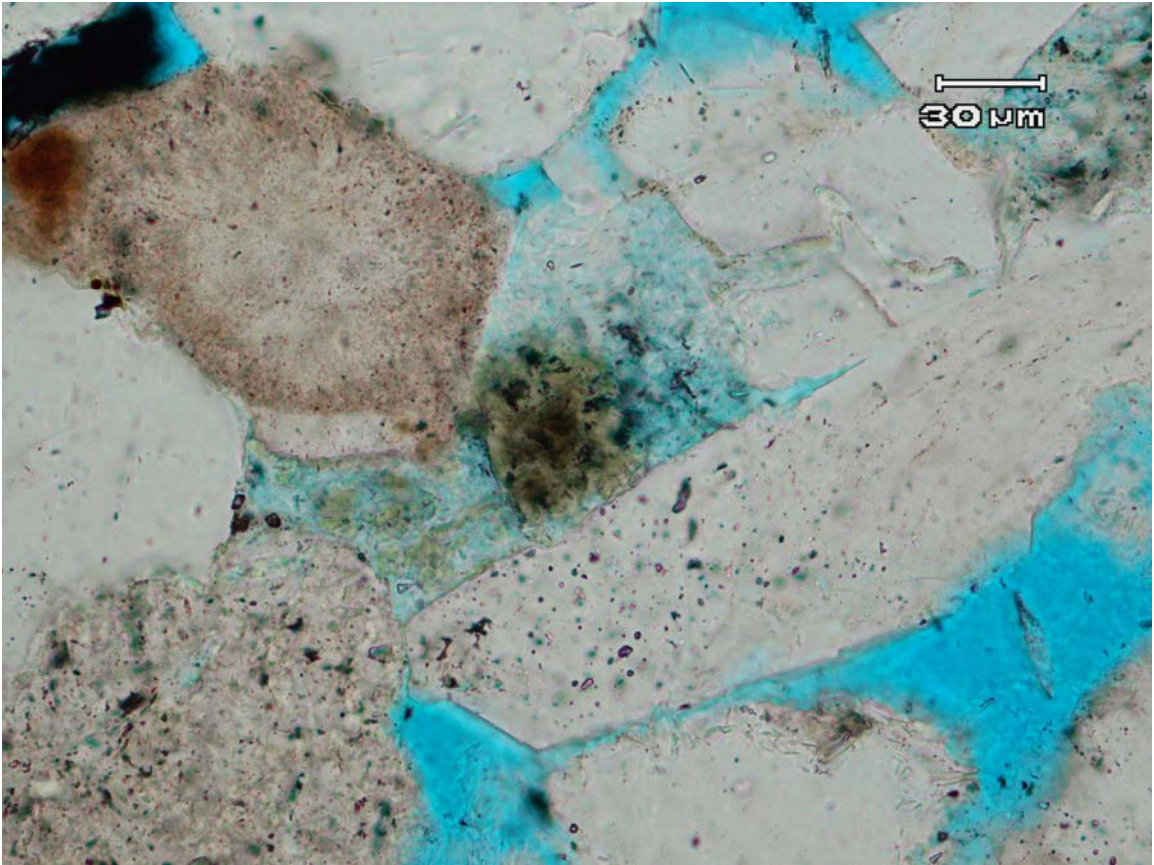


Figure 7 Dark green rounded detrital glauconite.

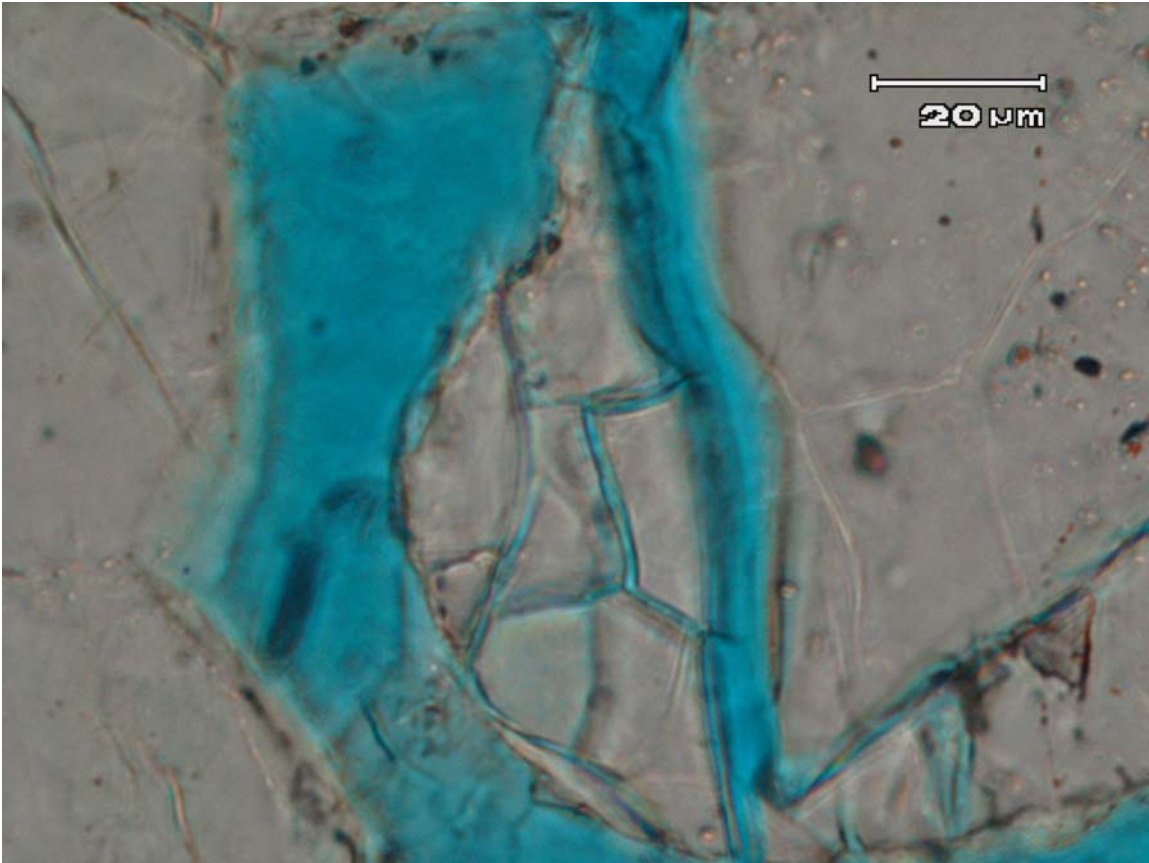


Figure 8 Micro fractures in quartz grain. Example of the secondary porosity development.

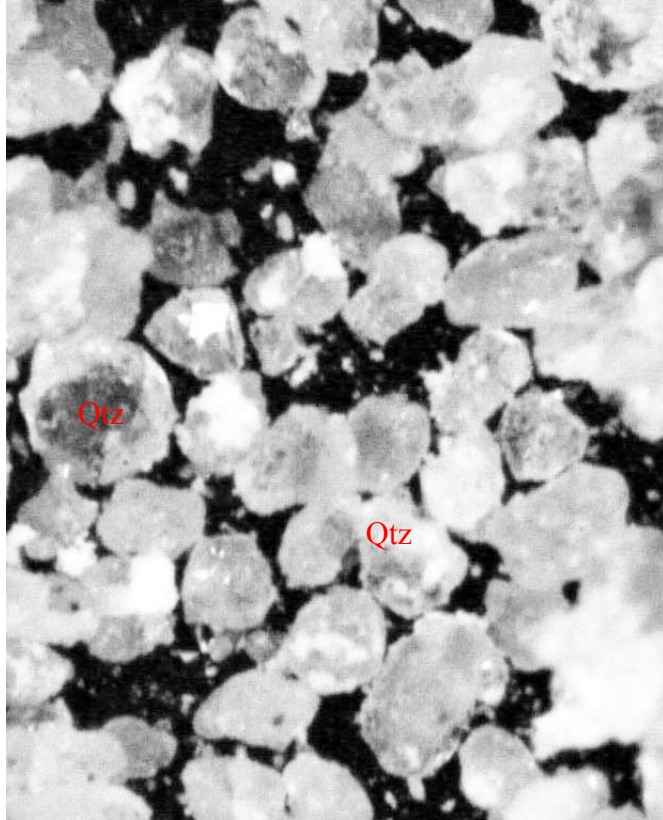


Figure 9 High magnification view of decremented Berea sandstone. The sand is carefully prepared and extracted from the rock sample before lasing. Note the roundness and the well sorting of framework grains. The grains sizes are medium grains, the shape of the grains commonly rounded to subrounded, the sorting of the grains are well sorted. Grains color translucent to clear white. (32 X)

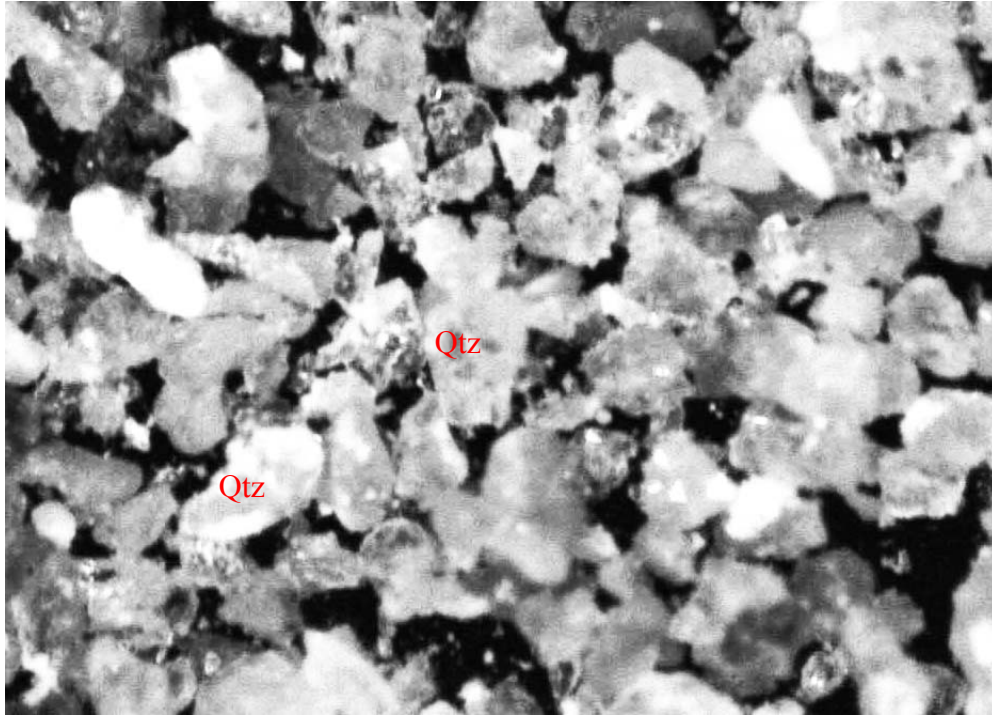


Figure 10 high magnification view of decemented sand collected from inside the tunnel after lasing. Note the different between this sample and the sample described before lasing specially in the distribution of grains framework. Note the angularity and poor sorting of the grains which indicates induced fracturing within the grains which associated with sudden exposure to high temperature. (32 X)

Figure 11 Section through biserial foraminifera. Not the typical Double-walled, calcareous structure.

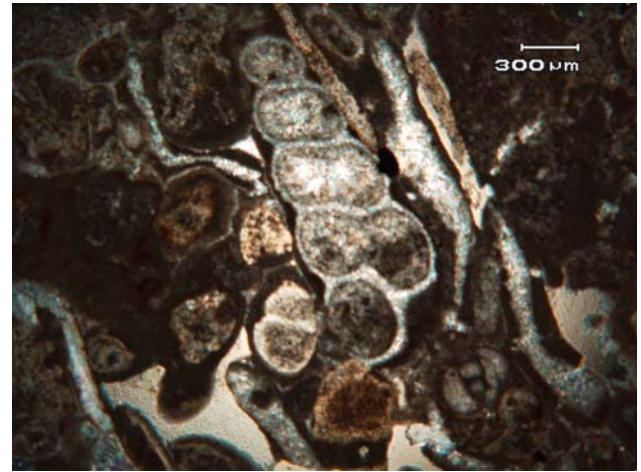


Figure 12 Longitudinal sections through brachiopod shell. The fabric within the shells caused by placcations and shell ornaments.

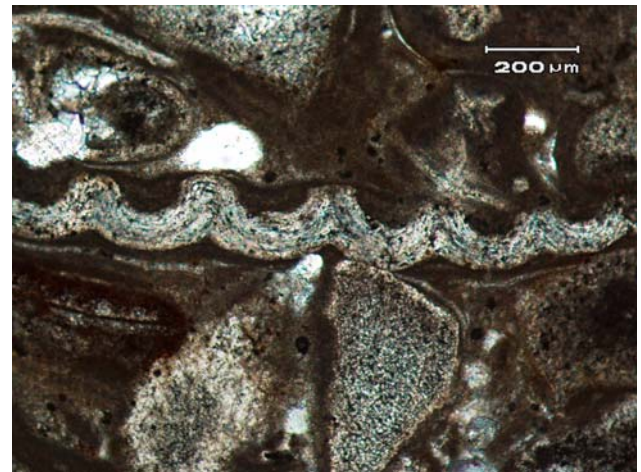


Figure 13. Transverse section, through a single echinoid spine showing the characteristic of the flower-like structure. The structure of the spine is delineated because of micritic infill and cementation.

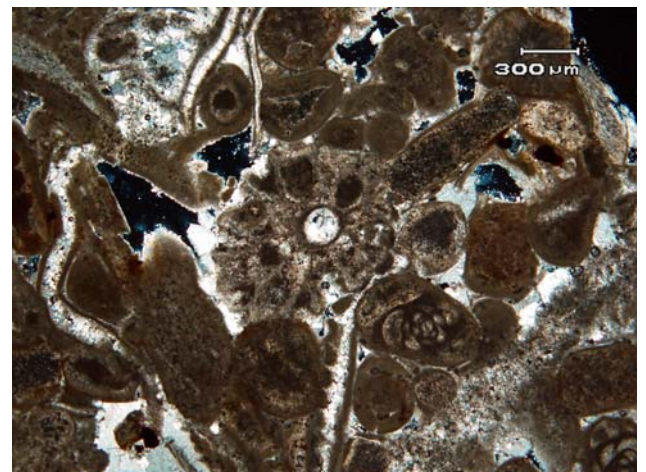


Figure 14. Example of intercrystal porosity (dark blue).

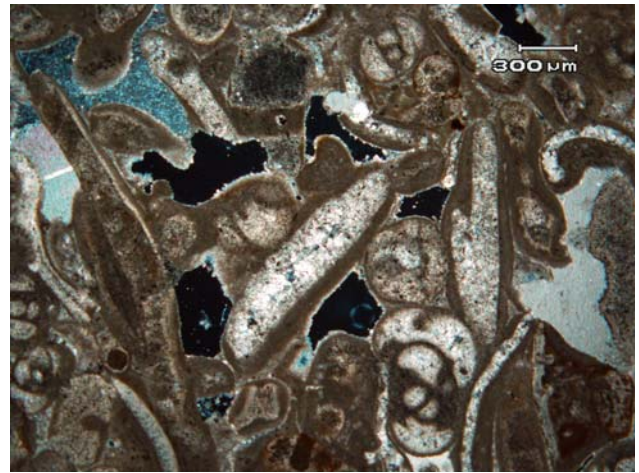


Figure 15. Example of complete bladed calcite cement crusts surround the envelope of leached bioclast.

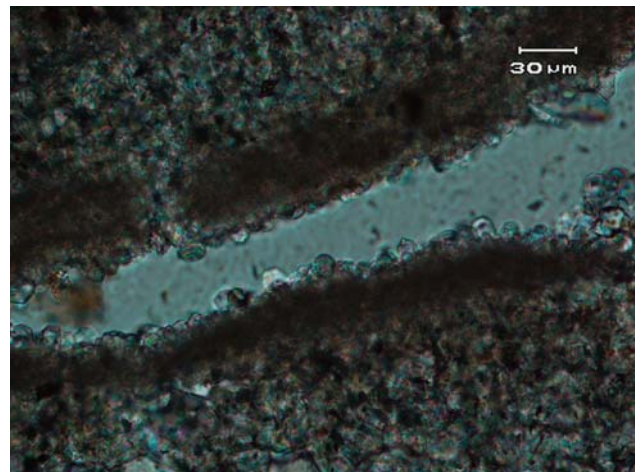


Figure 16. Calcite cement with complete filling of the primary porosity.

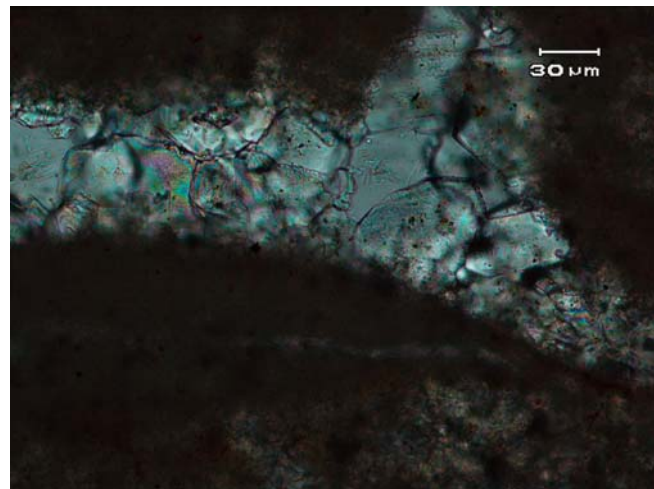
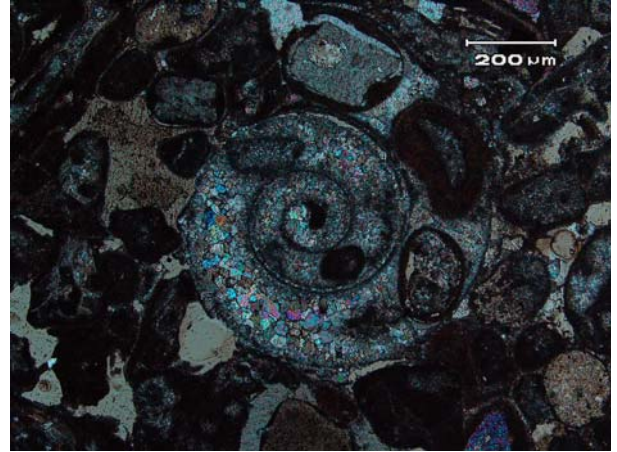


Figure 17. A complete dissolution of the fossil structure and were filled with calcite cement.



F: IPG Optical Fluids Report

Study for Gas Technology Institute

Contract #: KI00024110

November 21, 2003

Report on fluids for near IR transmission

By Victor Ilyashenko, IPG Photonics, Inc.

Introduction

The purpose of this research is to find a liquid media that posse's good transparency at the 1.54 microns wavelength. Besides water, we will consider three classes of liquids that can be found in Nature and industry. First class is carbohydrogens. It includes all organic liquids such as pure carbohydrogens of different molecular weight (up to the mineral oils) as well as alcohols, acids etc. All these molecules are full of CH₃ and CH₂ groups that control its spectroscopy. Another class is semi-organic or hybrid molecules (mostly silicone oils, that safe and inexpensive). Their backbone is built of silicon (Si) and oxygen atoms, rather than carbon. The third class is halogenated carbon based molecules. There are a lot of very stable perfluorinated and chlorinated fluids available.

Experimental setup

Two types of measurements were made for potential candidates. Low power spectrophotometer setup was built out of Ando AQ-4303B white light source operated as CW in the 400-1800 nm wavelength range. Ando AQ-6315E Optical Spectrum Analyzer was used as a receiver. Liquids were placed in the 1cm wide disposable cuvette from OceanOptics and the CUV-UV Cuvette Holder for 1-cm path length cuvette couples via SMA-terminated optical fibers to Ocean Optics high-sensitivity miniature fiber optic spectrometers and light sources to create

small-footprint spectrophotometer systems for absolute absorbance measurements of fluids. This compact cuvette holder is optimized for UV-VIS-NIR (~200 nm-2 μm) applications.

“The cuvette holder for 1-cm path length cuvette consists of these key components:

- Two adjustable 5-mm diameter f/2 quartz collimating lenses
- Spring-loaded ball plungers for precise cuvette positioning
- Built-in 1/4" filter slot
- Internal channels designed to accept a constant-temperature water source (for heating and cooling of the base and cuvette, by means of convection)
- SMA 905 terminations for coupling to fiber optics “

Second type of measurement was done using our 15-Watt laser ELR-15-1550 and Molectron power meter. Liquids were placed into 10cm path quartz cuvette. Laser beam diameter after collimation was 5mm.

Brief theory of NIR absorption

Molecules are made up of atoms bonded together. Bonds are produced by atoms, which share or give up electrons to another atom. These bonds actually act similar to little springs. As an electron moves about the atom(s), the bonded atom is drawn or repulsed from the atom to which it is bonded creating a vibrating motion. Whenever something moves consistently (vibrates) in time in this manner, it is said to have a frequency (n =frequency). The frequency is the number of times the atom vibrates in a second. The absorptions occurring in the NIR region will therefore be considered to be vibrational absorptions. These possible absorptions are also quantum mechanical in nature; only discrete energy amounts can be absorbed. These levels can be roughly calculated using Equation 1

$$E_n = \left(n + \frac{1}{2} \right) \frac{h}{2\pi} \sqrt{\frac{k}{\mu}} \quad \text{Equation 1}$$

Where E_n = the molecule vibration energy, $n = (0,1,2,3 \dots)$, h = Plank's constant, k = the force constant, μ = the reduced mass. n is considered a quantum number and take on only whole integer values.

$$\mu = (m_1 \cdot m_2) / (m_1 + m_2) \quad \text{Equation 2}$$

m_1 and m_2 mass of atoms.

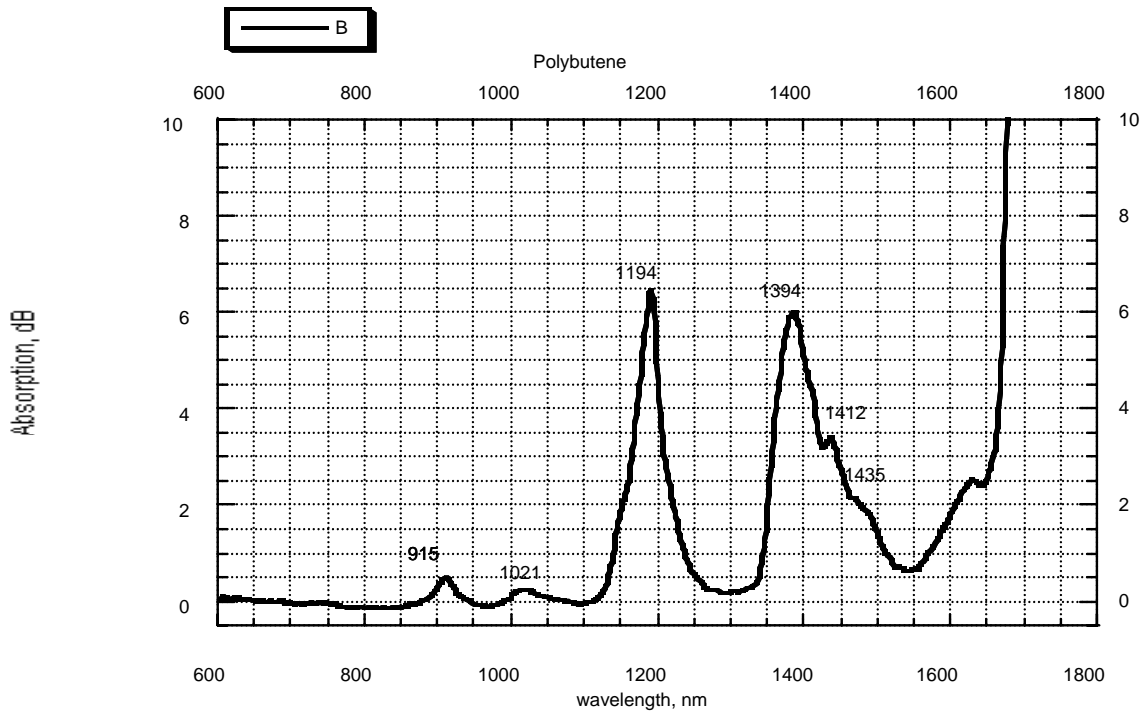
A transition where $n=1$, is known as a fundamental absorption. These fundamental absorptions are about 100 times less energetic than the electronic absorptions. Less energetic means longer wavelength. These absorptions occur in the Infrared portion of the spectrum. When n is greater than 1, the transition is known as an overtone. By looking at equation 1, it is evident that as n increases the energy to be absorbed also increases. This in turn indicates that shorter wavelengths will need to be absorbed. These absorptions generally occur in the NIR region. Additional absorptions (overtones and harmonics) occur at the wavelengths multiple to the fundamental frequency. It is clear, that the position of the fundamental bands considerably depends on the weights of the atoms participating such vibrations. **The fundamental tones of these vibrations are observed in the IR-region, and their overtones- in the visible and near IR regions.**

Organic fluids

Organic fluids include various carbohydrogen based materials, such as mineral oils, organic polymers, alcohols etc. These materials have a lot of CH_3 and CH_2 groups that control overall near IR absorption. Hydrogen, being the lightest atom, causes the fundamental vibrations of the CH vibration to occur at the relatively short wavelength of $3.2\mu\text{ m}$. The harmonics influence the attenuation loss in the visible and near infrared regions.

Following data is very good illustration of NIR bands due to vibrations and deformations between carbon and hydrogen in the CH_3 and CH_2 groups of organics

Our low power measurements of organic fluids (polybutene oil) yield following spectrum:



Picture 1.

Band assignments well known from the literature represented in table [1].

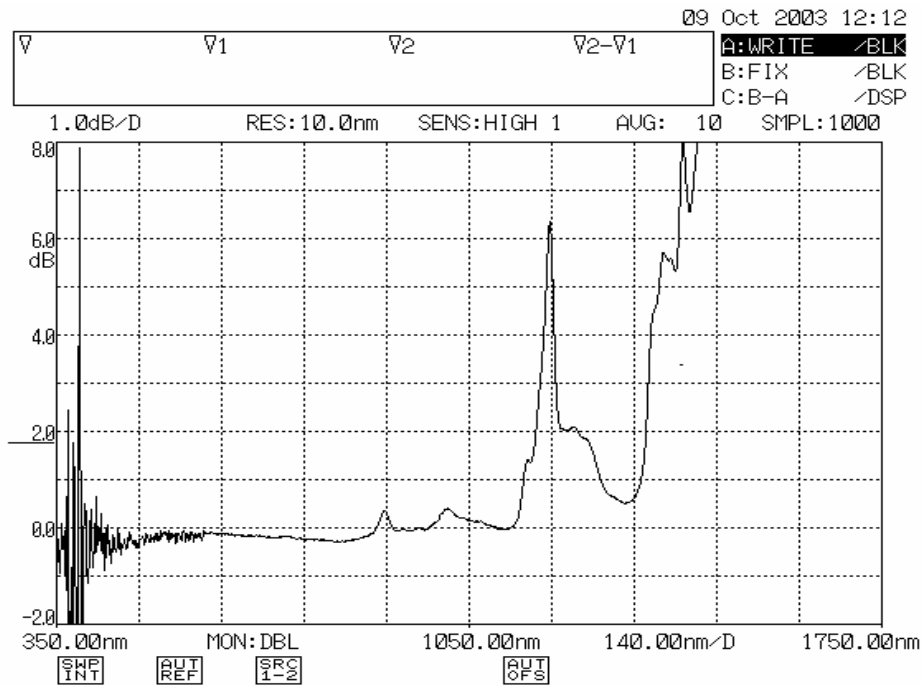
Table 1.

Bands (nm)	Assignments
915	C-H str third overtone (CH ₂)
1021	Combination bands (CH ₂ and CH ₃)
1151	C-H str second overtone (CH ₃)
1194	C-H str second overtone (CH ₃)

1394	Combination bands for CH ₂
1412	2 x C-H str + C-H def (CH ₃)
1435	2 x C-H str + C-H def (CH ₂)
1542	(CH ₂)
1634	(CH ₃)
1698	C-H str first overtone (CH ₃)
1710	(CH ₂)
1728	C-H str first overtone (CH ₂)
1764	C-H str first overtone (CH ₂)

Here we have plenty of stretching and bending C-H overtones that impact transparency at 1540nm (~0.42dB/cm). It is a very typical number for all carbohydrates because they all consist of the same “building blocks”.

Situation with alcohols as well as water even worse due to additional OH bands that absorb severely at 1540 nm:

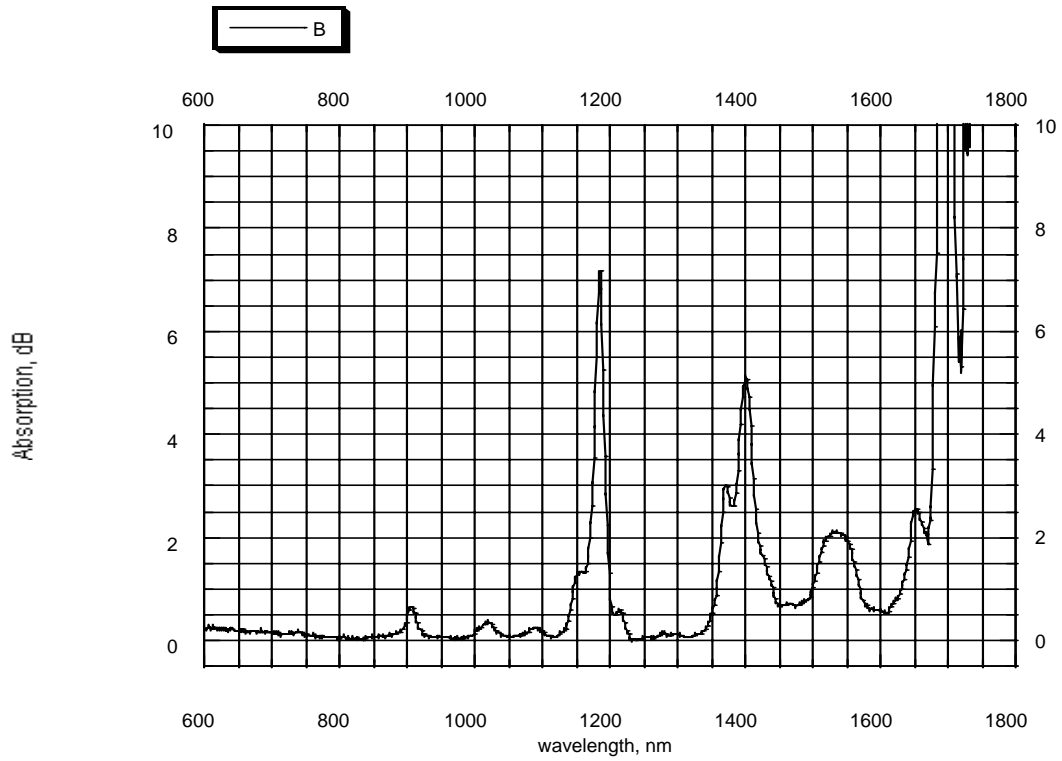


Picture 2.

Thus, we can conclude that polymeric (high molecular weight) carbohydrates without OH groups are more suitable for our purpose among organic molecules. Higher molecular weight in this case is necessary to provide higher boiling temperature because short carbohydrates are very volatile and easy flammable. Still, ~ 0.42 dB/cm absorption losses are somewhat worrisome. We have tested these materials at 1550nm and 15Watts power and observed similar absorption (about 5 dB after 10 cm path length). However, overtime (5 minutes), losses built-up to 86% of initial power due to distorted (scattered) laser beam. **Thus, even relatively small absorption can increase losses significantly due to local warm-up of liquid and following change of refractive index and probably thermal convection. Taking all this into account, we concluded that carbohydrates based materials are not perfect candidates, unless can be used in thin layers.**

Semi-organics molecules

Siloxane based fluids are very stable nonvolatile media. Though containing some C-H bonds, it can behave differently, because carbon in this case connected to silicon directly or through oxygen. We have screened tens of different Siloxane based fluids. Regardless of some variations for different polysiloxanes they all look similar around 1500nm:



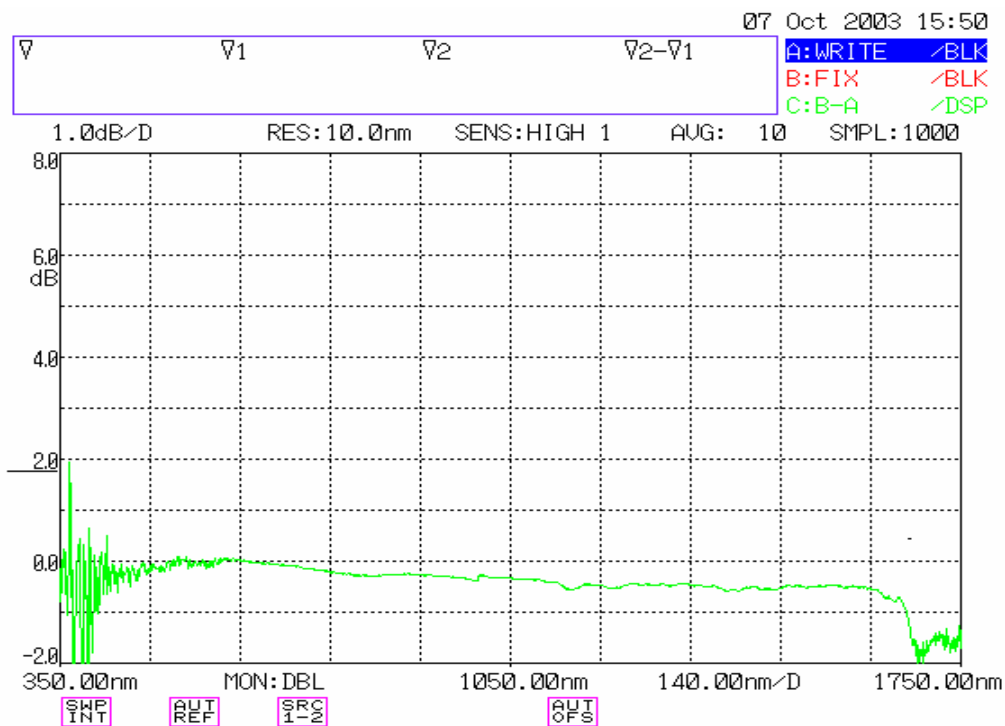
Picture 3.

New unfortunate peak arrived close to 1500nm due to carbon-silicon introduced shift. **Because of it, polysiloxanes even less suitable than carbohydrates.**

Halocarbons

It is becoming clear that we are not going to make a significant progress in our search, unless get rid of C-H bonds. The possibility that substitution of fluorine and chlorine atoms for hydrogen atoms may open the way to lower near IR absorption has been investigated [2]. If the C-H atom pairs within liquid molecule were replaced by carbon-fluorine (C-F) or carbon-chlorine (C-Cl), the increase in reduced mass would cause the fundamental absorptions to shift to the longer wavelength region, according to equations 1 and 2. This shift would allow to clear-up near IR region from various absorption bands. We took a look on several halogenated materials.

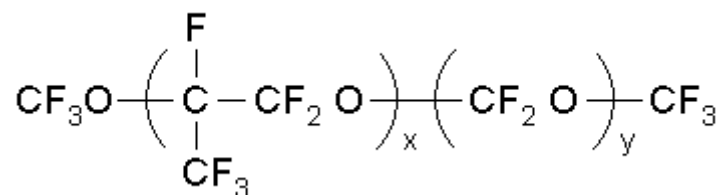
Halocarbon, Inc (Halocarbon.com) produces a variety of halocarbon oils: “Halocarbon oil is a low molecular weight polymer of chlorotrifluoroethylene (PCTFE). This oil is manufactured by a controlled polymerization process and then is stabilized to give it some very unique properties. This oil is safe, chemically inert and nonflammable and can be used with oxygen or chlorine. It has good lubricity, high thermal stability and low compressibility”. Following picture is our measurements for Halocarbon-400 oil:



Picture 4.

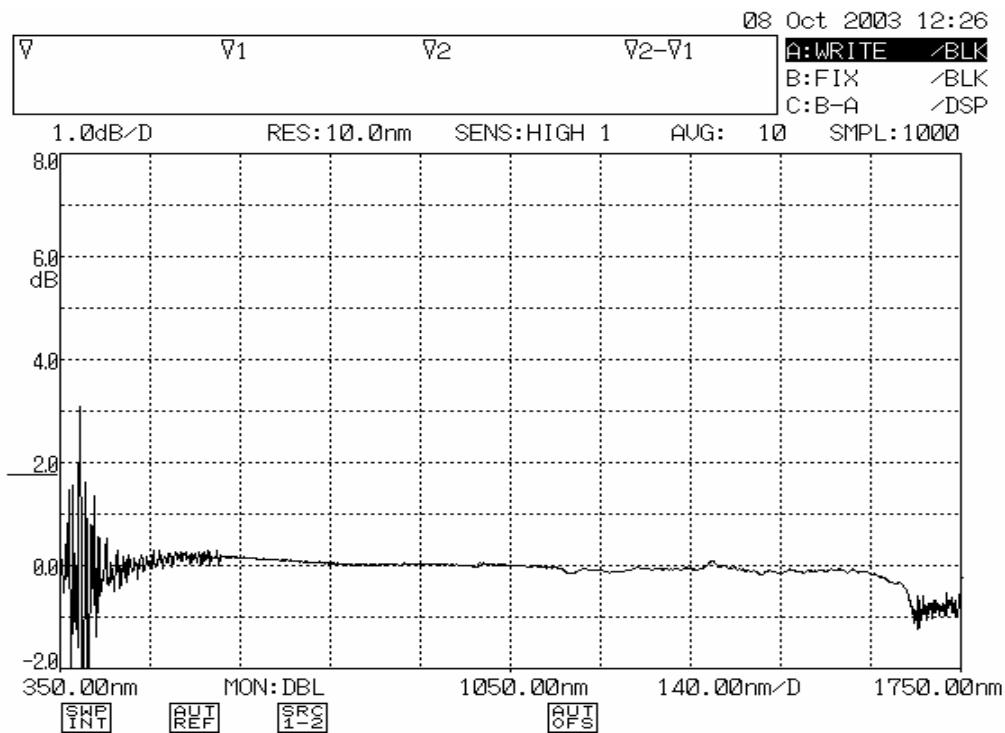
Amazing near IR transparency can be seen everywhere. Slight tilt (negative absorption) can be explained by reduction of back reflection from cuvette's walls due to differences in refractive index of oil and air. This very perspective candidate was tested by high power measurements. We observed virtually no loss (just cuvette back reflection) in 10cm long path length. These oils are available in different molecular weight that provides varieties of viscosities and boiling temperatures [3].

Second family of halogenated fluids available in the form of perfluorinated molecules (oils). Having extremely low refractive index comparing to organics and even Halocarbon oils, they also transparent in near IR. Known as Fomblins, perfluoropolyethers of general formula:



As you can see, there are no Carbon-Hydrogen bonds.

Fomblins are manufactured by Ausimont. Typical absorption spectrum:



Picture 5.

Same scenario is here. Virtually no near IR bands. High power measurements, described earlier (15 Watt at 1550nm and 10 cm path length), support outstanding transparency of carbohalogens, where we saw only losses coming from back reflection of curette's walls. We bought Fomblin-Y-40-11 for this study from Aldrich.

Conclusions

Among all classes of fluids considered in this study, we can definitely point to halogenated materials as the most transparent medium in the near IR region, namely 1540 nm. It is stipulated by absence of stretching and bending absorption overtones from Carbon-Fluorine and Carbon-Chlorine bonds, due to heavy atom mass of Chlorine and Fluorine atoms. **We have studied two product lines of halogenated oils from Halocarbon, Inc [3] and Ausimont [4,5] that have excellent transmission at 1540 nm as well as whole near IR region (Picture 4,5). We recommend these fluids as a laser transmission medium in the region from 800 to 1750 nm.** However, halocarbons and perfluorinated fluids exist in large variety as technical fluids, vacuum oils with respect to molecular weight, viscosity, boiling temperature etc. Also, there are many similar oils made by 3M, Lancaster, DuPont etc. that can utilized. Typical applications: lubrication, vacuum pumps, hydraulic fluids, instrument fill fluids etc., thus, widely available in technical field.

References

1. Himamitsu Higashiyama, Masahiro Watari and Masahiro Tomo *J. Near Infrared Spectrosc.*, **6**, 317-324 (1998)
2. Toshikuni Kaino, Polymer Optical Fibers, *NTT Opto-electronic Laboratories*
3. <http://halocarbon.com/e10.htm>
4. http://www.qualityvacuumpumps.com/fomblin_pfpe.html
5. <http://www.sisweb.com/vacuum/sis/fomblin.htm>

Laser Drilling – Drilling with the Power of Light

Part 2. High Energy Laser Perforation and Completion Techniques

Table of Contents

Disclaimer	ii
Abstract	iv
1 Executive Summary	1
1.1 GRI Project, 1997-2000	1
1.2 DOE Project, 2000-2007	1
1.2.1 Conclusions and Recommendations	1
2 Introduction.....	2
2.1 Drilling Today In the USA.....	2
2.2 1997-2000 GRI Laser Drilling Research Project	3
2.3 DOE Investigation.....	4
2.3.1 Phase I – Determination of Energy Requirements.....	4
2.3.2 Phase II – Multiple Beam Bursts	5
Experimental Approach	7
2.4 Proposed Tasks.....	7
2.4.1 Determining “Absolute” Specific Energy.....	7
2.4.2 Determining the Value of Pulsed Lasers	10
2.4.3 Saturated and Submerged Tests.....	12
2.5 Lasers Used in Drilling Research.....	13
2.5.1 Laser Parameters.....	13
2.5.2 Characteristics Of The Lasers Used In This Study.....	13
2.6 Experimental Approach Summary	15
3 Experimental Procedures and Results.....	16
3.1 Introduction	16
3.2 Purge Optimization and Calculating Specific Energy.....	16
3.2.1 Purge Optimization	16
3.2.2 Methods of Calculating Specific Energy	17
3.2.3 Result and Analysis:	19
3.3 Orientation Effect Test:	25
3.4 Determination of Boundary Effect.....	27
3.5 Effect of Beam Density on Specific Energy	29
3.6 Effect of laser power on Specific Energy (focused beam).....	36
3.6.1 Spallation Test:	39
3.6.2 Thermal Effects on Berea Sample	41
3.6.3 Thermal Effects on Limestone Sample.....	47
Effect of laser power on Specific Energy (Collimated beam)	77

Effect of laser power on Specific Energy (Collimated beam)	110
3.7 Laser Drilling Systems	116
3.7.1 Nd:YAG System	116
3.7.2 Nuvonyx Diode System	116
3.8 Saturated and Submerged Tests	116
3.8.1 Saturated	116
3.8.2 Submerged	117
4 Results and Discussion	118
4.1 Data Analysis	118
4.2 Important Rock Parameters	118
4.3 Spallation and Melting Zones Identified	119
4.4 Spallation Tests with Dry Samples	120
4.4.1 Lithology Samples	121
4.4.2 Specific Energy as Power Increases: Non-melt vs. Melt	122
4.4.3 Effects of Pulse Width and Repetition Rate	122
4.4.4 Temperature Factors	124
4.4.5 Spallation Tests with Saturated Samples	124
4.4.6 Submerged Sample Test	125
4.4.7 Diode Laser Tests with Dry Samples	125
5 Conclusions	127
6 Recommendations	129
6.1 Phase 2 Research Plan	129
6.1.1 Additional Fundamental Research	129
6.1.2 Modeling and Theoretical Studies	130
6.1.3 Engineering Studies	130
7 References	133
8 Appendix: A-F	134
A: GTI Laser Applications Bibliography	135
B: Tables of Results	139
C: Glossary	194
D: Nomenclature	199
ν = Poisson's ratio	201
E: Petrophysical and Petrographic Studies	202
F: IPG Optical Fluids Report	218
Study for Gas Technology Institute	219
Contract #: KI00024110	219
November 21, 2003	219
Report on fluids for near IR transmission	219
Introduction	219
Experimental setup	219
Brief theory of NIR absorption	220
Organic fluids	221
Picture 1	222
Semi-organics molecules	224
Picture 3	225
Halocarbons	226
Picture 4	227
As you can see, there are no Carbon-Hydrogen bonds.	228
Picture 5	228

Conclusions	228
References	230
List of Graphical Materials	234
Introduction	236
8.1 An Alternative Method: High Power Lasers	237
8.2 Laser Parameters	239
Executive Summary.....	241
Experimental	242
8.3 Proposed Tasks.....	242
8.4 Experimental Methods	246
8.4.1 Specific Energy Calculations.....	246
8.5 Rocks Used in this Investigation	248
8.5.1 Characterization of the Samples	248
8.5.2 General Rock Properties	248
Results and Discussion.....	249
High Pressure Perforation Simulation	249
8.5.3 High Pressure Perforation Cell Design and Development.....	250
Perforation of Core Samples under High Pressure Conditions.....	260
Perforation of Saturated Core Samples under High Pressure Conditions	269
Perforation of Composite Core Samples under High Pressure Conditions	271
Conclusion.....	275
References	276
Publications	276
Presentations.....	277
List of Acronyms and Abbreviations.....	278
Appendix A: Experimental Data	280
Appendix B: DOE Project Review Presentation	284

List of Graphical Materials

Figure 1. 2-D post-laser permeability map of perforation demonstration in 30.48 cm (12.0 in) per side block of Berea sandstone showing 15-30% permeability increase along the lased tunnel surface.....	237
Table 1. Comparison of laser characteristics for CO ₂ ; lamp-pumped and diode-pumped Nd:YAG; and high power fiber lasers at 4 kW output power.	238
Figure 2. Standard tri-axial cell design prior to modification for HPFL perforation. ...	251
Figure 3. High pressure perforation cell proof-of-concept tube with a cover lens.....	252
Figure 4. Cover lenses before and after lasing during high pressure perforation cell experiment.....	253
Figure 5. High pressure perforation cell proof-of-concept tube with funnel and a cover lens.....	254
Figure 6. Experimental set-up of high pressure perforation cell proof-of-concept test.	255
Figure 7. Laser firing during high pressure perforation cell proof-of-concept test.	255
Figure 8. Interior (A) and exterior (B) views of 5.08 cm (2.0 in) ID copper tube mock-up used to test high pressure perforation test cell design.....	256
Figure 9. Copper tube mock-up with the purging connection.	257
Figure 10. Copper tube mock-up assembly ready for laser application.	257
Figure 11. High pressure tri-axial cell concept for laser perforation testing under pressure conditions.....	258
Figure 12. High pressure tri-axial cell design for laser perforation testing under pressure conditions.....	259
Figure 13. Completed high pressure tri-axial cell for in-situ laser perforation testing..	260
Figure 14. Experimental set up for perforation test in high pressure cell.....	262
Figure 15. Perforation test in progress.....	262
Figure 16. Comparison of SE values in sandstone as observed at various test cell pressure conditions.....	263
Figure 17. Comparison of SE values in limestone as observed at various test cell pressure conditions.....	264
Figure 18. Comparison of SE values in limestone and sandstone as observed at various test cell pressure conditions.	264
Figure 19. Post-high pressure perforation test of limestone exhibiting stress fractures .	266
Figure 20. Sandstone samples show no post-test stress fractures.....	266
Figure 21. Thin section analysis from limestone used in perforation tests show low porosity and permeability with close grain contact.	267
Figure 22. Heat transfer in sandstone by conduction (solid to solid) and convection (solid to air).....	269
Figure 23. Comparison of SE values in sandstone as observed at various test cell pressure conditions, including brine and oil saturated samples.....	270
Figure 24. Comparison of SE values in limestone as observed at various test cell pressure conditions, including brine and oil saturated samples.	271

Figure 25. Composite core samples were to simulate physical conditions of a completed wellbore..... 272

Figure 26. Composite sample as prepared for the high pressure cell, illustrating modified design to avoid melting of core sleeve..... 273

Figure 27. CT scan image of 10.16 cm (4.0 in) diameter by 15.24 cm (6.0 in) length limestone clad sample and outline of penetration path after perforation of three 30 s shots by 5.34 kW ytterbium fiber laser with a 0.889 cm (0.35 in) diameter beam. 274

Figure 28. Pre- and post-lased images of 10.16 cm (4.0 in) diameter by 15.24 cm (6.0 in) length limestone core inset with 5.08 cm (2.0 in) diameter by 1.27 cm (0.5 in) thick steel plate..... 274

Introduction

The oil and gas industry has attempted for many years to find acceptable non-explosive alternatives to creating downhole reservoir connectivity with the wellbore. Although some methods have proven capable in providing an economic and technical solution, the use of high shaped charges remains the preferred technology for most applications.

Shaped charge explosives have drawbacks which alternative perforation methods seek to improve, primarily by crushing the tunnel zone and inhibiting flow from the reservoir into the wellbore. Remedial work with some form of stimulation is often required to overcome this flow restriction. Other concerns voiced by the industry include the inherent safety concerns regarding transport, storing and use of the perforating assembly. Also, regulatory concerns focus on limitations that may be raised on the use of explosive charges, challenging the industries ability to economically complete wells around the world.

The application of high power lasers to create the path between the wellbore and reservoir could significantly reduce the primary drawbacks of using explosives. In addition to perforating, laser applications should perform other on-site tasks including cutting windows for side exiting casing or laterals, extended perforations that connect additional reservoir rock to the wellbore, and removal of objects lost downhole that would normally require drill out or fishing operations.

Laser perforation experiments in the past have been performed using combinations of laser input parameters on several rock lithologies to determine specific cause and effect relationships. Optimized variables were identified and demonstrations conducted to show the capability of lasers to cut tunnels of at least 30.48 cm (12.0 in) deep into sandstone and limestone. One notable advantage resulting from laser perforation on sandstone is the improvement of near-tunnel fluid flow characteristics. Measured permeability increased 15-30% along the tunnel face of a perforation demonstration on a 30.48 cm (12.0 in) block of Berea sandstone (Figure 1).

Although the application of lasers for perforation provided promising results, downhole pressure conditions had not been investigated. All high power laser applications experiments performed to date had been conducted under ambient pressure conditions in the laboratory. In order to perform high pressure tests on rock, a tri-axial pressure cell would need to be designed to allow multiple pressure conditions, a simulated pressurized wellbore, a window for the laser beam to interface with the sample, and ejection ports for lased material.

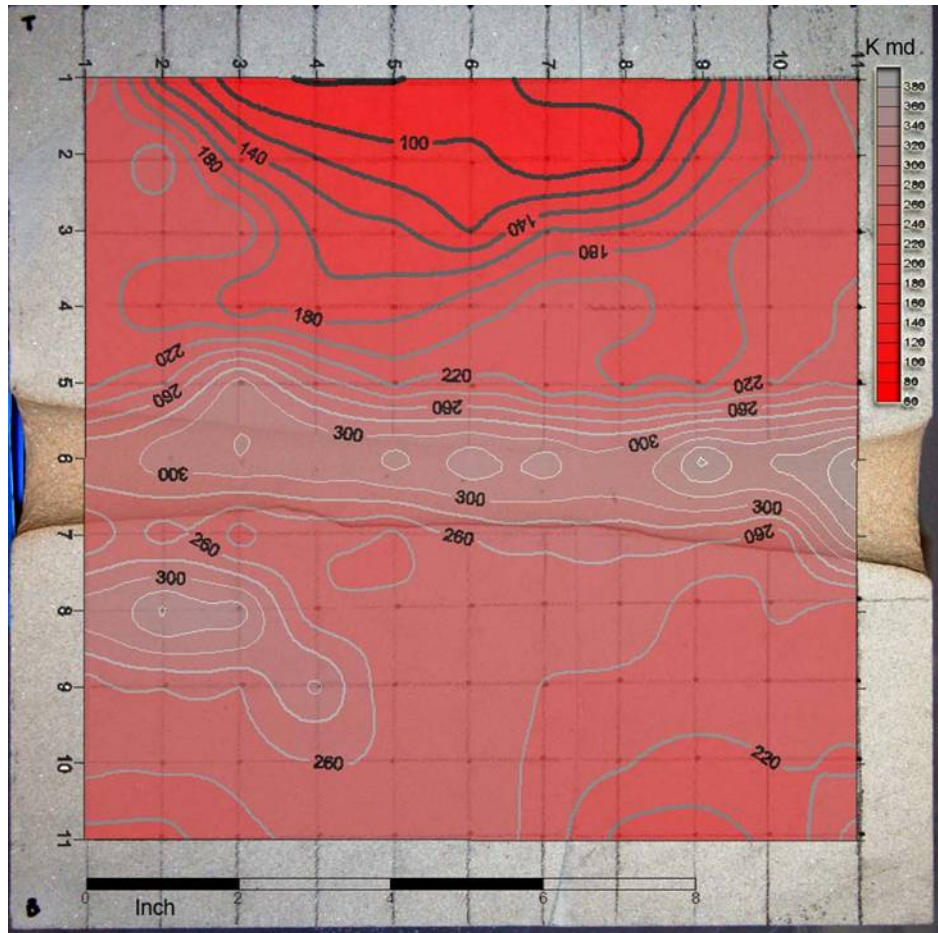


Figure 1. 2-D post-laser permeability map of perforation demonstration in 30.48 cm (12.0 in) per side block of Berea sandstone showing 15-30% permeability increase along the lased tunnel surface.

8.1 An Alternative Method: High Power Lasers.

Reducing costs and eliminating problems of current drilling and completion methods would have a significant positive impact on the oil and gas industry. New technologies and tools operate using basic rock destruction mechanisms like thermal spalling, fusion and vaporization, mechanical stresses and chemical reactions¹³. All of these destruction mechanisms can be achieved using lasers. For example, at low laser power, spalling (chipping) can be obtained. Increase in the laser power, with a fixed beam diameter, results in phase changes and reactions in the rock, like dehydration of clays, releasing of gases and inducing thermal stresses. At a certain power, the rock will melt (fuse) and at higher power the rock will vaporize.

¹³ Maurer, 1968, 1980

Laser technology applied to drilling and completion operations has the potential to reduce drilling time, eliminate the necessity to remove and dispose of drilling cuttings and improve well performance through improved perforation operations.

Although initial GRI laser drilling investigations utilized megawatt-class military lasers, it was soon apparent that an oversized laser could effectively remove a rock mass, however, it did so quite inefficiently due to material phase change and other phenomenon unrelated to cutting and removing rock.

Less powerful industrial lasers were then utilized providing improved SE values when exposed to the same or similar rock types. Under lab conditions, the researchers were successful in proving that the current generation of industrial lasers was capable of removing rock with energy levels comparable to those of existing mechanical rock drilling methods. However, for a laser system to be applied under field conditions, a number of conditions would have to be met, including requisite power delivery to target, reliability, portability, and greater efficiency. Although the overall size or footprint per kilowatt output was improving, industrial class lasers were not necessarily designed to withstand field conditions and would be difficult to economically operate given their low wall plug efficiencies.

8.1.1.1 Characteristics of Fiber Lasers

Recently, high power fiber lasers have become commercially available and have positioned themselves as a serious alternative to other solid-state and carbon dioxide lasers for industrial material-processing. Over the past two years, fiber lasers have increased in power from several watts to kilowatts, and are fully capable of delivering sufficient rock cutting power via fiber optics.

Of interest to the GTI research team were the nearly 10x higher wall plug efficiency; and greater mobility through a smaller overall size and solid state design. In addition, the beam quality was improved, and projected diode failure was in excess of 50,000 continuous hours, projecting low or no maintenance operations (Table 1).

Table 1. Comparison of laser characteristics for CO₂; lamp-pumped and diode-pumped Nd:YAG; and high power fiber lasers at 4 kW output power.

	CO ₂	LP Nd:YAG	DP Nd:YAG	HPFL
E/O Efficiency, %	5-10	2-3	4-6	16-20
Electric Power, kW (no chiller)	~ 50	~ 130	~ 80	20-25
Footprint, m ² (no chiller)	6	5	3	0.5
Water, m ³ /hr	6-8	20-25	~ 15	<2
Maintenance, Khrs	1-2	0.5	2-3	10-15

Pump Replace, Khrs	n/a	0.5-1	2.5	>50
--------------------	-----	-------	-----	-----

Source: IPG Photonics Corporation

Together, these improvements have rapidly advanced fiber lasers as a leading candidate for on-site applications, including hard rock mining, tunneling, pavement cutting and rock drilling.

GTI acquired an IPG Photonics 5.34 kW ytterbium-doped multi-clad fiber laser in 2003, at the time the most powerful of its kind available for research in the United States. Power output is rapidly increasing, as more powerful fiber lasers have been manufactured.

For oil and gas industry applications, the fiber laser presents itself as the most likely near-term candidate for successful laser applications in remote locations, capable of delivering a beam to a rock target some 1 to 2 km (3281 to 6562 ft) beneath the Earth's surface. Given the improvement in the fiber laser's wall plug efficiency (16%) over a comparable diode pumped Nd:YAG (6%), an ytterbium fiber laser requires about 62.5% less electrical energy to produce the same output power beam.

For many of the same reasons fiber lasers represent a breakthrough for field applications in oil and gas, it is also being considered for other applications that include cutting or breaking rock and/or similar materials in remote locations, including those in the energy, mining, defense, space, demolition and construction industries.

Results from experiments to date continued to suggest the application of photonic energy may prove to offer a non-explosive alternative for perforating oil and gas wells. By applying this technique downhole through casing and cement, perforations and other directionally controlled completion and stimulation methods could be employed without creating damage to the reservoir. Clearly, with the use of photonic energy, no perforating materials or explosive products are left to contaminate the wellbore and the perforation tunnel; therefore cleaning the perforated tunnel and the wellbore around the perforation area are not required. In fact, the use of lasers in downhole completions techniques, including perforation, has the potential to stimulate the perforation tunnel while it is constructed.

8.2 Laser Parameters

LASER is an acronym for Light Amplification by Stimulated Emission of Radiation. Albert Einstein predicted the possibility of stimulated emission (generation of photons or discrete bundles of energy via transitions between atomic or molecular energy levels) in 1917. Laser use in many applications such as medical, metallurgical, and military, is becoming well understood. The principle of the laser is transforming different kinds of energy (chemical, electrical, etc.) into intense electromagnetic beams of monochromatic and

coherent waves. The wavelength of a laser beam (λ) depends on laser's active medium, and ranges from 0.1 micrometers (μm) to $103\mu\text{m}$, spanning the ultraviolet, visible, infrared and sub-millimeter ranges of the photonic spectrum¹⁴.

Laser drilling is a developing technology that has been applied to industrial uses such as creating small holes in metal and other materials. This research examines the possibility of expanding the use of lasers to remove rock for oil and gas exploration and production applications, including conventional and horizontal drilling, cutting windows in steel casing and cement, and other completion techniques.

In rock drilling, the type of laser used plays a crucial role in the efficiency and quality of the cut. Laser properties, including discharge type (continuous or pulsed), wavelength, peak power, average power, intensity, repetition rate, and pulse width define the type of laser rock interaction obtained, and thus, affect the amount of energy transfer to the rock. The results of the previous experimental work show that lasers penetrate well through rocks, as they have a low reflectivity of electromagnetic waves, resulting in a good coupling with the laser radiation. Also, the low thermal conductivity of rocks allows for a rapid heating of the rock sample in the vicinity of the beam.

¹⁴W.T. Silfvast, 1996

Executive Summary

The overall objective of this study is to conduct research to establish the technical feasibility of using laser tools to drill and complete natural gas wells and conduct engineering studies leading to prototype tool development. The proposed tasks for this report include developing an in-situ laser/rock interaction test plan based on Phase I plan and results, including design of pressure vessel and data acquisition using pulsed and continuous wave lasers.

Experiments were performed at Gas Technology Institute in Des Plaines, IL at their High Power Laser Applications Laboratory. The 5.34 kW ytterbium-doped multi-clad fiber laser was used exclusively to perform the experimental work. Tests were conducted on Berea sandstone and Bedford limestone samples. Berea sandstone is a standard quarry rock used in the petroleum industry for laboratory testing. Bedford limestone was procured from a local Illinois quarry, and was selected due to its relatively consistent and uniform characteristics.

All laser/rock experiments performed to date have been conducted under ambient laboratory conditions. As part of a recent laser perforation proof-of-concept study, it was critical to understand how a laser would perform under downhole pressure conditions. In order to perform high pressure tests on rock, a tri-axial pressure cell was designed to allow multiple pressure conditions, a simulated pressurized wellbore, a window for the laser beam to interface with the sample, and ejection ports for lased material.

Initial tests were performed on cores of Berea sandstone and Bedford/Indiana limestone under various conditions of axial, pore and confining pressures. For all cases, the laser settings remained the same. Full output power of the ytterbium fiber laser, 5.34 kW, was applied continuously to each sample through the sapphire window of the pressure cell with a beam diameter of 0.889 cm (0.35 in) for 8.0 s.

Additional tests were performed on sandstone and limestone core saturated in a brine solution and oil. Finally, composite cores consisting of rock, cement and steel plate were constructed to simulate laser perforation in a completed wellbore under in-situ pressure conditions.

The results from these tests were successful in proving the ability of the high power fiber laser to perforate the samples under high pressure conditions. Next steps include design and testing of a downhole prototype laser perforation tool.

Experimental

8.3 Proposed Tasks

The work performed by GTI during the 2005 fiscal period was based on the following overall scope of work presented and accepted by DOE (Work performed during this period and presented in this report are in bold):

Task 2.0: Continuation of Fundamental Research and Development

GTI shall continue previous investigations into the feasibility of using high-powered lasers for the purpose of drilling and completing natural gas wells. The objectives of the project are to:

- a) Experimentally determine the best laser parameters for creating a hole of a given size, deep into a given lithology under in-situ conditions.
- b) Develop a model for the laser/rock interaction process, and
- c) Develop the conceptual design of a laser drilling system based on the results of a) and b).
- d) Experimentally determine the effect of liquid saturated lithologies on laser beam-rock interactions
- e) Ability of lasers to interact with rock in a liquid filled pressure vessel
- f) Advantages and disadvantages of pulsed vs. continuous wave CO₂ lasers
- g) Specific Energy (SE) dependencies on laser and other process parameters, and
- h) Mineralogy changes that occur with exposure to laser energy.

Task 2.1 Experimental Plans

1. Develop an in-situ laser/rock interaction test plan based on Phase I plan and results, including design of pressure vessel and data acquisition using pulsed and continuous wave lasers
2. Develop a laser/rock interaction test plan to be performed using a high-power free electron (FE) laser to determine effect of various beam wavelengths on rock samples

Task 2.2 Rock Preparation and Analysis

Acquire and prepare sandstone, shale and limestone target samples for all planned tests, and analyze rock properties pre- and post-test.

Task 2.3 Data Analysis

Collect and analyze diagnostic data, calculate SE and penetration rates, determine lithology-specific relationships and general relationships, and evaluate effect of pulsed vs. continuous wave lasers, wavelength, and in-situ conditions on the application of laser energy to remove rock.

Task 2.4 Topical Report

Prepare, as part of the Continuation Application, a draft topical report on the technical progress of the project. This report shall follow guidelines set forth in the Federal Assistance Reporting Checklist and accompanying reporting instructions and shall include, but not necessarily be limited to:

1. The diagnostic data, SE and penetration rate calculations for each lithology tested,
2. The conditions that result in spallation, melt, and vaporization mechanisms for rock removal in each lithology, including laser and rock properties
3. An analysis of changes in physical and chemical properties to rock samples following laser exposure
4. The contributory effects of laser beam wavelength on rock removal

Task 2.5 Modeled Effects of Energy Transfer From Lasers to Non-Homogeneous Porous Media

Develop a predictive model of the processes that occur during laser/rock interaction based principally on transport equations of mass, momentum and energy conservation.

Task 3.0 Systems Development Issues in Laser Well Construction

GTI shall investigate the significant technical hurdles that are required to allow downhole laser applications in oil and gas wells, including energy delivery downhole, rock cuttings from the wellbore as a material resource for well construction, alternative techniques (i.e., clear water or other transparent coaxial jets) for drilling with a weighted fluid environment.

This study will focus primarily on laser drilling systems development issues. Proposed is a two-phase program that encompasses idea/concept development and demonstration of concept. All phases and tasks proposed will be performed at Gas Technology Institute.

Task 3.1 Downhole Energy Delivery Assessment

Perform a literature review and analysis to determine available commercial options for laser systems and fiber optics, laser optics and lenses, conventional electric transmission applications and energy transfer issues.

Task 3.2 Laser Created Rock Melt Characteristic Study

Investigate the material properties of rock melted by laser energy as a material resource in well construction (i.e., ceramic casing), including strength properties, mineralogy, structure, thermal properties, porosity and permeability, and influence of additives on melt properties.

Task 3.3 Experimental Plans

Develop an in-situ laser/rock interaction test plan to simulate a variety of downhole drilling environments, including balanced, overbalanced, and underbalanced conditions, in combination with anticipated downhole fluids (i.e., drilling mud, water, brine, hydrocarbons).

Task 3.4 Rock Preparation and Analysis

Acquire and prepare sandstone, shale and limestone target samples for all planned tests, and analyze rock properties pre- and post-test.

Task 3.5 Data Analysis

Collect and analyze diagnostic data, calculate SE and penetration rates, determine lithology-specific relationships and general relationships, and evaluate effect of downhole drilling environments in combination with drilling fluids on these relationships.

Task 3.6 Topical Report

Prepare, as part of the Continuation Application (see Article 2.6, "Continuation Application" contained in Section II -Special Terms and Conditions), a draft topical report on the technical progress of the project. This report shall follow guidelines set forth in the Federal Assistance Reporting Checklist and accompanying reporting instructions, and shall include, but not necessarily be limited to:

- Bibliography and analysis from literature study,
- Laser Created Rock Melt Characteristic Study analysis and results,
- The diagnostic data, SE and penetration rate calculations for each material tested,
- The conditions that result in spallation, melt, and vaporization mechanisms for rock and cement removal in each lithology, including laser and rock properties, and conditions that optimize cutting through a steel liner,

- An analysis of changes in physical and chemical properties to rock, cement and steel samples following laser exposure.

Task 4.0: High Energy Laser Perforation and Completion Techniques

GTI is currently investigating the feasibility of laser perforation and completion techniques with a major service company partner. A proof of concept with planned subsequent investigations are aimed at creating engineering systems for adapting laser energy to puncture steel casing and the cement bonding agent, into the formation deep enough to allow the free flow of hydrocarbons into the wellbore.

GTI proposes to perform investigations into understanding and modeling laser/material interactions involving composite perforation targets, representing steel casing, cement, and reservoir rock. Although literature exists on the use of lasers for cutting steel in controlled factory environments, limited information addresses laser cutting of steel in the extreme conditions that exist downhole. These investigations will directly complement GTI's existing systems analysis and prototype development with our industry partner.

As with Task 2.0, all tasks proposed will be performed at Gas Technology Institute, however in unforeseen situation where laser or other similar equipment from laser or petroleum industry partners would be required, GTI is confident that access would be made available and supported.

Task 4.1 Experimental Plans

Develop an in-situ laser/rock interaction test plan matrix, including design of pressure vessel and data acquisition using a laser(s) capable of cutting steel, cement and rock samples.

Task 4.2 Rock Preparation and Analysis

Acquire and prepare combinations of sandstone, limestone, cement and steel target samples (individual and composite) and analyze material properties pre- and post-test.

Task 4.3 Data Analysis

Collect and analyze diagnostic data, calculate SE and penetration rates, determine material-specific relationships and general relationships, and evaluate effect of laser energy to remove combination of materials.

Task 4.4 Topical Report

Prepare, as part of the Continuation Application (see Article 2.6, "Continuation Application" contained in Section II -Special Terms and Conditions), a draft topical report on the technical progress of the project. This report shall follow guidelines set forth in the Federal Assistance Reporting Checklist and accompanying reporting instructions, and shall include, but not necessarily be limited to:

- The diagnostic data, SE and penetration rate calculations for each material tested,
- The conditions that result in spallation, melt, and vaporization mechanisms for rock and cement removal in each lithology, including laser and rock properties, and conditions that optimize cutting through a steel liner
- An analysis of changes in physical and chemical properties to rock, cement and steel samples following laser exposure.

Task 4.5 Modeled Effects of Energy Transfer in a Laser Perforation Shot

Develop a predictive model of the processes that occur during laser/material interaction based principally on transport equations of mass, momentum and energy conservation.

8.4 Experimental Methods

Experiments were performed at Gas Technology Institute in Des Plaines, IL at their High Power Laser Applications Laboratory. This lab was developed as a means to investigate alternative methods to conventional rock removal in accessing targeted subsurface accumulations, including energy reserves, minerals, aquifers, and pollutants. The 5.34 kW ytterbium-doped multi-clad fiber laser was used exclusively to perform the experimental work.

8.4.1 Specific Energy Calculations

In order to break rock by mechanically or thermally induced stresses, sufficient power must be applied to the rock such that the induced stresses exceed the rock's strength. Similarly, when fusing rock, sufficient heat must be generated that exceed the melting temperature of the rock. Once these threshold values of power and energy are exceeded, the amount of energy required to break or remove a unit volume of rock remains nearly constant. This energy parameter, which is a measure of the efficiency of the rock destruction technique, is defined as specific energy (SE). The term SE is associated with various definitions and is commonly used by the drilling industry in discussions of the efficiency of mechanical drilling, particularly in measuring effectiveness of new bit designs. SE is defined in this experimental work as the amount of energy required to remove a unit volume of rock and is relationally represented as follows:

$$SE \text{ (kJ/ cc)} = \text{Energy input / volume removed} \quad (1)$$

8.4.1.1 Parameters Affecting SE Measurements.

There are three basic phenomena evident in the process of radiant energy transfer to solids: reflection, scattering and absorption of radiation. The flow of energy of an incident electromagnetic wave (E_{inc}) is divided into these parts:

$$E_{\text{inc}} = E_{\text{refl}} + E_{\text{sc}} + E_{\text{abs}} \quad (2)$$

Where E_{refl} , E_{sc} , and E_{abs} are reflected, scattered and absorbed fractions of the energy flow of the incident wave, respectively.

If a surface is a planar one, like a mirror, then much of the energy is reflected. Rough surfaces mainly scatter the incident radiation. The reflectivity is determined by the composition of the solid, while the scattering of radiation is determined by wavelength, λ . It is the absorbed energy that gives rise to the rock heating and destruction. Reflection and scattering represent energy losses that occur apart from the absorbed energy. Minimizing fractions of reflected and scattered energy losses will, consequently, maximize the energy available for transfer to a rock for destruction.

There are factors that affect the amount of absorbed energy transferred to the rock samples, known as secondary effects, and include the creation of melted materials, beam absorbing exsolved gases in the lased hole and induced fractures in the surrounding rock. When applying high power lasers on rocks, the laser can spall, melt, or vaporize the rock as the energy transferred to the rock raises its temperature locally. Mineral melt begins to occur when the rate of heat dissipation by the rock is exceeded by the rate of energy absorbed by the rock. As time increases, energy accumulates in the form of heat, raising the local temperature of the minerals to their melting points, forming a glassy melt.

The amount of melt is a function of the mineralogy of the rock and the intergranular space of the rock matrix. The closer the grains are to one another, the more heat will be transferred, resulting in more melt in the rocks. However, for tightly packed grains, the heat conductivity could reach higher values dissipating the heat at a faster rate, reducing the amount of melted material. Also, some minerals decompose and produce gas. As a result, the melt and gases require part of the laser energy for their creation, so a smaller percentage of the total laser energy is transmitted to rock.

Fractures that form in the samples also have an impact on SE. It may be that fractures extending out from the laser created hole are beneficial to the removal process. However, it is our conclusion that the fractures seen in the tests are an artifact of the sample size and do not represent what will occur in the subsurface under in situ conditions.

For the purposes of this study, fractures represent losses of energy, which result in higher SE values. Fractures are classified as macro- and micro- fractures. The behavior of fractures is different from one rock type to another. This difference depends on intrinsic factors such as mineralogy, thermal properties of the rocks,

volume of void space, dimension of the sample and the amount of stress applied. Mineralogy also affects fracture formation. Clays contain water and by subjecting the clays to higher temperatures, water will escape in the form of vapor. This increases the volume and pressure in the pore and can cause fractures. Sandstones and shales have high thermal conductivities and contain clays. Limestones, on the other hand, have low thermal conductivity and have low amounts of clay and quartz. Therefore, fractures are expected in sandstones and shales, but not in limestones.

Rocks, having a high thermal conductivity, transfer heat more efficiently and the temperature is more uniform within the rock. Therefore, for this type of rock, cooling occurs gradually along the core sample. For example, fractures in sandstones developed regularly, not randomly. High temperatures resulting from the energy of the laser beam causes quartz grains to expand. At 600 °C (1112 °F) quartz grains expand by 1.75% of the original size. In the case of full grain contact (low void space), grains have less space to expand and fractures develop¹⁵.

The dimensions of the sample can affect the behavior of the fractures. It has been observed from the previous tests¹⁶ that the 2.54 cm (1.0 in.) diameter cores are highly fractured around the hole, while the 5.08 cm (2.0 in.) diameter cores are less fractured. Finally, stress applied to the core minimizes the macro fractures, while the micro fractures will still remain.

8.5 Rocks Used in this Investigation

8.5.1 Characterization of the Samples

Tests were conducted on sandstone and limestone samples. Berea sandstone is a standard quarry rock used in the petroleum industry for laboratory testing. Other notable Berea sandstone characteristics include: relative homogeneous physical characteristics including high silica content; common use in laboratory studies of rock; and extensive body of experimental data and literature.

Bedford limestone was procured from a local Illinois quarry, and was selected due to its relatively consistent and uniform characteristics.

For both rock types selected, it was important that both were available in large block sizes due to experimental design. Although actual sandstone and limestone reservoir core samples were available, sample size and consistent physical characteristics were more limited than quarry samples.

8.5.2 General Rock Properties

Microscopic properties, such as mineralogy, clay content, and microfractures, were determined using a scanning electron microscope with the energy dispersive

¹⁵ W.H. Somerton, 1992.

¹⁶ R.M. Graves and D.G. O'Brien, 1998

system (SEM-EDS), x-ray diffraction (XRD), and thin sections. Melting temperatures of these rocks were measured using differential thermal analysis (DTA).

The Pressure Decay Profile Permeameter (PDPK) was used to characterize the rocks before and after lasing. The PDPK measures point permeability at ambient conditions, Klinkenberg slip factor and the non-Darcy flow coefficient (Forchheimer). The PDPK is reliable down to a permeability of 0.001 md and experience has shown it to be repeatable and accurate. This non-destructive, unsteady-state test can measure permeability on irregular shapes, therefore, it an excellent tool to analyze permeability before and after beam exposure.

Results and Discussion

High Pressure Perforation Simulation

Objective: To simulate perforation under in-situ conditions by applying axial, pore and confining pressures on sandstone and limestone core samples.

Procedure: In order to perform high pressure tests on rock, a tri-axial pressure cell was designed to allow multiple pressure conditions, a simulated pressurized wellbore, a window for the laser beam to interface with the sample, and ejection ports for lased material.

As part of the laser perforation study, tests were conducted with the tri-axial pressure cell to give us an initial understanding on how high pressure conditions similar to that found downhole influence the laser/rock interaction process. The laser used in this experiment was a 5.34 kW ytterbium-doped multicladd fiber laser with an emission wavelength of 1.07 microns. The tri-axial pressure cell rated at 20,684 kPa (3000 psig) was designed for this experiment to allow laser beam exposure to a 10.16 cm (4.0 in) diameter by 15.24 cm (6.0 in) length pressure-charged rock core by means of a sapphire window. Maximum testing pressures performed by the manufacturer were 31,026 kPa (4500 psig).

Between the window and the core is a chamber that simulates a wellbore, and can be independently charged with pressure to simulate over-balanced conditions. At-balance conditions are simulated with ambient pressure in the wellbore chamber and no pore pressure in the rock sample. Underbalanced conditions are simulated with ambient conditions in the wellbore chamber and pore pressure in the rock sample.

Ports located in the wellbore chamber allow ejection of cuttings and other materials. The design of the wellbore chamber minimizes the exposure of the

optics to all material ejected from the sample during the lasing process. The design has proven successful in this application, and will be incorporated in future field prototype tool designs.

The concepts integrated into this high pressure perforation cell were developed at GTI and tested several times before the test chamber was built. Concepts that were developed for the cell included:

- Simultaneous application of axial, confining and pore pressure
- Testing of effective purge system under confined volume at high pressure (Removing debris from confined volume at high pressure was a major issue)
- Lasing core inside a cell at high pressure with minimum temperature rise of cell parts (safety issue)

Pressure transducers for confining, axial and pore pressure ports were calibrated, connected to cell assembly and tested for tri-axial pressure conditions.

8.5.3 High Pressure Perforation Cell Design and Development

When designing the high pressure laser perforation cell, the following key design criteria were identified as part of the unique application and complexity of the operation:

- Safety
- Pore pressure flexibility
- Purging under tri-axial pressure conditions
- Maintaining clear optics path and clean lenses

Operating the laser perforation testing cell under high pressure conditions and with a high power laser beam presents a serious safety issue. The cell also required the capability to apply multiple combinations of confining, axial and pore pressure, while circulating a fluid to remove cuttings in a manner to keep the optics clean and a clear path for the beam.

The original design for the laser perforation cell was of a conventional tri-axial cell used for flow measurement (Figure 2). Evaluation of this design determined that major modifications would need to be identified, designed, and tested before a prototype could be built.

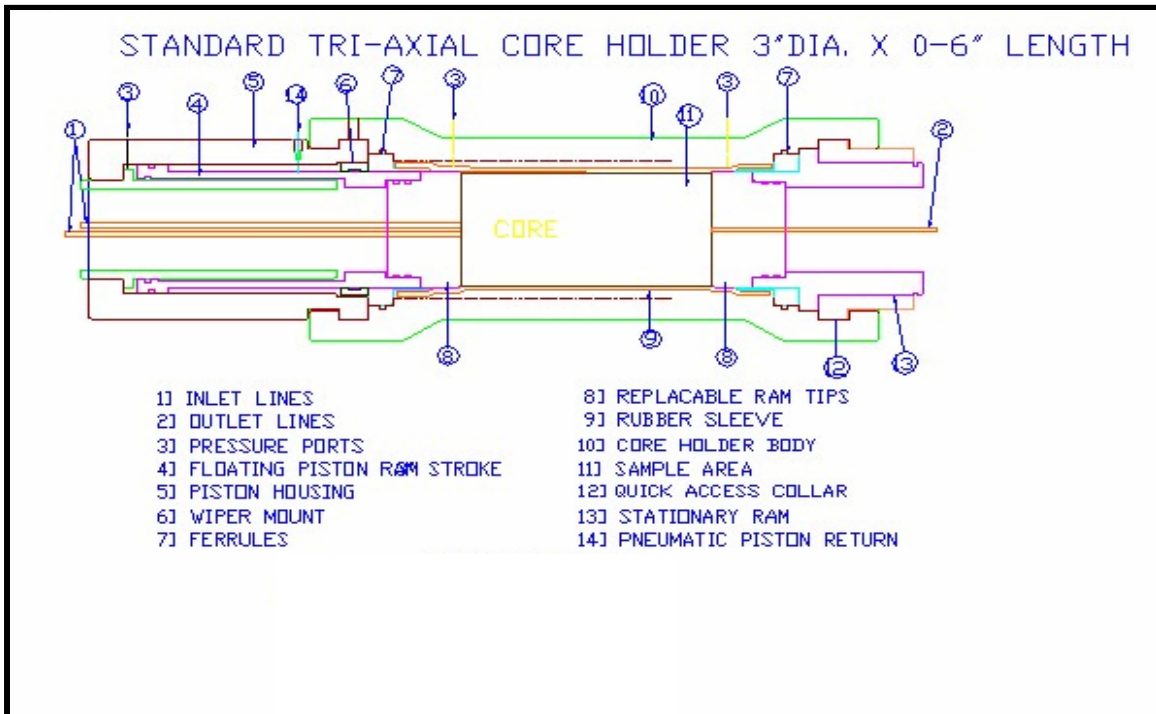


Figure 2. Standard tri-axial cell design prior to modification for HPFL perforation.

Concept experiments were designed and tested to understand how best to circulate a fluid, while lasing, to assist in the cuttings removal. An initial test was conducted with a 5.08 cm (2.0 in) ID tube fitted with a cover lens window on one end, a target rock core on the other and ventilation holes to allow debris to exit. Compressed air is used to keep the cover lens free of cuttings dust and debris, as well as provide an assist for material removal for the beam (Figure 3). The purpose of this experiment was to determine if the rock cuttings could be removed from inside the tubing without material accumulating on the cover lens window.

The result of this experiment was as expected: Dust had accumulated on the cover lens. Energy from the beam was transferred to the dust, and then to the cover lens. The temperature of the glass increased non-uniformly and led to its failure. Figure 4 shows the lens before and after the experiment.

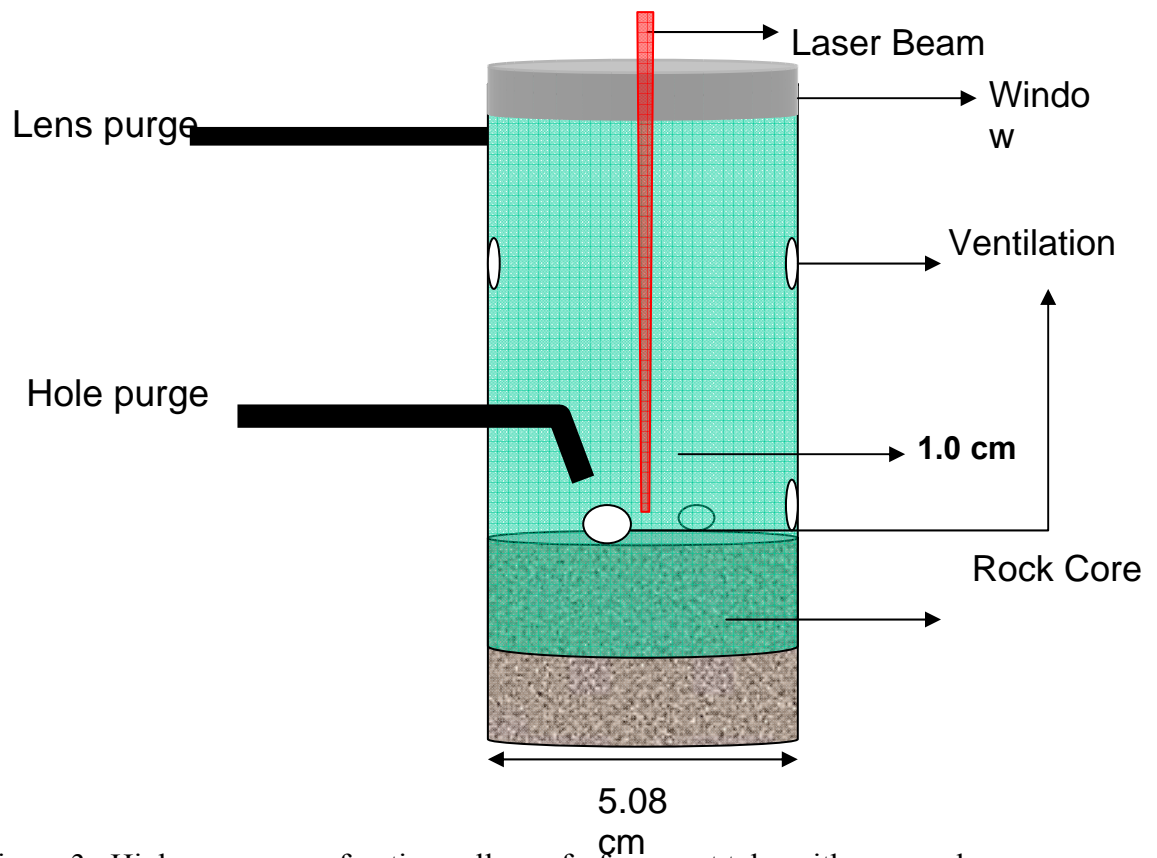


Figure 3. High pressure perforation cell proof-of-concept tube with a cover lens.

Before lasing



After lasing



Figure 4. Cover lenses before and after lasing during high pressure perforation cell experiment.

Since lasing directly through tube resulted in dust accumulation and beam blocking, an alternative design was needed to prevent dust from reaching the cover lens. A conical design was investigated that would reduce the area available for dust to reach the cover lens. In this experiment, the same set-up was used with a conical restriction put in place between the cover lens and the sample. The larger diameter of the cone was closer to the cover glass. The purging tube was inserted between the cone and the cover lens such that the compressed air flowed through the narrow opening in the direction of and coaxially with the laser beam, thereby deflecting debris away from the cover lens and toward the ventilation holes (Figure 5).

Ventilation holes are located around the tube between the cone and the rock sample which will allow the dust and the particles to exit. The shape of the cone assists in directing debris to the ventilation holes. Figure 6 shows the experimental set-up for the cone structure, while Figure 7 shows the chamber while the laser is firing.

The cone was inserted in a transparent tube to allow visibility and monitoring particle and dust behavior in the tube. Modifications were made to optimize location of system elements, including the distance between the cover lens and the surface of the sample, the purging angle and ventilation opening diameter.

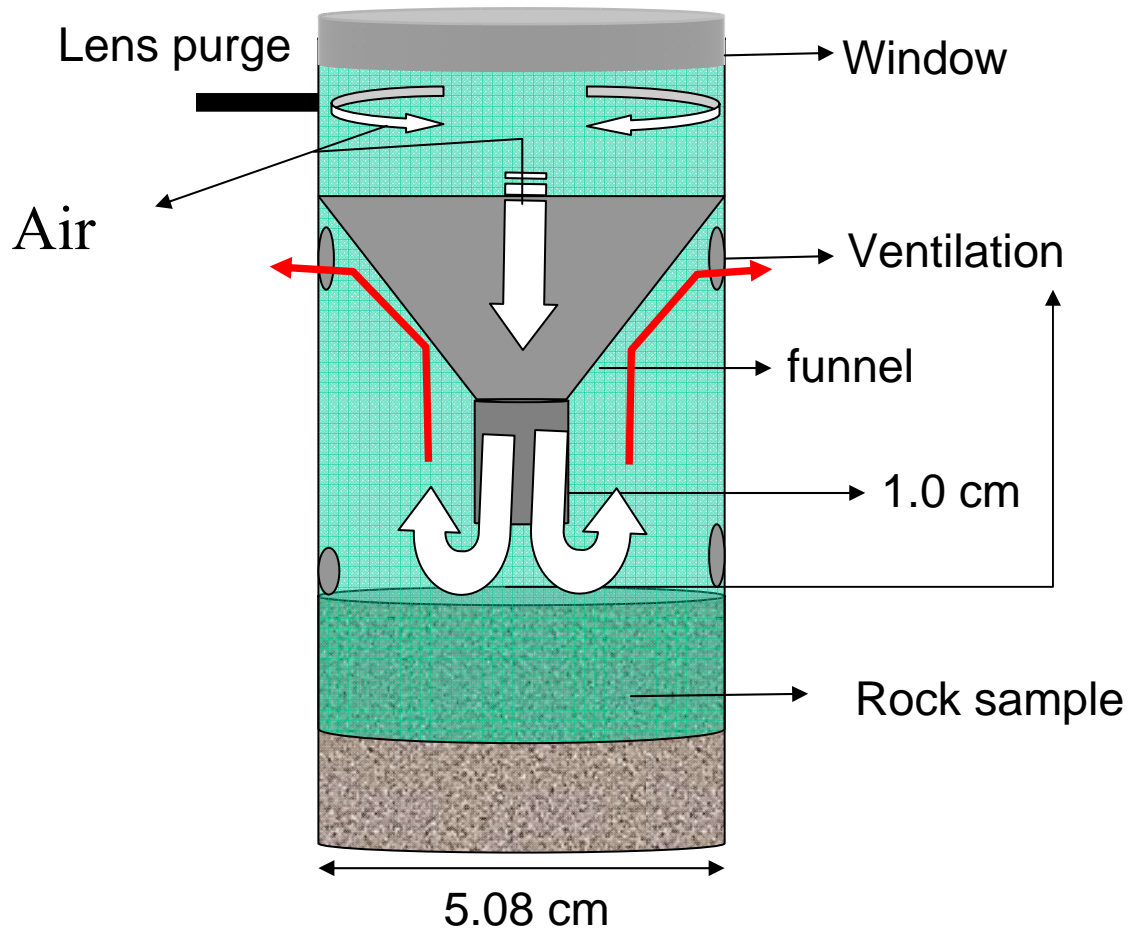


Figure 5. High pressure perforation cell proof-of-concept tube with funnel and a cover lens.

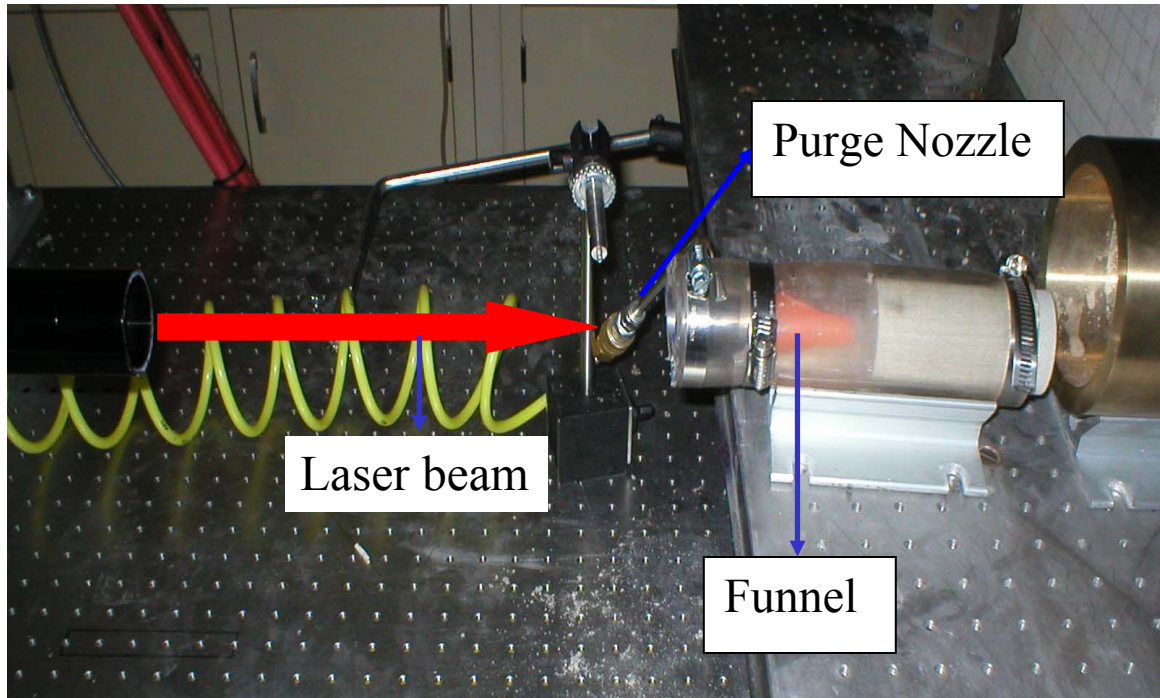


Figure 6. Experimental set-up of high pressure perforation cell proof-of-concept test.

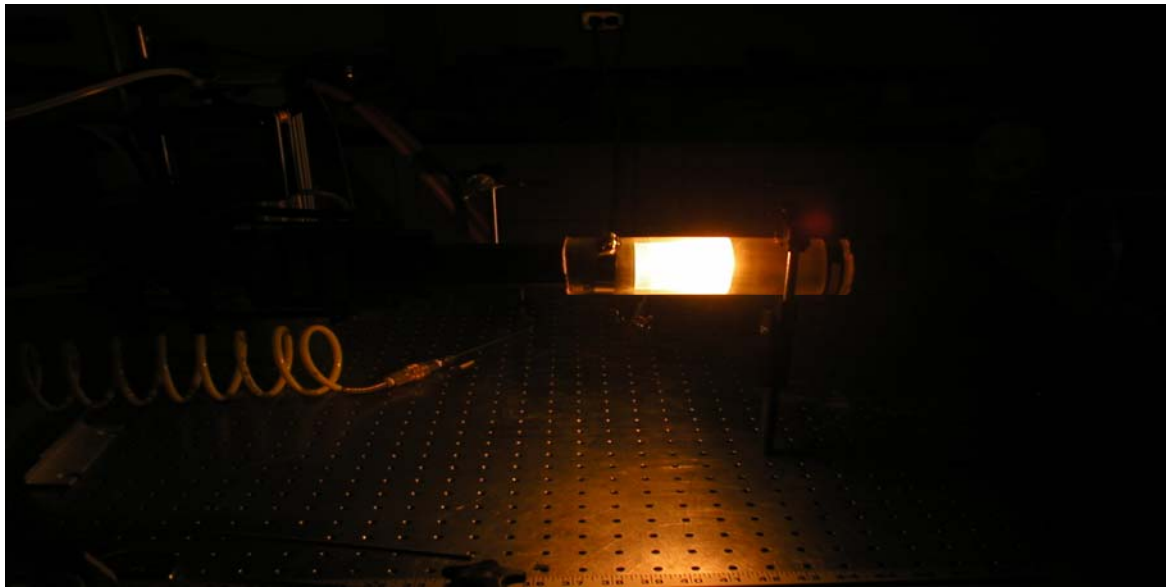


Figure 7. Laser firing during high pressure perforation cell proof-of-concept test.

Once the chamber design was optimized on the transparent plastic tube prototype, a 5.08 cm (2.0 in) ID copper test chamber was assembled. In the Figure 8A, the interior of the chamber is shown with cone and ventilation holes. Figure 8B depicts the exterior view of the chamber with the ventilation holes.

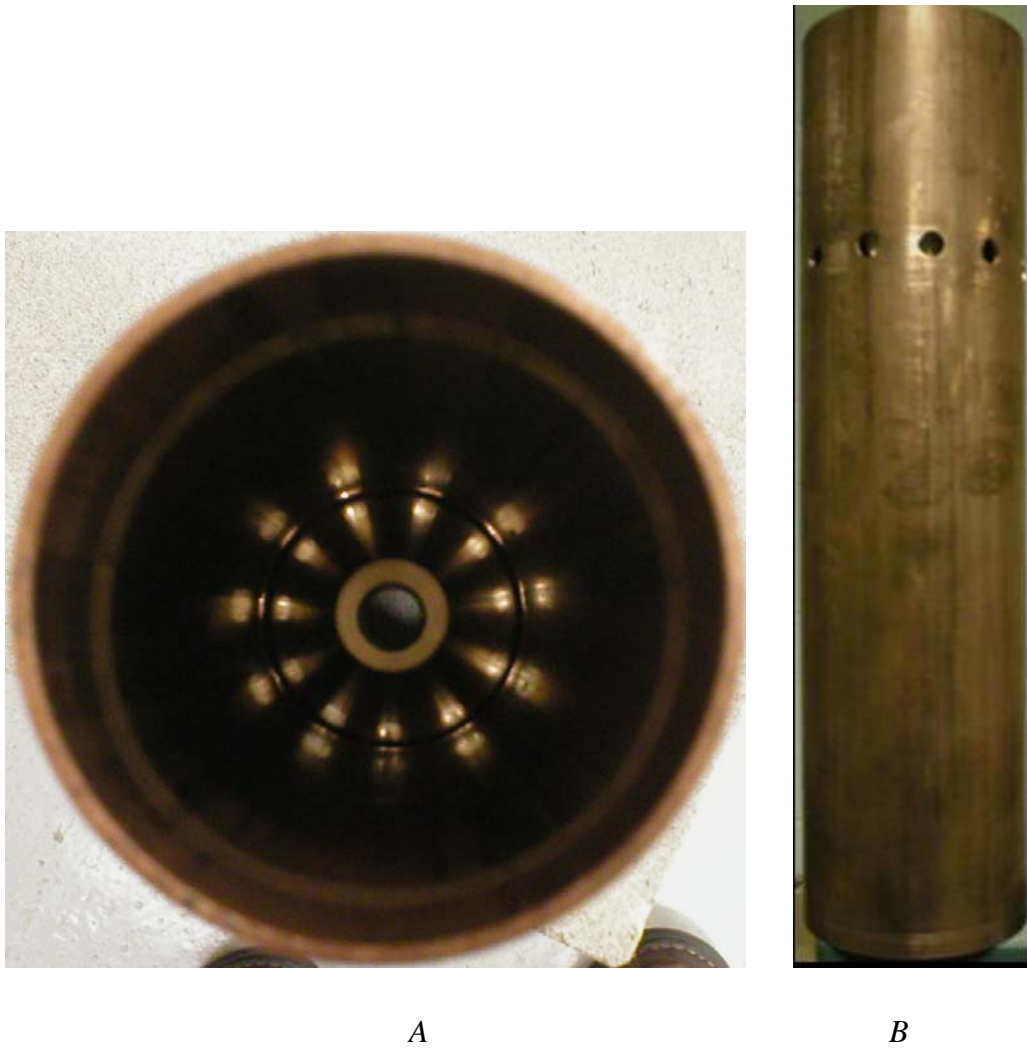


Figure 8. Interior (A) and exterior (B) views of 5.08 cm (2.0 in) ID copper tube mock-up used to test high pressure perforation test cell design.

Figure 9 shows the connection of the chamber tube with the purging system ready for the laser beam, and Figure 10 shows the tube in the dust enclosure before lasing.

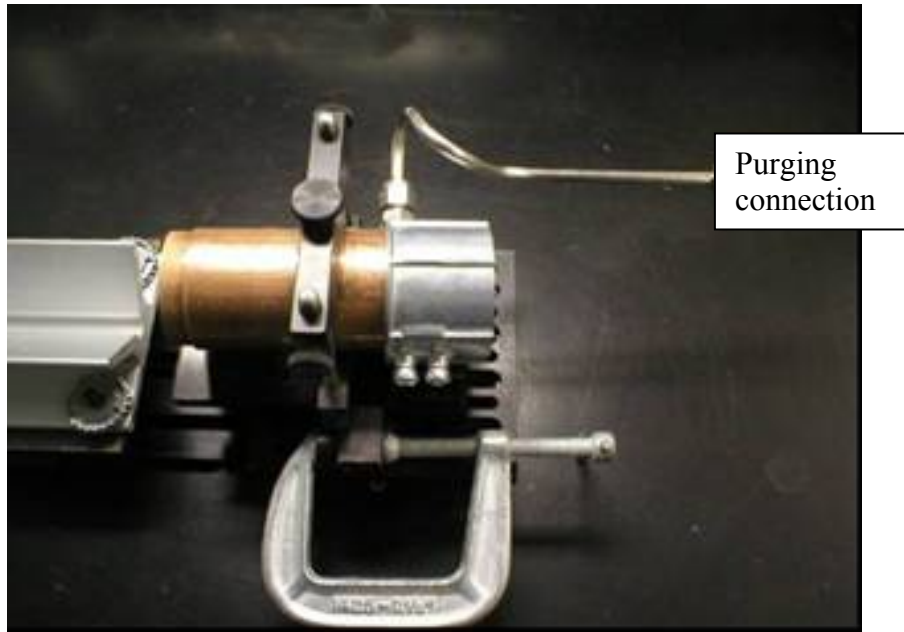


Figure 9. Copper tube mock-up with the purging connection.

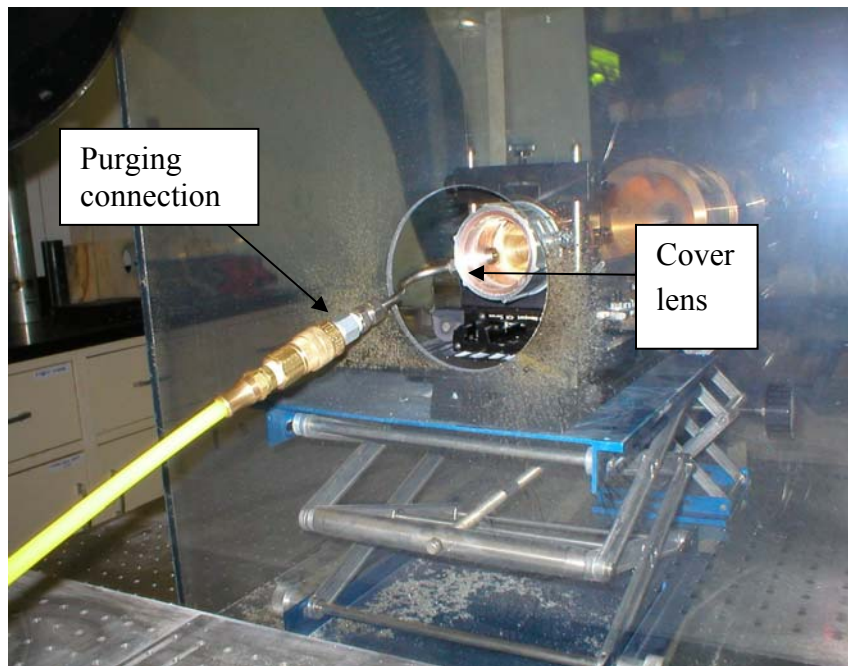


Figure 10. Copper tube mock-up assembly ready for laser application.

An initial concept drawing of the high pressure laser perforation test cell is represented in Figure 11. The design incorporates the elements tested thus far, including optimized purging and ventilation with a cone structure. Additionally, safety chambers have been added with in the event a breach occurs in an optical window. Relief valves were also added for safety.

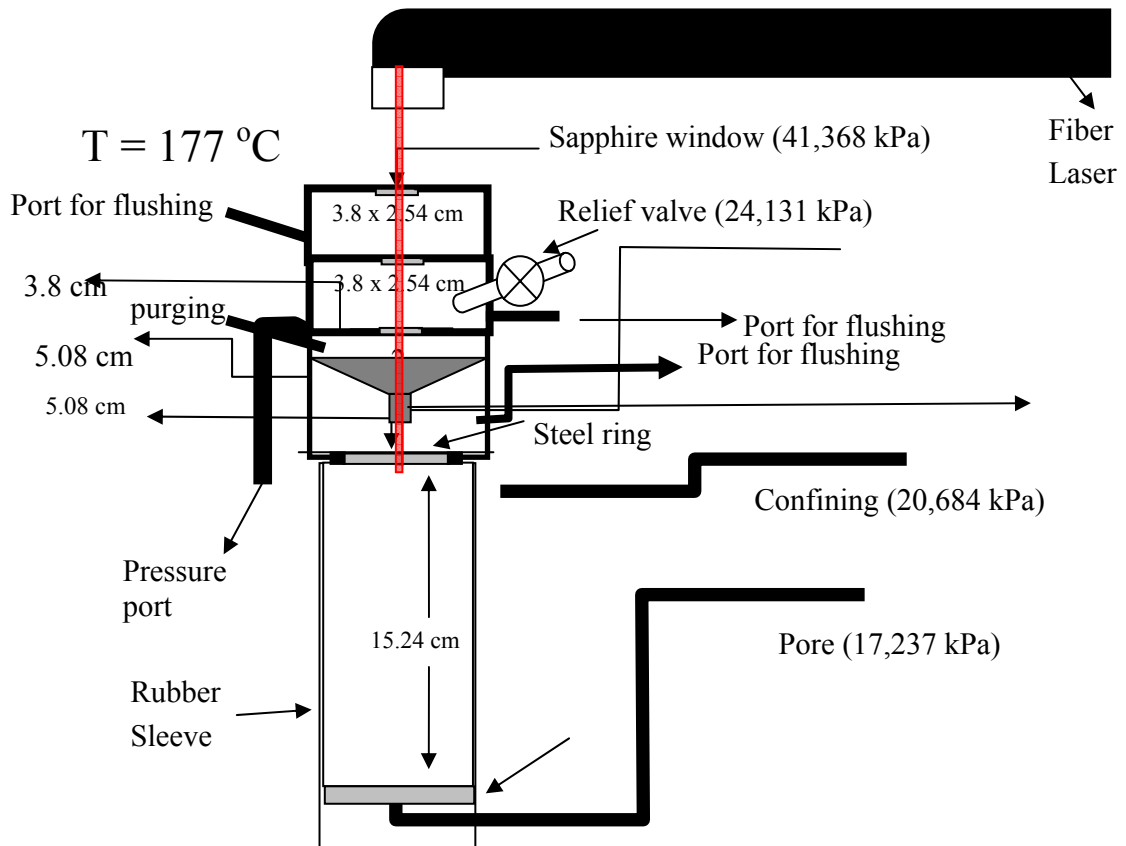


Figure 11. High pressure tri-axial cell concept for laser perforation testing under pressure conditions.

The high pressure laser perforation cell has the flexibility to

11. Perforate in under- or over-balanced conditions up to 20,684 kPa (3000 psig)
12. Apply pore pressure and tri-axial pressure conditions
13. Purge with gas or liquid fluid

14. Test samples up to 10.16 cm (4.0 in) in diameter and 15.24 cm (6.0 in) length

15. Test wellbore simulated samples of rock, cement and steel

Three chambers were designed through which the laser beam is transferred to the target. The chamber closest to the sample incorporates the deflection cone, purging fluid line and exhaust ports for ventilation. The remaining two chambers were designed to contain the system should an optical window fail. A pressure port is available to provide a positive pressure differential for simulating overbalanced conditions. Sapphire optical windows are rated up to 41,368 kPa (6000 psig). Relief valves allow excess pressure to exit the cell.

The final design of the high pressure cell is presented in Figure 12, and the disassembled cell is pictured in Figure 13.

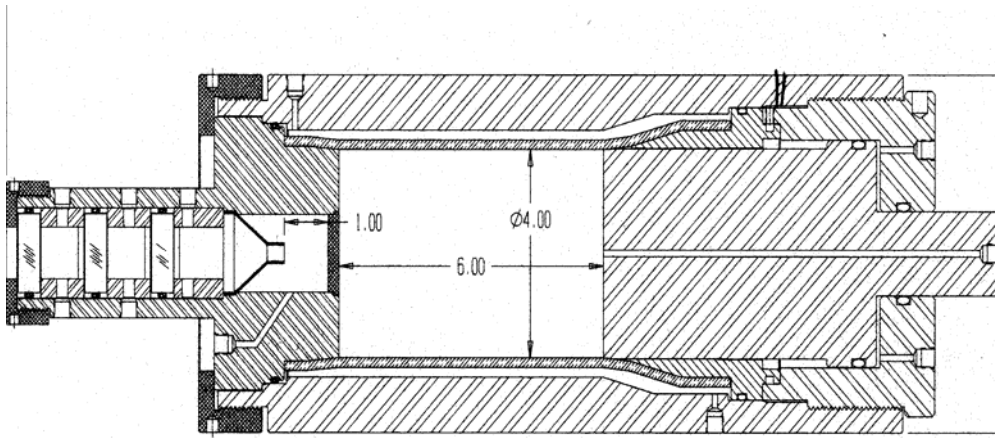


Figure 12. High pressure tri-axial cell design for laser perforation testing under pressure conditions.

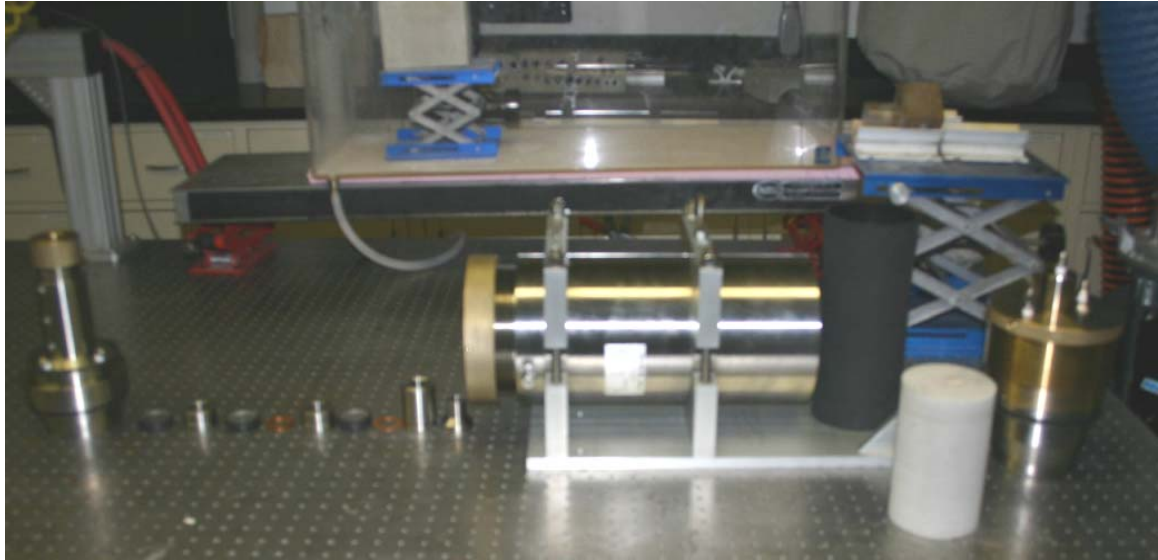


Figure 13. Completed high pressure tri-axial cell for in-situ laser perforation testing.

Perforation of Core Samples under High Pressure Conditions

Objective: To simulate perforation under downhole conditions by applying axial and confining pressures (tri-axial load) on sandstone and limestone core samples.

Procedure: Initial tests were performed on cores of Berea sandstone and Bedford limestone under various conditions of axial, pore and confining pressures. For all cases, the laser settings remained the same. Full output power of 5.34 kW was applied continuously to each sample through the sapphire window of the pressure cell with a focused beam diameter of 0.889 cm (0.35 in) over 8.0 s. The 0.889 cm (0.35 in) diameter beam was previously found to generate no boundary effects with 10.16 cm (4.0 in) diameter core. The amount of laser exposure time was calculated from previous laser rock interactions to allow penetration into the core without risk of penetrating the core's full length and avoiding possible damage to the pressure cell.

Results and Analysis

Five trials were performed on unsaturated samples of each rock type. A base case was established for each rock type by lasing samples in the cell at ambient pressure conditions. A second condition was tested on each rock type with confining and axial stress limited to about 6895 kPa (1000 psig). Since the cores were not charged with pore pressure, a high pressure gas purge of 620.5 kPa (90 psig) through a 0.635 cm (0.25 in) nozzle assisted in particle removal.

A third condition was then tested for each rock type combined confining and axial stress limited to about 6895 kPa (1000 psig), while charging the core to a pore pressure. No gas purge was provided as underbalanced conditions (greater pore pressure than wellbore pressure) served to eject particles from the charged core

through pressure cell exit ports. Two additional trials were performed at balanced and underbalanced conditions with double the pressure settings.

To better understand the in-situ performance of lasers in the presence of reservoir fluids, sandstone and limestone cores were saturated in brine and liquid hydrocarbon prior to high pressure lasing. Pressure conditions for each rock type included confining and axial stress limited to about 6895 kPa (1000 psig) with no pore pressure.

Figure 14 shows the experimental set up and Figure 15 shows the high pressure cell during the experiment.

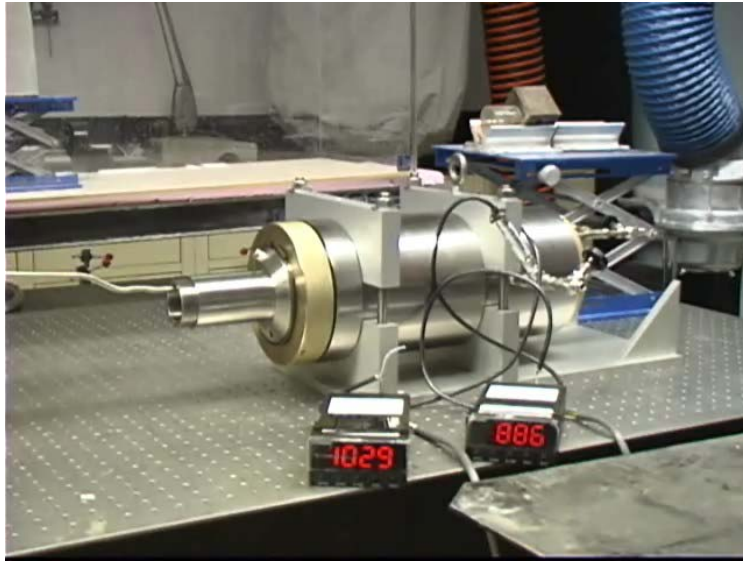


Figure 14. Experimental set up for perforation test in high pressure cell

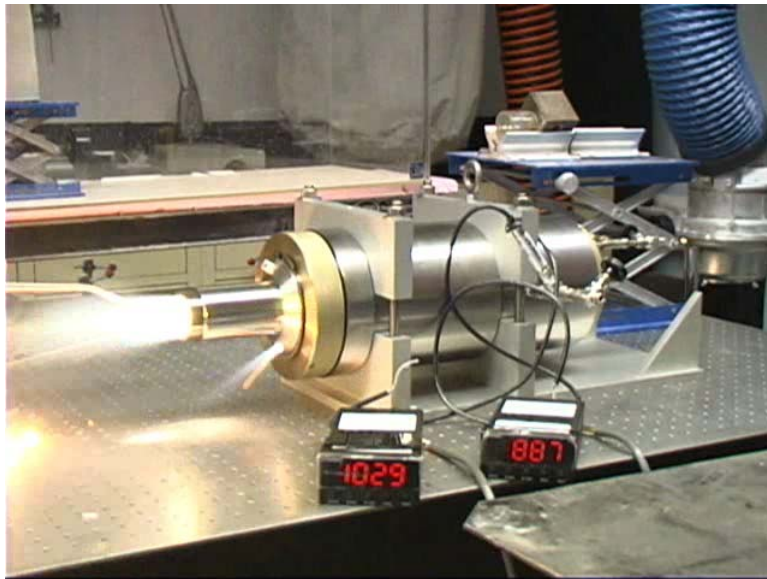


Figure 15. Perforation test in progress.

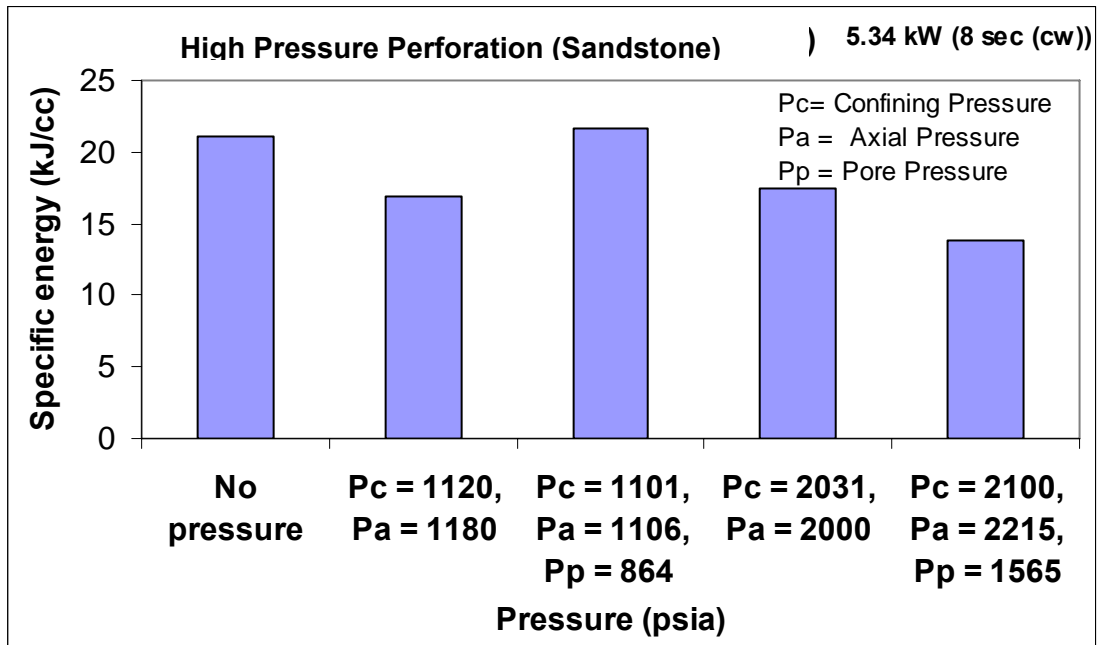


Figure 16. Comparison of SE values in sandstone as observed at various test cell pressure conditions.

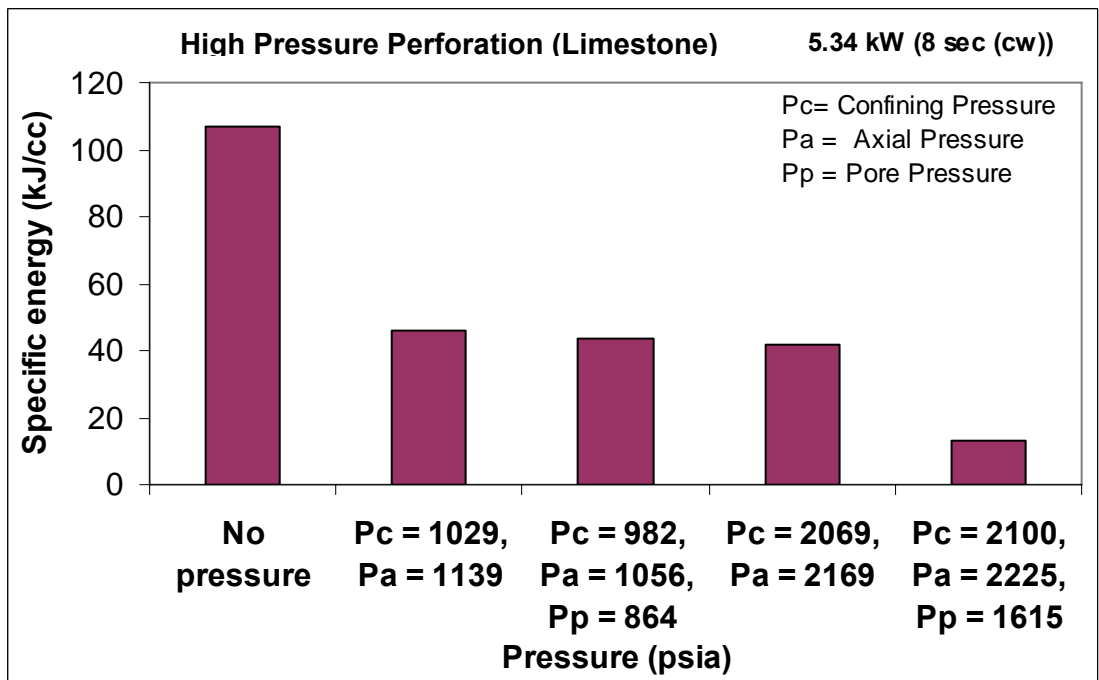


Figure 17. Comparison of SE values in limestone as observed at various test cell pressure conditions.

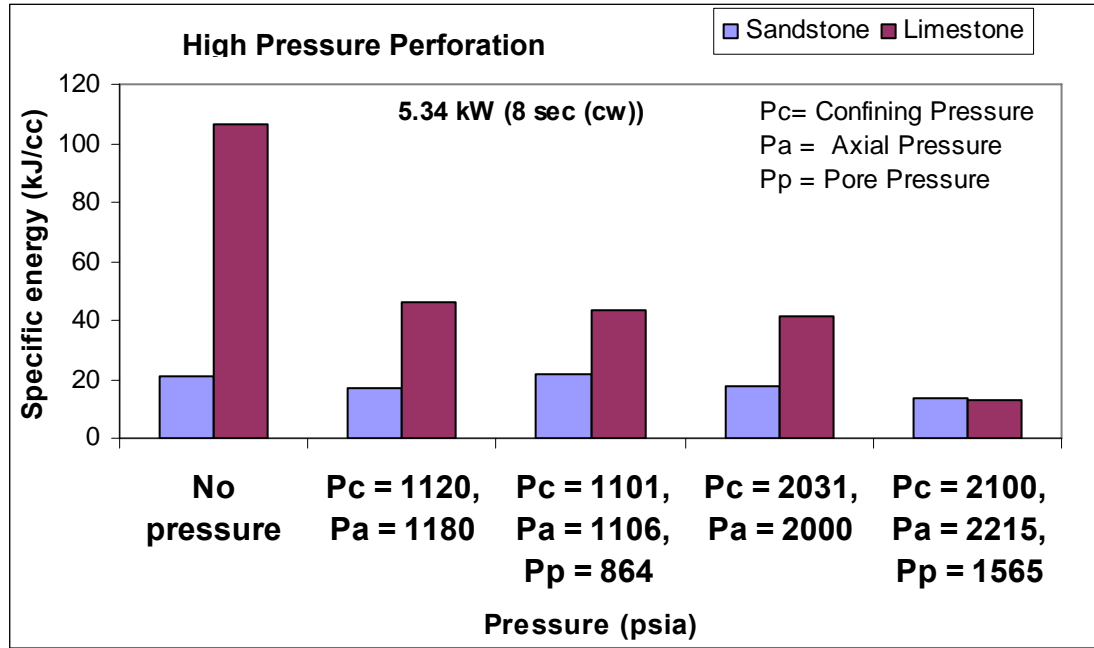


Figure 18. Comparison of SE values in limestone and sandstone as observed at various test cell pressure conditions.

The resulting data generated from the series of sample trials on sandstone and limestone have demonstrated that a laser perforation system will significantly benefit from the high pressure conditions encountered downhole. For both rock types, SE values decreased as confining and axial stresses increased. The effect was more apparent in the limestone than in the sandstone samples. Results from the sandstone and limestone core tests are presented in Figures 16, 17, and 18. Tabular results are presented in Appendix A.

Sandstone. The removal mechanism for Berea sandstone is spallation, where rapid differential thermal expansion causes grains and cementitious material to fracture. The base case for sandstone with no pressure had an SE value of 19.75 kJ/cc. The conditions are similar in many respects to much of the previous work performed in the lab. The sample is at ambient conditions during lasing and a gas purge nozzle assists in removing broken material.

The lowest SE value observed in sandstone was 12.91 kJ/cc, a 35% reduction from the base case, resulting from the highest pressure values tested. Material removal was assisted with the differential between the pore pressure and wellbore chamber pressure. As this differential increases, material is more rapidly ejected from the tunnel, thus minimizing travel through the cutting beam and absorbing less beam energy after detaching from the rock matrix. With less beam energy

absorbed by exiting particles, more is available for cutting, as evidenced by the drop in SE value.

At the pressures tested, confining and axial stress had a limited impact on SE values for sandstone. The stresses imparted on the sandstone matrix create tighter grain-to-grain contact and improved the thermal diffusivity of the rock. In both cases, material is purged with an assist gas with the same conditions for each trial.

Limestone. The removal mechanism for limestone is calcination where the energy of the laser beam causes a thermal dissociation of carbonates into carbon dioxide and calcium oxide (lime). Just as axial and confining stress compressed the sandstone, the effect was more evident in the limestone samples. This quarry limestone was originally unstressed, contributing to an SE drop of at least 60 percent due to closer grain-to-grain contact and a more efficient calcination process.

The lowest SE value observed in limestone was at the highest pressure and stress conditions. Again, the differential pressure assisting in material removal was evident with a significantly lowered SE of 12.27 kJ/cc, 88% lower than the base case.

The application of stress to the rock core allows the grains within the rock matrix to move closer to each other as the pore volume decreases. Failure of the rock can occur when the applied stress exceeds the strength of the rock. This failure was observed in the quarry limestone cores as they developed fractures along their length. Figure 19 shows a fracture that developed in a limestone test core when 15,272 kPa (2215 psig) stress was applied. Stress fractures were not evident in a similarly stressed sandstone sample in Figure 20. The strength properties of the sandstone were greater than the applied stress.

The sandstone core samples consist of grains bound by cementation, and have higher values of porosity and permeability than the limestone core samples (Figure 21). When a high power laser beam interacts with a core sample, heat transfer takes place from grain-to-grain by the more direct method of conduction, and across the void space by convection as seen in Figure 22. By applying stress to the limestone sample, more grains are in contact with one another, the void space is reduced, and heat is more efficiently transferred by conduction. This is evident in the data presented in Figure 17, as SE is substantially reduced from the base case under ambient conditions to each case under stressed conditions.

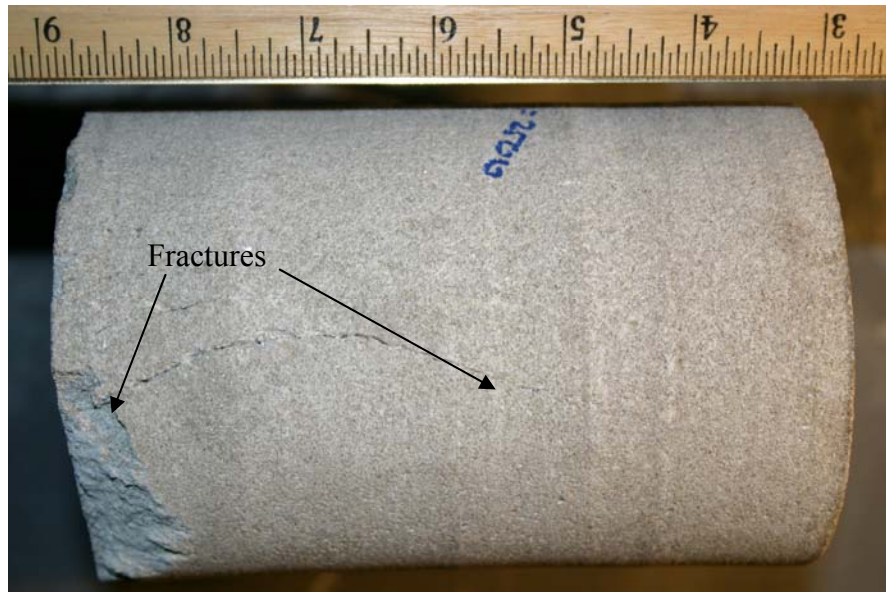


Figure 19. Post-high pressure perforation test of limestone exhibiting stress fractures

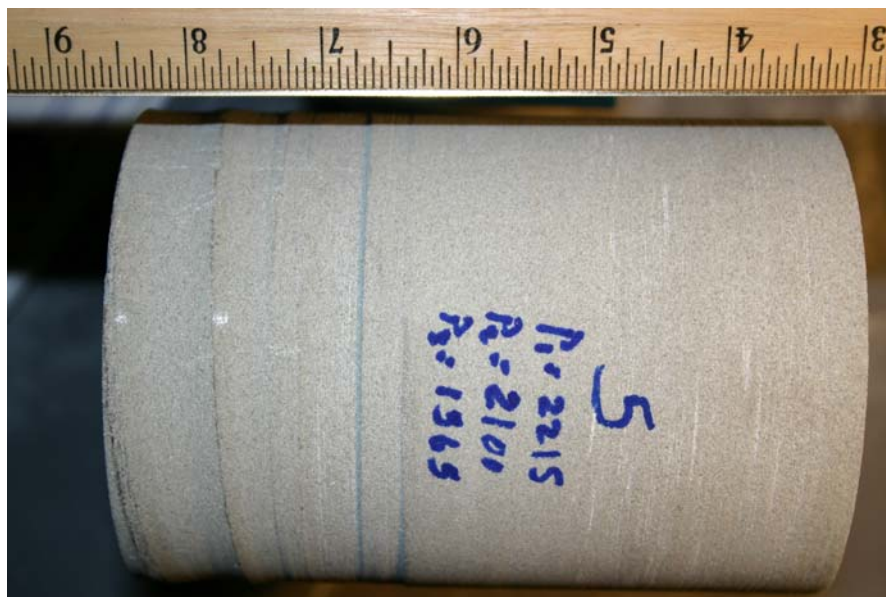


Figure 20. Sandstone samples show no post-test stress fractures.

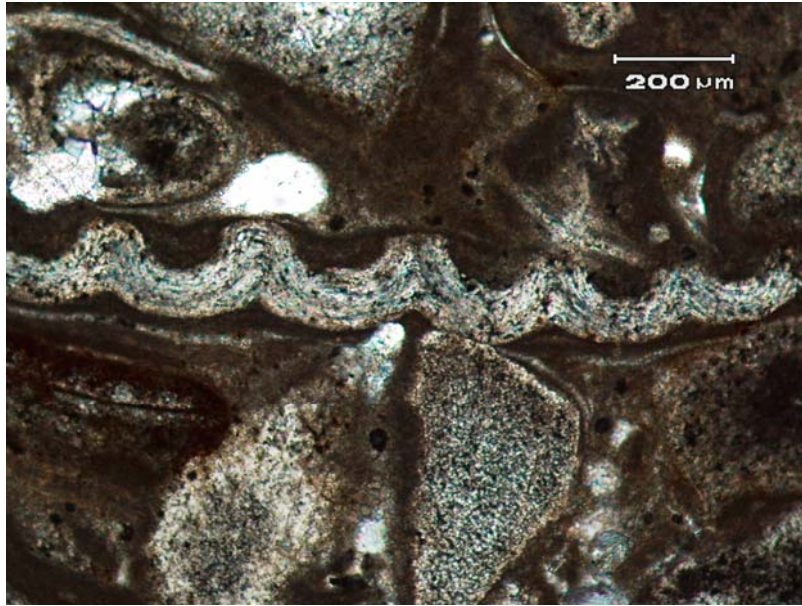


Figure 21. Thin section analysis from limestone used in perforation tests show low porosity and permeability with close grain contact.

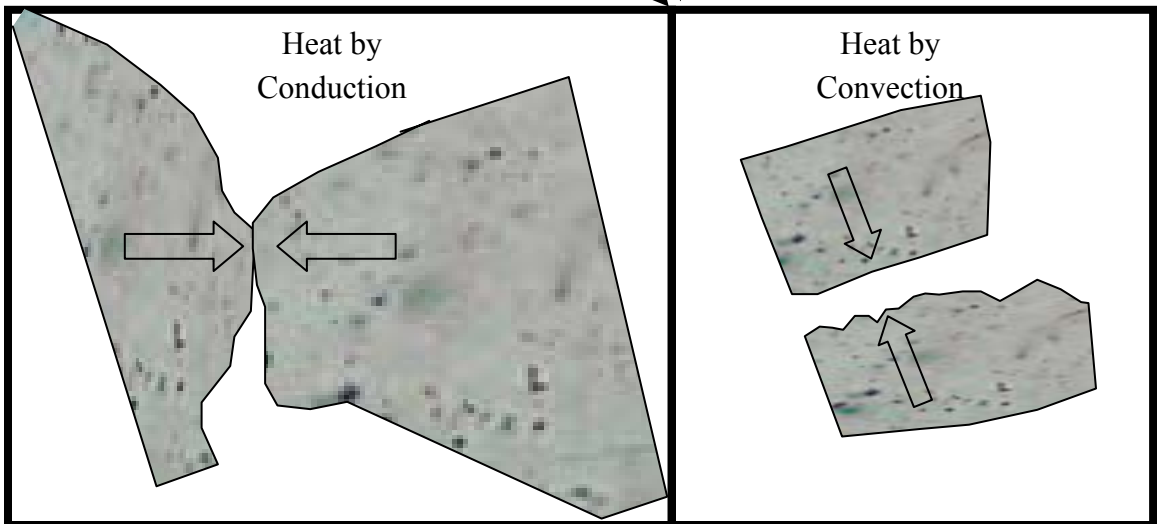
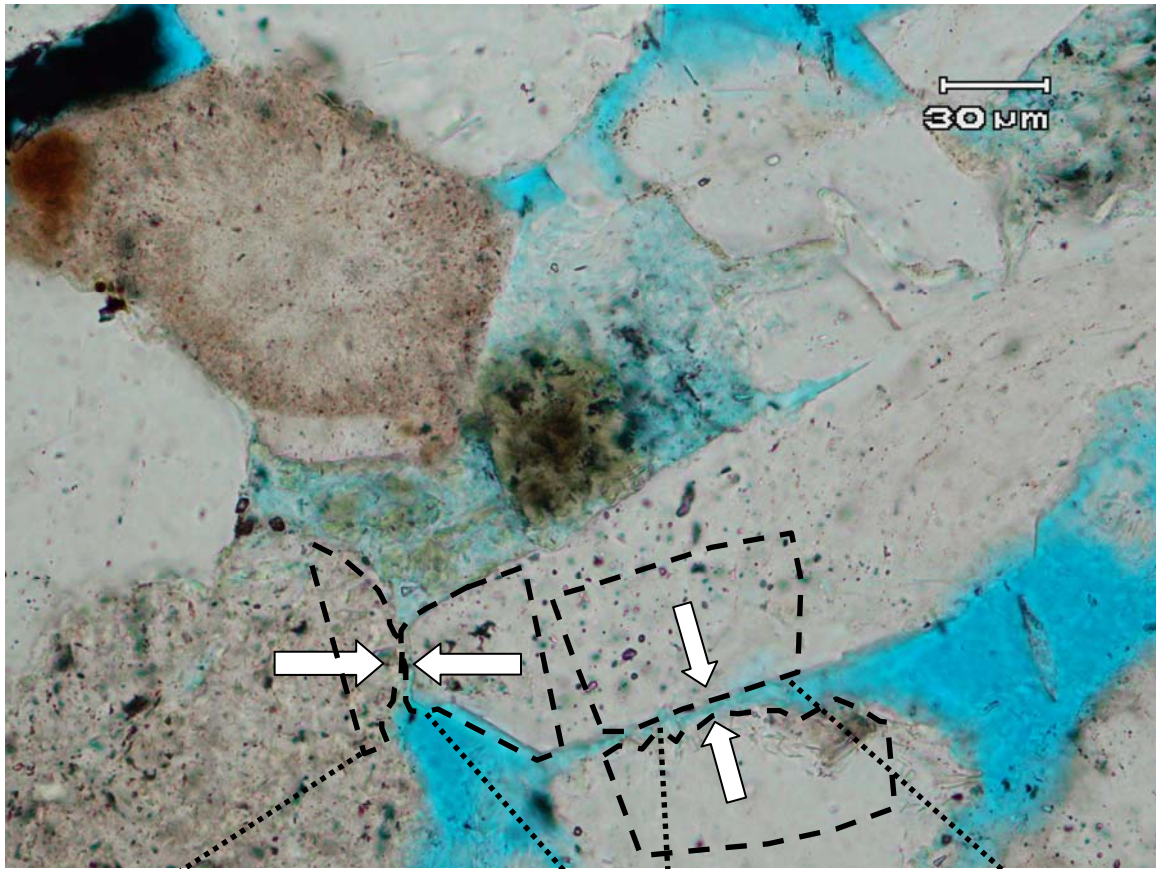


Figure 22. Heat transfer in sandstone by conduction (solid to solid) and convection (solid to air).

Perforation of Saturated Core Samples under High Pressure

Conditions

Objective: To simulate perforation under downhole conditions by applying axial and confining pressures (tri-axial load) on sandstone and limestone saturated core samples.

Procedure: Sandstone and limestone cores 10.16 cm (4.0 in) diameter and 15.24 cm (6.0 in) length were placed in a vacuum environment for about 6.0 hrs and then saturated with brine solution or oil for at least 24 hrs.

The composition of the brine was a mixture of 25,000 ppm potassium chloride (KCl) and 25,000 ppm sodium chloride (NaCl) in 1,000 ml of water. The density of the brine was 1.039 g/cm³. The oil used in testing had a density of 0.841 g/cm³.

Each saturated sample was placed in the high pressure cell and was pressurized for confining and axial pressures to approximately 13,790 kPa (2000 psig). Each saturated sample was lased for 8.0 s with 5.34 kW laser power. Spot size was kept constant at 0.889 cm (0.35 in). Pore pressure was not applied to the saturated samples.

Results for both the rock types are shown in Figures 23 and 24 with previous data from unsaturated samples to compare SE values. Tabular results are presented in Appendix A.

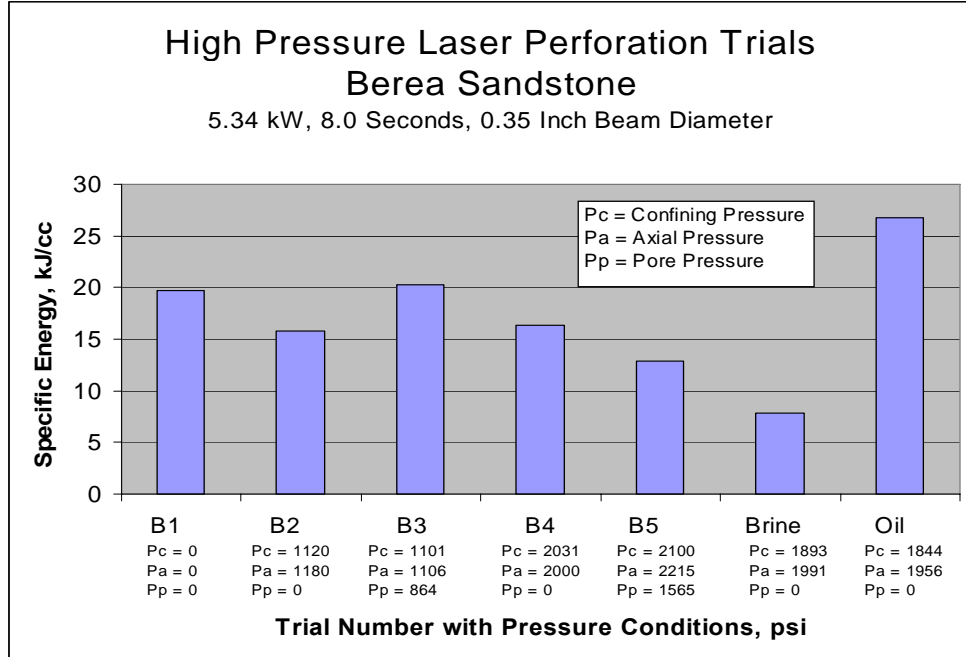


Figure 23. Comparison of SE values in sandstone as observed at various test cell pressure conditions, including brine and oil saturated samples.

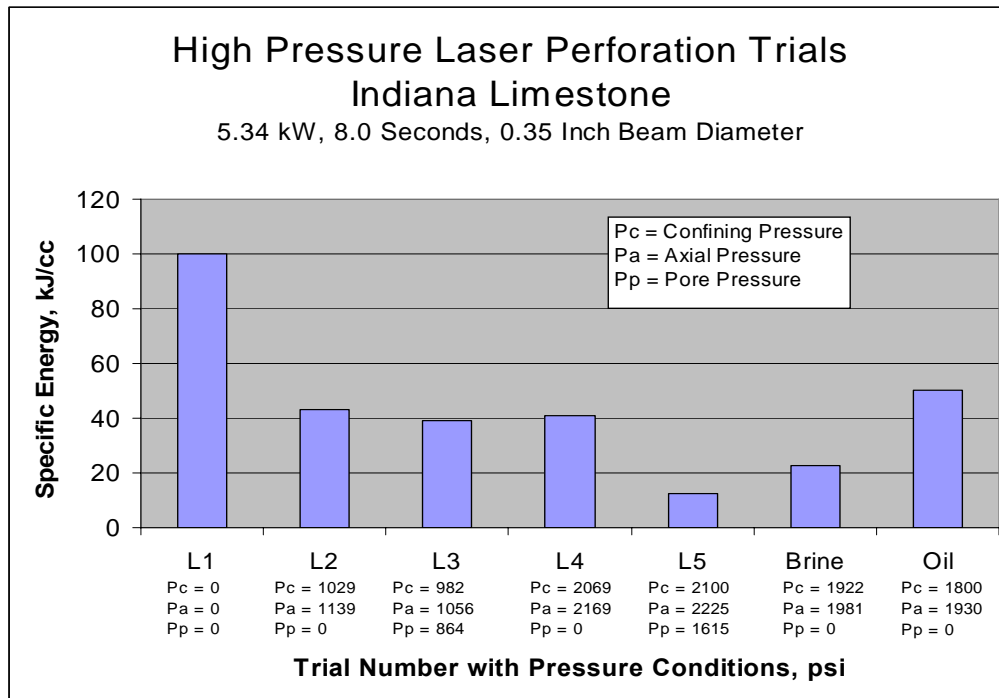


Figure 24. Comparison of SE values in limestone as observed at various test cell pressure conditions, including brine and oil saturated samples.

Results and Analysis:

The effect of liquid saturation on the rock samples gave us an indication as to how their presence in the reservoir may affect the laser's ability to create a perforation. Regarding brine, sandstone received an added boost in efficiency with an SE of 7.84 kJ/cc. This is 60% lower than the base case (B1), and 50% lower than the best stressed case (B2). Rapid vaporization of the brine is suspected to provide assistance in the spallation process, as has been previously observed with water saturated sandstone samples. The limestone also exhibited some improvement with an SE of 22.78 kJ/cc, a 77% reduction from the base case (L1), and a 42% reduction from the best stressed case (L3).

The presence of a hydrocarbon in sandstone raised the SE to 26.76 kJ/cc. This is a 35% increase in energy required from the base case (B1), and a 63% increase from a similar unsaturated case (B4). This effect may be a result of the hydrocarbon and its byproducts absorbing more beam energy than is provided by rapid vaporization in the pores. A similar result was observed in limestone, although not as pronounced. The observed SE in the oil saturated limestone sample was 50.36 kJ/cc, about 50% lower than the base case (L1) SE, and 24 % higher than the similar unsaturated case (L4).

As explained previously, the stress because grains to get closer there for more heat transfer. In figure 23 and 24 the graphs show sandstone and limestone under confined, axial and saturation conditions.

The figure shows that sample saturated with oil present the high SE value. Then lasing with oil saturation, the oil consumes energy to heat up and the vapor and the product of lasing is like a dark cloud with blocks the beam from reaching the sample. In the case of brine, the water evaporates and the sample path gets clear for the beam.

For limestone the same trend was observed where the Oil saturated sample shows more SE than the brine, but for limestone the SE value oil is still less than dry with no stress because there void space is very small in limestone, therefore the amount of the oil injected in the sample is very small or even insignificant.

Perforation of Composite Core Samples under High Pressure Conditions

Objective: To estimate the perforation depth for composite samples under tri-axial pressure condition and simulate the perforation of a completed wellbore under in-situ pressure conditions.

Procedure: The design of the composite material sample for high pressure perforation was to allow the laser to penetrate materials as they would be encountered in a completed wellbore as depicted in Figure 25. Specific concerns

were addressed in the design of the composite cores, given the thermal conductivity of the materials involved. With any exposure of the beam on steel, we could expect that thermal energy would rapidly rise evenly throughout the steel sample. Should this occur, the confining pressure sleeve would likely melt at any point where it came into contact with the hot steel. The system would be unable to maintain stress and pressure on the core, as well as potential safety concerns.

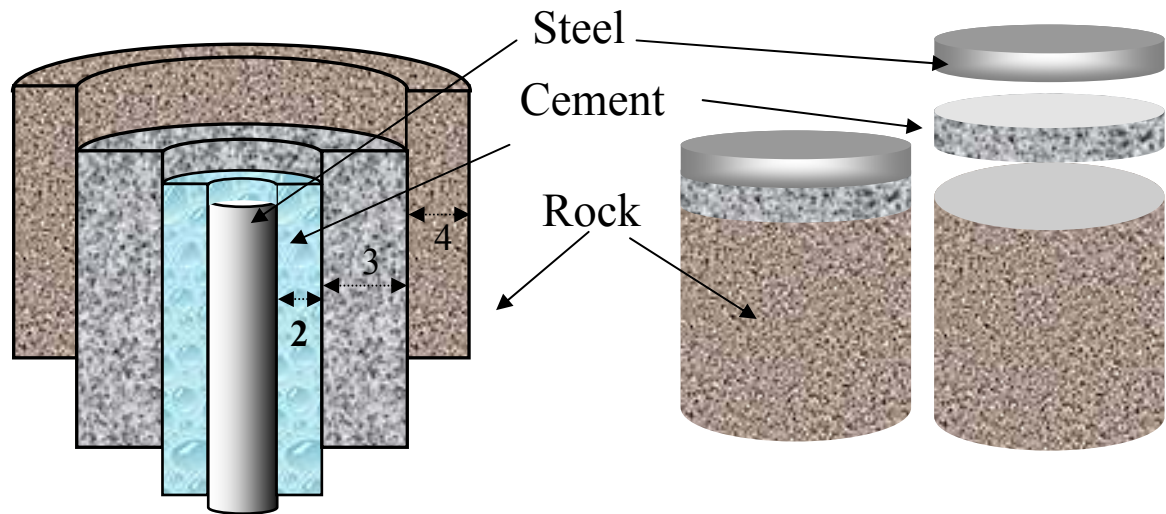


Figure 25. Composite core samples were to simulate physical conditions of a competed wellbore.

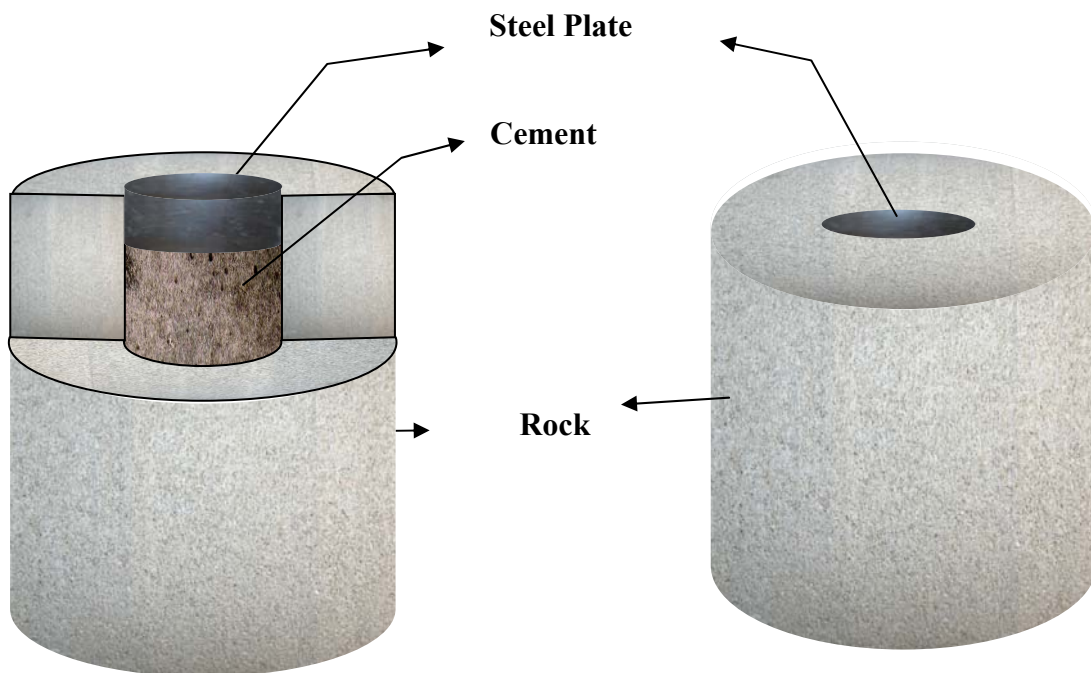


Figure 26. Composite sample as prepared for the high pressure cell, illustrating modified design to avoid melting of core sleeve.

Composite samples of steel, cement and rock were prepared by cementing in place a 5.08 cm (2.0 in) diameter by 1.27 cm (0.5 in) thick steel plate. By using a smaller steel diameter inset, the rubber pressure sleeve jacketing the sample core would not be at risk of melting through direct contact with a full diameter steel plate.

After observing the laser/rock interactions of sandstone and limestone under high pressure conditions and the resulting SE values, in-situ demonstrations were then executed to best simulate downhole conditions and material encountered during laser perforation.

The sandstone and limestone clad samples were exposed to the same laser beam conditions as performed under previous high pressure trials. For the sandstone sample, axial and confining pressures were measured at 14,479 and 13996 kPa (2100 and 2030 psig), respectively. Axial and confining pressures for the limestone sample were measured at 14,300 and 13,555 kPa (2074 and 1966 psig), respectively.

Total time of beam exposure was 90 s per composite sample. The time was calculated based on earlier laser exposure times to remove a unit volume of steel, cement and rock materials. The laser fired for thirty second intervals buffered with 20 s between shots as a precaution to avoid overheating the cell assembly. Before and after lasing images of the limestone clad sample are shown in Figure 28.

As a result of the high pressure clad sample trials, the laser penetrated about 6.35 cm (2.5 in) into the sandstone clad sample, or 1.27 cm (0.5 in) beyond the steel and cement. The laser penetrated 11.43 cm (4.5 in) into the limestone clad sample, or 6.35 cm (2.5 in) beyond the steel and cement. An X-ray CT scan image of the limestone clad sample is shown in Figure 27.

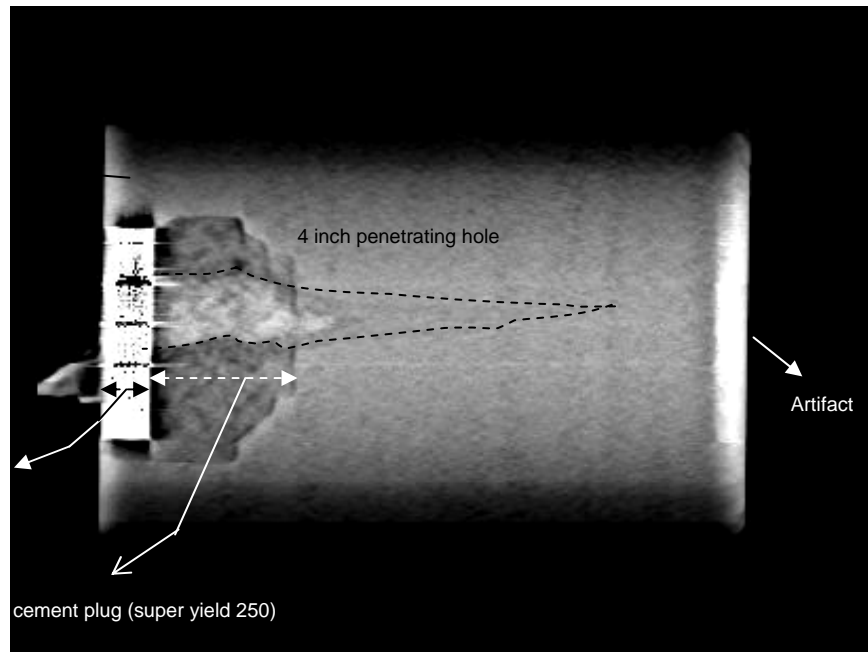


Figure 27. CT scan image of 10.16 cm (4.0 in) diameter by 15.24 cm (6.0 in) length limestone clad sample and outline of penetration path after perforation of three 30 s shots by 5.34 kW ytterbium fiber laser with a 0.889 cm (0.35 in) diameter beam.



Figure 28. Pre- and post-laser images of 10.16 cm (4.0 in) diameter by 15.24 cm (6.0 in) length limestone core inset with 5.08 cm (2.0 in) diameter by 1.27 cm (0.5 in) thick steel plate.

Conclusion

The recent commercial introduction of high-power fiber lasers represented a significant step forward in realizing field-based applications of photonic energy for well construction and completion. Fiber lasers meet the multiple demands from industry regarding a field deployable system, including overall size limitations, mobile rugged on-site deployment, requisite energy delivery to target, real-time controllability and penetration of multiple materials. From an economic perspective, the order of magnitude improvement in efficiency significantly lowers input energy and waste heat dissipation requirements. They also require minimal maintenance and repair, and are commercially available.

High power laser applications for cutting and boring rocks have been successfully demonstrated under ambient pressure conditions; however, this is the first time samples have been lased at in-situ pressure conditions. Research results demonstrated the beneficial effect of stress and pressure on the laser's ability to perforate reservoir rock. Additionally, we were able to demonstrate the capability of a single wavelength laser to penetrate a combination of steel, cement and rock at in-situ pressures that would be encountered while perforating downhole.

Operating the laser in underbalanced conditions demonstrated the ability of the laser to perform at downhole conditions without requiring a supplemental assist purge system. The differential pressure between the reservoir pore pressure and the wellbore pressure provided the means for ejecting the cuttings.

Operating the laser on rock under axial and confining stress improves the conditions for laser perforation due to a closer grain-to-grain contact and resulting improvement to thermal diffusivity. This extends the influence of the beam energy further into the rock.

References

27. DeGolyer and MacNaughton, One Energy Square, Dallas, Texas, 2000.
28. Andersen, et al, "Deep Drilling Basic Research: Volume 2 - Deep Drilling," GRI 90/0265.2, June 1990, 78p.
29. W.C. Maurer, Novel Drilling Techniques, Pergamon Press, 1968.
30. W.C. Maurer, Advanced Drilling Techniques, Petroleum Publishing, 1980.
31. W.T. Silfvast, Laser Fundamentals, Cambridge, 1996.
32. W.H. Somerton, Thermal Properties and Temperature-related Behavior of Rock/Fluid System. University of California, Development in Petroleum Science. Elsevier, Amsterdam-London-New York-Tokyo, 1992.
33. R.M. Graves and D.G. O'Brien, "Star Wars Laser Technology Applied to Drilling and Completing Gas wells," SPE 49259, 1998.

Publications

Publications by GTI staff from October 2004 to September 2005:

24. Gahan, B.C. "Processing Rocks," Industrial Laser Solutions, Sept.(2005):16-18.
25. Gahan, B.C. "Fiber Laser Offers Fast Track to Clean Perforations" GTI Document No. GTI-05/0226, *GasTIPS*, 11, No. 2 (Spring 2005), pp. 17-20.
26. Gahan, B.C., Batarseh, S. 2004. "An Overview of High Power Laser Applications Research from Well Construction and Completion," 2004 International Gas Research Conference (IGRC), Vancouver, BC, November 1-4.
27. Batarseh, S., Gahan, B.C., Sharma, B., Gowelly, S. 2004. "Evaluation of High Power Ytterbium Fiber Lasers for Rock Cutting and Removal Applications," Paper 1402, 23rd International Congress on Applications of Lasers and Electronics, San Francisco, CA, October 4-7.

Presentations

Presentations delivered from October 2004 to September 2005:

High Power Laser Applications for Well Drilling and Completions
Innovations in Exploration Drilling, Memorial University of Newfoundland
St. Johns, NL, Canada, August 23, 2005 (invitation)

Improving Gas Well Drilling and Completion with High Energy Lasers
American Petroleum Institute, Delta Chapter
New Orleans, LA, August 17, 2005 (invitation)

Improving Gas Well Drilling and Completion with High Energy Lasers
American Institute of Chemical Engineers (AIChE), Chicago Section
Chicago, IL, March 9, 2005 (invitation)

Improving Gas Well Drilling and Completion with High Energy Lasers
International Coiled Tubing Association (ICoTA), Gulf Coast Section
Houston, TX, February 8, 2005 (invitation)

An Overview of High Power Laser Applications Research from Well Construction and Completion
2004 International Gas Research Conference (IGRC)
Vancouver, BC, Canada, November 2, 2004

Evaluation of High Power Ytterbium Fiber Lasers for Rock Cutting and Removal Applications
23rd International Congress on Applications of Lasers and Electronics
San Francisco, CA, October 4-7, 2004

List of Acronyms and Abbreviations

C	= Celsius/centigrade
cc	= cubic centimeter
CO ₂	= carbon dioxide
CW	= continuous wave
DP	= diode-pumped
DTA	= differential thermal analysis
E _{abs}	= absorbed energy
E _{inc}	= incident electromagnetic wave
E _{ref}	= reflected energy
E _{sc}	= scattered energy
EDS	= energy dispersive system
E/O	= electrical to optical
F	= Fahrenheit
g	= gram
J	= joule
HPFL	= high power fiber laser
ID	= inside diameter
LP	= lamp-pumped
m	= meter
md	= millidarcy (Permeability Unit)
Nd:YAG	= neodymium-doped yttrium aluminum garnet (Nd:Y ₃ Al ₅ O ₁₂)
P _a	= Axial pressure
P _c	= Confining pressure
P _p	= Pore pressure
Pa	= Pascal
PDPK	= pressure decay profile permeameter
ppm	= parts per million
psig	= pounds per square inch gauge
s	= seconds
SE	= specific energy
SEM	= scanning electron microscope
W	= watt
x ,X	= times

XRD = x-ray diffraction

λ = wavelength

Appendix A: Experimental Data

Experiment: High Pressure Perforation**Material: limestone****Laser power: 5.34 kW****Lasing time: 8 s****Spot size: 0.889 cm (0.35 in)**

Name	Conf. Pressure (psia)	Axial Pressure (psia)	Pore Pressure (psia)	Core dia. (cm)	Core length (cm)	Weight before lasing (gm)	Weight after lasing (gm)	Weight removed (gm)	Density (gm/cc)	Volume removed (cc)	Specific energy (kJ/cc)
1	0	-	-	10.11	13.80	2489.60	2488.70	0.90	2.25	0.40	106.77
2	1029	1139	-	10.11	15.39	2785.80	2783.70	2.10	2.26	0.93	45.92
3	2069	2169		10.11	15.56	2793.40	2791.20	2.20	2.24	0.98	43.43
4	982	1056	864	10.11	15.62	2814.80	2812.50	2.30	2.24	1.02	41.69
5	2100	2225	1625	10.11	15.34	2731.20	2723.90	7.30	2.24	3.26	13.11
Saturated-Brine	1922	1981	-	10.11	15.34	2987.20	2983.00	4.20	2.24	1.87	22.78
Saturated-Oil	1800	1930	-	10.11	15.34	2850.80	2848.90	1.90	2.24	0.85	50.36

Conditions Tested:

Bi axial load

Tri axial load

Perforation of saturated sample (brine, oil)

Experiment: High Pressure Perforation

Material: sandstone

Laser power: 5.34 kW

Lasing time: 8 s

Spot size: 0.889 cm (0.35 in)

Name	Conf. Pressure (psia)	Axial Pressure (psia)	Pore Pressure (psia)	Core dia. (cm)	Core length (cm)	Weight before lasing (gm)	Weight after lasing (gm)	Weight removed (gm)	Density (gm/cc)	Volume removed (cc)	Specific energy (kJ/cc)
1	-	-	-	10.11	15.19	2589.30	2585.00	4.30	2.12	2.03	21.09
2	1120	1180		10.12	15.39	2638.60	2633.20	5.40	2.13	2.53	16.88
3	1101	1106	864	10.10	15.34	2622.00	2617.80	4.20	2.13	1.97	21.69
4	2031	2000		10.11	15.34	2616.90	2611.70	5.20	2.13	2.44	17.50
5	2100	2215	1565	10.11	15.34	2437.00	2430.40	6.60	2.13	3.10	13.79
Saturated-Brine	1893	1991	-	10.11	15.34	2866.30	2854.70	11.60	2.13	5.45	7.84
Saturated-Oil	1844	1956	-	10.11	15.34	2776.60	2773.20	3.40	2.13	1.60	26.76

Conditions Tested:

Bi axial load

Tri axial load

Perforation of saturated sample (brine, oil)

Experiment: High Pressure Perforation (sandstone composite)

- Perforation of composite samples: 10.16 cm (4.0 in) diameter x 15.24 cm (6.0 in) length sandstone core
Inset thickness: 1.27 cm (0.5 in) steel plate; 3.81 cm (1.5 in) SY 250 cement

Spot size: 0.889 cm (0.35 in)

Name	Conf. Pressure (psia)	Axial Pressure (psia)	Pore Pressure (psia)	Core dia. (cm)	Core length (cm)	Lasing time (sec)	Depth of penetration (inch)
1	2030	2100	-	10.1	15.2	90 (On time) (30 sec on/20 sec off)	2.5

Experiment: High Pressure Perforation (limestone composite)

- Perforation of composite samples: 10.16 cm (4.0 in) diameter x 15.24 cm (6.0 in) length limestone core
Inset thickness: 1.27 cm (0.5 in) steel plate; 3.81 cm (1.5 in) SY 250 cement

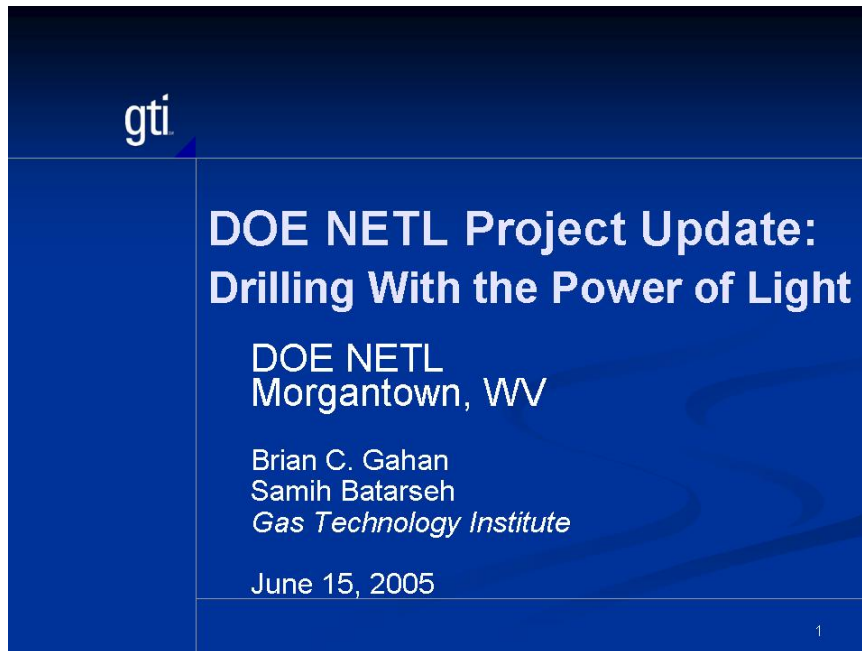
Spot size: 0.35”

Name	Conf. Pressure (psia)	Axial Pressure (psia)	Pore Pressure (psia)	Core dia. (cm)	Core length (cm)	Lasing time (sec)	Depth of penetration (inch)
1	1966	2074	-	10.15	15.2	90 (On time) (30 sec on/20 sec off)	4.5

Appendix B: DOE Project Review Presentation

June 15, 2005
Morgantown, WV

Slide 1



gti

DOE NETL Project Update: Drilling With the Power of Light


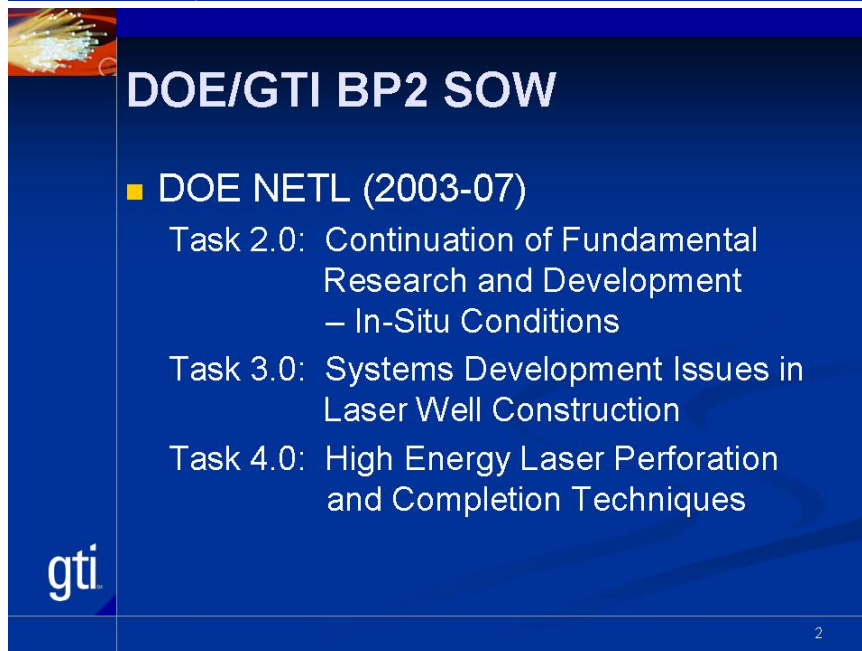
DOE NETL
Morgantown, WV

Brian C. Gahan
Samih Batarseh
Gas Technology Institute

June 15, 2005

1

Slide 2



DOE/GTI BP2 SOW

- DOE NETL (2003-07)
 - Task 2.0: Continuation of Fundamental Research and Development – In-Situ Conditions
 - Task 3.0: Systems Development Issues in Laser Well Construction
 - Task 4.0: High Energy Laser Perforation and Completion Techniques

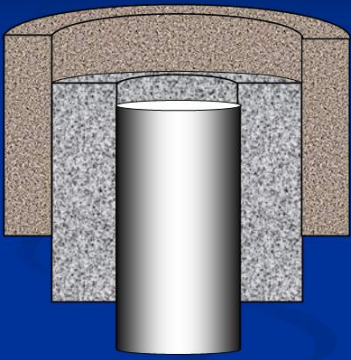
gti

2

Slide 3

Downhole Laser Applications

- Drilling
- Perforating
- Seismic Shot Holes
- Casing Cutting/ Abandonment
- Offshore Platform Abandonment
- Casing "Windows" for Multi-Laterals
- Downhole Slotted Liners/Screens



The diagram shows a cross-section of a wellbore with a central metal pipe. A laser toolstring is positioned inside the pipe, extending from the top. The toolstring is shown as a series of connected segments, with a red line indicating the laser path. The wellbore is surrounded by a casing and a cement sheath.

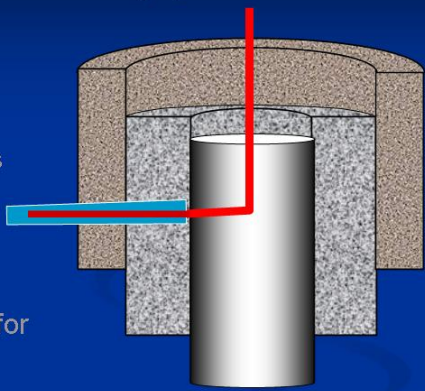
gti

3

Slide 4

Downhole Laser Applications

- Drilling
- **Perforating**
- Seismic Shot Holes
- Casing Cutting/ Abandonment
- Offshore Platform Abandonment
- Casing "Windows" for Multi-Laterals
- Downhole Slotted Liners/Screens




The diagram shows a cross-section of a wellbore with a central metal pipe. A laser toolstring is positioned inside the pipe, extending from the top. The toolstring is shown as a series of connected segments, with a red line indicating the laser path. The laser path is shown as a red line that turns 90 degrees to the right, entering the wellbore wall. A blue rectangular area is shown on the wellbore wall, indicating the perforating zone. The wellbore is surrounded by a casing and a cement sheath.

gti

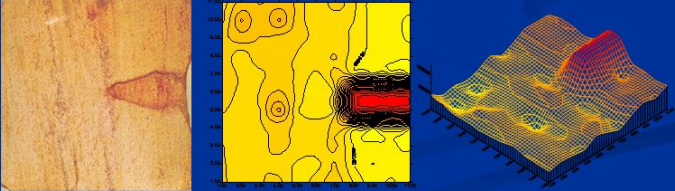
4

Slide 5



Benefits of Laser Perforation


- Non-Explosive Technology
- Real-Time Control: Input vs. Output
- Potential for “Extended Perforation” and Other Completion Methods
- Stimulate While Creating Perforations



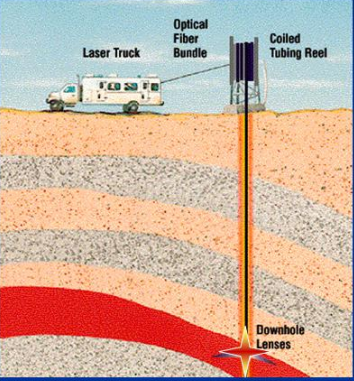
gti

5

Slide 6



Downhole Laser Applications



Laser Truck

Optical Fiber Bundle

Coiled Tubing Reel


Downhole Lenses

Field Applications Concept

gti

6

Slide 7



Laser Applications Background


GTI High Power Laser R&D

- GRI Feasibility Study (1997-00)
- GTI/DOE BP1 - Phase I (2000-01)
- GTI/DOE BP1 - Phase II (2002-03)
- GTI/DOE BP2 (2003-07)
- Laser Perforation POC (2003-04)
 - Halliburton/GRI \$1.5M
 - Complements GTI/DOE Task 4.0
 - Applications Focused
 - Filled in During DOE Funding Delay and Rescope

gti

7

Slide 8



Specific Energy


$$SE = \frac{\text{Energy Input}}{\text{Volume Removed}} = \frac{P}{dV/dt}$$
$$= \frac{\text{kW}}{\text{cm}^3/\text{sec}} = \frac{\text{kJ}}{\text{cm}^3}$$

gti

Reference: SPE 77627

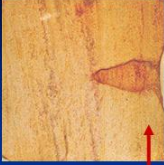
8

Slide 9




GRI Feasibility Study

Can Lasers Penetrate Rock?



- Laser Drilling Experiments (1997 to 2000)
- Three High-Powered Military Lasers

Type	Power (kW)	λ (μm)	Branch
COIL	6.8	1.34	USAF
CO ₂	50,150	10.6	USAF
MIRACL	1600	3.4	US Army




- Various Rock Lithologies Studied

gti

Reference: SPE 56625 9

Slide 10



GTI/DOE Study - Phase I

How Much Energy Does it Take?

- Laser Drilling Experiments (2000 - 2001)
- Three High-Powered Industrial Lasers

Type	Power (kW)	λ (μm)	Location
Nd:YAG	1.6	1.06	ANL
CO ₂	6	10.6	ANL
Diode	4	0.8	NA Tech

- Lithologies Studied: SS, LS, Sh

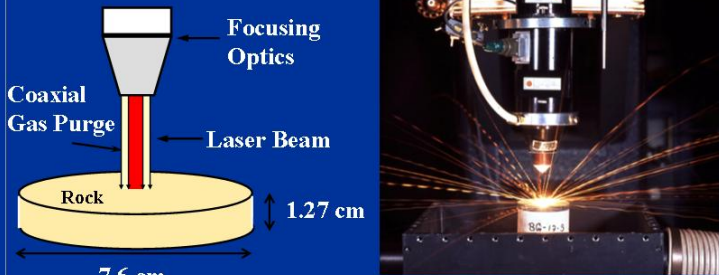
gti

Reference: SPE 71466 10

Slide 11

Nd:YAG Laser

Neodymium Yttrium Aluminum Garnet

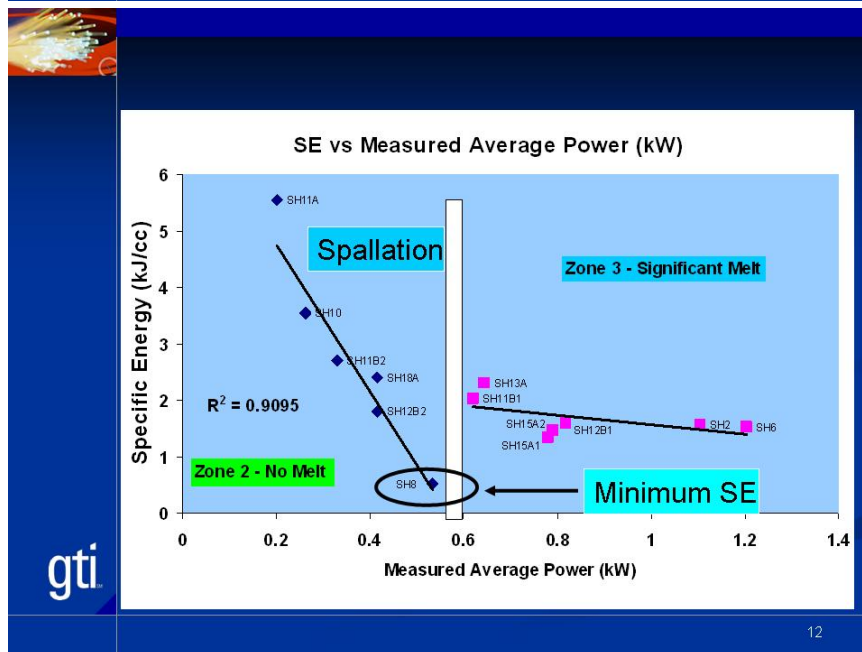


Labels in diagram: Focusing Optics, Coaxial Gas Purge, Laser Beam, Rock, 7.6 cm, 1.27 cm.

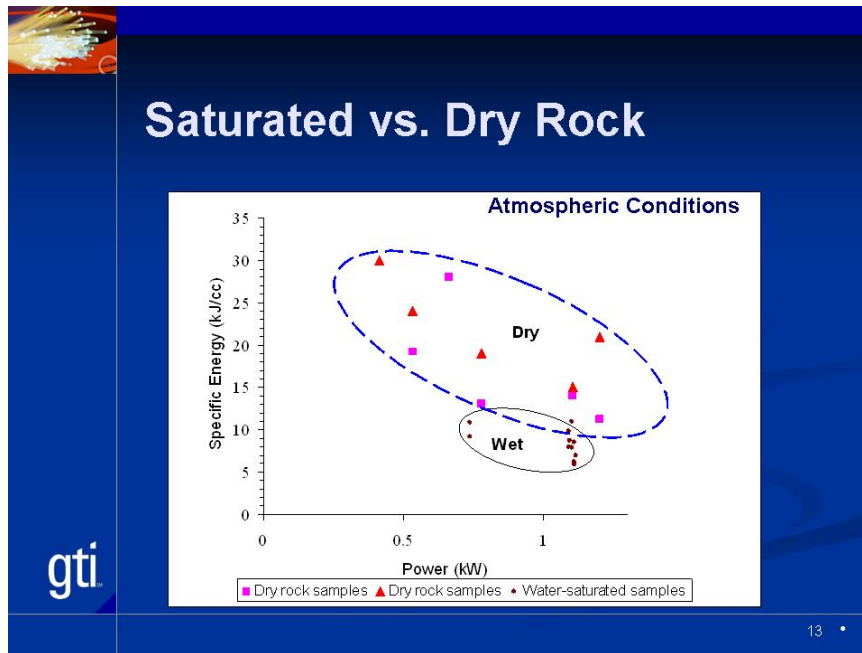
gti

11

Slide 12




Slide 13



Slide 14

- ## Paradigm Shift Results
- Change in Application Theory – Rate of Application: Blasting vs Chipping
 - Unlimited Downhole Applications due to Precision and Control (i.e., direction, power, etc.)
 - Off-Ramp Approach to Commercialization and Technology Integration
 - Completions Less Complex Than Drilling
 - Allows Technology Leveraging
 - Rolling Integration Into Industry
- gti
- 14

Slide 15



GTI/DOE Study - Phase II

How Can Lasers Create Larger Holes?

- Laser Drilling Experiments (2002 - 2003)
- Two High-Powered Industrial Lasers

Type	Power (kW)	Λ (μm)	Location
Nd:YAG	1.6	1.06	ANL
CO ₂	6	10.6	ANL


- Lithologies Studied: SS, LS

gti

Reference: SPE 71466

15

Slide 16



GTI/DOE Study - Phase II

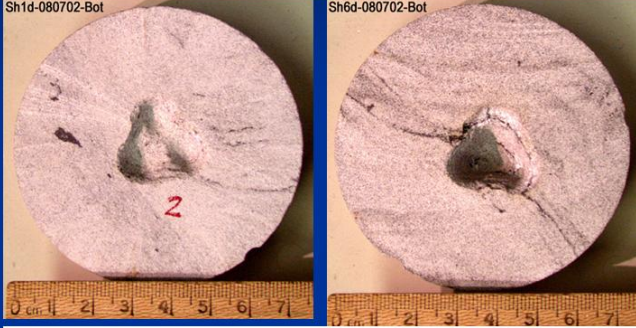
- Test Effects of Laser Application Techniques on Specific Energy
 - Avoid Melt
 - Minimize SE Values
- Apply Multiple Beam Bursts in Varied Geometric Patterns
 - Mimics Results of Rock Cutters
 - Cumulative Effects of Multiple Bursts
 - Not Continuous Blast

gti

16

Slide 17

GT/DOE Study - Phase II



Sh1d-080702-Bot

Sh6d-080702-Bot

Photos of the lowest SE result (SH1D-2, left), and highest SE (SH6D, right). Sample SH6D exhibits a small amount of melt inside the hole.

gti

17

Slide 18


HES Laser Perf POC Tasks

- 1.0 Laser Selection and Testing
- 2.0 Preliminary Tests and Analysis
- 3.0 In-Situ Rock Tests
- 4.0 In-Situ Clad Tests
- 5.0 Final Reports

gti

18

Slide 19



Downhole Laser Requirements

- **Technical**
 - Provide Required Output Power
 - Deliver Beam to Downhole Target
 - Operate at Downhole Conditions
 - Cut / Drill Multiple Materials
 - Mobile, Rugged On-site Deployment

gti

19

Slide 20



Downhole Laser Requirements

- **Economic**
 - Existing, Commercially Available
 - Minimal Maintenance and Repair
 - High Energy Conversion Efficiencies
 - Minimal Energy Losses
 - Attenuation
 - Absorbtion

gti

20

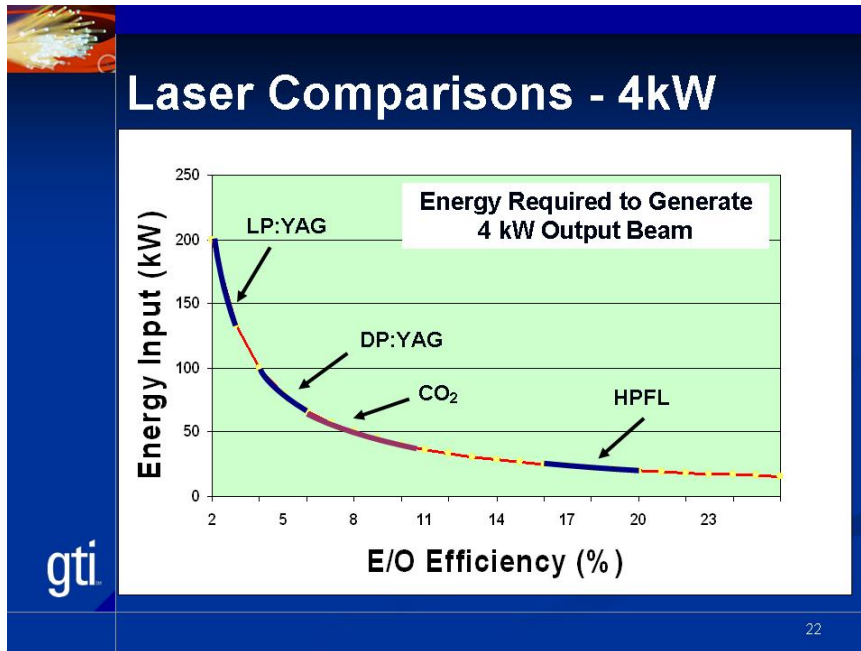
Slide 21

Laser Comparisons - 4kW

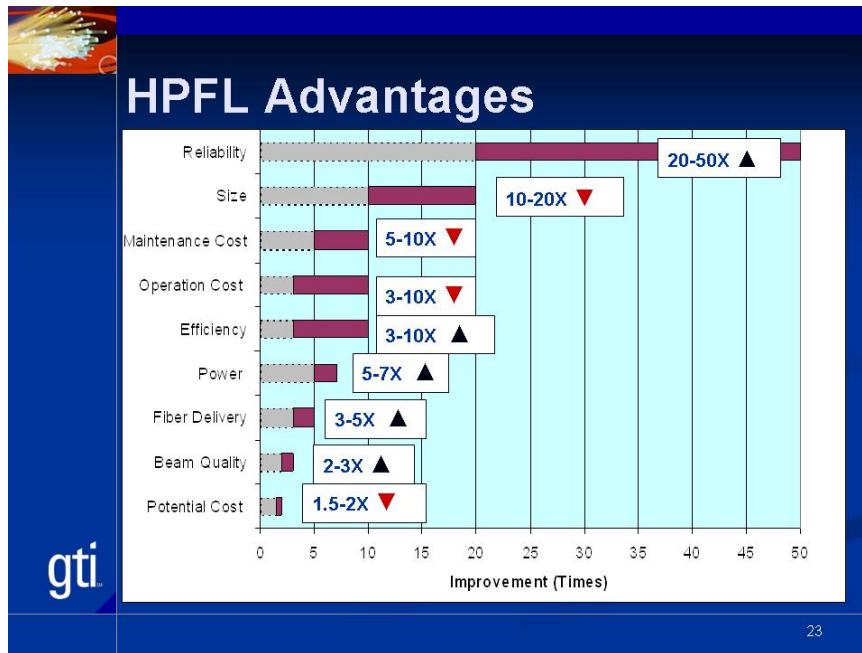
	CO ₂	LP:YAG	DP:YAG	HPFL
E/O Efficiency, %	5-10	2-3	4-6	16-20
Electric Power, kW (no chiller)	40-80	130-200	~ 80	20-25
Footprint, m ² (no chiller)	6	5	3	0.5
Water, m ³ /hr	6-8	20-25	~ 15	<2
Maintenance, Khrs	1-2	0.5	2-3	10-15
Pump Replace, Khrs	n/a	0.5-1	2.5	>50

21

Slide 22



Slide 23



Slide 24

Fiber Laser Background

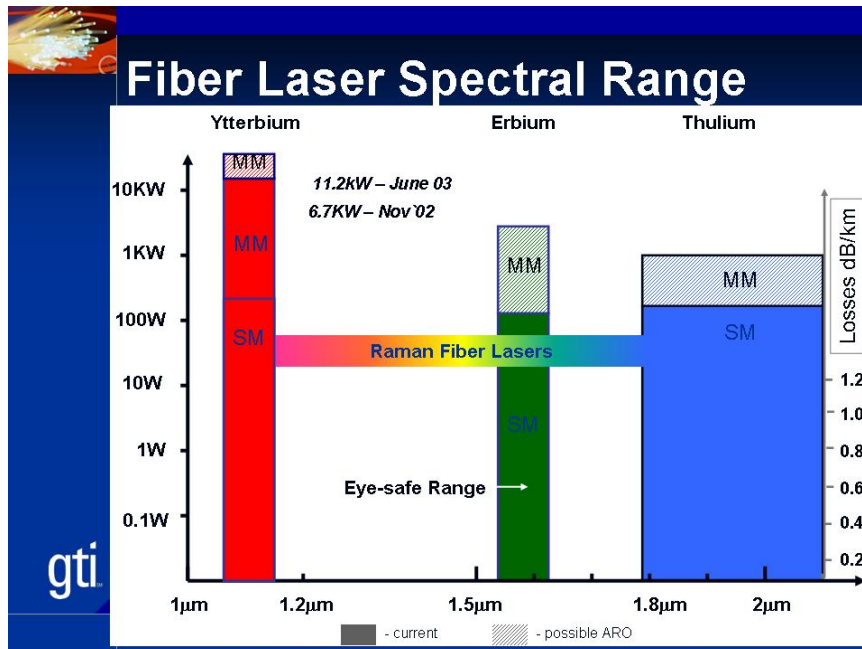
Path to Technology Breakthrough

- **1963** – First Demonstration
- **1980's** – Fiber Optic Communications
 - Signal Boosters (amplifiers)
- **2000's** – High Power Fiber Lasers
 - Single to Multimode Configuration
 - 100-10,000 W over 18 months

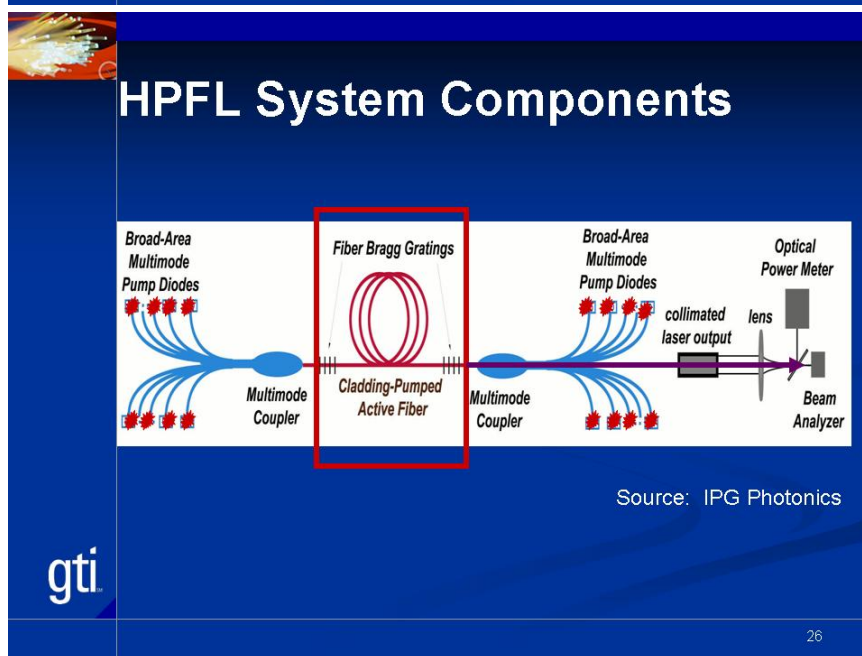
gti

24


Slide 25



Slide 26




Slide 27



GTI High Power Fiber Laser

Largest US Research HPFL

- 5.34 kW, 1.07 micron
- E/O Efficiency $\geq 20\%$
- Size: 60 x 80 x 160 cm
 - Footprint: 0.5 m²
- Weight: 400 kg



gti

27

Slide 28




GTI High Power Fiber Laser



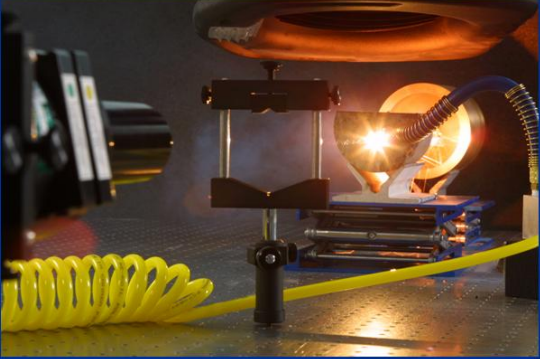
gti

28

Slide 29




GTI High Power Fiber Laser



gti

29

Slide 30




HES Laser Perf POC Tasks

- 1.0 Laser Selection and Testing
- 2.0 Preliminary Tests and Analysis**
- 3.0 In-Situ Rock Tests
- 4.0 In-Situ Clad Tests
- 5.0 Final Reports

gti

30

Slide 31



HES Experimental Tasks

- Deep Penetration Tests
 - Evaluate SE Calculation
 - Optimizing HPFL Parameters
- Saturation Tests
 - Oil, Water and Gas
- Fiber Efficiency Test
 - Compare Results with Other Laser Data
- Simulated Casing Tests
- Optical Fluid Transmission Test

gti

31

Slide 32



Material Removal Mechanisms

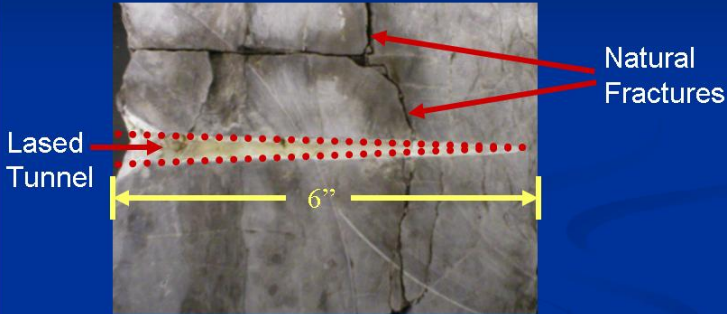
- Several Methods Observed
- Function of Thermal Properties
 - Carbonates – Dissociation
$$\text{CaCO}_3 \rightarrow \text{CaO} + \text{CO}_2$$
 - Sandstones – Spallation
 - Shales – Spallation
 - Steel - Melt

gti

32

Slide 33

HPFL Perforation: Limestone



Lased Tunnel

Natural Fractures

6"

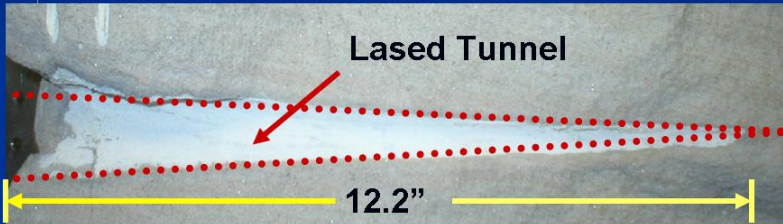
gti

HPFL Perforation in Reservoir Limestone
Length: 6 inches Power: 5.34 kW Beam: CW

33

Slide 34

HPFL Perforation: Limestone



Lased Tunnel

12.2"

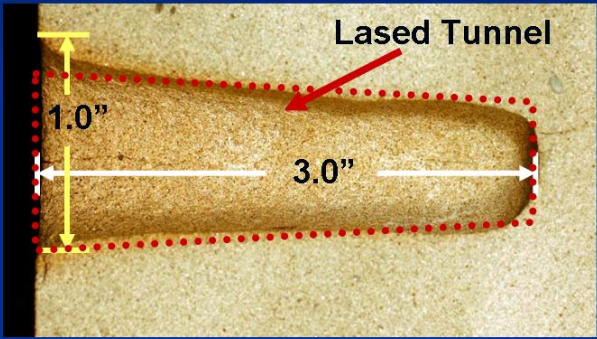
gti

HPFL Perforation in Quarry Limestone
Length: 12.2 inches Power: 5.34 kW Beam: CW

34

Slide 35

HPFL Perforation: Sandstone



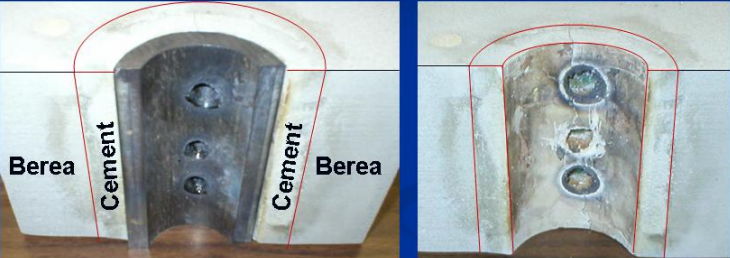
HPFL Perforation in Berea Sandstone
Length: 3.0 inches Power: 3 kW Beam: CW

gti

35

Slide 36

HPFL Perforation: Composite




HPFL Perforation Through Steel, Cement, and SS
Power: 4.4 kW Beam: CW

gti

36

Slide 37

Small Block Perf Test



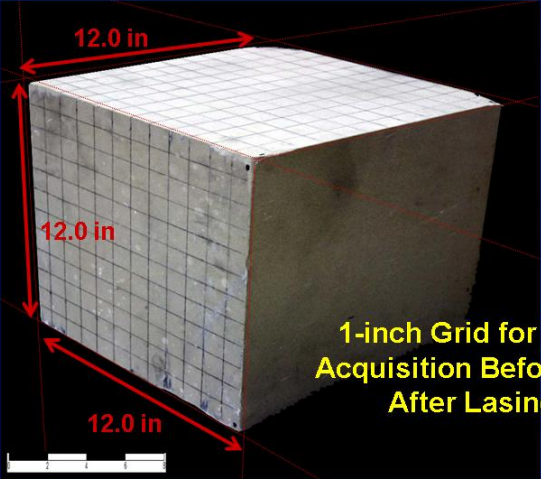
gti

Creating 1 x 3 Inch Tunnel in Small Berea Block

37

Slide 38

Large Block Perf Test

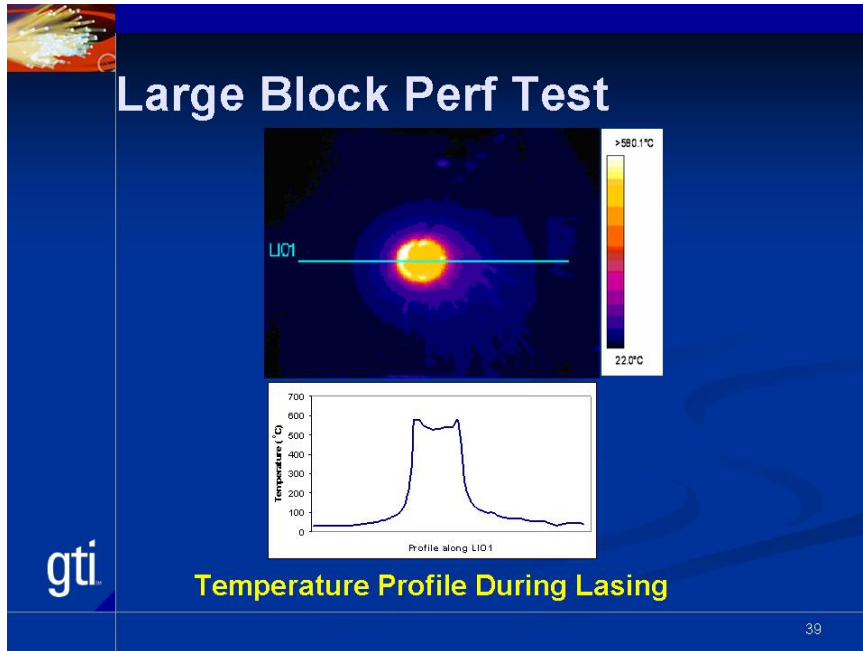


gti

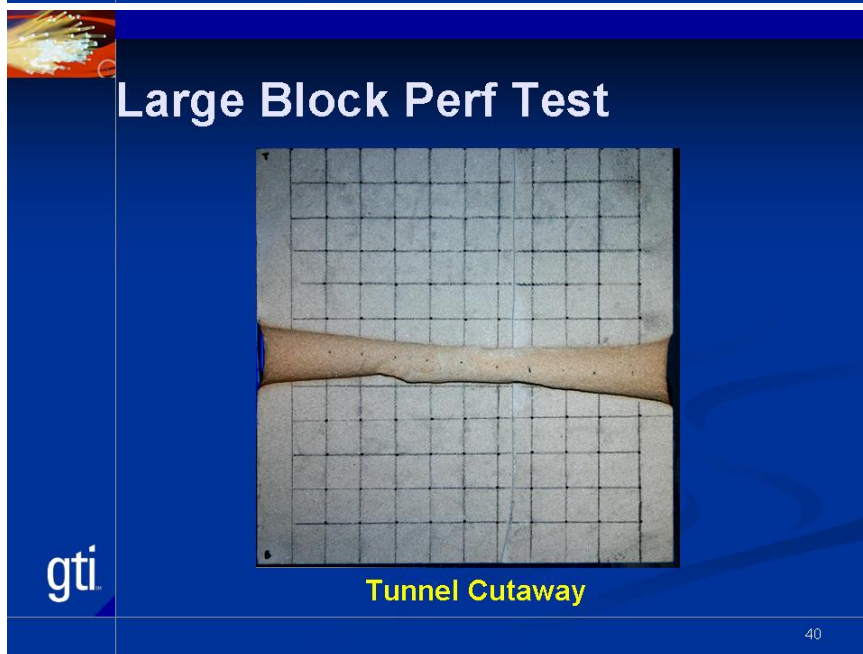
1-inch Grid for Data Acquisition Before and After Lasing

38

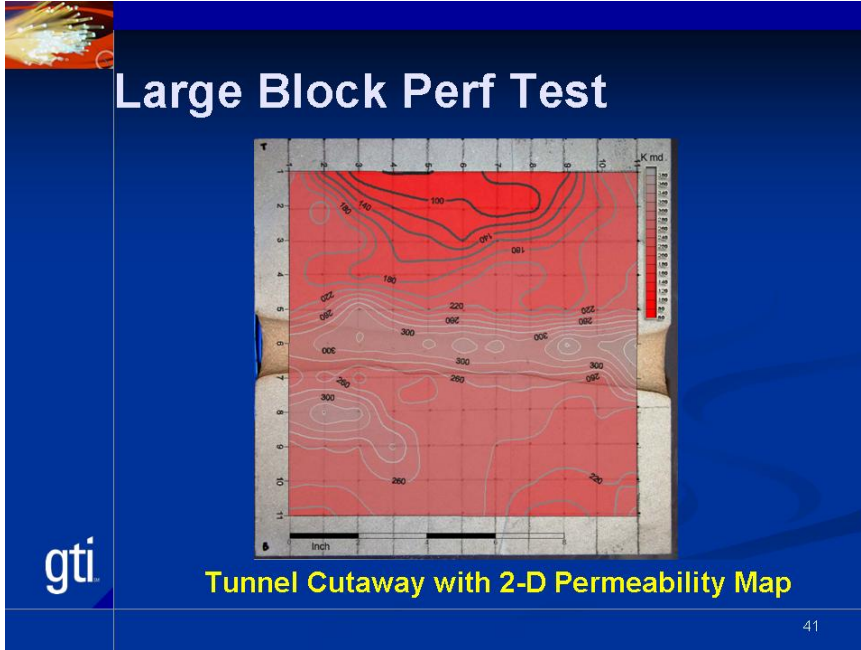
Slide 39



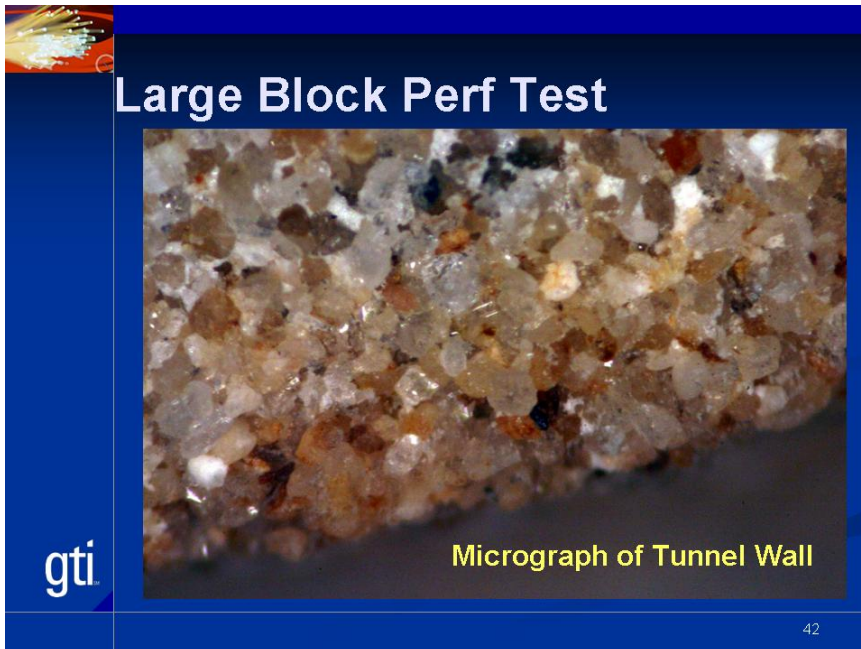
Slide 40



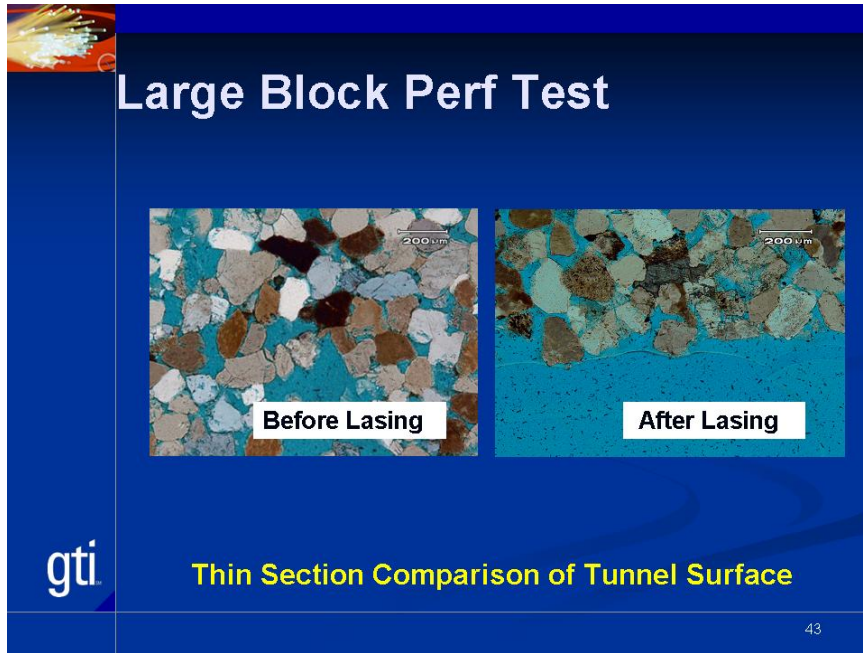
Slide 41



Slide 42



Slide 43



Large Block Perf Test

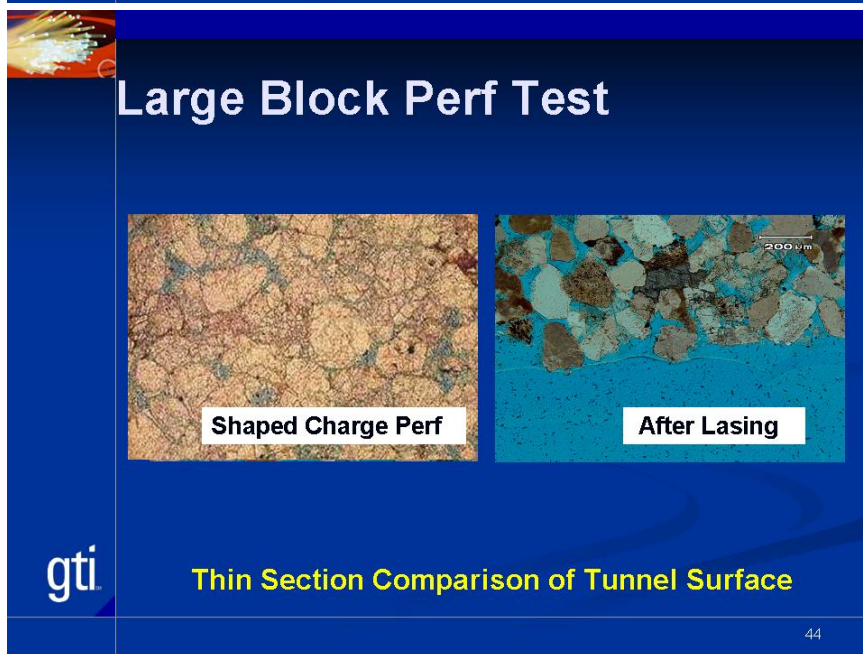
Before Lasing **After Lasing**

gti **Thin Section Comparison of Tunnel Surface**

43

Detailed description: This slide features a blue background with a small fiber optic image in the top-left corner. The main title is 'Large Block Perf Test'. Below it are two side-by-side micrographs. The left micrograph, labeled 'Before Lasing', shows a porous, irregular rock surface with a 200 µm scale bar. The right micrograph, labeled 'After Lasing', shows a smoother, more uniform surface with a 200 µm scale bar. At the bottom left is the 'gti' logo, and at the bottom center is the text 'Thin Section Comparison of Tunnel Surface'. The number '43' is in the bottom right corner.

Slide 44



Large Block Perf Test

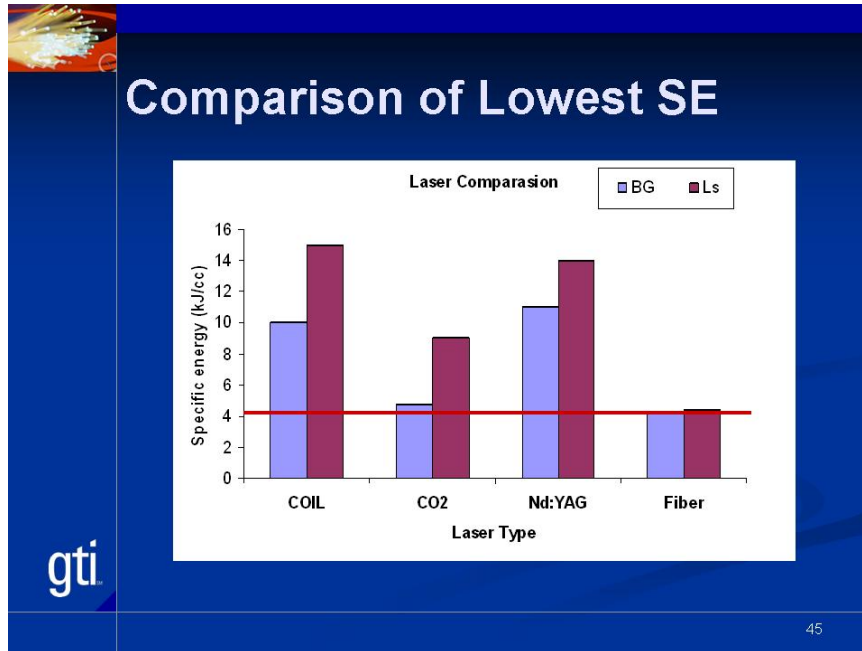
Shaped Charge Perf **After Lasing**

gti **Thin Section Comparison of Tunnel Surface**

44

Detailed description: This slide features a blue background with a small fiber optic image in the top-left corner. The main title is 'Large Block Perf Test'. Below it are two side-by-side micrographs. The left micrograph, labeled 'Shaped Charge Perf', shows a highly textured, porous rock surface. The right micrograph, labeled 'After Lasing', shows a smoother, more uniform surface with a 200 µm scale bar. At the bottom left is the 'gti' logo, and at the bottom center is the text 'Thin Section Comparison of Tunnel Surface'. The number '44' is in the bottom right corner.

Slide 45



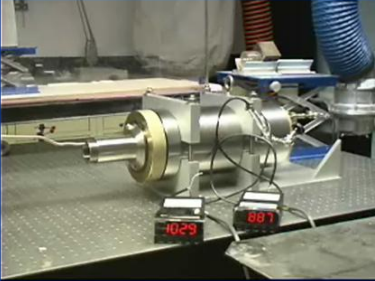
Slide 46

- ### HES Laser Perf POC Tasks
- 1.0 Laser Selection and Testing
 - 2.0 Preliminary Tests and Analysis
 - 3.0 In-Situ Rock Tests**
 - 4.0 In-Situ Clad Tests**
 - 5.0 Final Reports
- gti
- 46

Slide 47

HES Perf Tests – Pressure

- High Pressure Cell for Laser Applications
 - Simulates Downhole Pressure Conditions
 - Initial Tests Successful (Triaxial)
 - Testing Under Various Configurations



gti

47

Slide 48


Conclusions

- Lasers Can Break/Cut All Rock
- Previous Literature Outdated
- HPFL: Breakthrough Technology
 - Meets Field Deployment Needs
 - Commercially Available
- Potential Non-Explosive Perf Option

gti

48

Slide 49



Conclusions

- **Successful Well Perforation Lab Demo**
 - Longest Laser Tunnel to Date in SS
 - Minimal SE Observed
 - Optimal Fluid Flow Conditions Result
 - Temperature Control Key to SS Spallation
- **Multiple Applications – Multiple Industries**

gti

49

Slide 50




Next Steps in Laser R&D

- **Additional Fundamental Research**
 - Beam Wavelength Effects (Jeff Labs FEL)
 - Expand Simulation of Downhole Conditions
 - Modeled Effects of Energy Transfer
- **Field Experiments - Perforation**
 - Develop Prototype Tool
 - Test Suite of Conditions
- **Explore Drilling Issues and Applications**
 - i.e., Microhole and Laser Assist

gti


50

Slide 51




Publications 2004-2005

- Gahan, B.C. "Application of Fiber Lasers with Rock and Non-Metal Materials," *Industrial Laser Solutions*, September (2005).
- Gahan, B.C. "Fiber Laser Offers Fast Track to Clean Perforations," *GasTIPS* (Spring 2005).
- Gahan, B.C., Batarseh, S. 2004. "An Overview of High Power Laser Applications Research from Well Construction and Completion," 2004 *International Gas Research Conference* (IGRC), Vancouver, BC.
- Batarseh, S., Gahan, B.C., Sharma, B., Gowelly, S. 2004. "Evaluation of High Power Ytterbium Fiber Lasers for Rock Cutting and Removal Applications," 23rd *International Congress on Applications of Lasers and Electronics*, San Francisco, CA.




51

Slide 52




Publications 2004-2005

- Gahan, B.C., Batarseh, S., Reilly II, J.F., Wilcox, B.H. 2004. "Geological Investigation of the Lunar and Martian Surface and Subsurface Using High Power Lasers," American Institute of Aeronautics and Astronautics (AIAA) *Space 2004* Conference and Exhibit, San Diego, CA.
- Gahan, B.C., Batarseh, S., Sharma, B., Gowelly, S. 2004. "Analysis of Efficient High-Power Fiber Lasers for Well Perforation," SPE Paper 90661, *SPE Annual Technical Conference and Exhibition*, Houston, TX.
- Batarseh, S., Gahan, B.C. 2004. "Deep Hole Penetration for Oil Production Using Ytterbium Fiber Laser," *SPIE High-Power Laser Ablation V*, Taos, NM.
- Gahan, B.C., Shiner, B. 2004. "New High-Power Fiber Laser Enables Cutting-Edge Research," *GasTIPS* (Winter 2004).



52

Slide 53



Accepted Publications 2005

- "Influence of Downhole Pressure Conditions on Laser Perforation," 2005 SPE ATCE, Houston, TX.
- "Innovation in Wellbore Perforation Using High Power Lasers," 2005 SPE IPTC, Doha, Qatar.
- "High Pressure Testing Advances Underground Fiber Laser Rock Cutting Applications," 2005 ICALEO, Miami, FL.
- GasTIPS, Fall 2005

gti

53

Slide 54



GTI Leading Laser Apps R&D

- Unique Capabilities, Expertise, Network
- Successful R&D Results
- Advanced HPFL Lab
- Attracting R&D With Industry Partners
- Exclusive Laser Industry Partner (IPG)
- Near and Long Term Project Portfolio

gti

54

